MRC | National Institute for Medical Research

UCL

Motoring merozoites: the role of gliding-associated proteins GAP45 and GAP50 in erythrocytic invasion

A thesis presented in partial fulfilment of the requirements for the degree of Doctor of Philosophy of the University of London

Roxanne Rhiannon Rees-Channer

Divisions of Parasitology and Physical Biochemistry
National Institute for Medical Research
Mill Hill, London
NW7 1AA

Department of Biochemistry and Molecular Biology
University College London
Gower Street, London
WC1E 6BT

ProQuest LLC
789 East Eisenhower Parkway
P.O. Box 1346
Ann Arbor, MI 48106-1346

ABSTRACT

Apicomplexan parasites utilise an acto-myosin motor for host cell invasion and/or gliding motility. Until recently, only actin, myosin A (MyoA) and its putative light chain (MLC1 in *Toxoplasma gondii*) or myosin tail domain interacting protein (MTIP) in *Plasmodium* spp., had been identified as central to the function of this motor. Isolation of two additional components in *T. gondii*, the gliding-associated proteins (GAP)45 and GAP50, has provided a valuable insight into how the motor complex may be anchored in the pellicular membrane network lining the periphery of invasive zoites.

Results presented here demonstrate that the tetrameric complex comprising MyoA, MLC1/MTIP, GAP45 and GAP50 is conserved in *Plasmodium falciparum* (*P. falciparum*). *P. falciparum* (Pf)GAP45 and PfGAP50 are expressed and co-localise with PfMTIP at the periphery of blood-stage merozoites. As in *T. gondii*, PfGAPs are membrane-bound and found in association with PfMyoA and PfMTIP; a complex that appears to be assembled in two distinct stages. PfGAP50 is incorporated subsequent to the formation of a cytoplasmic ternary complex comprising PfGAP45, PfMyoA and PfMTIP.

Expression of recombinant forms of PfGAPs has facilitated structural and functional analyses. While both PfGAP50 and PfGAP45 are at least partially folded, the latter has a low overall content of secondary structure. Despite investigation using a number of techniques, direct interaction of PfGAP45 with PfMyoA or PfMTIP has not been found. PfGAP45 is *N*-myristoylated and palmitoylated in developing merozoites. Thus, the protein may target and tether complex components to membranes. PfGAP45 is also phosphorylated in the parasite; a modification potentially important in protein function and/or regulation of the motor. A calcium-dependent protein kinase (PfCDPK1) expressed at the periphery of merozoites, is one potential candidate kinase. Recombinant PfGAP45 is a substrate for recombinant PfCDPK1 *in vitro* and phosphopeptides have been identified. An overlapping phosphopeptide isolated from digests of PfGAP45 extracted from merozoites suggests this kinase also modifies the protein *in vivo.*

ACKNOWLEDGEMENTS

First and foremost, I must express my sincerest gratitude to a number of people within NIMR whose help and support has been invaluable to me. Primarily, I would like to thank Tony Holder and Justin Molloy for giving me the opportunity to develop my research skills in such a rewarding field. Their encouragement and support have been vital for my development throughout the project and provided me with excellent tools for the future. Many thanks also to Judith Green, for her endless patience and encouragement in the lab. Her enthusiasm in all aspects of research projects and dry sense of humour has kept me grounded and laughing through many a scatty bench disaster. I must also extend my appreciation to Stephen Martin, who was always available for advice, practical help and whose knowledge of all things spectroscopic to this day overwhelms me. Particular thanks must also go to Muni Grainger for culturing and preparing endless quantities of parasite material for a wide range of experiments. I should also thank Steven Howell for his boundless theoretical and practical experience in mass spectroscopy and for his patience in sharing a meagre portion of this knowledge with me.

Members of the Holder lab, divisions of Parasitology and Physical Biochemistry who have helped me at one time or another are too many to mention but I thank all of you. In particular, I thank Sola Ogun and Madhu Kaddekoppala for performing immunisations and Anton Dluzewski for immunoEM analyses.

There are a number of others from outside the instutite I would also like to acknowledge. Firstly, Paul Bowyer, whose optimistic, helpful advice regarding *N*-myristoylation assays was essential to my research. A huge thank you must also go to my parents and friends who have put up with the everyday ups and downs that accompany the PhD process. Lastly and most importantly, my warmest thanks go to my partner Chris, for his unwavering love and support through thick and thin. For that, I am eternally grateful.

PREFACE

The work described in this thesis was carried out at the National Institute for Medical Research (NIMR) between September 2004 and April 2008 while the author was in receipt of a Medical Research Council (MRC) studentship. The scientific work performed and presented here was performed solely by the author except where specifically acknowledged. No part of this thesis has been submitted for any other degree or diploma. Scientific papers related to this thesis that have been published by the author are listed below:

Rees-Channer, R.R, Martin, S.R., Green, J.L., Bowyer, P.W., Grainger, M., Molloy, J.E., Holder, A.A. (2006) "Dual acylation of the 45 kDa gliding-associated protein GAP45 in Plasmodium falciparum merozoites" Mol Biochem Parasitol **149**(1): 113-116.

Roxanne Rees-Channer

April, 2008

CONTENTS

ABSTRACT 2

ACKNOWLEDGEMENTS 3

PREFACE 4

CONTENTS 6

FIGURES 11

TABLES 13

ABBREVIATIONS 14

Chapter One - Introduction

1.1 History of malaria 18

1.1.1 Ancient literature 18

1.1.2 Scientific discoveries 18

1.2 Life-cycle of the malaria parasite 20

1.2.1 Sporozoite entry and exo-erythrocytic schizogony 20

1.2.2 Erythrocytic schizogony 21

1.2.3 Gametogenesis and sporogony 22

1.3 Global impact of malaria 24

1.3.1 Distribution and burden of disease 24

1.3.2 Control and treatment 24

1.4 Host-pathogen interplay 27

1.4.1 Pathogenesis 27

1.4.2 Immunity 28

1.5 Maintenance of an intracellular lifestyle 30

1.5.1 Host cell invasion 30

1.5.2 Gliding motility 31

1.6 Apicomplexan zoite morphology 33

1.6.1 The cytoskeleton 33

1.6.2 Apical organelles 34

1.7 Erythrocytic invasion by *Plasmodium* spp 37

1.7.1 Initial attachment 37
1.7.2 Re-orientation and apical attachment 39
1.7.3 The moving junction and cell penetration 41
1.8 The glideosome 45
1.8.1 Apicomplexan actin 45
1.8.2 Apicomplexan myosin 47
1.8.3 Intra-extracellular anchorage 50
1.9 Aims of research 53

Chapter Two - Materials and Methods

2.1 Materials 65
2.1.1 Chemical reagents 65
2.1.2 Solutions - Media 65
2.1.3 Centrifuges 66
2.1.4 Host strains 66
2.1.5 Plasmids 67
2.1.6 Oligonucleotides 68
2.2 Manipulation of DNA 69
2.2.1 Concentration 69
2.2.2 Quantification 69
2.2.3 Agarose gel electrophoresis 69
2.3 Plasmid construction 70
2.3.1 Isolation of parasite genomic DNA 70
2.3.2 Polymerase Chain Reaction (PCR) 70
2.3.3 Restriction endonuclease digestion 71
2.3.4 Ligation of DNA fragments 71
2.3.5 Purification of DNA 71
2.3.6 Ligation Independent Cloning (LIC) 72
2.3.7 Isolation of plasmid DNA 72
2.3.8 Sequencing of DNA 73
2.3.9 Codon optimisation 73

2.4 Manipulation of host cells: *E. coli and P. pastoris* 74
2.4.1 Transformation 74
2.4.2 Cell culture for protein expression 75
2.4.3 Cell storage 76
2.5 Parasite manipulation 77
2.5.1 Cell culture 77
2.5.2 Synchronisation and isolation of parasites 77
2.5.3 Biosynthetic labeling 78
2.5.4 Total protein extraction and solubility tests 79
2.6 Protein Analyses 80
2.6.1 Purification of recombinant proteins and co-precipitations 80
2.6.2 Factor Xa cleavage 81
2.6.3 Quantification 81
2.6.4 Buffer exchange and concentration 81
2.6.5 SDS-Polyacrylamide gel electophoresis (SDS-PAGE) 82
2.6.6 Synthetic peptides 82
2.7 Production and application of antisera 83
2.7.1 Raising antisera 83
2.7.2 Purification of antibodies 83
2.7.3 Purification of PfGAP45 from merozoites 84
2.7.4 Western blotting 85
2.7.5 Immunofluorescence assays (IFA) 85
2.7.6 Immunoelectron Microscopy (ImmunoEM) 86
2.7.7 Immunoprecipitation (IP) 87
2.8 Bioinformatic analyses 89
2.8.1 Search engines and databases 89
2.8.2 Proteomic tools 89
2.9 *In vitro* post-translational modification assays 90
2.9.1 *N*-myristoylation assay 90
2.9.2 [γ-^{32}P] Adenine trinucleotide (ATP) kinase assay 90
2.9.3 Nicotinamide adenine dinucleotide (NADH)-coupled enzyme assay 90
2.10 Biophysical analyses 92

2.10.1 Circular dichroism (CD) spectroscopy 92
2.10.2 Fluorescence spectroscopy 92
2.10.3 Electrospray ionisation mass spectrometry (ESI-MS) 94
2.10.4 MALDI-TOF mass spectrometry 95

Chapter Three - Expression of GAPs in P. falciparum

3.1 Introduction 108
3.2 Results 112
3.2.1 PfGAPs are expressed in late blood stages 112
3.2.2 PfGAPs are associated with parasite membranes 113
3.2.3 PfGAPs are located at the periphery of merozoites 113
3.2.4 PfGAPs form a complex with PfMyoA and PfMTIP 114
3.2.5 The tetrameric motor complex is assembled in two stages 115
3.2.6 PfGAP45 is directly associated with parasite membranes 115
3.3 Discussion 117

Chapter Four - Structural analyses of PfGAPs and investigation of intra-complex associations

4.1 Introduction 148
4.2 Theory and data analysis 153
4.2.1 Circular dichroism (CD) spectroscopy 153
4.2.2 Fluorescence spectroscopy 157
4.3 Results 160
4.3.1 Preparation of recombinant PfGAPs expressed in *E. coli* 160
4.3.2 Structural analyses 162
4.3.2.1 Secondary structure prediction for recombinant PfGAPs 162
4.3.2.2 Conformational analyses of recombinant PfGAPs using CD 164
4.3.3 Interactions of PfGAPs within the tetrameric complex 165
4.3.3.1 Co-immunoprecipitations 165
4.3.3.2 CD analyses 166

4.3.3.3 Fluorimetric analyses 167
4.3.4 Preparation of recombinant PfGAP45 in *P. pastoris* 167
4.3.5 Far-UV CD of recombinant PfGAP45 expressed in *P. pastoris* 169
4.4 Discussion 170

Chapter Five - Post-translational modification of PfGAP45

5.1 Introduction 209
5.2 Results 213
5.2.1 *In silico* prediction of co- and post-translational modifications 213
5.2.2 *In vitro N*-myristoylation of PfGAP45 214
5.2.3 Modification of PfGAP45 in the parasite 215
5.2.4 PfGAP45 is a substrate for PfCDPK1 *in vitro* 216
5.2.5 Isolation of recombinant PfGAP45 phosphopeptides 217
5.2.6 Identification of phosphorylation sites within parasite-derived PfGAP45 218
5.2.6.1 Extraction of PfGAP45 from purified merozoites 218
5.2.6.2 MALDI-TOF analyses 219
5.3 Discussion 221

Chapter Six - Conclusions and perspectives

6.1 Conservation of the tetrameric motor complex 250
6.2 Structure of PfGAPs 252
6.3 Direct intra-complex associations 253
6.4 The role of PfGAPs 255
References 263

FIGURES

Chapter One

1.1 Life-cycle of *P. falciparum* 54
1.2 Global distribution of malaria 56
1.3 Apicomplexan zoite morphology 58
1.4 Erythrocytic invasion by *P. falciparum* merozoites 60
1.5 The glideosome complex 62

Chapter Two

2.1 NADH-coupled kinase assay enzyme reactions 105

Chapter Three

3.1 Transcriptional profiles of genes coding for PfGAPs 130
3.2 PfGAPs are expressed in the late blood stages 132
3.3 PfGAPs are predominantly associated with membranes 134
3.4 PfGAPs are located at the periphery of merozoites 136
3.5 PfGAPs are associated with pellicular membranes 139
3.6 The tetrameric complex is conserved in *P. falciparum* 141
3.7 The *P. falciparum* tetrameric complex is formed in two stages 143
3.8 PfGAP45 is directly associated with membranes 145

Chapter Four

4.1 The structure of myosins 176
4.2 Purification of recombinant PfGAPs (*E. coli*) 179
4.3 Removal of the N-terminal tag from recombinant PfGAP50 181
4.4 Secondary structure predictions for PfGAPs 183
4.5 Helical wheel presentation of an α-helical coiled coil motif 186
4.6 The secondary structure of recombinant PfGAPs (*E. coli*) 188
4.7 The tertiary structure of recombinant PfGAPs (*E. coli*) 190
4.8 Conformational stability of recombinant PfGAP50 192

4.9 PfMTIP does not co-precipitate with PfGAP45 *in vitro* 194
4.10 PfMTIP-PfGAP45 interaction is not detectable by CD analyses 196
4.11 PfMTIP-PfGAP45 interaction is not detectable by fluorescence analyses. 198
4.12 Purification of recombinant PfGAP45 (*P. pastoris*) 200
4.13 PfGAP45 is glycosylated in *P. pastoris* 202
4.14 Different recombinant forms of PfGAP45 adopt a similar conformation .. 204
4.15 Comparison of apicomplexan GAP45 amino acid sequences 206

Chapter Five

5.1 PfGAP45 is a substrate for PfNMT *in vitro* 231
5.2 PfGAP45 is dually acylated and phoshorylated in merozoites 233
5.3 PfGAP45 is a substrate for PfCDPK1 *in vitro* 235
5.4 The kinetics of PfCDPK1-catalysed phosphorylation 237
5.5 Recombinant PfGAP45 is modified at three different sites 239
5.6 Phosphates are incorporated between residues 81-112 of PfGAP45 241
5.7 Determination of metastable fragment ion true molecular masses 243
5.8 Purification of PfGAP45 from merozoites 245
5.9 Identification of two parasite-derived phosphopeptides 247

Chapter Six

6.1 The updated glideosome complex 260

TABLES

Chapter Two

Table 2.1 Constructed plasmids 97
Table 2.2 Oligonucleotides 99
Table 2.3 Polymerase chain reactions (PCR) 101
Table 2.4 Antibodies 103

Chapter Three

Table 3.1 Solubility of PfGAPs in developing merozoites 122
Table 3.2 Immunoprecipitation of the tetrameric complex 124
Table 3.3 Variation in the motor components ~42-44 h post-invasion 126
Table 3.4 Variation in solubility of PfGAP45 ~42-44 h post-invasion 126

Chapter Four

Table 4.1 Secondary structure contents of PfGAP50 during thermal unfolding 174

Chapter Five

Table 5.1 Predicted phospborylation sites in PfGAP45 227
Table 5.2 Phosphopeptides identified in parasite-derived PfGAP45 229

ABBREVIATIONS

ABC	ammonium bicarbonate
ABRA	acidic basic repeat antigen
AMA-1	apical membrane antigen-1
ARF1	ADP-ribosylation factor 1
ADP/ATP	adenosine di/triphosphate
BDM	2,3-butanedione monoxime
BM(G/M)Y	buffered (glycerol/methanol) complex
BSA	bovine serum albumin
CDPK1	calcium-dependent protein kinase 1
CD	circular dichroism
CTRP	circumsporozoite- and TRAP-related protein
DAPI	4'-6-diamidino-2-phenylindole
DBL	duffy binding-like
dNTP	Deoxyribonucleoside triphosphate
DOC	sodium deoxycholate
DTNB	5,5'-dithio-bis(2-nitrobenzoic acid)
DTT	dithiothreitol
DRM	detergent-resistant membrane raft
EBA	erythrocyte binding antigen
EDTA	ethylenediaminetetraacetic acid
EGTA	ethylene glycol bis(2-aminoethyl ether)-*N*,*N*,*N'N'*-tetraacetic acid
EGF	epidermal growth factor
EM	electron microscopy
EMP-1	erythrocyte membrane protein-1
ESI-MS	electrospray ionisation mass spectroscopy
FITC	fluorescein isothiocyanate
GAP45/50	45 kDa/50 kDa gliding-associated protein
GFP	green fluorescent protein
GPI	glycosylphosphatidylinositol
GST	glutathione *S*-transferase

HEPES	4-(2-hydroxyethyl)-1-piperazineethanesulfonic acid
HRP	horse-radish peroxidase
IFA	immunofluorescence assay
IMAC	immobilised metal affinity chromatography
IMC	inner membrane complex
IP	immunoprecipitation
IPTG	isopropyl-β-D-thiogalactopyranoside
JAS	jasplakinolide
LB	Luria-Bertani
LDH	lactate dehydrogenase
LDS	lithium dodecyl sulphate
LIC	ligation independent cloning
MACS	Magnetic-Activated Cell Sorting
MALDI-TOF	matrix-assisted laser desorption/ionisation time-of-flight
MD	minimal dextrose
MIANS	2-(4'-maleimidylanilino) naphthalene-6-sulfonic acid
MIC	microneme protein
MJ	moving junction
MLC1	myosin light chain 1
MSP	merozoite surface protein
MTIP	myosin tail domain interacting protein
MTRAP	merozoite TRAP homologue
Myo	myosin
NADH	nicotinamide adenine dinucleotide
NMT	*N*-myristoyl transferase
NP-40	nonidet P-40
Ni-NTA	nickel-nitrilotriacetic acid
PAGE	polyacrylamide gel electrophoresis
PAP	purple acid phosphatase
PAS	periodic acid/Schiff's reagent
PAT	palmitoyltransferase
PBS(T)	phosphate buffer saline (tween)

PCR	polymerase chain reaction
PEP	phosphoenolpyruvate
PI	protease inhibitor cocktail
PK	pyruvate kinase
pRBC	parasitised red blood cell
PV(M)	parasitophorous vacuole (membrane)
PTRAMP	*Plasmodium* thrombospondin-related apical merozoite protein
RAMA	rhoptry-associated membrane antigen
RBL	reticulocyte binding-like
Rh	reticulocyte binding protein homologue
RhopH	high molecular mass rhoptry complex
RIMA	ring membrane antigen
RKIP	raf kinase inhibitor protein
ROM	rhomboid protease
RON	rhopty neck protein
ROPE	repetitive organellar protein
RPMI	Roswell Park Memorial Institute
SERA	serine repeat antigen
SDS	sodium dodecyl sulphate
SUB	subtilisin-like protease
TBE	tris-borate ethylenediaminetetraacetic acid
TE	tris ethylenediaminetetraacetic acid
TFA	trifluoroacetic acid
TFE	trifluoroethanol
Trx	thioredoxin
TSR	thrombospondin type I repeat
YEPD/YPD	yeast extract peptone dextrose
YNB	yeast nitogen base
YND	yeast nitrogen base dextrose

Chapter One

Introduction

1.1 History of malaria

1.1.1 Ancient literature

Malaria is among the most ancient of diseases. Descriptions of symptoms believed to be caused by malaria can be found in Chinese, Roman, Greek, Indian, Egyptian and European literature up to the 19th century. In 2700 BC, the Chinese Nei Ching (The Canon of Medicine) refers to the epidemic occurrence of paroxysmal fevers associated with enlarged spleens (Oaks, Mitchell et al. 1991). Vedic and Brahmanic scriptures (1,900-3,500 years ago) from the Indus valley in Northern India contain numerous references to fevers that are likely to have been caused by malaria. The *Atharva Veda* specifically details that fevers were more prevalent after excessive rainfall or in areas of high grass cover. It was believed that a fever demon "Takman" was the culprit (Carter and Mendis 2002).

Malaria appeared in Greek literature from around 500 BC. Hippocrates was the first physician to make a connection between the proximity of stagnant bodies of water and the infection of nearby populations (Oaks, Mitchell et al. 1991). A number of Roman writers also associated marshes with fevers. In the first century A.D., Marcus Terrentius Varro reported that "in swampy places minute creatures live that cannot be discerned with the eye and they enter the body through the mouth and nostrils and cause serious diseases" (Amici 2001). In 1718, Italian physician Francisco Torti described the ill-effects caused by stagnant bodies of water as "mal'aria" (bad air), a term which entered the English language as malaria many years later (Jarcho 1993).

1.1.2 Scientific discoveries

Scientific understanding of malaria did not begin until the end of the 19th century when the disease began to threaten many parts of European empires. In 1880, French army surgeon Charles Laveran identified the protozoan parasite that was responsible for causing malaria in fresh blood smears (Laveran 1880; Capanno 2006). In 1884, Italian scientists Ettore Marchiafava and Angelo Celli used optical microscopy, with an oil immersion objective lens in order to visualise the micron-sized parasites. They named the genus *Plasmodium* (Marchiafava and

Celli 1885; Capanno 2006), a title that has remained in literature ever since. The belief that mosquitoes were involved in transmitting malaria extends into antiquity. Cuneiform scripts several thousand years old attribute malaria to Nergal, the Babylonian god of destruction and pestilence. Nergal was depicted as a double-winged mosquito-like insect. Proof of the mosquito theory eventually came in 1897. British physician Ronald Ross identified what are now known to be oocysts (see section 1.2.3) in the gut of mosquitoes that had fed on a blood meal containing crescented parasites (Ross 1897; Capanno 2006). In 1898, he demonstrated that the bite of the *Culicine* mosquito was responsible for delivery of the parasite in birds. He was able to trace the different forms of the avian parasite from the bloodstream of the vertebrate through its proliferation in the mosquito gut to its accumulation in salivary glands (Ross 1898; Capanno 2006). This development of the parasite through its various stages in host organisms is known as its "life-cycle".

Italian malariologist Giovanni Grassi, alongside Amico Bignami and Giuseppe Bastianelli identified *Anopheline* mosquitoes as carriers of parasites that infect humans (Bastianelli, Bignami et al. 1898; Capanno 2006). By 1899, the group had elucidated the life-cycles of three of the species known to infect man: *Plasmodium falciparum (P. falciparum)*, *P. vivax* and *P. malariae* (Grassi 1900; Capanno 2006). The fourth species (*P. ovale*) was finally identified and described by John Stephens in 1922 (Stephens 1922). It has now been established that there are in fact over two hundred species of *Plasmodium* that infect a wide range of mammalian, avian and reptilian hosts (Rich and Ayala 2003).

Although our understanding of the parasite and the disease itself are still somewhat limited, it is from this base of knowledge that modern research in malaria has expanded and developed.

1.2 Life-cycle of the malaria parasite

The complete life-cycle of *Plasmodium* consists of alternating patterns of asexual and sexual growth and division in invertebrate as well as vertebrate hosts (figure 1.1). Of the 60 species of *Anopheles* mosquito that can transmit malaria in natural conditions, the Afrotropical *Anopheles gambiae* is the most effective vector of human malaria (Coluzzi 1999). For *P. falciparum*, *P. vivax* and *P. ovale*, the exclusive vertebrate hosts are humans. Conversely, *P. malariae* is capable of transmitting disease in higher apes and can therefore complete its life-cycle without infecting man. The four species of *Plasmodium* that infect man all have similar life-cycles but they display subtle differences that are described in the relevant sections.

1.2.1 Sporozoite entry and exo-erythrocytic schizogony

When a female *Anopheles* mosquito probes the skin of its human host, infective sporozoites contained in the saliva are injected into the avascular portion (Sidjanski and Vanderberg 1997). It was originally thought that sporozoites rapidly move away from the site of infection (Vanderberg 1975). However, recent evidence suggests a large proportion remain at the injection site for hours, with only slow release into the circulation (Yamauchi, Coppi et al. 2007). Once in the bloodstream, sporozoites migrate to the liver and within 30 minutes, they will invade hepatocytes (Shin, Vanderberg et al. 1982). The precise mechanism of targeting and invading specific hepatocytes is still unclear, although it has been suggested that traversal of both Kupffer cells (resident macrophages of the liver) and hepatocytes may be essential (Mota and Rodriguez 2004; Frevert, Usynin et al. 2006).

Upon invasion of the selected hepatocyte, parasites form a parasitophorous vacuole (PV) and reside in the cell for 9-16 days where they undergo asexual replication known as exo-erythrocytic schizogony. Hepatic schizogony can give rise to between ~10,000 (*P. vivax*) and ~40,000 (*P. falciparum*) merozoites that are released into the bloodstream upon rupture. Recent data have suggested that liver-stage parasites manipulate hepatocytes to ensure the safe delivery of

merozoites. Hepatocyte-derived merosomes appear to bud from schizonts, shuttling merozoites directly into the bloodstream so they are protected from the host immune system (Sturm, Amino et al. 2006). The time taken to complete the tissue stage of infection is dependent on the species. The durations are 8-25 days for *P. falciparum*, 8-27 days for *P. vivax*, 9-17 days for *P. ovale* and 15-30 days for *P. malariae*.

In *P. falciparum* and *P. malariae*, all sporozoites appear to develop directly into hepatic schizonts and none persist chronically in the liver. However, in *P. vivax* and *P. ovale*, a varying proportion of sporozoites will differentiate into latent forms called hypnozoites (Krotoski, Collins et al. 1982). Hypnozoites can remain dormant in the liver for months or even years before commencing schizogony that results in a relapse of infection.

1.2.2 Erythrocytic schizogony

Once the merozoites are released into the bloodstream, they locate, attach to and subsequently invade erythrocytes. In order to limit exposure of the parasite to the host immune system, this process is highly efficient and occurs rapidly, within 60 seconds (Bannister, Butcher et al. 1975).

Upon entry into the erythrocyte, the erythrocyte membrane invaginates and eventually forms a PV in which parasites develop into early trophozoites or 'ring forms'. The cytoplasm of the parasite then increases in quantity and becomes pigmented as ring forms transform into trophozoites. Parasites are highly metabolically active at this stage and thus, enlargement occurs as a result of the uptake and subsequent digestion of erythrocytic material in food vacuoles. The by-product of haemoglobin digestion, heme, is toxic to the parasite and is therefore polymerised into crystalline haemozoin that produces the characteristic pigment observed.

Parasites then undergo a series of nuclear divisions, each nucleus forming an individual merozoite bud that forms around the remaining cytoplasm. These rosettes of merozoites enclosed within erythrocytes are called schizonts and the number of parasites contained in each red cell is dependent on the species of

Plasmodium. *P. falciparum* schizonts usually contain a larger number of merozoites (8-32), whereas the other species generally generate fewer; 8-24 for *P. vivax*, 4-8 for *P. ovale* and 8 for *P. malariae*.

For survival, merozoites must then exit depleted erythrocytes and find new ones to invade. Recent evidence suggests that a subset of organelles contained within merozoites release specific proteases required to disrupt the PVM and/or erythrocyte membrane (Yeoh, O'Donnell et al. 2007). This membrane disruption causes schizonts to burst explosively, rapidly dispersing merozoites (Glushakova, Yin et al. 2005). Released merozoites will then rapidly find a new erythrocyte to invade, thus potentiating a repetitive synchronous cycle of either tertian or quartan periodicity, depending on the species (see section 1.3.1).

1.2.3 Gametogenesis and sporogony

Some of the merozoites contained within erythrocytes will differentiate into female and male macro and micro-gametocytes respectively. The precise stimulus governing this transformation is unknown and the timescale is also variable, depending on the species. For *P. falciparum*, gametogenesis takes 10-12 days whereas in *P. vivax* and *P. ovale*, gametocytes begin to appear within 5 days of infection. The process can be more variable in *P. malariae*, taking 5-23 days to occur.

Gametocytes are ingested by the female *Anopheles* mosquito when she takes a blood meal and develop within the lumen of the midgut. The female macrogametocytes and male microgametocytes escape from their respective erythrocytes and mature into gametes. For the microgametocyte, this involves exflagellation: nuclei divide rapidly to form filamentous flagella, enabling the microgamete to move away in search of a macrogamete. Gametes then fuse to form zygotes known as ookinetes that penetrate midgut epithelial cells and develop into oocysts on the basal lamella of the gut. Each oocyst contains thousands of sporozoites that subsequently escape into the haemocaelic cavity and migrate to salivary glands. Here, they invade the acinal cells of the salivary glands and mature into infective forms. After further penetration of the salivary glands,

sporozoites finally appear in the salivary duct, where they await injection into the next human host.

1.3 Global impact of malaria

1.3.1 Distribution and burden of disease

Evidence suggests that malarial parasites have been our co-evolutionary companions for millions of years (Carter and Mendis 2002). Although precise trajectories are unclear, parasite populations infecting early man are thought to have originated in Africa and subsequently dispersed across the globe. A number of factors are likely to have influenced the evolution of human malaria throughout the centuries. The gradual warming of the planet to present-day temperatures heralded the dawn of agriculture, which, eventually took root in Africa ~5,000 years ago (Carter and Mendis 2002). The tropical climate combined with the change of lifestyle transformed human settlements into ideal breeding grounds for mosquitoes. Anopheline mosquitoes evolved into highly anthropophilic vectors capable of maintaining stable and intense transmission required for endemicity (Coluzzi 1994; Coluzzi 1999). Following the agrarian revolution, rapid population expansion then necessitated widespread migration of human hosts and their parasite hijackers (Hume, Lyons et al. 2003).

Malaria reached its global limits around 1900. A total of 140 countries were malarious, ~77% of the population was exposed to the disease and of those affected, 1 in 10 could expect to die (Hay, Guerra et al. 2004). However, at the end of the 19th century, malaria entered a dramatic decline throughout North America and Northern and Western Europe where it is currently non-existent. Today, although control efforts have reduced the area of malaria risk by approximately half (53% to 27% of the Earth's surface), malaria still casts a considerable shadow over the tropics (figure 1.2). It is estimated that ~40% of the world population are now at risk in a total of 107 countries. Each year, 300-500 million people are affected by malaria, 60% of those cases and 80% of associated mortality occurring in Africa alone (World Health Organisation 2005).

1.3.2 Control and treatment

As malaria continued to extend its global reign, humanity began to fight back. In the 1950s, the World Health Organisation endorsed the malaria

eradication programme (Litsios 2002) in an attempt to block transmission over a large geographical area. Although campaigns did successfully reduce the burden of malaria in some parts of the world, global eradication was never achieved and the disease is subsequently re-emerging. However, important lessons have been learnt that can be applied to future control strategies. One key message is that the tools applied in the past were, and remain to be, very effective.

During the eradication era, extensive spraying with the insecticide dichlorodiphenyltrichloroethane (DDT) resulted in a substantial reduction in mosquito populations that helped to eradicate malaria in Southern Europe, Russia and parts of Asia (Guerin, Olliaro et al. 2002). However, control efforts were not so successful in the tropics where breeding is more intense and widespread. This may have been due to inadequate accessibility to health facilities and a gradual increase in insecticide resistance. Preventative efforts have since moved towards the use of bed nets impregnated with pyrethroid insecticides (Guillet, Alnwick et al. 2001; Lengler 2004). Although this strategy has had some success in reducing morbidity and or mortality in China and Africa (Aikins, Fox-Rushby et al. 1998; Utzinger, Tozan et al. 2001), extensive coverage would be needed to obtain more substantial reductions in transmission. Additionally, resistance to the pyrethroids appears to be increasing (Curtis, Miller et al. 1998; Chandre, Darriet et al. 1999), compounding the urgent need to develop new classes of insecticides.

If applied effectively, treatment with antimalarial drugs can prevent progression to severe disease and reduce associated morbidity and mortality (World Health Organisation 1993). The first antimalarial agent identified was quinine, isolated from the bark of the *cinchona* tree in 1820. The efficacy, affordability and low toxicity of the synthetic derivative chloroquine have led to its global use in antimalarial therapy for the last 40 years. However, parasite resistance to chloroquine is now widespread and few countries are unaffected (Bloland, Lackritz et al. 1993). Pyramethamine-sulphodoxine has been deployed as a cheap alternative therapy but resistance has also begun to develop and is spreading rapidly (Ronn, Msangeni et al. 1996). In 1972, an active antimalarial agent was isolated from the Quin Hao herb and named artemisinin. Although somewhat pricier, artemisinin and its derivatives are considered the most potent,

tolerable and rapidly acting of the antimalarial drugs (White 1997). Combination therapy with artemisinin or one of its many derivatives and slowly eliminated drugs such as mefloquine or lumefantrine has been highly effective, even against multidrug-resistant *P. falciparum* (Price, Nosten et al. 1997; van Vugt, Brockman et al. 1998). Although no significant resistance has yet been observed in clinical isolations or laboratory experiments, only time will tell if these new compounds are destined to suffer the same fate as their predecessors.

The development of a malaria vaccine has been the "holy grail" for many research groups since the early 20th century. However, progress has been stunted by a lack of funding as well as an incomplete understanding of the parasite and the immune mechanisms underlying infection (Rogers and Hoffman 1999). As a consequence, there has been a recent shift away from animal models and greater emphasis placed upon clinical trials (Richie and Saul 2002). Vaccines are currently being targeted at different stages of the parasite life-cycle, each having a unique antigenic repertoire (Facer and Tanner 1997). Unfortunately, various problems including extensive polymorphism in antigenic regions of proteins and poor immunogenicity has meant few candidates have progressed to the later stages of vaccine development (Guerin, Olliaro et al. 2002).

1.4 Host-pathogen interplay

1.4.1 Pathogenesis

The clinical manifestations and pathology of malaria are caused primarily by erythrocytic stages of the parasite; hepatic schizogony and gametogenesis are relatively asymptomatic. The early stages of infection are characterised by acute paroxysms that occur at 48 hr (*P. falciparum*, *P. vivax* and *P. ovale*) or 72 hr (*P. malariae*) intervals, coinciding with the rupture of erythrocytes and release of merozoites into the bloodstream (Golgi 1889; Capanno 2006). Detailed symptoms associated with paroxysms are specific to the species of parasite and can include fever, chills, rigor and sweating. The severity of febrile attack is dependent on the synchronisation of parasites within erythrocytes and the level of parasitaemia (Kitchen 1949).

It is well established that malaria-related fever is caused by the release of endogenous pro-inflammatory cytokines, such as tumour necrosis factor α (TNFα) (Kwiatkowski, Cannon et al. 1989; Karunaweera, Grau et al. 1992; Kwiatkowski 1995). It has been suggested that glycosylphosphatidylinositol (GPI) anchor glycolipids are prominent toxins contributing to malarial pathogenesis by activating the pro-inflammatory response (Schofield and Hackett 1993; Tachado, Gerold et al. 1996; Krishnegowda, Hajjar et al. 2005). The physiological significance of this is still unclear at present and other toxic products may exist.

In some circumstances, infection can progress and cause more severe clinical manifestations. A number of different syndromes can be present either alone or in combination including severe anaemia, acidosis and respiratory complications, multi-organ failure and cerebral malaria (World Health Organisation 2000). Severity of disease is influenced by a number of factors including host age, immune status and species of parasite involved. Destruction of parasitised red blood cells (pRBCs) and uninfected erythrocytes as well as marked dyserythropoiesis can lead to severe anaemia in both *P. falciparum* and *P. vivax* infections (Looareesuwan, Ho et al. 1987; Abdalla 1990; Phillips and Pasvol 1992; Mendis, Sina et al. 2001). However, other clinical manifestations of severe malaria that inflict the most morbidity and mortality are caused by *P. falciparum*.

Where *P. vivax* and *P. ovale* are restricted to reticulocytes, *P. falciparum* can invade erythrocytes of all ages, leading to higher levels of parasitaemia (Garnham 1966). Additionally, *P. falciparum* can modify the surface of an occupied erythrocyte, allowing pRBCs to adhere to vascular endothelium. Cytoadherence of pRBCs prevents parasite destruction, as uninfected erythrocytes are cleared by the spleen (Langreth and Peterson 1985). The surface of pRBCs containing either trophozoites or merozoites is covered with knob-like structures (Luse and Miller 1971) comprising *P. falciparum* erythrocyte membrane protein-1 (PfEMP-1), a family of genetically variable proteins. PfEMP-1 mediates the binding of pRBCs to various host receptors, allowing parasites to sequester in different organs of the body (Baruch, Pasloske et al. 1995; Baruch, Gormely et al. 1996; Baruch 1999). Platelet-mediated clumping (Pain, Ferguson et al. 2001) and the binding of pRBCs to uninfected erythrocytes (rosetting) (David, Handunnetti et al. 1988) are both processes that increase the number of cells sequestered in various locations.

It is unclear exactly how cytoadherence leads to severe pathology. Obstruction of blood flow to tissues is likely to be an important factor as well as systemic and local production of inflammatory cytokines (Chen, Schlichtherle et al. 2000).

1.4.2 Immunity

An individual's experience of malaria is correlated with the degree of antimalarial immunity acquired. Immune status is determined by the degree of exposure to infection and age of the host. For *P. falciparum*, it is possible to obtain a degree of immunity to some aspects of severe disease after only one or two infections (Gupta, Snow et al. 1999). However, immunity to other non-life threatening clinical symptoms of malaria and effective antiparasitic immunity require a large number of frequent inoculations (Trape and Rogier 1996; Carter and Mendis 2002). In tropical Africa, where transmission levels are very high, a large percentage of the population will have acquired a strong protective immunity by the age of 4 or 5 (Trape and Rogier 1996; Carter and Mendis 2002).

Very young children appear to have a low capacity to acquire any kind of antimalarial immunity and therefore tend to suffer a greater burden of disease (Baird, Jones et al. 1991; Baird 1995).

Development of effective immunity is a slow process. In addition to genetic variation between different species, there is antigenic diversity within individual species. This is due to polymorphisms in allelic gene products as well as antigenic variation as a result of expression of alternative genes in a particular family. To combat infection, the host must therefore mount a specific response to each distinct parasite inoculum. Effective immunity is only obtained when a sufficient range of parasites have been experienced (Powell, McNamara et al. 1972; Mendis, David et al. 1991).

Ironically, as arduous a task acquiring immunity is to the host, protection is lost again with relative ease. Evidence suggests that without reinfection, a period of six months to a year is sufficient to leave an individual at risk of experiencing the full impact of a malarial infection (Taliaferro 1949).

1.5 Maintenance of an intracellular lifestyle

Plasmodium belongs to the phylum Apicomplexa, one of the largest groups of eukaryotic protozoa containing over 5000 species of parasite. Many of the apicomplexan parasites are responsible for important diseases of humans and animals, contributing to substantial morbidity and mortality in both. Another important and well-studied parasite is *Toxoplasma gondii* (*T. gondii*), the causative agent of toxoplasmosis. Toxoplasmosis can be life-threatening in immuno-compromised individuals and can lead to blindness or cognitive impairment in infected infants. Other members include *Cryptosporidium*, an opportunistic pathogen of humans and animals, *Eimeria* spp., pathogens of chicken and cattle and *Theileria* spp., tick-borne parasites of cattle in Africa.

One important and unifying feature of Apicomplexa is that they are all obligate intracellular parasites, maintenance of this lifestyle being essential for their survival.

1.5.1 Host cell invasion

Host organisms have a number of defence mechanisms to protect against infection. By entering a host cell, a parasite can effectively avoid recognition whilst assuring itself a readily available source of nutrients. Some parasites, including the trypanosomatid *Leishmania* utilise the voracious appetite of phagocytic cells for passive uptake (Chang and Dwyer 1976). However, although uptake is efficient and rapid, phagocytes are hydrolytic, short-lived cells that are not suited to every parasitic lifestyle.

In contrast, non-phagocytic cells offer a much more stable living environment for the parasite that is adept enough to gain entry. Some bacterial pathogens such as *Shigella* and *Salmonella* achieve this by intoxicating their host cells, forcing them to gorge uncontrollably (Francis, Ryan et al. 1993; Galan and Bliska 1996). Apicomplexa have evolved a distinct and unique strategy where parasites actively gain entry to host cells utilising their own protein machinery. It is worth noting that there are some exceptions to the rules: e.g. *T. gondii*, a somewhat promiscuous parasite, is known to routinely invade phagocytic cells.

Not withstanding this, the parasite still uses its own machinery to actively invade these cells (Sibley 1995). Conversely, *Theileria* does not actively invade host cells but instead manipulates their physiology in order to gain entry (Shaw, Tilney et al. 1991; Shaw and Tilney 1995).

1.5.2 Gliding motility

Survival is not as simple as just gaining entry to the host cell in question. Parasites must also be able to exit the cell when reproduction is complete and locate a new cell to infect. In order to achieve all of these goals, many forms of apicomplexan parasites are motile and can migrate extensively within their host organisms. In *Toxoplasma*, tachyzoites initially cross intestinal epithelial cells before disseminating into deep tissues and traversing biological barriers such as the blood-brain barrier and the placenta (Barragan and Sibley 2002). In *Plasmodium,* sporozoites have to journey through the circulation to locate liver cells. Additionally, ookinetes need to traverse the mosquito midgut epithelium in order to complete sporogony.

In order to fulfil their travel requirements, cells demonstrate distinct types of locomotion. One of the most common forms of motility is cell crawling or amoeboid locomotion. Dynamic reorganisations of the actin cytoskeleton give rise to protrusions of the leading edge of cells that extend and attach to new substrates. Retraction of the trailing portion then allows the cell to move forward. Crawling is generally a slow process but rates can range from 0.01 $\mu m\ s^{-1}$ to well over 1 $\mu m\ s^{-1}$ depending on the cell type (Bray 2001). A variety of cells or whole organisms utilise cilia or flagella to propel themselves through an aqueous environment. This type of locomotion is powered by dynein motors located in microtubule-based axonemes (Wemmer and Marshall 2004). Rates of swimming can vary from 10 $\mu m\ s^{-1}$ to over 1 $mm\ s^{-1}$ permitting swimmers to generally outpace crawlers (Bray 2001).

With the exception of microgametocytes, apicomplexan zoites lack cilia or flagella and do not undergo any of the distortions in shape necessary for crawling. Instead they adopt a substrate-dependent locomotion that is known as gliding

motility; gliding being defined as a smooth and continuous movement across a solid surface. Interestingly, gliding behaviour has also been observed in some other eukaryotic cell types, including the raphid diatom *Bacillariophyceae* and colonial protozoan *Labyrinthula* (Reviewed in (Heintzelman 2006)). Close examination suggests there are a number of physical movements associated with gliding motility although precise patterns observed depend on the species and specific stage involved.

In *Toxoplasma* tachyzoites, forward movement appears to be achieved by a combination of both circular and helical gliding. In circular gliding, parasites rotate anti-clockwise yet progress inconsistently at a rate of ~1.5 μm s^{-1}. Progression by helical gliding occurs at rates of ~1-3 μm s^{-1} and invariably involves a 360° clockwise rotation of parasites around their long axis. A third form of gliding known as upward twirling has also been identified. Parasites attach to a substrate by their posterior end and rotate clockwise at a rate of ~0.5 revolutions/second. The role of this third type of motion remains unclear (Hakansson, Morisaki et al. 1999).

Patterns of motility exhibited by *Plasmodium* ookinetes have also been examined. Parasites appear to display three distinct forms of locomotion: stationary rotation as well as two types of translocational motility. Translocational spiralling, akin to helical gliding, has an average speed of ~2.6 μm min^{-1} whereas straight-segment translocation, where ookinetes are elongated and move forward in straight segments, is more rapid (~5 μm min^{-1}) (Vlachou, Zimmermann et al. 2004). Observation of both *Plasmodium* and *Eimeria* sporozoites suggests that these parasites predominantly glide in a clockwise circular motion (Vanderberg 1974; Russell and Sinden 1981).

Despite some differences observed in both rates and patterns of locomotion, these data imply that gliding motility is conserved and representative of the phylum Apicomplexa.

1.6 Apicomplexan zoite morphology

Despite the diverse range of hosts infected and various modes of transmission, the necessity to internalise unifies apicomplexan parasites functionally. As a consequence, their invasive/motile forms share a number of morphological features. Zoites are highly polarised cells containing an elaborate invasive apparatus known as the "apical complex" that comprises a prominent cytoskeleton and specialised regulated secretory organelles (figure 1.3).

1.6.1 The cytoskeleton

The overall shapes and sizes of zoites vary between different species as well as life-cycle stages. *P. falciparum* merozoites are oval-shaped and probably the smallest of all the *Plasmodium* spp., measuring ~1 by 1.6 μm (Aikawa and Seed 1980). In contrast, a number of other stages are larger in size and have an elongated crescent shape of varying proportions, e.g. *P. falciparum* sporozoites measure ~1 by 11 μm (Aikawa and Seed 1980) and *T. gondii* tachyzoites, ~2 by 6 μm (Dubey, Lindsay et al. 1998).

Shape is determined by the number of subpellicular microtubules in the cell, their length and the angles they lie at (reviewed in (Morrissette and Sibley 2002)). The number of subpellicular microtubules ranges from only 3 or 4 in *P. falciparum* merozoites, to ~60 in the larger ookinete. Most apicomplexan parasites have evenly spaced microtubules that terminate near the nucleus at the posterior end of the cell. However, *P. falciparum* merozoites represent a major exception to this spacing rule. Their assembly of microtubules extends solely along one side of the parasite body and they are anchored into a unique microtubule organising centre (MTOC) known as the apical polar ring (Bannister and Mitchell 1995). In some parasites, such as *T. gondii*, the polar ring is enveloped by a cylindrical tubulin structure called the conoid (Hu, Roos et al. 2002). However, in *Plasmodium* zoites there are only 3 polar rings and the microtubule network extends from the distal ring (Bannister and Mitchell 1995).

The microtubules underlie an unusual tri-laminar pellicle that lines the length of the cell body. The pellicle comprises the plasma membrane closely

aligned to an inner membrane complex (IMC) consisting of one or more flattened vesicles fused together in longitudinal rows (Foussard, Gallois et al. 1990; Bannister and Mitchell 1995). The intramembranous space between the plasma membrane and the IMC contains a number of proteins that are essential for both gliding motility and active invasion of host cells (see section 1.8). Interestingly, members of *Plasmodium* spp. appear to have a thick surface coat that overlies their plasma membranes.

Detailed ultrastructural analyses of *P. knowlesi* merozoites established that the coat is comprised of clusters of closely aligned filaments. The majority of these filaments measure ~18-20 nm by 2 nm and have an expanded bifurcal apical tip. However, some filaments can extend to up to ~150 nm and may project outwards or lie flat, parallel to the surface of the parasite (Bannister, Mitchell et al. 1986). Similar observations in a number of other species of *Plasmodium* suggest the coat is morphologically conserved (Galinski and Barnwell 1996). Although the precise composition of the surface coat is still unknown, a number of important cell surface proteins have been identified (see section 1.7.1). The proposed role of the surface coat is in capturing and attaching to erythrocytes prior to invasion.

1.6.2 Apical organelles

Zoites contain sets of specialised secretory vesicles known as the apical organelles, since they are located at the parasite apex. They are membrane-bound structures of varying proportions that contain densely packed granular material. Precise size, shape, number and content are dependent on the species and life-cycle stage. Secretion appears to be sequential (Carruthers and Sibley 1997) and thus, individual organelles are discussed here in their likely order of discharge. The downstream effects of secretion are likely to be complex. Nonetheless, some important molecular components and their proposed roles in host cell invasion are discussed in section 1.7.

Micronemes are relatively small organelles that are often numerous, e.g. in larger zoites such as *Plasmodium* sporozoites or zoites of *Toxoplasma* and

Eimeria that are required to glide extensively (Scholtyseck and Mehlhorn 1970; Aikawa and Seed 1980). Conversely, in *P. falciparum* merozoites, there are relatively few (Langreth, Jensen et al. 1978) and they exist as elongated fusiform sacs ~120 nm long that surround and extend from the ducts of another set of apical organelles; the rhoptries (see below).

Subsequent to primary erythrocyte attachment, micronemes secrete their contents onto the surface of merozoites through the apical prominence, probably through fusion with the rhoptry ducts. Recent evidence suggests that this is a regulated process. Microneme secretion seems to be dependent on the release of Ca^{2+} from intracellular parasite stores (Carruthers and Sibley 1999; Gantt, Persson et al. 2000; Lovett and Sibley 2003). Interestingly, observations made in *P. knowlesi* suggest there may also be partial discharge of micronemes upon merozoite release from erythrocytic schizonts (Bannister and Mitchell 1989). Additionally, *in P. falciparum*, certain components of micronemes such as apical membrane antigen 1 (AMA-1) (see section 1.7.3), have been shown to translocate to the surface of merozoites before or during egress from the erythrocytes (Healer, Crawford et al. 2002; Mitchell, Thomas et al. 2004). Therefore, subsets of micronemes may exist that are discharged at different times before and during invasion of host cells.

Rhoptries are the largest of the organelles and are generally pear-shaped. In *P. falciparum* they measure ~550 by 250 nm, whereas in larger zoites of *T. gondii* they are more elongated, measuring up to ~2 μm (Nichols, Chiappino et al. 1983; Bannister, Hopkins et al. 2000). They are most commonly found in pairs, as seen in the *Plasmodium* merozoite. However, *T. gondii* zoites can contain 8 or more rhoptries and *Cryptosporidium* sporozoites appear to have just the one (Tetley, Brown et al. 1998). Rhoptries consist of a basal bulb region and a ductal portion at the apex, each with a distinct structure and unique composition (Bannister, Hopkins et al. 2000). Following erythrocytic attachment, the rhoptry ducts initially fuse with each other as well as the parasite plasma membrane. They then discharge their contents through the apical prominence and collapse, dramatically changing in appearance (Aikawa, Miller et al. 1978; Carruthers and Sibley 1997).

Dense granules are the least well classified organelle as they can sometimes be mistaken for either the rhoptries or micronemes. For this reason, there is still some confusion regarding their identity in some genera, including *Plasmodium*. In *P. knowlesi* and *P. falciparum* merozoites, they appear to be spheroidal vesicles with a diameter of ~80 nm that lie in the cytoplasmic space of the apical region. For secretion, dense granules migrate to various points along the parasite surface, breach the pellicular membranes and release their contents into the PV via exocytosis (Bannister and Mitchell 1989; Aikawa, Torii et al. 1990; Culvenor, Day et al. 1991). Similar events have been observed in both *Toxoplasma* (Leriche and Dubremetz 1990) and *Sarcocystis* (Entzeroth 1985).

Secretion from dense granules appears to respond to signals of both a regulated (Dubremetz, Achbarou et al. 1993; Carruthers and Sibley 1997) and constitutive secretion pathway (Chaturvedi, Qi et al. 1999; Liendo, Stedman et al. 2001), implying different populations may exist. Very recent evidence in *P. falciparum* has shown that dense granules are more heterogenic than previously recognised (Yeoh, O'Donnell et al. 2007). Their protein content and function appears to be sufficiently distinct that a new organelle has been defined; the exoneme. As exonemes were found to contain specific proteases required for schizont rupture, this work provides clear evidence that subsets of dense granules have a specific role in merozoite exit from erythrocytes.

Interestingly, another novel secretory organelle has recently been identified in *P. falciparum* called the mononeme (Singh, Plassmeyer et al. 2007). The mononeme appears to be a thread-like structure located on one side of the merozoite, in close proximity to the sub-pellicular microtubules. A rhomboid protease, ROM1, involved in the transmembrane cleavage of specific merozoite surface proteins during invasion (see section 1.7.3), is contained within the mononeme. As one of the targets of ROM1 is micronemal protein AMA-1, this compartmentalisation is likely to provide the parasite with a mechanism of keeping the two proteins separate until their association is necessary.

1.7 Erythrocytic invasion by *Plasmodium* spp.

While some apicomplexan zoites invade many different cell types, merozoites of *Plasmodium* spp. are highly specific in their choice of cellular niche. They are exquisitely adapted for the successful identification and invasion of erythrocytes. However, unlike sporozoites or ookinetes, merozoites do not appear to be motile. Gliding across inert substrates has not been observed *in vitro* (Mitchell and Bannister 1988) but it is unclear how merozoites behave in the confines of the host bloodstream. Recent insights into erythrocyte exit suggest that propulsion of merozoites from ruptured schizonts may be sufficient to bring them into contact with neighbouring erythrocytes (Rayner 2006). Thus, active motility may not be a prerequisite for the lifestyle of these zoites.

The small size and extracellular instability of *Plasmodium* merozoites (Johnson, Epstein et al. 1980) has somewhat hindered the biochemical characterisation of invasion. Therefore, a large proportion of our current knowledge has been obtained from more tractable life-cycle stages such as *Plasmodium* sporozoites or in other genera, in particular *T. gondii*. A detailed depiction of the various stages of erythrocytic invasion is shown in figure 1.4.

1.7.1 Initial attachment

Merozoites must first be able to distinguish between erythrocytes and other blood cell types unsuitable for invasion. Primary adherence and recognition appears to be reversible and of low affinity (Bannister and Dluzewski 1990). Erythrocytes are captured by the proteinaceous coat of merozoites and thus, contact can occur at any point on the parasite surface.

GPI-anchored membrane proteins constitute a large proportion of the merozoite surface and several have been identified in *P. falciparum*. Their localisation is not always evenly spread across the surface, e.g. merozoite surface protein (MSP)-10 (Black, Wang et al. 2003) and Pf38 (Sanders, Gilson et al. 2005) also appear to be apical. Some of the GPI-anchored proteins have cysteine-rich domains that may be important in adherence. MSP-1 (Holder and Freeman 1981), MSP-4 (Marshall, Silva et al. 1997), MSP-5 (Marshall, Tieqiao et al. 1998) and

MSP-10 contain single or double epidermal growth factor (EGF)-like domains at the C terminus. The most abundant of these, MSP-1, is a large ~200 kDa protein that is cleaved during invasion leaving only the C-terminal 19 kDa fragment, $MSP\text{-}1_{19}$ (Blackman, Heidrich et al. 1990). This EGF-like domain has been shown to be an important target of antibodies that protect against invasion and recombinant proteins incorporating this region are leading vaccine candidates (Hirunpetcharat, Tian et al. 1997; O'Donnell, de Koning-Ward et al. 2001; Stowers, Cioce et al. 2001). However, the precise function of this domain is still unclear. Although binding to erythrocyte receptor band 3 has been suggested (Goel, Li et al. 2003; Li, Chen et al. 2004; Kariuki, Li et al. 2005), it seems the domain can be drastically altered without affecting the ability of merozoites to invade (Drew, O'Donnell et al. 2004).

Another two surface proteins, Pf12 and Pf38 contain "6-cys" modules (Sanders, Gilson et al. 2005; Gilson, Nebl et al. 2006). Additional proteins containing these domains have been identified on the surface of both *Plasmodium* gametes (van Dijk, Janse et al. 2001) as well as sporozoites (Ishino, Chinzei et al. 2005) and are thought to have roles in adhesion. Furthermore, the 6-cys family appear to have a surface antigen related sequence (SRS)-type fold, present in adhesive surface antigens of *T. gondii*. Interestingly, another member of the MSP family, MSP-2 (Smythe, Coppel et al. 1988), is an intrinsically unstructured protein with a partially structured core shown to form amyloid-like fibrils (Yang, Adda et al. 2007). Consequently, it may be that this protein is an important structural component of the merozoite surface coat.

Peripheral membrane proteins also exist on the surface of merozoites and have potential roles in erythrocytic adhesion. These proteins are secreted into the PV during schizogony and are thought to associate with the parasite surface via non-covalent interaction with a GPI-anchored membrane protein (Trucco, Fernandez-Reyes et al. 2001; Sanders, Gilson et al. 2005; Pachebat, Kadekoppala et al. 2007). In *P. falciparum*, the peripheral membrane proteins include the MSP3/6 (McColl and Anders 1997; Trucco, Fernandez-Reyes et al. 2001; Pearce, Mills et al. 2005) MSP-7 (Stafford, Stockley et al. 1996) and serine repeat antigen (SERA) (Miller, Good et al. 2002; McCoubrie, Miller et al. 2007) families as well

as acidic basic repeat antigen (ABRA)/MSP-9 (Stahl, Bianco et al. 1986), S-antigen (Cowman, Saint et al. 1985) and another member of the 6-cys family, Pf41 (Sanders, Gilson et al. 2005). Members of the MSP-7 family and Pf41 appear to have a strong interaction with the merozoite surface whereas others, including the MSP-3/6 family proteins, are more weakly associated (Sanders, Gilson et al. 2005).

Owing to their low affinity associations with erythrocytes, it remains to be determined which of the integral and peripheral proteins are important in establishing primary contact. It may be that the contribution of several low-affinity interactions involving a number of surface proteins is sufficient for initial attachment.

1.7.2 Re-orientation and apical attachment

Merozoites penetrate erythrocytes exclusively from their apex. Therefore, after initial contact has been established, parasites must re-orientate themselves and establish a firm connection between their apex and the erythrocyte surface. A number of proteins have been implicated in these high-affinity interactions.

The Duffy binding-like (DBL) proteins are micronemal proteins that share homology with the Duffy binding protein identified in *P. vivax* (Wertheimer and Barnwell 1989). In *P. falciparum*, they include erythrocyte binding antigen (EBA)-175 (Camus and Hadley 1985), EBA-140/BAEBL (Mayer, Kaneko et al. 2001) and EBA-181/JESEBL (Gilberger, Thompson et al. 2003). The cysteine-rich DBL domains interact with erythrocyte glycophorins A, C and unknown receptor E respectively. These interactions are dependent on sialic acid present in the receptor; treatment of erythrocytes with neuraminidase will ablate binding by removal of sialic acid.

The reticulocyte-binding protein homologues (Rh or RBL family) are located in rhoptry necks and are homologues of reticulocyte-binding proteins identified in *P yoelii* (Holder and Freeman 1981; Ogun and Holder 1996). PfRh1 interacts with putative glycosylated erythrocytic receptor Y in a sialic-acid dependent manner (Rayner, Vargas-Serrato et al. 2001; Triglia, Duraisingh et al.

2005). The PfRh2b and PfRh4 interactions are sialic-acid independent, the former utilising unknown receptor Z (Rayner, Galinski et al. 2000; Kaneko, Mu et al. 2002; Baum, Maier et al. 2005) whereas no association has yet been observed for PfRh2a (Duraisingh, Triglia et al. 2003).

Although having potentially important roles in determining host cell specificity, individual DBLs and Rhs do not appear to be essential. Moreover, the multitude of ligands appears to provide merozoites with a number of different pathways they can utilise to enter erythrocytes. Differential expression of PfRh proteins as well as the ability to switch between EBL and Rh/RBL pathways may be important in maintaining phenotypic variation (Duraisingh, Triglia et al. 2003; Stubbs, Simpson et al. 2005). Successful invasion is dependent on sufficient interactions between merozoites and erythrocytes. Specific erythrocytic ligands can be extensively polymorphic across the human population and surface abundance may vary (Miller, Baruch et al. 2002). Additionally, the host immune system could potentially block certain invasion pathways. Therefore, multiple invasion pathways may be important for the survival and fitness of the parasite.

Other micronemal proteins also appear to have important roles in both apical attachment and/or re-orientation. The thrombospondin-related anonymous protein (TRAP) family are a group of type I transmembrane proteins that contain adhesive integrin A-like domains (A domains) and/or thrombospondin type I repeats (TSRs). Members of the TRAP family have been identified in *Plasmodium* sporozoites (circumsporozoite protein (CS) and TRAP) (Menard, Sultan et al. 1997; Sultan, Thathy et al. 1997) as well as ookinetes (circumsporozoite- and TRAP-related protein, CTRP) (Yuda, Sawai et al. 1999) and merozoites (merozoite TRAP homologue, MTRAP and *Plasmodium* thrombospondin-related apical merozoite protein, PTRAMP) (Thompson, Cooke et al. 2004; Baum, Richard et al. 2006). A TRAP homologue known as microneme protein (MIC)2 is also expressed in *T. gondii* (Carruthers, Giddings et al. 1999). Both TRAP and MIC2 have been shown to bind some host surface molecules and extracellular matrix components including erythrocyte glycosaminoglycans (Müller, Reckmann et al. 1993; Robson, Frevert et al. 1995; McCormick, Tuckwell et al. 1999; Harper, Hoff et al. 2004). As yet, there is no

evidence that either MTRAP or PTRAMP bind erythrocytes. Although this does not rule out the possibility of a direct interaction, it may be that these proteins bind erythrocytes indirectly via association with another parasite protein.

AMA-1 is a type I integral membrane protein that is highly conserved across Apicomplexa and has been shown to be essential for invasion in *P. falciparum* (Triglia, Healer et al. 2000) and *T. gondii* (Mital, Meissner et al. 2005). Parts of the N-terminal ectodomain resemble PAN modules, domains known to be important in protein-protein and protein-carbohydrate interactions (Pizarro, Vulliez-Le Normand et al. 2005). *In vitro*, AMA-1 has been shown to bind erythrocytes in both *P. yoelii* (Fraser, Kappe et al. 2001) and *P. falciparum* (Kato, Mayer et al. 2005) and thus, these domains may be significant in this interaction. Although the precise role of AMA-1 in invasion is still unclear, evidence from *T. gondii* and *P. knowlesi* (Mitchell, Thomas et al. 2004) suggest it is not involved in initial attachment but is important in both re-orientation and apical attachment.

1.7.3 The moving junction and cell penetration

Subsequent to apical attachment, merozoites form an even more intimate contact called the moving junction (MJ) (Aikawa, Miller et al. 1978). Until recently, only one cytosolic protein, merozoite capping protein (MCP)-1 of *P. falciparum*, had been shown to have association with the MJ (Klotz, Hadley et al. 1989). Recent observations in *T. gondii* suggest that AMA-1 is located at the MJ in association with at least three other rhoptry neck (RON) proteins; RON2, RON4 and Ts4705 (RON5) (Alexander, Mital et al. 2005; Lebrun, Michelin et al. 2005). AMA-1 and RON4 co-localise at the moving junction but precise locations of the other two proteins are still unclear. The specific role of individual proteins in this complex is unknown but it appears AMA-1 is essential. When AMA-1 is not expressed, RON4 is still secreted at the apex but cannot form an organised MJ. Two additional rhoptry neck proteins, RON1 and RON3 have also been identified in *T. gondii* (Bradley, Ward et al. 2005) and homologues of TgRON1-4 have been isolated in *P. falciparum* (Alexander, Arastu-Kapur et al. 2006). Further analyses

should help determine which of these proteins constitute the MJ and identify their function.

As invasion ensues, the MJ moves from the anterior to the posterior end forming the border of the developing PV. Evidence from *T. gondii* suggests that the MJ acts as a molecular sieve, selectively excluding host and parasite proteins on the basis of their membrane association. GPI-anchored proteins and some AMA-1 appear to pass through the junction whereas other transmembrane adhesins are refused entry (Mordue, Desai et al. 1999; Charron and Sibley 2004).

As the MJ migrates, there appears to be a concomitant "shaving" of the surface coat (Bannister, Butcher et al. 1975; Aikawa, Miller et al. 1978). The ectodomains of several transmembrane adhesins are shed during invasion, a process that appears to be essential for invasion (Conseil, Soête et al. 1999; Carruthers and Blackman 2005). Proteolytic shedding may provide a means of disengaging contact with erythrocytes, thereby facilitating host cell penetration and allowing parasites to separate from the moving junction once invasion is complete.

In *P. falciparum*, two classes of subtilisin-like proteases (SUBs) have been identified. SUB-2 (Barale, Blisnick et al. 1999; Hackett, Sajid et al. 1999) is a micronemal integral membrane protein that translocates across the merozoite surface and appears to mediate juxtamembrane cleavage of MSP-1, AMA-1 (Howell, Well et al. 2003; Harris, Yeoh et al. 2005) and PTRAMP (Green, Hinds et al. 2006). In contrast, SUB-1 is located in exonemes and is released onto the parasite surface in a soluble, truncated form (Blackman, Fujioka et al. 1998; Yeoh, O'Donnell et al. 2007). SUB-1 is involved in the processing of SERA5, required for efficient release of merozoites from erythrocytes (Yeoh, O'Donnell et al. 2007; Arastu-Kapur, Ponder et al. 2008). It is unknown whether there are additional substrates or whether this protease plays a role in shedding of the surface coat.

A number of transmembrane adhesins are cleaved within their transmembrane domains by a class of polytopic membrane serine proteases called rhomboids. PfROM1 is located in the mononeme and has been shown to cleave AMA-1 (Baker, Wijetilaka et al. 2006). In contrast, PfROM4 is distributed at the merozoite surface and mediates cleavage of EBL and Rh/RBL proteins as well as

members of the TRAP family, with the exception of PTRAMP (Baker, Wijetilaka et al. 2006; O'Donnell, Hackett et al. 2006).

As merozoites penetrate erythrocytes, the host plasma membrane invaginates and develops into the PVM that ultimately encapsulates the parasite within the cell. Although a considerable fraction of the PVM appears to be derived from host cell components (Ward, Miller et al. 1993), PV biogenesis seems to involve a complex parasite-derived reorganisation of host and parasite material. Rhoptries contain internal membranous structures comprised of protein and lipid components. Early observations showed that these are discharged and incorporated into the developing PVM as merozoites penetrate erythrocytes (Bannister, Mitchell et al. 1986; Sam-Yellowe, Shio et al. 1988). Although still quite poorly characterised, a number of rhoptry proteins have been identified in *Plasmodium* that appear to have potential roles in the development of the PV.

Penetration of erythrocytes appears to coincide with a localised reorganisation of the spectrin-actin network (Aikawa, Miller et al. 1981). A protein with some characteristics of spectrin, repetitive organellar protein (ROPE), has been identified in *P. chabaudi* and may be important in rearranging the host cell cytoskeleton (Werner, Taylor et al. 1998).

A number of other rhoptry bulb proteins appear to be transferred to the PV during invasion and/or bind erythrocytes. These include the high molecular mass rhoptry complex (RhopH)1, 2 and 3 (Campbell, Miller et al. 1984; Holder, Freeman et al. 1985; Doury, Bonnefoy et al. 1994; Ling, Florens et al. 2004), rhoptry-associated membrane antigen (RAMA) (Topolska, Lidgett et al. 2004) and stomatin (Hiller, Akompong et al. 2003). Observations in *P. falciparum* suggest that stomatin and RhopH2 reside and are transferred to the PVM in detergent-resistant membrane rafts (DRMs) (Hiller, Akompong et al. 2003). Thus, the PVM appears to be enriched in both erythrocyte and parasite-derived DRMs. The precise role of these microdomains is unclear although their disruption in erythrocytes has been shown to block infection (Samuel, Mohandas et al. 2001).

Once the PV is formed, the dense granules are discharged. One of their protein components, ring membrane antigen (RIMA) is transported to the ring plasma membrane (Trager, Rozario et al. 1992). Its disappearance during

subsequent growth stages suggests it may be important in maintenance of the PV after invasion.

1.8 The glideosome

Early observations in a number of apicomplexan parasites have shown that zoites can translocate molecules that bind to their surface at a similar speed to their forward locomotion (Dubremetz and Ferreira 1978; King 1981; King 1988). In *Plasmodium* sporozoites, gliding has been shown to associate with posterior deposition of its predominant surface protein, CS (Stewart and Vanderberg 1991). Similar trails of specific surface proteins and lipids appear to delineate gliding patterns in a number of apicomplexan zoites (Arrowood, Sterling et al. 1991; Dobrowolski and Sibley 1996).

These observations have led to the proposal of a capping model for both gliding motility and invasion (King 1988). In this model, parasite derived-ligands are released and their interaction with either a solid substrate or host cell receptors leads to forward movement or cell penetration respectively.

1.8.1 Apicomplexan actin

Actin is a highly conserved cytosolic protein that constitutes a large proportion of the cytoskeleton in a wide range of eukaryotic cells. It has a number of important roles including determining cell shape, driving motility and powering muscle contraction in mammalian cells. There are two forms of actin present in cells, monomeric G-actin and filamentous F-actin. Polymerisation of G-actin and depolymerisation of F-actin occurs at the barbed (plus) and pointed (minus) ends respectively, giving rise to polarised helical filaments (Pollard and Borisy 2003).

A number of experiments using cytochalasins (toxins that prevent the polymerisation of G-actin) have established the essential role of apicomplexan parasite actin networks in both gliding motility and invasion (Russell and Sinden 1981; Dobrowolski and Sibley 1996).

Apicomplexan actins appear to be highly divergent, sharing only 73-83% homology with other eukaryotic actins that are usually more than 90% homologous (Wesseling, Smits et al. 1988). Whereas most apicomplexan parasites have a single gene coding for actin, *Plasmodium* have two genes, *Pf-actin I* and *Pf-actin II* (Baum, Papenfuss et al. 2006). Actin-I is the asexual blood-stage

protein whereas actin II is predominantly expressed in the sexual stages (Wesseling, Snijders et al. 1989). Observations in a number of species show that blood-stage actin is expressed at the cell cortex with some concentration at the apex (Webb, Fowler et al. 1996; Dobrowolski, Niesman et al. 1997; Forney, Vaughan et al. 1998). However, precise architecture has been difficult to establish as actin filaments cannot be observed using electron microscopy (EM) under standard conditions (Bannister and Mitchell 1995; Shaw and Tilney 1995). Evidence from both *T. gondii* (Sahoo, Beatty et al. 2006) and *P. falciparum* (Field, Pinder et al. 1993) suggests that parasites contain ~8-10 μM cytosolic actin. Despite this, the majority of the protein appears to be in its monomeric form.

Recently, it has been shown that both *T. gondii* (Sahoo, Beatty et al. 2006) and *P. falciparum* (Schmitz, Grainger et al. 2005) actin can polymerise to form very short filaments. Interestingly, the critical concentrations of G-actin at each end of the filament were shown to be 3-4 times lower than those of other vertebrate and yeast (varies from 0.1 to 0.6 μM at the barbed and pointed ends respectively) (Pollard and Borisy 2003; Sahoo, Beatty et al. 2006; Pollard 2007). The low abundance of F-actin present within parasites is therefore surprising and the exact basis of this phenomenon remains elusive. However, it does suggest that regulation of actin filament assembly is tightly controlled *in vivo.*

When *P. falciparum* and *T. gondii* parasites are treated with the actin-filament-stabilising drug jasplakinolide (JAS), instead of forming parallel organised sets of actin filaments, densely-packed bundles form that appear to be arranged in random orientations (Shaw and Tilney 1999; Mizuno, Makioka et al. 2002; Wetzel, Hakansson et al. 2003). Although treated parasites are still motile, they change direction frequently and are unable to invade, suggesting that both polarity and rapid turnover of filaments is essential.

A number of actin-binding proteins and actin-regulatory proteins have been identified in apicomplexan parasites that may contribute to the organisation of actin networks (Baum, Papenfuss et al. 2006). Monomer binding proteins such as profilin, cofilin and cyclase-associated protein (CAP) are likely to play a key role in promoting the sequestration of G-actin. In a system where such proteins

are likely to prevent spontaneous polymerisation, factors stimulating the formation of F-actin may be essential for motor engagement.

Many protein families that are considered key actin regulators in yeast and higher eukaryotes are absent in Apicomplexa, and where orthologs do exist they often display prominent heterologies (Gordon and Sibley 2005). Notably absent are the severing protein gelsolin, cross-linking proteins such as fimbrin or α-actinin and the Arp2/3 complex, an actin nucleator and branching protein widely conserved across eukaryotes (Pollard 2007). However, some proteins have been identified in *P. falciparum* that may promote polymerisation or stabilise F-actin filaments *in vivo*. Formin1 is expressed in merozoites and follows the moving tight junction between the invading parasite and the host cell. *In vitro*, formin1 was found to be a potent nucleator, implicating its potential important role in the polymerisation of actin during invasion (Baum, Tonkin et al. 2008). A gene coding for F-actin binding, bundling protein coronin has also been identified and shown to associate with F-actin in the parasite (Tardieux, Liu et al. 1998). It is possible that other regulators do exist but perhaps their divergent sequences have so far made them difficult to identify.

1.8.2 Apicomplexan myosin

Shortly after actin was identified as an essential component in gliding and invasion, the collaborative role of parasite myosin was established using the adenosine triphosphate (ATP)-ase inhibitor 2,3-butanedione monoxime (BDM) (Dobrowolski, Carruthers et al. 1997; Pinder, Fowler et al. 1998; Matuschewski, Mota et al. 2001).

Myosins are molecular motors utilised by many eukaryotes for various processes including mitosis, organellar transport, cell locomotion and muscle contraction. Myosin heavy chains commonly comprise three domains. Highly conserved head domains bind actin as well as ATP and are responsible for generating movement. The neck domain acts as a mechanical lever arm for the motor. Calmodulin family light chains that bind in this region can regulate motor activity by means of their calcium-binding motifs, EF-hands (Mooseker MS and

Cheney 1995; Lewit-Bentley and Rety 2000). Tail domains are generally more variable and are important in determining cell localisation as well as cargo specificity.

It is thought that all myosins work by a similar molecular mechanism: cyclical interactions between the myosin head and an actin filament are coupled to the breakdown of ATP causing force and movement to be generated. The current model for force generation is that myosin binds to filamentous actin with the products of ATP hydrolysis (adenosine diphosphate (ADP) and phosphate) bound in its catalytic site. Then, as the products are sequentially released (phosphate first, then ADP), myosin changes conformation to produce a translational movement or "working-stroke". After the products have been released the catalytic site is vacant and myosin forms a tightly-bound "rigor" complex with actin. Binding of a new ATP molecule to myosin causes the rigor complex to dissociate and subsequent ATP hydrolysis resets the original myosin conformation so that the cycle can be repeated.

Myosins are a diverse superfamily; the most recent phylogenic sequence analyses suggest there are at least 24 different classes (Foth, Goedecke et al. 2006). Apicomplexan parasites appear to possess a limited array of myosins, many of which belong to a distinct class (XIV) that also encompasses some closely related ciliate myosins. Current evidence suggests that members of *Plasmodium* spp. have six genes coding for myosins, all of which are expressed (not always exclusively) in the blood stages and may contribute to different biological processes (Chaparro-Olaya, Margos et al. 2005). Current evidence suggests that Myosin (Myo)A (Pinder, Fowler et al. 1998), MyoB and MyoE (Chaparro-Olaya et al, 2005) are all class XIV myosins, MyoD (Hettmann, Herm-Gotz et al. 2000) and MyoF (Chaparro-Olaya, Margos et al. 2005) form part of an extended class VI and MyoC (Hettmann, Herm-Gotz et al. 2000) is a member of newly categorised class XXII (Foth, Goedecke et al. 2006). It should be noted that PfMyoC, D and F are not homologues of other apicomplexan myosins that have been designated with the same letters (Foth, Goedecke et al. 2006).

MyoA was the first apicomplexan myosin to be identified (Heintzelman and Schwartzman 1997; Pinder, Fowler et al. 1998). Conditional knockouts have

been generated in *T. gondii* and demonstrated that in its absence, gliding and invasion are both inhibited (Meissner, Schluter et al. 2002). MyoA is highly conserved across Apicomplexa and homologues have been identified in various parasite stages (Pinder, Fowler et al. 1998; Margos, Siden-Kiamos et al. 2000; Lew, Dluzewski et al. 2002). Like a number of other class XIV members, MyoA is an unconventional myosin. It appears to lack consensus IQ motifs (IQXXXRGXXXRK) that would normally bind light chains and does not follow the TEDS rule, i.e. position 16 upstream of a conserved DALAK sequence is either negatively charged or able to be phosphorylated (Bement and Mooseker 1995). Furthermore, it is unusually small (~91-93 kDa); the neck and tail domains are extremely short and not easily defined (Heintzelman and Schwartzman 1997). Despite these differences, studies in both *T. gondii* (Herm-Gotz, Weiss et al. 2002) and *P. falciparum* (Green, Martin et al. 2006) have shown that MyoA is a fast, plus-end directed, single-headed motor that can move actin at ~3.52-5.2 μm s^{-1}, rates that are suitable for its participation in gliding and invasion.

In both *T. gondii* (Heintzelman and Schwartzman 1999; Hettmann, Herm-Gotz et al. 2000) and *Plasmodium* (Pinder, Fowler et al. 1998; Margos, Siden-Kiamos et al. 2000; Matuschewski, Mota et al. 2001), MyoA is expressed at the periphery of all actively invading zoites. Early biochemical and immunoEM studies showed that it is tightly associated with pellicular membranes but could not firmly establish a plasma membrane or IMC localisation (Pinder, Fowler et al. 1998; Heintzelman and Schwartzman 1999). However, transfection of *T. gondii* with deletion constructs of MyoA demonstrated that the tail domain was critical for membrane localisation (Hettmann, Herm-Gotz et al. 2000).

More recently, TgMyoA was found to co-purify with a protein designated myosin light chain 1 (MLC1) (Herm-Gotz, Weiss et al. 2002). Homologues have since been identified in *Plasmodium* sporozoites (Bergman, Kaiser et al. 2003) as well as merozoites (Baum, Richard et al. 2006; Green, Martin et al. 2006; Jones, Kitson et al. 2006) and designated myosin tail-domain interacting proteins (MTIPs).

Studies in *Plasmodium* sporozoites convincingly demonstrated that MTIP, and thus MyoA, is located at the outer face of the IMC, not the plasma membrane

(Bergman, Kaiser et al. 2003). Although biochemical and structural analyses in *P. falciparum* have shown that MTIP binds the MyoA tail domain (Bosch, Turley et al. 2006; Green, Martin et al. 2006; Bosch, Turley et al. 2007), it appears to be only distantly related to calmodulin and other well-characterised light chains. It is proposed to contain at least one EF-hand domain (Herm-Gotz, Weiss et al. 2002; Bergman, Kaiser et al. 2003), although a critical residue needed for coordination of Ca^{2+} ions is missing and its binding to MyoA appears to be calcium-independent (Linse and Forsén 1995; Green, Martin et al. 2006).

As a number of other apicomplexan myosins are not yet fully characterised, their precise roles within parasites are unknown. However, evidence suggests that PfMyoB may also be involved in invasion as it is also expressed only in mature trophozoites and schizonts (Chaparro-Olaya, Dluzewski et al. 2003). Additionally, a myosin with similar properties to MyoA (MyoD) has been identified in *T. gondii* and *Eimeria Tenella* that may also have potential roles in motility and invasion (Hettmann, Herm-Gotz et al. 2000; Herm-Gotz, Weiss et al. 2002).

1.8.3 Intra-extracellular anchorage

For the acto-myosin motor to generate force required for gliding and invasion, it must be both rigidly anchored in the cell and associate with plasma membrane components that can attach external substrates. The sequences of MTIPs contain no potential transmembrane domains or consensus sites that might give rise to lipid-based membrane attachment, therefore IMC attachment is probably dependent on one or more accessory proteins.

Two candidates, 45 kDa and 50 kDa gliding-associated proteins (GAP45 and GAP50) have recently been identified. Evidence from both *T. gondii* (Gaskins, Gilk et al. 2004) and *P. falciparum* (Baum, Richard et al. 2006; Jones, Kitson et al. 2006) elucidated that GAPs are expressed and located at the periphery of merozoites, forming part of a tetrameric complex with both MLC1/MTIP and MyoA. This tetrameric complex in association with actin is known as the acto-myosin motor complex. GAP50 is proposed to act as a transmembrane receptor for the motor complex but the precise function of GAP45 is unknown. How the

individual components are associated with each other and held stationary within the IMC is also unclear, although connection to microtubules (Nichols and Chiappino 1987; Morrissette, Murray et al. 1997) or subpellicular filaments (Mann and Beckers 2001) is possible.

Association of the acto-myosin complex with specific parasite adhesins appears to provide the surface attachment necessary for successful gliding and invasion. Disruption of the TRAP gene in *Plasmodium* sporozoites has been shown to abolish their ability to glide and inhibits invasion of both the mosquito salivary gland and the vertebrate liver (Sultan, Thathy et al. 1997; Matuschewski, Nunes et al. 2002). Similar effects have been observed upon disruption of homologues expressed in *Plasmodium* ookinetes (Yuda, Sawai et al. 1999) and in *T. gondii* (Huynh, Rabenau et al. 2003; Huynh, Opitz et al. 2004).

The importance of the cytoplasmic tail domain of TRAP was established when its deletion gave rise to sporozoites with reduced invasive potential and whose gliding was non-productive. The function of this domain appears to be conserved as its substitution in TRAP with the tail of TgMIC2 restores both motility and invasion (Kappe, Bruderer et al. 1999). Evidence that the surface translocation of TgMIC2 is sensitive to cytochalasins implicated these adhesins in providing links to the motor system (Carruthers, Giddings et al. 1999; Carruthers and Sibley 1999; Jewett and Sibley 2003).

The tetrameric glycolytic enzyme aldolase has been shown to bind actin in mammalian cells, having effects on either cell contraction or motility (O'Reilly and Clarke 1993; Wang, Morris et al. 1996). Recently, it has been shown that the cytoplasmic tail domains of TgMIC2 (Jewett and Sibley, 2003) TRAP (Buscaglia, Coppens et al. 2003) and MTRAP (Baum, Richard et al. 2006; Bosch, Buscaglia et al. 2007) interact with aldolase. Deletion of the tail domains or mutation of specific residues abolishes binding and leads to impairment of both gliding and invasion. At present, it is unknown whether additional cell surface adhesins may also participate in association with the motor complex.

Although subject to change, the identification of a molecular machine or "glideosome" comprising a number of protein components has provided a

working model for how the diverse range of apicomplexan parasites penetrate and traverse their host cells (figure 1.5).

1.9 Aims of research

The extracellular environment is a dangerous place for apicomplexan parasites. Members of *Plasmodium* spp. express a diverse array of surface ligands in order to evade the host immune system and counteract the polymorphic nature of erythrocytes within a population. Surface adhesins also show extensive variation across the genera and probably account for the range of different host organisms and tissues utilised. Consequently, efforts at developing effective vaccines against a number of these ligands have so far been unsuccessful.

In contrast, the intracellular environment is under far less selective pressure. The components of the acto-myosin complex are all well conserved across the genera, highlighting their important role in both gliding motility and host cell invasion. Given that these functions are essential for parasite survival, it is plausible that these proteins may constitute effective targets for the design of novel anti-malarial drugs.

The nearly complete genome sequencing of the 3D7 clone of *P. falciparum* has provided a formidable tool for identifying and characterising a number of parasite genes and proteins. When this project began, the GAPs had not yet been characterised in *P. falciparum*. The primary aim was therefore to establish a conserved role for these proteins in host cell invasion. To expand on this, other research goals were to examine their structure, identify their interactions with other motor components and elucidate specific functions within the complex and/or in regulation of the motor during invasion.

Figure 1.1

Life-cycle of *P. falciparum*

Depicted here are the main phases of *P. falciparum* infection that occur in the liver and erythrocytes of the human host as well as the salivary glands of the mosquito (Bannister and Mitchell 2003). See section 1.2 for a full description of the life-cycle.

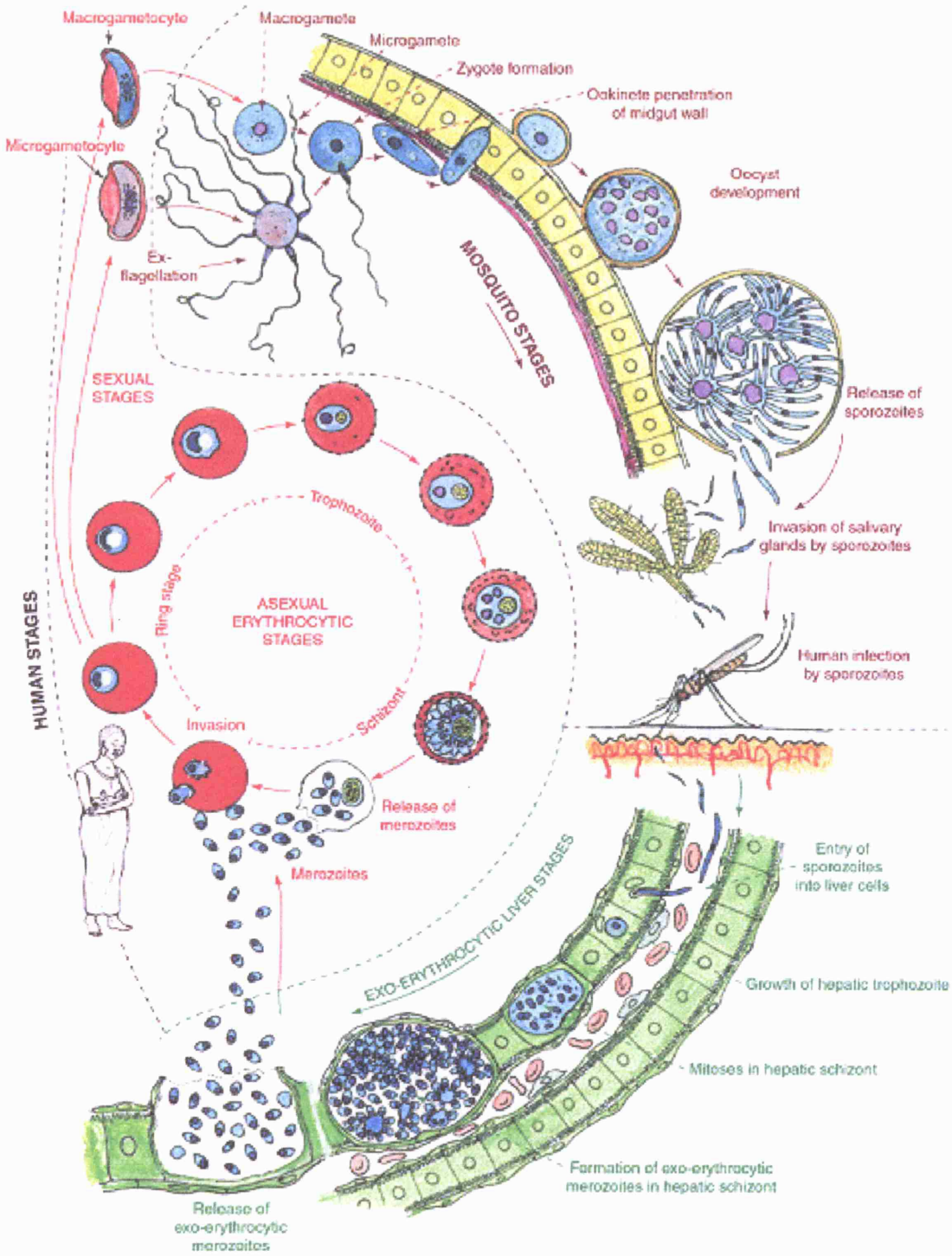
Macrogametocyte
Macrogamete
Microgamete
Zygote formation
Ookinete penetration of midgut wall
Microgametocyte
Oocyst development
Ex-flagellation
MOSQUITO STAGES
SEXUAL STAGES
Release of sporozoites
Trophozoite
Invasion of salivary glands by sporozoites
Ring stage
ASEXUAL ERYTHROCYTIC STAGES
HUMAN STAGES
Human infection by sporozoites
Schizont
Invasion
Release of merozoites
Merozoites
Entry of sporozoites into liver cells
EXO-ERYTHROCYTIC LIVER STAGES
Growth of hepatic trophozoite
Mitoses in hepatic schizont
Formation of exo-erythrocytic merozoites in hepatic schizont
Release of exo-erythrocytic merozoites

Figure 1.2

Global distribution of malaria

Overlaid all-cause malaria distribution maps from pre-intervention (circa 1900) to 2002. Low and high risk regions were merged in individual maps (Hay, Guerra et al. 2004).

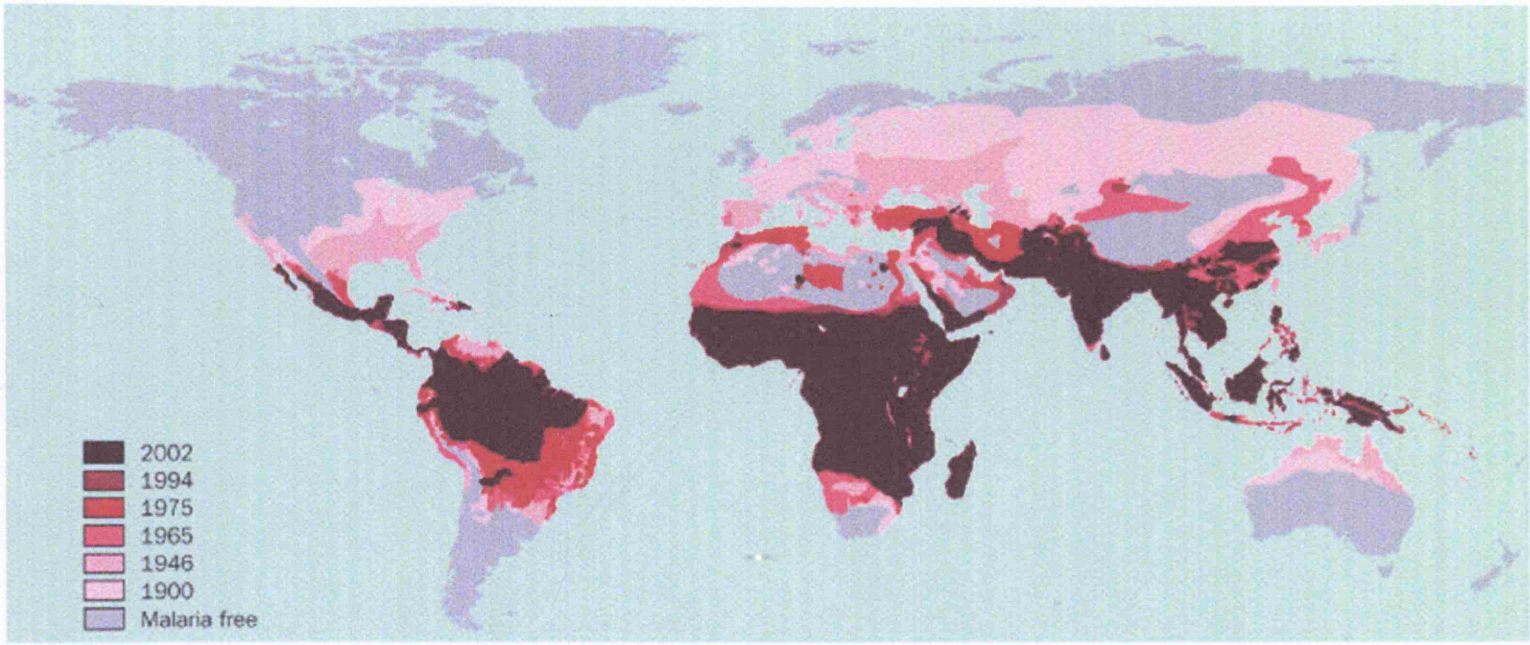
2002
1994
1975
1965
1946
1900
Malaria free

Figure 1.3

Apicomplexan zoite morphology

Comparitive morphology between a *Toxoplasma* tachyzoite and a *Plasmodium* merozoite (diagram not to scale) (Baum, Papenfuss et al. 2006). The apical structure comprising the secretory organelles and cytoskeletal network is a conserved feature of this phylum although subtle differences exist between different life-cycle stages, species and genera (see section 1.6).

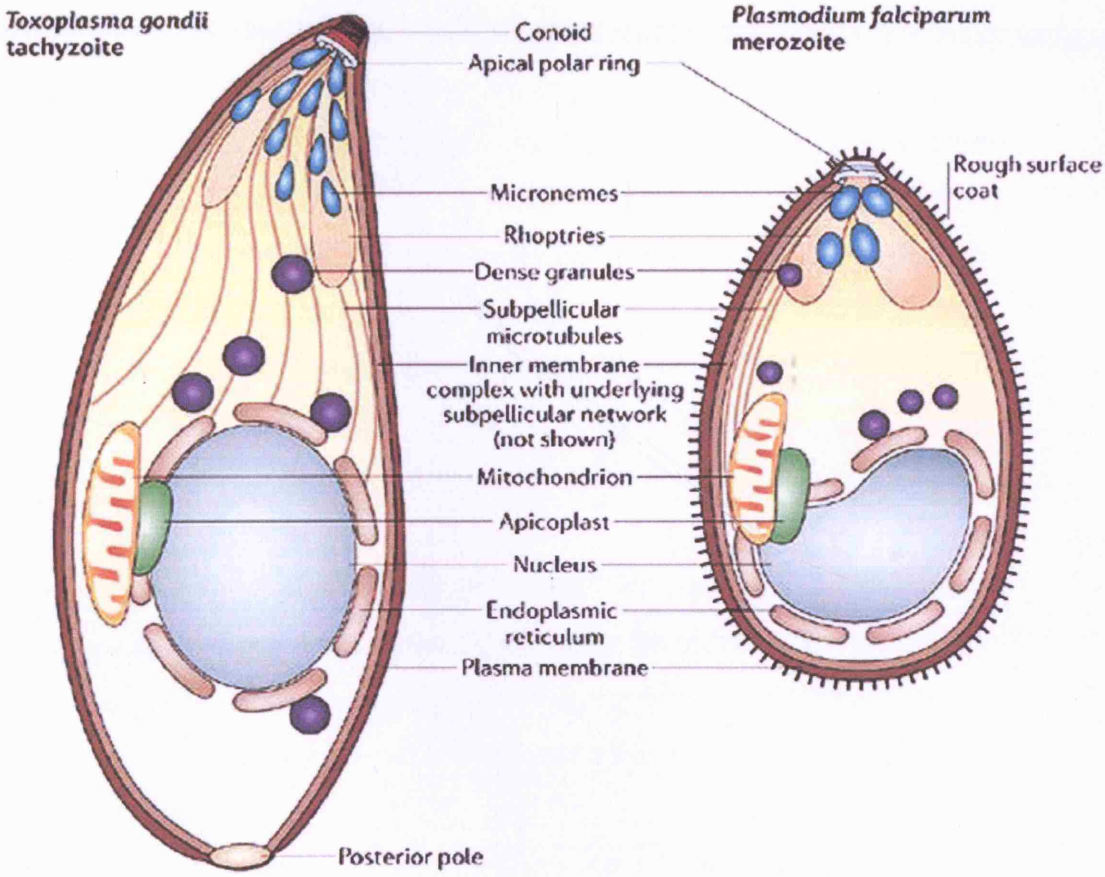
Toxoplasma gondii tachyzoite
Plasmodium falciparum merozoite
Conoid
Apical polar ring
Micronemes
Rhoptries
Dense granules
Subpellicular microtubules
Inner membrane complex with underlying subpellicular network (not shown)
Mitochondrion
Apicoplast
Nucleus
Endoplasmic reticulum
Plasma membrane
Posterior pole
Rough surface coat

Figure 1.4

Erythrocytic invasion by *P. falciparum* merozoites

A current working model of erythrocytic invasion (Carruthers and Boothroyd 2007). See section 1.7 for full details of individual steps. (1) Initial attachment is reversible and involves low affinity association of erythrocyte surface receptors with a number of merozoite surface proteins including the MSP superfamily. (2) Apical attachment is associated with Ca^{+}-dependent secretion of micronemes. Several proteins are secreted onto the parasite surface including AMA-1, which may be involved in parasite re-orientation. Members of other protein families (EBAs, Rhs and TRAPs) are involved in high affinity binding with erythrocyte surface receptors. (3) The MJ is formed when members of the RON family associate with AMA-1 at the parasite apex. This is thought to occur during or after rhoptry duct discharge. (4) Simultaneously or soon after, the rhoptries fully discharge and a number of additional proteins are secreted, some of which may be transferred to the developing PVM during invasion. (5) To penetrate the erythrocyte, merozoites pull transmembrane adhesins and/or the MJ to their posterior end, invaginating the host cell membrane. (6 and 7) Closure and separation appear to be the rate limiting steps of invasion. Closure involves fission of the PVM and erythrocyte membrane and may involve the residual MJ complex or other host or parasite proteins.

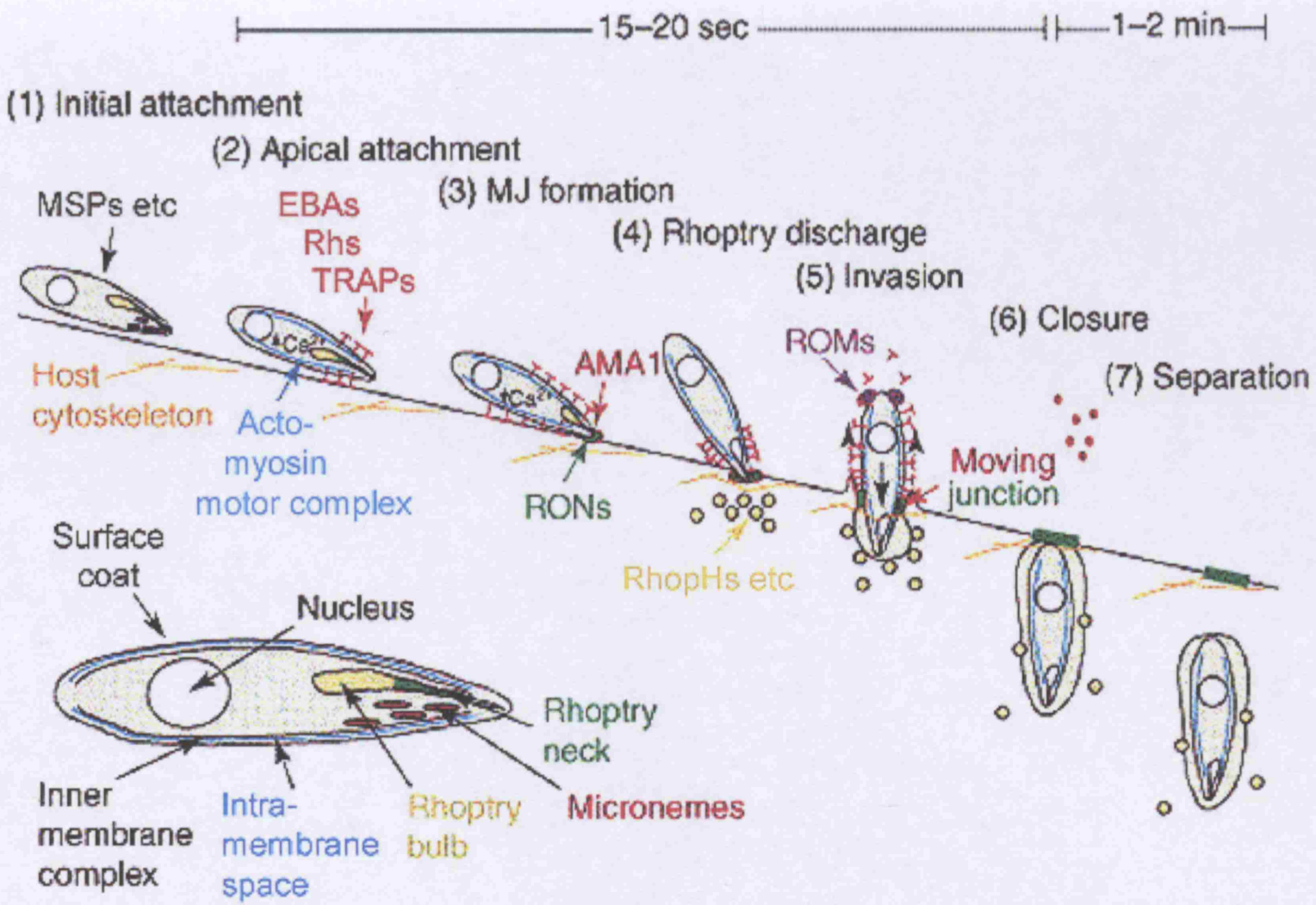
15–20 sec
1–2 min
(1) Initial attachment
(2) Apical attachment
(3) MJ formation
(4) Rhoptry discharge
(5) Invasion
(6) Closure
(7) Separation
MSPs etc
EBAs
Rhs
TRAPs
Host cytoskeleton
Acto-myosin motor complex
AMA1
RONs
ROMs
Moving junction
RhopHs etc
Surface coat
Nucleus
Rhoptry neck
Micronemes
Inner membrane complex
Intra-membrane space
Rhoptry bulb

Figure 1.5

The glideosome complex

A model of the glideosome complex depicted at the zone of contact between substrates. MyoA is anchored in the IMC by association with MTIP, GAP45 and GAP50 (with the exception of MyoA and MTIP, direct protein interactions were not defined at the start of this project). Mechanical force is converted into forward penetration by association of actin, through tetrameric aldolase, with parasite transmembrane adhesins that bind to erythrocyte surface receptors. A detailed description of the glideosome and its individual components is given in section 1.8.

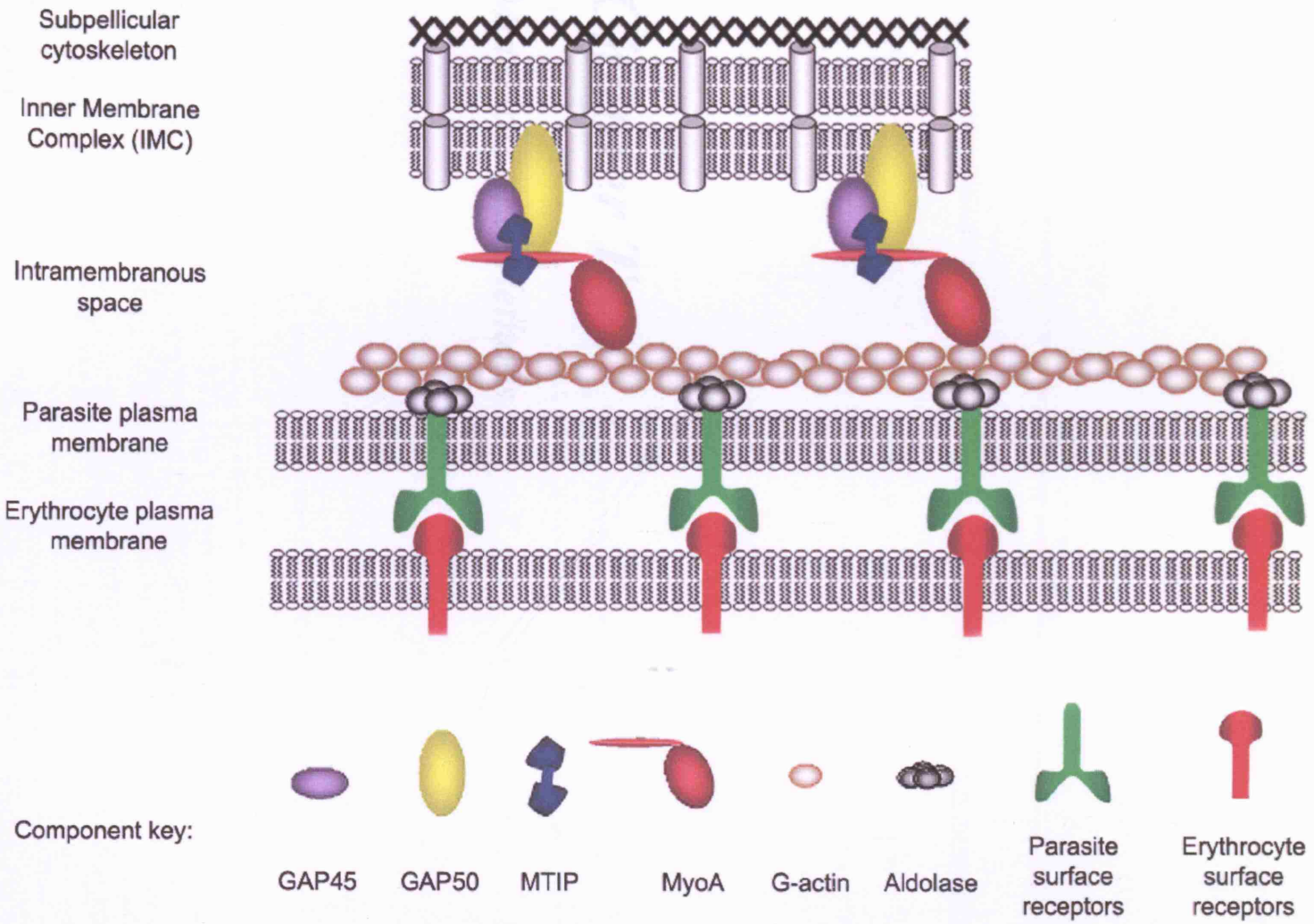
Subpellicular cytoskeleton
Inner Membrane Complex (IMC)
Intramembranous space
Parasite plasma membrane
Erythrocyte plasma membrane
Component key:
GAP45
GAP50
MTIP
MyoA
G-actin
Aldolase
Parasite surface receptors
Erythrocyte surface receptors

Chapter Two

Materials and Methods

2.1 Materials

2.1.1 Chemical reagents

All chemicals used were obtained from Sigma-Aldrich Company Ltd (Poole, UK) unless otherwise stated.

2.1.2 Solutions - Media

All media were prepared according to standard protocols (Sambrook and Russell, 2001) and sterilised by autoclaving prior to storage.

Buffered Glycerol-complex (BMGY):	1% (w/v) Yeast extract, 2% (w/v) Peptone, 1.34% (w/v) YNB (Yeast Nitrogen Base with Ammonium Sulphate without amino acids), 4 X 10^{-5}% (w/v) Biotin, 1% (v/v) Glycerol, 100 mM Potassium Phosphate pH 6.0.
Buffered Methanol-complex (BMMY):	1% (w/v) Yeast extract, 2% (w/v) Peptone, 1.34% (w/v) YNB, 4 X 10^{-5}% (w/v) Biotin, 0.5% (v/v) Methanol, 100 mM Potassium Phosphate pH 6.0.
Luria-Bertani (LB) broth:	1% (w/v) Bacto-tryptone, 0.5% (w/v) Bacto-yeast extract, 1% (w/v) NaCl in distilled water. The pH was adjusted to 7.0 using NaOH.
LB agar:	LB broth supplemented with 1.5% (w/v) Bacto-agar.
Minimal Dextrose agar (MD):	1.34% (w/v) YNB, 4 X 10^{-5}% (w/v) Biotin, 2% Dextrose, 1.5% (w/v) agar.

SOC:	2% (w/v) Bacto-tryptone, 0.5% (w/v) Bacto-yeast extract, 0.5% (w/v) NaCl in distilled water. The pH was adjusted to 7.5 using NaOH.
Yeast Extract Peptone Dextrose (YPD/YEPD):	1% (w/v) Yeast extract, 2% (w/v) Peptone, 2% (w/v) Dextrose.
YPD/YEPD agar:	YPD/YEPD supplemented with 1.5% (w/v) agar.
YND:	1.34% (w/v) YNB, 2% (w/v) Dextrose in distilled water.

Other solutions used in specific procedures are listed in the relevant section.

2.1.3 Centrifuges

Parasite material was handled using either a Sigma 4-10 bench-top centrifuge, rotor Nr.11140 or a Sigma 112 microcentrifuge, rotor Nr. 12026 for smaller volumes. All other material was handled using either a Beckman J-6B centrifuge, rotor JS-5.2, a Heraeus Biofuge Primo R centrifuge, rotor Nr. 7591 or a Sigma 1K15 microcentrifuge, rotor Nr. 12024-H for smaller volumes. Ultracentrifugation was carried out using a Beckman L7-65 ultracentrifuge, rotor 70TI or a Beckman TL-100 ultracentrifuge, rotor TLA 100.3 for smaller volumes.

2.1.4 Host strains

Escherichia coli (*E. coli*) One Shot® TOP10 chemically competent cells (Invitrogen) were used for all plasmid manipulations in both bacterial and yeast expression systems. For expression of recombinant proteins in *E. coli*, BL21Gold or BL21Gold(DE3)pLysS strains (Stratagene) were used, depending on the choice of plasmid. The latter cell line expresses the lambda bacteriophage T7 RNA

polymerase and is used when expression of a recombinant protein is driven by the T7 promoter. This strain also contains an additional plasmid that expresses lysozyme. Lysozyme inhibits the activity of T7 RNA polymerase, providing tighter control over induction. Protein was expressed in *Pichia pastoris* (*P. pastoris*) using GS115 (Invitrogen); a histidine-deficient, methanol utilisation strain (His^-Mut^+). The first step in the metabolism of methanol is its oxidation to formaldehyde by alcohol oxidase. Alcohol oxidase has a low affinity for oxygen and thus, the cells will compensate by generating large quantites of the enzyme. Expression of a recombinant protein is therefore driven by the strong alcohol oxidase (*AOX1*) promoter.

2.1.5 Plasmids

For expression in *E. coli*, vectors used in this work were pQE60 (Qiagen, Crawley, UK) and pET32 Xa/LIC (Novagen). The DNA sequence of pQE60 encodes a hexa-His tag that can be incorporated at the C-terminus of a recombinant protein. Expression using pQE60 is constitutive; no induction is necessary. The pET32 Xa/LIC plasmid encodes *E. coli* thioredoxin (Trx) upstream of an S-tag and a hexa-His tag. This large tag can be incorporated at the N-terminus of a recombinant protein and may assist in proper folding. The vector also encodes the T7 promoter and thus, proteins were expressed in BL21gold(DE3)pLysS upon induction with isopropyl-β-D-thiogalactopyranoside (IPTG).

For expression in *P. pastoris*, the vector used was pPIC9K (Invitrogen) and cloning was performed by GENEART GmbH, Regensburg, Germany. This plasmid is linearised with an appropriate restriction endonuclease and integrates into the yeast genome via homologous recombination. Integration re-generates the *His4* gene that is not functional in strain GS115, allowing transformants to synthesise histidine. Subsequent selection is therefore made using minimal dextrose medium (MD). The plasmid also encodes kanamycin that confers resistance to geneticin® (Invitrogen) in *P. pastoris*. Multiple integration of the

plasmid can give rise to a gene dosage effect (Cregg, Vedvick et al. 1993) and references therein) and thus, increased concentrations of geneticin® can be used to screen for transformants harbouring multiple gene copies. Table 2.1 shows a list of plasmids constructed, their features and accompanying host cell strains.

2.1.6 Oligonucleotides

Oligonucleotides were purchased from Sigma-Aldrich Company Ltd (Poole, UK) and used for plasmid construction either by cohesive end ligation or ligation independent cloning (Sections 2.3.4 and 2.3.6). Table 2.2 shows a list of oligonucleotides used in this project.

2.2 Manipulation of DNA

2.2.1 Concentration

Ethanol precipitation was used to concentrate DNA. 1/10 volume of 3 M sodium acetate was added to the DNA sample, followed by 2 volumes of 100% ethanol. DNA was left to precipitate overnight at -20°C and pelleted by centrifugation (20,937*g*, 20 min). The pellet was washed in 70% (v/v) ethanol and spun again prior to air-drying and re-suspension in an appropriate volume of buffer.

2.2.2 Quantification

DNA was quantified using UV absorbance spectrometry. Appropriate dilutions were made and absorbance at 260 nm recorded using a UNICAM UV1 spectrophotometer. An absorbance of 1 corresponds to approximately 50 μg ml^{-1} dsDNA (Freifelder, 1982).

2.2.3 Agarose gel electrophoresis

Gels were prepared by melting agarose (Roche) in 0.5X TBE (45 mM Tris-Borate pH 8.0, 1 mM ethylenediaminetetraacetic acid (EDTA)) to a final concentration of 0.7-2% (w/v) depending on the resolution required. For UV detection of DNA, 0.5 μg ml^{-1} ethidium bromide was added to melted agarose prior to casting gels in horizontal plates (Anachem Ltd, Luton, UK). Once cooled, gels were immersed in 0.5X TBE and DNA samples were supplemented with 20% (v/v) GelPilot DNA loading dye (Qiagen) before loading into wells. Separation was conducted at 6-10 V cm^{-1} using an EPS 500/400 DC Power Supply (Pharmacia).

2.3 Plasmid construction

2.3.1 Isolation of parasite genomic DNA

Synchronised parasite cultures containing erythrocytes infected with parasites of predominantly trophozoite/early schizont stages and at ~5% parasitaemia were centrifuged (815*g*, 10 min) and the supernatant discarded. The pellet was re-suspended in 4 pellet volumes of Buffer A (50 mM NaAc pH 5.2, 100 mM NaCl, 1 mM EDTA) and 1 pellet volume of 18% (w/v) sodium dodecyl sulphate (SDS) added. Efficient lysis was achieved by inverting the tubes several times before leaving to settle for 2 min at room temperature (RT). To precipitate the DNA, 6 pellet volumes of phenol/chloroform was added and the tube inverted to mix the contents before centrifugation (1,520*g*, 10 min). The supernatant containing DNA was removed carefully and subjected to ethanol precipitation (section 2.2.1) in Corex tubes (Corning). The following day, DNA was re-suspended in TE buffer (10 mM TrisHCl pH 7.6, 1 mM EDTA) and transferred to Eppendorf tubes. Phenol/chloroform extraction was repeated but after addition of 1/10 volume NaAc to the supernatant, 1 volume cold isopropanol was added instead of ethanol. The tubes were inverted and left on dry ice for 1 hr to allow precipitation of DNA. The samples were then centrifuged (20,937*g*, 10 min, 4°C) and the pellet washed in 75%-80% ethanol prior to re-suspension in an appropriate volume of TE.

2.3.2 Polymerase Chain Reaction (PCR)

DNA was amplified from parasite genomic DNA using high fidelity AccuPrime™ *Pfx* DNA polymerase (Invitrogen). Reactions contained 10 pg-200 ng template DNA, 0.3 μM each oligonucleotide and 1-2.5 U enzyme in supplied reaction buffer. Reaction buffer (10X) contained 10 mM $MgSO_4$, 3 mM dNTPs and thermostable proteins that enhance template-primer hybridization.

For amplification from plasmid DNA or in colony PCR to screen *E. coli* transformants, Taq DNA polymerase (Roche) was used. For plasmid DNA,

reactions were as described for genomic DNA except for the addition of 200 μM of each dNTP. Reaction buffer supplied (10X) contained 15 mM $MgCl_2$. For colony PCR, a single *E. coli* colony was picked from an agar plate and suspended in 19 μl distilled water. This sample was then used as a template for the PCR reaction.

PCR programmes used in this project are described in Table 2.3.

2.3.3 Restriction endonuclease digestion

For a typical reaction, 1 μg DNA was digested for 2 h at 37°C, in reaction buffer supplied with the specific enzyme being used. All enzymes were purchased from New England Biolabs, 1 Unit being defined as the amount of enzyme required to digest 1 μg DNA in 1 h at 37°C, in a 50 μl reaction. Where more than one enzyme was used in any given reaction, buffers were chosen in order to retain optimal activity of both enzymes.

2.3.4 Ligation of DNA fragments

Where restriction digestion was used in cloning, the resulting cohesive ends were ligated using T4 DNA ligase (New England Biolabs). Reactions contained 200 U enzyme, 50 ng vector DNA and a 3:1 molar excess of insert to vector DNA. Samples were incubated at 16°C overnight, in the supplied buffer.

2.3.5 Purification of DNA

Digested plasmid DNA and PCR amplicants were separated by agarose gel electrophoresis and the resulting bands were excised from gels. The DNA was subsequently purified from gel pieces using a gel extraction kit (Qiagen, Crawley, UK). DNA was eluted from the spin columns using 30 μl of the provided elution buffer and quantified.

2.3.6 Ligation Independent Cloning (LIC)

Cloning into pET32 Xa/LIC was achieved by ligation independent cloning (LIC), using kits purchased from Novagen. The vector is linearised and non-complementary 12-14 base single stranded overhangs are generated by treating DNA with T4 DNA polymerase in the presence of dGTP. The 3' to 5' exonuclease activity of the enzyme removes nucleotides until it encounters a guanine residue where the DNA polymerase activity prevents further excision.

Oligonucleotides were designed to generate PCR amplicants with complementary overhangs so that the two DNA fragments can be joined by annealing (see Table 2.2). DNA fragments for cloning were amplified from genomic DNA and purified, eluting in TlowE buffer (10 mM TrisHCl pH 8.0, 0.1 mM EDTA). To generate overhangs, 0.2 pmol DNA was incubated with 1 U T4 DNA polymerase, 2.5 mM dGTP, 5 mM dithiothreitol (DTT) in reaction buffer for 30 min at 22°C. The enzyme was then inactivated by heating at 75°C for 20 min. For annealing, 0.02 pmol insert was incubated with 0.01 pmol vector at 22°C for a total of 10 min. After 5 min, EDTA was added to the mixture to a final concentration of 6.24 mM.

2.3.7 Isolation of plasmid DNA

Plasmid DNA was isolated from *E. coli* overnight cultures using either the QIAprep Spin Miniprep or QIAGEN Plasmid Maxi kits (Qiagen, Crawley, UK) following the protocols provided in the QIAGEN plasmid purification handbook. If resulting DNA was to be used for transformation or sequencing, 2-5 ml culture was sufficient and DNA was extracted using the Miniprep kit. For electroporation of *P. pastoris*, larger quantites of DNA were required and thus 500 ml cultures were grown and DNA extracted using the QIAGEN-tip 500 from the Maxiprep kit. All DNA was eluted and stored in buffer EB, with the exception of samples used for sequencing that were eluted in de-ionised distilled water.

2.3.8 Sequencing of DNA

All DNA for sequencing was sent to the Advanced Biotechnology Centre (ABC), Imperial College London. Samples comprised 1 μg plasmid DNA obtained from Miniprep kit purification and 12.8 pmol of each oligonucleotide in 12 μl de-ionised distilled water. ABI chromatogram files were viewed and manipulated using BioEdit sequence alignment editor (Hall 1999).

2.3.9 Codon optimisation

The gene coding for PfGAP45 was re-synthesised by GENEART GmbH, Regensburg, Germany. The sequence was optimised for protein expression in *P. pastoris* and potential N-glycosylation sites were removed. For purification, additional nucleotides were incorporated at the C-terminus of the gene encoding a hexa-His tag.

2.4 Manipulation of host cells: *E. coli and P. pastoris*

2.4.1 Transformation

Chemically competent *E. coli* strains purchased commercially were transformed by heat-shock. Cells were thawed on ice prior to the addition of 1-50 ng purified plasmid DNA, 1-3 µl ligation reaction or 1 µl annealed LIC fragments. The cells were then subjected to a short heat-pulse at 42°C before incubation on ice. Pre-warmed SOC was then added to the cells and the samples incubated for 1 hr at 37°C. Transformed cells were then plated onto agar plates containing appropriate antibiotic for selection (Ampicillin 100 µg ml^{-1}, Kanamycin 50 µg ml^{-1}, Chloramphenicol 50 µg ml^{-1}) and incubated at 37°C overnight. The precise amount of DNA added to cells and conditions of transformation varied depending on the strain, so these factors were adapted as advised in the handbooks supplied with individual strains.

P. pastoris strain GS115 was transformed using an electroporation protocol that was adapted from the *Pichia* expression kit manual (Invitrogen) by Dr Chrislaine Withers-Martinez, NIMR, UK. Prior to transformation, the constructed plasmid was linearised with SacI restriction endonuclease to facilitate integration into the host genome. An agar stab of *P. pastoris* strain GS115 (Invitrogen) was used to inoculate 4 ml YPD which was then incubated overnight. The overnight cultures were then diluted 1:10,000 in 100 ml YPD and incubated overnight to give an optical density at 600nm (OD_{660}) of 1.2-1.5 cm^{-1}. Cells were harvested by centrifugation (3,000*g*, 10 min), re-suspended in 40 ml 50 mM Potassium Phosphate, 25 mM DTT, and incubated at 30°C for 15 min. Cells were then spun again and washed twice in electroporation buffer (STM) (10mM TrisHCl pH 7.5, 270 mM sucrose, 1mM $MgCl_2$), initially with 200 ml and then with 100 ml. Subsequent to the addition of STM to cells, the suspensions must be kept on ice to retain competency. Once harvested, the cells were re-suspended in 1 ml STM and 1-5 µg linearised DNA added to 60 µl cell suspension. The mixture was added to a pre-chilled 2 mm electroporation cuvette (Bio-Rad) and an electric

field (1.5 kV, 400 Ω, 25 μF) was applied using a Gene Pulser II (Bio-Rad). The suspension was then incubated at 30°C for 1 hr in 1 ml YPD and plated onto MD agar. The plates were incubated at 30°C for up to 3 days to select for transformants. Positive transformants were subjected to a further selection process. Colonies were suspended in distilled water to give an OD_{660} of 1.0 cm^{-1} (5.10^7 cells). Samples were then diluted 1:2.5 in distilled water and plated onto YPD agar containing increasing concentrations of geneticin® (0.25-4 mg ml^{-1}). Plates were incubated at 30°C for 3-7 days to select for transformants containing a high copy number of the integrated plasmid.

2.4.2 Cell culture for protein expression

For expression of recombinant proteins in *E. coli*, individual colonies were picked from agar plates and used to inoculate 10 ml LB (plus appropriate antibiotic). Cultures were incubated at 37°C overnight and subsequently used to inoculate a larger culture volume of 500 ml-2 litres LB. These cultures were incubated at 37°C to an OD_{600} of 0.6 cm^{-1} and induced if necessary, by the addition of 1 mM IPTG. For maximal expression, cultures were then incubated overnight at 18°C. All cultures were incubated at 220 rpm in a Multitron II incubator shaker (Infors, Switzerland).

For protein expression in *P. pastoris*, colonies were picked from YPD geneticin® agar plates and used to inoculate 5 ml Buffered Glycerol-complex (BMGY) which was incubated at 30°C overnight. The overnights were used to inoculate 150 ml BMGY which was again incubated at 30°C overnight. The following day the cells were harvested by centrifugation (1,500-3,000*g*, 10 min) and re-suspended in 500 ml Buffered Methanol-complex (BMMY). The starting OD_{600} should be 1-5 cm^{-1} for optimal protein expression (to confirm this, cultures were diluted appropriately). Cultures were then incubated for a total of 96 hrs at 30°C, with addition of 0.5% (v/v) methanol every 24 hrs to maintain induction. All cultures were incubated at 250 rpm in a Multitron II incubator shaker.

2.4.3 Cell storage

Glycerol stocks of bacterial and yeast strains were made for long term storage of cells. Overnight cultures were grown and 800 µl cells added to 200 µl 100% glycerol in cryogenic vials (Nalgene). Cells were then vortexed briefly to mix the contents and stored at -80°C. For short term storage (1-2 months) of bacteria and yeast, cells were streaked onto appropriate agar plates from either overnight cultures or glycerol stocks. Plates were then incubated at the appropriate temperature to permit growth of colonies.

2.5 Parasite manipulation

All parasite manipulations except for those described in section 2.5.4 were conducted by Munira Grainger, NIMR, UK.

2.5.1 Cell culture

P. falciparum 3D7 lines were originally obtained from Professor David Walliker and were cultured using a method modified from that described by Trager and Jenson (Trager and Jensen 1976). Erythrocytic stages were maintained in human erythrocytes at up to 15% parasitaemia, 0.5-1% haematocrit by culturing in Roswell Park Memorial Institute (RPMI) 1640 medium (Invitrogen) that was supplemented with 0.5% (w/v) AlbuMAX I, 25 mM HEPES, 27 mM $NaHCO_3$, 2 mM L-glutamine, 25 μg ml^{-1} gentamycin, 50 μg ml^{-1} hypoxanthine and 2 mg ml^{-1} glucose. Cultures were gassed with a mixture of 5% O_2, 7% CO_2, 88% N_2 and incubated at 37°C. To replace culture medium (every 2 days for cultures at 5% parasitaemia), parasitised erythrocytes were centrifuged (815*g*, 3 min) and old medium removed by aspiration. To examine cultures, thin blood smears were made on glass slides and cells stained using 1:1 Giemsa's stain:distilled water for 10 min. Slides were then viewed using a light microscope.

2.5.2 Synchronisation and isolation of parasites

For crude synchronisation, parasite cultures were centrifuged (815*g*, 5 min) and pellets re-suspended in 5% (w/v) sorbitol in PBS. The suspension was incubated at 37°C for 10 min to ensure late stages were lysed and then centrifuged (815*g*, 5 min) and re-suspended in fresh culture medium. Late-stage schizonts and merozoites were purified by Magnetic-Activated Cell Sorting (MACS®) (Miltenyi, Muller et al. 1990) using a Super Macs II magnetic separator in conjunction with a MACS type D depletion column. Schizonts were purified using a method described by Taylor et al (Taylor, Grainger et al. 2002). The MACS column was initially washed with 100% (v/v) ethanol, followed by

distilled water and then equilibrated using RPMI 1640 (Invitrogen). Infected erythrocytes were harvested by centrifugation (815*g*, 5 min) and re-suspended in an equal volume of RPMI. Suspensions were then passed through the column under gravity and washed with four column volumes RPMI. Trophozoites and schizonts older than 24 hours are retained on the magnet owing to their iron-containing pigment. The column was then removed from the magnet and schizonts eluted in 50 ml RPMI.

To isolate merozoites, purified schizonts (95% parasitaemia) were cultured in RPMI for 1-2 h and then centrifuged (815*g*, 5 min). Schizonts and uninfected erythrocytes were pelleted whereas released merozoites remained in the supernatant. Supernatants were removed and spun again before being passed through the column under gravity. Contaminating red cells and schizonts were retained on the column and the flow through contained highly purified merozoites. Resulting fractions obtained containing either purifed schizonts or merozoites were then separated into smaller aliquots and cells were pelleted by centrifugation (815*g*, 5 min).

2.5.3 Biosynthetic labeling

Populations of tightly synchronised late stage schizonts estimated to be ~42 hours (h) post-invasion were radiolabeled by growth in either L-[^{35}S] methionine and L-[^{35}S] cysteine (Pro-mix, GE healthcare), [^{3}H] myristic acid (GE healthcare) or [^{3}H] palmitic acid (GE healthcare). Pelleted schizonts were washed and grown for 2 h at 37°C in media supplemented with 37 MBq radiolabeled isotope. For pulse-chase experiments, schizonts were radiolabeled with L-[^{35}S] methionine and L-[^{35}S] cysteine for 15 min (pulse or t=0) and then grown in RPMI 1640 containing unlabeled L-methionine and L-cysteine for a further 1 h 45 min (chase), samples being taken at 15, 30, 60 and 120 min time points (t=15, 30, 60 and 120).

For labeling with [^{3}H] myristic acid and [^{3}H] palmitic acid, AlbuMAX I and human serum were excluded from the growth medium. Ethanol used in the

storage of the radiolabel was evaporated and 1.8% (w/v) defatted BSA added in a 1:1 molar ratio. The mixture was incubated for 1 hr, RT and added to the growth medium. Subsequent to labeling, cultures were centrifuged (815*g*, 5 min) and pellets washed twice in appropriate media and once in PBS prior to a final centrifugation (815*g*, 5 min). Pellets were stored at -80°C.

2.5.4 Total protein extraction and solubility tests

Tighly synchronised schizonts (~42 h post-invasion) or purified merozoites were re-suspended in a variety of lysis buffers in order to extract parasite proteins.

For whole cell extracts, pellets were re-suspended in 1 ml 1:1 NuPAGE® 4X lithium dodecyl sulphate (LDS) Sample Preparation Buffer: distilled water with or without the addition of 1X supplied reducing agent. Samples were boiled for 10 min to denature genomic DNA that may affect protein separation by SDS-polyacrylamide gel electrophoresis (PAGE).

For solubility tests, pellets were lysed in 1 ml of each sequential buffer. For each step, samples were ultracentrifuged (280,000*g*, 30 min, 4°C) subsequent to lysis and the supernatants retained on ice. Initial pellets were lysed in hypotonic lysis buffer (5 mM TrisHCl pH 8.0, 5 mM EDTA, 5 mM ethylene glycol bis(2-aminoethyl ether)-*N,N,N'N'*-tetraacetic acid (EGTA)) and subjected to 3 cycles of freeze/thawing. Resulting pellets were then lysed in high-salt buffer (5 mM TrisHCl pH 8.0, 5 mM EDTA, 5 mM EGTA, 500 mM NaCl), followed by Nonidet P-40 (NP-40, Roche) buffer (1% (v/v) NP-40, 50 mM TrisHCl pH 8.0, 500 mM NaCl, 5 mM EDTA, 5 mM EGTA), sodium deoxycholate (DOC) buffer (1% (w/v) DOC, 50 mM TrisHCl pH 8.0, 5 mM EDTA, 5 mM EGTA) and finally SDS buffer (1% (w/v) SDS, 50 mM TrisHCl, 5 mM EDTA). The final pellet was retained, re-suspended in distilled water and boiled to degrade haemozoin. For detection, extracted proteins were then separated by SDS-Polyacrylamide gel electrophoresis (SDS-PAGE) and transferred to nitrocellulose for Western blotting, as described in sections 2.6.5 and 2.7.4 respectively.

2.6 Protein analyses

2.6.1 Purification of recombinant proteins and co-precipitations

Recombinant proteins were expressed in *E. coli* and *P. pastoris* as described in section 2.4.2. Cultures were centrifuged (3,750*g*, 30 min) and relevant fractions were retained for purification. For *E. coli*, pellets were lysed in BugBuster™ Protein Extraction Reagent (Novagen) with shaking, at RT for 20-30 min. Lysates were then ultracentrifuged (80,000*g*, 30 min, 4°C) and the supernatants removed and kept on ice. For *P. pastoris*, 300 mM NaCl was added to culture supernatants and the pH adjusted to 8.0 using NaOH. Supernatants were then centrifuged (3,750*g*, 10 min) to pellet any salt precipitate. Recombinant hexa-His tagged proteins were captured using nickel-nitrilotriacetic acid (Ni-NTA) agarose (QIAGEN, Crawley, UK) or TALON™ metal affinity resin (Clontech) packed into disposable polypropylene columns (Pierce). Washes were conducted with binding buffer (50 mM sodium phosphate pH 8.0, 300 mM NaCl) and increasing concentrations of imidazole (10-50 mM). Proteins were eluted in binding buffer containing 250 mM imidazole, buffer exchanged with PBS as described in section 2.6.4 and stored at 4°C.

For co-precipitations, S-tagged proteins were captured using S-protein agarose (Novagen). For high specificity binding, proteins were incubated overnight with an appropriate volume of resin (minimum capacity 500 μg ml^{-1}) and washed X 3, both in 20 mM Tris-HCl pH 7.5, 150 mM NaCl, 0.1% (w/v) Triton X-100. For elution, proteins were re-suspended in 1:1 NuPAGE® 4X LDS Sample Preparation Buffer: distilled water plus 1X supplied reducing agent. Samples were heated to 95°C for 5 min, centrifuged (20,937*g*, 5 min) and proteins in the supernatant separated by SDS-PAGE as described in section 2.6.5 and visualised by staining with coomassie blue.

2.6.2 Factor Xa cleavage

For efficient processing of fusion proteins, 50 μg Factor Xa (Roche)/mg recombinant protein was used. Reactions were incubated at 20°C, overnight, in reaction buffer (50 mM TrisHCl pH 8.0, 100 mM NaCl, 5 mM $CaCl_2$) and buffer exchanged with Ni-NTA/TALON™ binding buffer (see section 2.6.1 for recipe). Unprocessed protein and tags were then removed from reactions by passing samples through pre-prepared Ni-NTA columns (section 2.6.1). Flow-through fractions were retained and buffer exchanged with PBS.

2.6.3 Quantification

Protein concentrations were determined by measuring absorbance at 280 nm using a UV spectrophotometer (section 2.2.2).

The Beer-Lambert law states: $A = \varepsilon.c.l$

A is the absorbance at 280 nm, ε is the extinction coefficient of the protein being analysed (M^{-1} cm^{-1}), c is the protein concentration (M) and l is the path length (cm). Spectra were obtained by recording absorbance at 250-350 nm and subsequently corrected for light scattering occuring at the longer wavelengths. Predicted extinction coefficients for proteins being analysed were obtained using ProtParam (www.expasy.org/tools/protparam.html).

2.6.4 Buffer exchange and concentration

Buffer exchange was performed using PD-10 desalting columns (GE Healthcare) following the protocol provided in the supplied notes. Protein was concentrated using Vivaspin 20 (20 ml) or 500 (500 μl) centrifugal concentrators (VWR International) with polyethersulphone (PES) membranes and 5 kDa molecular weight cut-off (MWCO).

2.6.5 SDS-Polyacrylamide gel electophoresis (SDS-PAGE)

All protein samples were separated using Nu-PAGE® pre-cast Bis-Tris gels and Xcell II™ Mini Cell gel cassette (Invitrogen). The acrylamide concentration used was either 10% or 12% depending on the resolution required and the molecular weight of the protein. Nu-PAGE® 4X LDS sample preparation buffer plus 1X supplied reducing agent (Invitrogen) was added to samples at a final concentration of 25% (v/v) and Precision Plus Protein™ standards (Bio-Rad) were used to monitor protein separation and determine sample molecular weights. Proteins were separated in Nu-PAGE® 3-(N-morpholino)-propanesulphonic acid (MOPS) or 2-(N-morpholino)-ethanesulphonic acid (MES) running buffer by applying a constant 200 Volts (V) using an EPS 500/400 DC Power Supply (Pharmacia). Proteins were either visualised by staining gels with Coomassie blue stain or transferred to nitrocellulose for detection by Western blotting (section 2.7.4). For staining, gels were immersed in Coomassie blue stain (0.1% (w/v) Coomassie Brilliant Blue R-250, 45% (v/v) methanol, 10% (v/v) acetic acid) for 1 h and then immersing in destain (45% (v/v) methanol, 10% (v/v) acetic acid) until the gel background became transparent.

2.6.6 Synthetic peptides

PfMyoA peptides were sythesised by Dr. Graham Bloomberg, Bristol, UK. For fluorescent labelling, a cysteine residue was incorporated at the N-terminus of peptide 1 (GAKILTKIQREKLVEWEN) and whereas the sequence of peptide 2 (VEWENCVSVIEAAILKHKYKQKVNKN) contained an internal cysteine. The N- and C-terminal residues were un-modified.

2.7 Production and application of antisera

A list of all antibodies used in this project is provided in table 2.4, including those that were kindly donated by others.

2.7.1 Raising antisera

Polyclonal antisera were raised against both PfGAP45 and PfGAP50 in both mice and rabbits. Rabbit polyclonal antisera was raised in New Zealand Whites (HsdIF:NZW) by Harlan UK Ltd, Oxon, UK. Mouse polyclonal antisera were raised in-house using 10 week old female BALB/c mice. Immunisations and blood collection were conducted by Solabami Ogun and Dr Madhu Kaddekoppala, NIMR, UK To raise antisera, 2 rabbits and 5 mice were immunised per antigen and concentrations used were 0.4 mg ml^{-1} for rabbits, 0.08 mg ml^{-1} (prime) - 0.16 mg ml^{-1} (boost) for mice. Animals were initially pre-bled and then primed using 1:1 antigen: Freund's Complete Adjuvant. An additional 3-5 boosts were given using 1:1 antigen: Freund's Incomplete Adjuvant at 3 week intervals before animals were sacrificed and blood collected.

2.7.2 Purification of antibodies

Total IgG was purified from rabbit polyclonal antisera using protein G sepharose (GE healthcare) in a method adapted from that given in the supplied notes. Binding buffer (20 mM $NaPO_4$ pH 7.0) was used to equilibrate 1 ml (settled resin volume) sepharose that was packed into a column. A 10 ml sample of antiserum was then diluted 1:1 in binding buffer and filtered through a 0.45 μM Minisart SRP25 (Sartorius). Antiserum was then passed through the resin under gravity and washed with 20 column volumes of binding buffer. Antibodies were eluted using 0.1 M glycine pH 2.7 and neutralised with 1 M TrisHCl pH 9.0. Samples were then buffer exchanged with PBS as described in section 2.6.4 and stored at -20°C.

For affinity purification, recombinant proteins were coupled to CNBr-activated sepharose. To remove additives, 0.3 g CNBr-activated sepharose (GE healthcare) was washed in 1 mM HCl and filtered by vacuum. For coupling, sepharose was re-suspended in coupling buffer (0.1 M $NaHCO_3$ pH8.3, 0.5 M NaCl) containing 5 mg recombinant protein and incubated with rotation overnight at 4°C. Sepharose was packed into columns and washed with coupling buffer. To block remaining active groups, sepharose was washed with 5 column volumes of 0.1 M TrisHCl pH 8.0 and left to stand in an additional 5 column volumes of buffer for 2 hrs at 4°C. Unbound antigen was removed by washing sepharose with 4 cycles of 0.1 M NaAc pH 4.0, 0.5 M NaCl followed by 0.1 M TrisHCl pH 8.0, 0.5 M NaCl. Purified IgG fractions were then diluted in PBS and allowed to pass through the sepharose under gravity. For antibody depletion, flowthrough would be collected and stored at this stage. Otherwise, subsequent to washing with 20 column volumes of PBS followed by 20 column volumes of 0.1 M TrisHCl pH 8.0, 0.5 M NaCl, affinity purified antibodies were eluted and stored as described for purification of IgG.

2.7.3 Purification of PfGAP45 from merozoites

Merozoites were purified from synchronised parasite cultures as described in section 2.5.2. Pellets were lysed in *N*-octylglucoside buffer (0.5% (w/v) N-octylglucoside (Calbiochem), 1 X protease inhibitor cocktail (PI) (Roche), 50 mM TrisHCl pH 8.0, 500 mM NaCl, 5 mM EDTA, 5 mM EGTA), incubated on ice for 30 min and centrifuged (20,937*g*, 20 min, 4°C). The supernatant was removed and kept on ice. PfGAP45 was purified from the supernatant using an affinity column which was made following the method described in section 2.7.2. Exceptions were that 0.9 g sepharose was used and 15 mg affinity-purified rabbit anti-PfGAP45 antibodies were used in the coupling reaction. Additionally, 1% (w/v) N-octylglucoside was added to all the buffers used throughout the purification to ensure PfGAP45 remained in solution.

2.7.4 Western blotting

Proteins were transferred from Nu-PAGE® gels to Hybond C-Extra nitrocellulose membrane (GE healthcare) using the Xcell II™ blot module (Invitrogen). The method followed was as described for blotting Novex® pre-cast gels in LINNEA™ protocols, available at www.invitrogen.com. Blots were blocked with 5% (w/v) milk powder (Marvel), 0.05% (v/v) Tween-20 in PBS (PBST) for 1 h-overnight at 4°C. Antibodies were diluted in blocking buffer at the concentrations specified in table 2.4 and used to probe blots. Blots were incubated in primary antibody for 1 h and washed 3 X 10 min in PBST. Secondary antibodies conjugated to horse-radish peroxidase (HRP) were then applied to blots and incubated for 30 min prior to an additional 3 X 10 min washes in PBST. Protein bands were detected using the enhanced chemiluminescence (ECL™) Advance Western Blotting Detection Kit (GE healthcare) following the supplied protocol. Blots were exposed to Biomax MR film (Kodak) for 1-15 min and developed using a FujiFilm FPM-3800 AD developer.

2.7.5 Immunofluorescence assays (IFA)

Synchronised parasite cultures containing erythrocytes infected with late-stage schizonts and free merozoites were smeared onto glass slides and air-dried. Parasites were fixed for 20 min with 1% (v/v) formaldehyde (Agar Scientific Ltd, Essex, UK) in PBS and permeabilised with 0.01% (v/v) Triton X-100 in PBS for 10 min. Slides were blocked with 0.2% (v/v) fish skin gelatin in PBS for 1 h at 4°C and rinsed in PBS. Antibodies were diluted in 1% (w/v) bovine serum albumin (BSA), 0.05% (v/v) Tween 20 in PBS at the concentrations given in table 2.4. Primary antibodies were applied to individual wells, incubated at 37°C for 1 h and washed 3 X 10 min in PBS. Secondary antibodies conjugated to either fluorescein isothiocyanate (FITC) or alexafluor®594 were applied and incubated at 37°C for 45 min followed by an additional 3 X 10 min washes. Nuclei were stained with 1 μg ml^{-1} 4'-6-Diamidino-2-phenylindole (DAPI) and mounted using

glycerol/PBS solution containing anti-quenching agent (Citifluor Ltd). Slides were viewed under oil immersion using an Axioplan fluorescence microscope (Carl Zeiss MicroImaging GmbH). Images were recorded by a digital camera and viewed using AxioVision software (Carl Zeiss MicroImaging GmbH).

2.7.6 Immunoelectron Microscopy (ImmunoEM)

This procedure was carried out by Dr. Anton Dluzewski, NIMR, UK.

For fixation, ~100 µl packed cells (merozoites) were suspended in 0.1% (v/v) double-distilled (dd)-EM grade gluteraldehyde diluted in RPMI (no serum) and incubated for 20 min, 4°C. Samples were then centrifuged (20,937g, 1 min) and washed 4 X in RPMI before a final centrifugation (as above) to give a firm pellet. Pellets were dehydrated by incubation with increasing concentrations of ethanol (50% (v/v), 20 min, 4°C; 70% (v/v), 30 min, -20°C; 90% (v/v), 60 min, -20°C; 100% (v/v), 60 min, -20°C) prior to infiltration with LR white resin (London Resin Company, Basingstoke, UK). For infusion, pellets were incubated with increasing concentrations of LR white, diluted in ethanol (75 : 25% (v/v) ethanol : LR white, 30 min, -20°C; 50 : 50% (v/v), 30 min, -20°C; 25 : 75% (v/v), 15 min, -20°C; 0 : 100% (v/v) 8 h-overnight, -20°C). Small crumbs were then picked and embedded in gelatin capsules. Resin was polymerised overnight at RT using indirect UV. Ultra-thin sections were cut using a diamond knife on a Reichert ultramicrotome and fixed on 400 mesh nickel grids using 0.5% (v/v) Pioloform. Sample grids were then stained dull side up by flotation on liquid surfaces. An initial incubation on 1% (v/v) glycine for 10 min was performed to block free aldehyde groups. Non-specific labelling was blocked by incubation on PBS-1% (w/v) BSA for 30 min, 37°C in a humidified chamber. Grids were then drained on filter paper (Whatman) and incubated on primary antibody solution for 1-2 h, 37°C. For washing, grids were floated 3 X 10 min on PBS-1% (w/v) BSA loaded into 96 well microtitre plates that were placed on a tilting stage. Protein A-

gold (2 nm) was diluted 1:70 in PBS-1% (w/v) BSA and grids incubated on this solution for 1 h, RT before being drained and washed 1 X 10 min on PBS-0.1% (v/v) BSA and 2 X 10 min on MilliQ dd-H_2O. Prior to viewing, grids were air-dried, contrasted using 2% (v/v) uranyl acetate and washed with dd-H_2O. Samples were viewed using a Hitachi H600 transmission electron microscope operated at 75 kV.

2.7.7 Immunoprecipitation (IP)

Antibodies were used to precipitate proteins from synchronised parasite cultures containing erythrocytes infected with late-stage schizonts at ~42 h post-invasion. Unlabeled or biosynthetically labeled parasites (section 2.5.3) were isolated as described in section 2.5.2. Parasites were lysed in either 1% SDS buffer (1% (w/v) SDS, 1 X PI, 50 mM TrisHCl pH 8.0, 5 mM EDTA, 5 mM EGTA, 150 mM NaCl) or 1% NP-40 buffer (1% (v/v) NP-40, 1 X PI, 50 mM TrisHCl pH 8.0, 5 mM EDTA, 5 mM EGTA, 150 mM NaCl) and incubated for 20 min at RT or 4°C respectively. Lysates were centrifuged (20,937*g*, 20 min) and supernatants were retained. Parasites lysed in SDS buffer were then diluted 1:10 in NP-40 buffer to prevent SDS precipitation at 4°C. Supernatants were pre-cleared with protein G sepharose for 1 h at 4°C and proteins were immunoprecipitated overnight at 4°C with antibodies diluted at concentrations given in table 2.4. To isolate antibody-protein complexes, protein G sepharose was added to supernatants and samples incubated for 1 h at 4°C. Sepharose was then washed X 4 in NP-40 buffer and re-suspended in 1:1 NuPAGE® 4X LDS Sample Preparation Buffer: distilled water plus 1X supplied reducing agent. Samples were heated to 95°C for 5 min, centrifuged (20,937*g*, 5 min) and proteins in the supernatant separated by SDS-PAGE as described in section 2.6.5. For detection of radiolabelled proteins, gels were then fixed for 20 min in 25% (v/v) isopropanol, 10% (v/v) acetic acid, 65% distilled water and treated with NAMP100 Amplify™ (GE healthcare) for 20 min. Gels were then dried using a

DryGel Sr. Slab gel dryer (Hoefer Scientific instruments, SF, USA) attached to a vacuum pump (Edwards high vacuum international, Crawley, UK). Dried gels were exposed to Biomax MR film at -70°C for as long as required before developing as described in section 2.7.4. For IP-Westerns, gels were transferred to nitrocellulose and blots developed as described in section 2.7.4.

2.8 Bioinformatic analyses

2.8.1 Search engines and databases

Protein sequences of *T. gondii* GAP45 and GAP50 were isolated from the protein databases in Entrez, the life sciences search engine at the National Center for Bioinformatics (NCBI). The sequences were then used in a Basic Local Alignment Search Tool (BLAST) query in the *Plasmodium* database (PlasmoDB), in order to isolate orthologues from *P. falciparum*. PlasmoDB was then used to analyse transcription profiles (Bozdech, Llinas et al. 2003; Bozdech, Zhu et al. 2003; Le Roch, Zhou et al. 2003) and examine protein expression (Florens, Washburn et al. 2002; Florens, Liu et al. 2004) in erythrocytic stages.

2.8.2 Proteomic tools

All tools for proteomic analyses were obtained from the Expert Protein Analysis System (ExPASy) Proteomics Server of the Swiss Institute for Bioinformatics (SIB). The multiple sequence alignment program ClustalW (Thompson, Higgins et al. 1994) was used to compare protein sequences and the secondary structure of recombinant proteins was predicted using PSIPRED (Jones 1999; Bryson, McGuffin et al. 2005). N-terminal signal sequences were analysed using SignalP (Nielsen, Engelbrecht et al. 1997; Bendtsen, Nielsen et al. 2004) and COILS (Parry 1982; Lupas 1996) was used to predict the likelihood of a protein sequence forming coiled-coils. Potential *N*-myristoylation and palmitoylation sites were determined using NMT- the MYR Predictor (Maurer-Stroh, Eisenhaber et al. 2002) and CSS-Palm (Zhou, Xue et al. 2006) respectively. NetPhos 2.0 (Blom, Gammeltoft et al. 1999) was used to predict potential Ser, Thr or Tyr residues that would likely be phosphorylated by kinases. Protein crystal structures were viewed and manipulated using PyMol (DeLano 2002).

2.9 *In vitro* post-translational modification assays

2.9.1 *N*-myristoylation assay

In-vitro *N*-myristoylation assays were set up where recombinant *P. falciparum* *N*-myristoyl transferase (PfNMT) was used to catalyse transfer of ^{3}H-labelled myristoyl-CoA (Amersham Biosciences) to substrate proteins. Assay conditions were developed by Dr Paul Bowyer, Stanford University, CA, USA, who also kindly donated aliquots of purified PfNMT. In each assay, 0.2 µM myristoyl-CoA (0.022 MBq) was incubated with 5-15 µM substrate and 0.38 µM PfNMT for 2 h at RT in reaction buffer (30 mM TrisHCl pH 6.8, 0.5 mM EGTA, 0.45 mM EDTA, 4.5 mM 2-mercaptoethanol, 1% (v/v) Triton X-100) to a final volume of 50 µl. Fractions from each reaction were separated by SDS-PAGE as described in section 2.6.5. Proteins were visualised either by Coomassie staining or gels were treated, dried and exposed to X-ray film as described in sections 2.7.4 and 2.7.7.

2.9.2 [γ-^{32}P] Adenine trinucleotide (ATP) kinase assay

Phosphorylation of recombinant proteins was achieved by incubating 5 µg substrate with 0.5 µg recombinant PfCDPK1 in reaction buffer (20 mM TrisHCl pH 8.0, 20 mM $MgCl_2$, 0.5 mM $CaCl_2$, 0.18 MBq [γ-P^{32}] ATP (Amersham Biosciences), 100 µM ATP) at 30°C for 30 min. For detection of transferred phosphate, proteins were separated by SDS-PAGE and treated, fixed and dried as described in section 2.7.7. Gels were then exposed to X-ray film and developed as described in section 2.7.4.

2.9.3 Nicotinamide adenine dinucleotide (NADH)-coupled enzyme assay

The kinetics of PfCDPK1 phosphorylation were examined using a continuous spectrophotometric assay based on that described by Cook et al (Cook, Neville et al. 1982). Phosphorylation was monitored by coupling the hydrolysis of ATP to two additional enzyme reactions. Phosphoenolpyruvate (PEP) is first

converted to pyruvate by pyruvate kinase (PK), re-generating ATP. Lactate dehydrogenase (LDH) is then converted pyruvate into lactate via the oxidation of NADH (figure 2.1). This oxidation was monitored by measuring the change in absorbance at 340 nm using a JASCO V-550 UV/Visible spectrophotometer. Reaction buffer (50 mM HEPES pH 7.5, 10 mM $MgCl_2$, 1 mM $CaCl_2$, 0.3 mM NADH, 1.45 mM PEP, 1.75 mM ATP, 10.8 U LDH, 5.4 U PK) was added to 10 mm quartz suprasil (QS) cuvettes (Hellma GmbH & Co. KG) and initially incubated at 30°C for 5 min to allow the signal to stabilise. PfCDPK1 was added at a fixed concentration of 15 μM and samples incubated at 30°C for 5 min to allow time for autophosphorylation to occur. Substrates were then added at different concentrations and initial rates were measured.

The Michaelis-Menton equation states: $$\text{Rate} = \frac{V_{Max}[S]}{[S] + K_M}$$

Values for the Michaelis constant (K_M) and V_{Max} were fitted to the above equation using CURFIT (in-house software developed by Dr Stephen Martin, NIMR, UK) by the non-linear least squares method.

2.10 Biophysical analyses

2.10.1 Circular dichroism (CD) spectroscopy

Dr Stephen Martin (NIMR, UK) assisted in the analysis of protein samples and in the interpretation of results obtained.

CD measurements were made using a Jasco J-715 spectropolarimeter equipped with a PTC-348WI Peltier temperature control system. CD spectra were recorded at 20°C in PBS, using 1 mm QS cuvettes (Hellma GmbH & Co. KG). The secondary structure of recombinant proteins was determined by monitoring CD in the far-UV region (190-250 nm) and measurements in the near-UV region (250-350 nm) were recorded to examine tertiary structure. Multiple scans were averaged and the appropriate buffer baseline was subtracted. Far and near-UV CD intensities are presented on a mean residue weight ($\Delta\varepsilon_{MRW}$) or molar ($\Delta\varepsilon_{M}$) basis respectively. Secondary structure contents were estimated from far-UV CD spectra using the methods described by Sreerama and Woody (Sreerama and Woody 2000). Thermal denaturation of protein samples was studied by heating from 5 to 85°C at 1°C min^{-1} whilst monitoring the CD signal at 220 nm. Theory and data analysis for CD are described in section 4.2.1.

2.10.2 Fluorescence spectroscopy

Dr Stephen Martin (NIMR, UK) assisted with experimental procedures and interpretation of results.

The amino acid sequences of synthetic PfMyoA peptides were designed to contain one cysteine for labelling but the protein sequence coding for PfMTIP contains 5 cysteine residues. However, if 4 of these residues are paired in disulphide bridges, one would remain free. The quantity of free thiol in PfMTIP was therefore determined using Ellman's reagent (5,5'-Dithio-bis(2-nitrobenzoic acid) or DTNB). Working DTNB reagent was prepared by diluting 50 µl of a

stock solution (50 mM NaAc, 5 mM DTNB) into 100 µl 1 M Tris HCl, pH 8.0, 830 µl dH_2O. A background scan for this solution (A1) was obtained at 412 nm using a UV spectrophotometer. PfMTIP was then added to the solution (20µl) which was stirred and incubated for 5 min at RT before taking a second reading (A2). The molarity (M) of free sulphydryl in the assay ($[SH]$) was then calculated from:

$$[SH] = \left(\frac{A2 - A1}{\varepsilon_{412} TNB^{-}} \right)$$

Where $\varepsilon_{412} TNB^{-}$ is the extinction coefficient of the coloured anion of 2-thio-5-nitrobenzoic acid (TNB) at 412 nm (13,600 $M^{-1}cm^{-1}$).

The molarity (M) of free sulphydryl in the original sample of PfMTIP ($[SH]_{SAMPLE}$) was then calcluated from:

$$[SH]_{SAMPLE} = [SH] \left(\frac{Vol_{TOTAL}}{Vol_{SAMPLE}} \right)$$

Where Vol_{TOTAL} is the total volume in the assay (1000 µl) and Vol_{SAMPLE} is the volume of PfMTIP added (20 µl). The value obtained for $[SH]_{SAMPLE}$ was approximately equal to the concentration of PfMTIP in the sample (M) (calculated previously as described in section 2.6.3), confirming that there was one free cysteine.

Cysteine residues contained in synthetic PfMyoA peptides and recombinant PfMTIP were subsequently labeled with the environmentally sensitive probe, 2-(4'-maleimidylanilino) naphthalene-6-sulfonic acid (MIANS)

(Invitrogen, Molecular Probes™) by incubation of the protein in 25 mM TrisHCl pH 7.25. A five-fold excess of fluorophore was used and unincorporated fluorophore was removed using a PD-10 column. The concentrations of fluorophore in the products were determined using UV-absorption (as described in section 2.6.3, ε_{330} = 20,400 M^{-1} cm^{-1} for MIANS). To ensure that a single MIANS group had been incorporated, protein concentrations were also calculated using far-UV CD.

To probe for potential interactions, recombinant PfGAP45 was titrated into fixed concentrations of either labelled peptides or recombinant PfMTIP. Uncorrected fluorescence emission spectra were recorded in PBS using a SPEX fluoromax fluorimeter with 4 X 10 mm QS cuvettes (Hellma GmbH & Co. KG). Excitation was at 330 nm (slits 1.7 nm) and emission was scanned from 400 to 600 nm (slits = 5 nm). Fluorescence polarisation measurements were made at a single wavelength (excitation at 330 nm and emission at 520 nm). Theory and data analysis for fluorescence spectroscopy are described in section 4.2.2.

2.10.3 Electrospray ionisation mass spectrometry (ESI-MS)

All machine procedures were conducted by Dr Steven Howell, NIMR, UK.

Protein molecular mass was determined using a stand alone syringe pump (Perkin Elmer, Foster City, CA) coupled to a Platform electrospray mass spectrometer (Micromass, Manchester, UK). Samples were desalted on-line using a 2 mm x 10 mm guard column (Upchurch Scientific, Oak Harbor, WA) packed with 50 micron Poros RII resin (Perseptive Biosystems, Framingham) inserted in place of the sample loop on a rheodyne 7125 valve. Proteins (100 pmol) were injected onto the column in 10% (v/v) acetonitrile, 0.10% (v/v) formic acid, washed with the same solvent and then step eluted into the mass spectrometer in 70% (v/v) acetonitrile, 0.1% (v/v) acetic acid at a flow rate of 10 μl min^{-1}. The mass spectrometer was calibrated using myoglobin.

2.10.4 MALDI-TOF mass spectrometry

All machine procedures were conducted by Dr Steven Howell, NIMR, UK.

Peptides were prepared either by in-gel protein digestion or digestion of proteins in aqueous solution using modified sequencing grade endopeptidase Asp-N (Roche) or trypsin (Promega). For in gel-digestion, proteins were separated by SDS-PAGE as described in section 2.6.5 and detected using the Colloidal Blue staining kit (Invitrogen) following the protocol described in the manual. Protein bands were excised and SDS and colloidal stain extracted with 200 mM ammonium bicarbonate (ABC), 50% (v/v) acetonitrile. Proteins were reduced with 20 mM DTT and washed with 200 mM ammonium bicarbonate (ABC), 50% (v/v) acetonitrile. Proteins were subsequently alkylated using 5 mM iodoacetamide and washed with 20 mM ammonium bicarbonate (ABC), 50% (v/v) acetonitrile. The bands were then dried using 100% (v/v) acetonitrile and re-swollen in 20 µl enzyme diluted to 2 ng μl^{-1} in 5 mM ABC. After overnight digestion at 32°C, the supernatant was acidified by the addition of a 1/10 volume of 4% (v/v) trifluoroacetic acid (TFA). For digestion of proteins in aqueous solution, samples were buffer exchanged with 5 mM ABC and enzymes added at a 1:200 enzyme:protein molar ratio. Reactions were incubated at 37°C for 2 h. Phosphopeptides were isolated from protein digests using a phosphopeptide isolation kit (Pierce). Sample pH was adjusted to 2.5 using 20% (v/v) acetic acid to allow binding of phosphopeptides to SwellGel® Gallium-chelated resin disks. The resin was then washed twice in 0.1% (v/v) acetic acid, twice in 0.1% (v/v) acetic acid, 10% (v/v) acetonitrile and peptides eluted using 0.1 M ABC, pH 9.0.

Experiments were performed using a Reflex III matrix-assisted laser desorption/ionisation time-of-flight (MALDI-TOF) mass spectrometer (Bruker Daltonik GmbH, Bremen, Germany), equipped with a nitrogen laser and a Scout-384 probe, to obtain positive ion mass spectra of digested protein with pulsed ion extraction in reflectron mode. For normal scans, an accelerating voltage of 26 kV was used with detector bias gating set to 2 kV and a mass cut-off of m/z 650.

Post-source decay (PSD) scans were calibrated using the known fragments of [Glu]-fibrinopeptide. Matrix surfaces were prepared using re-crystallised α-cyano-4-hydroxycinammic acid and nitrocellulose using the fast evaporation method (Vorm et al, 1994). Digestion supernatants (0.5 µl) were deposited on the matrix surface and allowed to dry prior to desalting with water. Proteins digested in aqueous buffer were diluted to 0.4 µM in 0.1% (v/v) TFA prior to loading. For peptide mass fingerprinting, ions obtained were searched against the non-redundant protein database placed in the public domain by the National Centre for Biotechnology Information (NCBI) using MASCOT (Perkins, Pappin et al. 1999).

Table 2.1

Constructed plasmids

Vector	Insert	Oligonucleotides	Restriction sites	Resistance	Tags
pQE60	PfGAP45	pQEG45F, pQEG45R	Nco1, BamH1	Ampicillin	C-term hexa-His
pET32Xa/LIC	PfGAP50	pETG50F, pETG50R	LIC cloning	Ampicillin	N-term Trx, S, hexa-His
pPIC9K	PfGAP45	N/A	N/A	Geneticin®	C-term hexa-His

* Construct was synthesised by GENEART and contained a synthetic gene codon-optimised for expression in *P. pastoris*.

Table 2.2

Oligonucleotides

Oligo Name	Forward Sequence 5'-3'	Reverse Sequence 5'-3'
pQEG45	GCGCCCATGGGAAATAAATGTTCA	GCGCGGATCCGCTCAATAAAGG
pETG50	ggtattgagggtcgcCTACGCTTTGCGTCTTT	agaggagagttagagccTTAGGTATCTTTATTTCCC

*Underlined sequences represent sites of action for restriction endonucleases. Lower case sequences represent 5' extensions required for Ligation Independent Cloning.

Table 2.3

Polymerase chain reactions (PCR)

Stage	**Temperature (°C)**	**Duration (min)**
Hot start	95	2
25-35 cycles:		
Denaturation	95	0.5
Annealing	60	0.5
Extension	68-72*	1 per kb
Final extension	68-72*	10
Hold	4	N/A

* The optimum extension temperature for AccuPrime™ Pfx DNA polymerase is 68°C, whereas extension using Taq DNA polymerase is optimal at 72°C.

Table 2.4

Antibodies

Name	Species	Type	*Dilutions for:*			Source
			Western	IFA	IP	
Primary:						
α-PfGAP45	Mouse	Polyclonal serum	1:1,000	1:1000	1:200	Raised in-house
α-PfGAP45	Rabbit	Polyclonal AP[a]	1:2,000	1:10,000	1:400	Raised by Harlan
α-PfGAP50	Mouse	Polyclonal serum	1:1,000	N/A[b]	N/A[b]	Raised in-house
α-PfGAP50	Rabbit	Polyclonal AP[a]	N/A[b]	1:200	1:400	Raised by Harlan
α-PfMTIP	Mouse	Polyclonal AP[a]	1:1,000	1:1,000	1:400	Dr JL Green
α-PfMTIP	Rabbit	Polyclonal AP[a]	1:1,000	1:2000	1:400	Dr JL Green
α-MyoA	Rabbit	Polyclonal serum	1:1,000	N/A[b]	N/A[b]	Dr JC Fordham
α-EBA175	Rabbit	Polyclonal serum	N/A[b]	1:500	N/A[b]	MR4
α-RhopH2	Rabbit	Polyclonal serum	N/A[b]	1:200	N/A[b]	Dr AA Holder
α-$MSP1_{19}$	Rabbit	Polyclonal serum	N/A[b]	1:500	N/A[b]	Dr C Uthaipibull
α-AMA-1	Mouse	Polyclonal serum	N/A[b]	1:100	N/A[b]	Dr CR Jarra
1E1 (α-MSP1)	Mouse	Monoclonal	N/A[b]	1:4,000	N/A[b]	TJ Scott-Finnigan
α-His	Rabbit	Monoclonal	1:1,000	N/A[b]	N/A[b]	Santa Cruz
Secondary:						
α-Mouse IgG HRP[c]	Goat	Polyclonal AP[a]	1:5,000	N/A[b]	N/A[b]	BioRad
α-Rabbit IgG HRP[c]	Goat	Polyclonal AP[a]	1:5,000	N/A[b]	N/A[b]	BioRad
α-Mouse IgG HRP[c]	Donkey	Polyclonal AP[a]	1:10,000	N/A[b]	N/A[b]	Jackson
α-Rabbit IgG HRP[c]	Donkey	Polyclonal AP[a]	1:10,000	N/A[b]	N/A[b]	Jackson
α-Mouse IgG FITC[d]	Rabbit	Polyclonal AP[a]	N/A[b]	1:1,000	N/A[b]	Sigma
α-Rabbit IgG FITC[d]	Mouse	Polyclonal AP[a]	N/A[b]	1:1,000	N/A[b]	Sigma
α-Mouse Alexa fluor®594	Goat	Polyclonal AP[a]	N/A[b]	1:5,000	N/A[b]	Invitrogen
α-Rabbit Alexa fluor®594	Goat	Polyclonal AP[a]	N/A[b]	1,5,000	N/A[b]	Invitrogen

[a]AP: Antibody affinity-purified
[b]N/A: Antibody not used in or was un-suitable for the marked procedure
[c]HRP: Antibody conjugated to horse radish peroxidase
[d]FITC: Antibody conjugated to fluorescein isothiocyanate

Figure 2.1

NADH-coupled kinase assay enzyme reactions

Diagrammatical representation of the enzymatic reactions taking place in NADH-coupled kinase assays. Phosphorylation of the substrate protein catalysed by PfCDPK1 involves the hydrolysis of ATP into ADP and phosphate (Pi). Phosphoenolpyruvate (PEP) is then converted to pyruvate by pyruvate kinase (PK), re-generating ATP. Finally, lactate dehydrogenase (LDH) converts pyruvate into lactate via the oxidation of NADH.

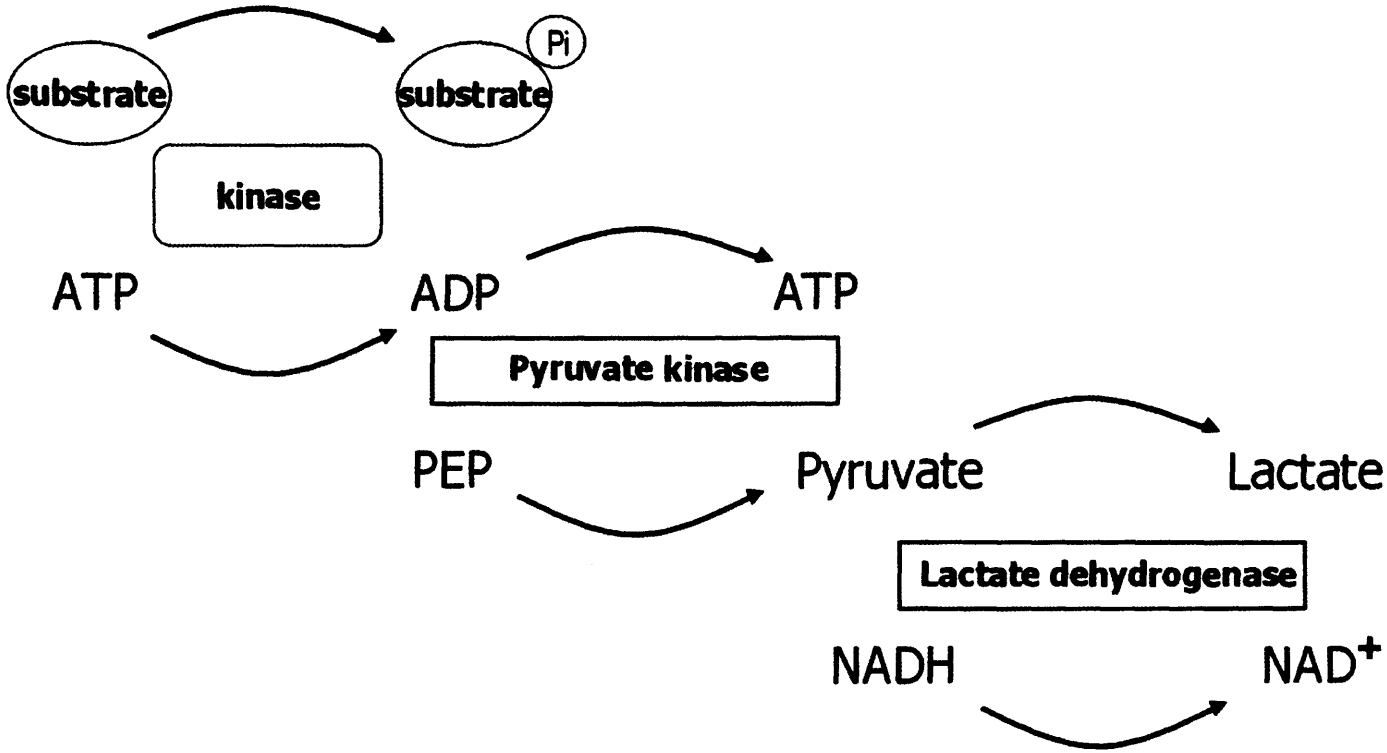
substrate
Pi
substrate
kinase
ATP
ADP
ATP
Pyruvate kinase
PEP
Pyruvate
Lactate
Lactate dehydrogenase
NADH
NAD+

Chapter Three

Expression of GAPs in P. falciparum

3.1 Introduction

In *T. gondii* tachyzoites (Gaskins, Gilk et al. 2004) and *P. falciparum* merozoites (Jones, Kitson et al. 2006; Baum, Richard et al. 2006), GAP45 and GAP50 are associated with MyoA and MLC1/MTIP, forming a tetrameric motor complex. The identification of GAP orthologues in a number of other apicomplexan parasites implies a conserved function for these proteins across the phylum (Gaskins, Gilk et al. 2004). However, at the start of this project, the *P. falciparum* orthologues of GAP45 and GAP50 had only recently been identified (Gaskins, Gilk et al. 2004). Research presented in this chapter is geared towards establishing whether GAPs are expressed in *P. falciparum* and if their functional roles are likely to be comparable throughout Apicomplexa.

Genomic and proteomic information was found in PlasmoDB using gene IDs *PFL1090w* and *PFI0880c*, coding for PfGAP45 and PfGAP50 respectively. Microarray analyses of *PFL1090w* and *PFI0880c* transcription in HB3, 3D7 and Dd2 lines throughout the erythrocytic cycle (Bozdech, Llin et al. 2003; Bozdech, Zhu et al. 2003; Le Roch, Zhou et al. 2003) suggest that levels of expression peak during early to late schizogony, at approximately 39-45 h and 34-42 h post-invasion respectively (figure 3.1). If levels of transcription are comparable to that of translation, these data are consistent with genes coding for proteins that may be involved in host cell invasion.

Polyclonal mouse and rabbit antisera were raised against recombinant forms of both PfGAP45 and PfGAP50, whose production is discussed fully in section 4.2.1. This chapter is focussed on the use of these antisera to examine the expression and specific location of PfGAPs within blood stages. Antisera were all tested individually as their effectiveness varied accordingly to the application. In some cases, purification of antibodies specific to PfGAPs was necessary and is discussed in the relevant sections. In order to establish the conserved role of PfGAPs in host cell invasion, analyses were performed in parasites synchronised at ~42-48 h post-invasion. At this timepoint, parasites will predominantly be late schizonts or free merozoites that have entered the blood post-rupture.

Analyses described in this chapter were developed based on the characterisation of GAPs in *T. gondii*, as described fully by Gaskins, Gilk et al. 2004.

TgGAP45 was initially identified in tachyzoite pellicle preparations extracted with DOC. This was the first evidence suggesting the protein is associated with membranes. Thus, to determine a more specific solubility profile for PfGAPs, parasites were lysed in a sequential series of buffers designed to separate proteins according to their location within cells. Parasites were initially lysed in a hypotonic buffer and subjected to freeze/thaw. The combination of increased osmotic pressure created by the buffer and contraction of ice crystals that occurs during freeze/thawing causes cells to swell and burst releasing soluble, cytoplasmic proteins. Proteins insoluble in this buffer were then extracted using a high salt buffer. High salt is known to disrupt ionic interactions between some peripheral membrane proteins and their protein or lipid binding components. The remaining insoluble proteins were then extracted in a series of detergents with increasing ionic strength.

Detergents are amphipathic molecules. Like biological membrane components, they have hydrophobic-associating properties as a result of their non-polar tails. However, they are also water-soluble and thus permit the solubilisation of otherwise water-insoluble membrane-bound components. Detergent strength is categorised by the nature of the hydrophilic head group that can be ionic, non-ionic or zwitterionic. NP-40 is a mild, non-ionic, non-denaturing detergent that can be used to solubilise membrane proteins and their associating protein partners in a native state. SDS is a strong, anionic detergent that will totally disrupt membranes as well as protein-protein interactions, solubilising proteins in a denatured form. DOC is another anionic detergent that is far less denaturing than SDS, although it can still disrupt non-covalent protein-protein interactions. Details regarding protein extraction methods are reviewed by Selinsky (Selinsky 2003) and Ahmed (Ahmed 2004).

For GAPs to function in the motor complex, they must not only be expressed at the right time but in the same location of the parasite as MyoA and MLC1/MTIP. Convincing immunofluorescence analyses performed in tachyzoites have shown that TgGAPs are located at the IMC. Furthermore, immunoEM experiments demonstrated that TgGAP45 was specifically located at the side of the IMC that faces the plasma membrane. Similar analyses were therefore undertaken to determine the specific location of PfGAPs in developing merozoites.

TgGAP45 can be immunoprecipitated with TgGAP50, TgMyoA and TgMLC1 when parasites were lysed in Triton X-100. Extraction using SDS was shown to disrupt these interactions and the antibody precipitated only GAP45, suggesting there was no cross-reactivity. To confirm the tetrameric complex also exists in *P. falciparum*, similar immunoprecipitations were performed by extracting parasites in SDS or NP-40. NP-40 is structurally similar to Triton X-100; it is also a mild, non-ionic detergent that solubilises proteins in their native state, often retaining protein-protein interactions.

GAP50 and its orthologues all contain a predicted C-terminal transmembrane domain. In addition, they contain an N-terminal hydrophobic stretch that in *T. gondii*, has been shown to act as a cleavable signal peptide (Gaskins, Gilk et al. 2004). Therefore, this protein is most likely co-translationally inserted into the endoplasmic reticulum and subsequently transported to the IMC via the secretory pathway. In contrast, MyoA, MLC/MTIP, GAP45 and their related orthologues do not contain N-terminal sequences coding for signal peptides or anchors. Moreover, their sequences do not contain any hydrophobic regions that may correspond to transmembrane anchors. Hence, these proteins are likely synthesised in the cytosol on cytoplasmic ribosomes.

In *T. gondii*, pulse-chase labelling experiments have suggested that TgMyoA, TgMLC1 and TgGAP45 form an initial complex in the cytosol before being trafficked to the IMC by an unknown mechanism. There, they associate with TgGAP50 to form the complete tetrameric motor complex. Consequently,

similar radiolabelling experiments were designed to examine the formation of the *P. falciparum* complex over time.

3.2 Results

3.2.1 PfGAPs are expressed in late blood stages

To determine whether PfGAPs are expressed in the late blood stages, antibodies were used to detect PfGAPs in both synchronised late schizonts (~42 h post invasion) and free merozoites. Rabbit and mouse PfGAP45 antisera detected a doublet in late schizonts and a single band in free merozoites (figure 3.2 A). In reduced samples, the doublet corresponded to apparent molecular masses of ~37 and ~39 kDa and the single band, ~40 kDa.

When rabbit PfGAP50 antiserum was used to probe membranes, a significant amount of background staining was observed that could not be reduced even after blots were blocked overnight. In an attempt to improve clarity, the antiserum was subjected to three rounds of purification (as described in section 2.7.2). Initial purification of IgG using protein G sepharose did reduce background, although not significantly. Subsequent affinity putification further reduced background staining although a significant amount remained such that bands corresponding to PfGAP50 were obscured. Recombinant PfGAP50 contained a large N-terminal tag comprising ~12 kDa *E. coli* Trx fused to an S-tag and a hexa-His tag. A recombinant form of this tag was expressed in *E. coli* BL21gold(DE3) cells and purified using Ni-NTA agarose, as described in sections 2.4.2 and 2.6.1. This protein was used to generate an affinity column in order to deplete antibodies raised against the tag region. Although background staining was significantly reduced after this step, PfGAP50 could not be detected in blots.

Conversely, mouse PfGAP50 antiserum was much more effective in Western blotting. A single ~45 kDa band was detected in both schizont and free merozoite extracts, reduced or non-reduced (figure 3.2 B).

3.2.2 PfGAPs are associated with parasite membranes

To determine whether PfGAPs are located in membranes, antibodies were used to detect protein extracted from late schizonts in a sequential series of buffers designed to separate proteins according to their location within cells.

Nitrocellulose blots probed using mouse PfGAP45 and PfGAP50 antisera are shown in figure 3.3. The majority of PfGAP45 (A) and PfGAP50 (B) were extracted using a detergent. The intensity of bands observed in each lane was measured using ImageJ software (National Institute of Health) and represented as a percentage of total intensity (table 3.1). It should be noted that these figures are approximations only and do not take into account that the relationship between protein abundance and band intensity may not be linear.

For PfGAP45, the majority of protein appeared to be soluble in NP-40 and the remainder in DOC. Interestingly, where both NP-40 and DOC solubilise similar quantities of the ~39 kDa band, a greater proportion of the ~37 kDa band was extracted in the milder detergent. Likewise, the majority of PfGAP50 appeared to be soluble in NP-40. Smaller proportions of the protein were also extracted in ionic detergents DOC and SDS although a fraction appeared to be insoluble even in the latter. Interestingly, in contrast to PfGAP45, ~15% of PfGAP50 was also soluble in the high salt buffer.

3.2.3 PfGAPs are located at the periphery of merozoites

To determine a more specific location for PfGAPs within developing merozoites, antibodies were initially used to detect proteins in IFAs (described in sections 2.7.5). Both mouse PfGAP45 antiserum and rabbit anti-PfGAP50 detected a ring of fluorescence around the periphery of developing merozoites within late schizonts (figure 3.4, A and B respectively). This pattern was distinct from that observed using antibodies detecting either micronemal (EBA-175 and PfAMA-1) or rhoptry (RhopH2) proteins. In contrast, counterstaining with antibodies raised against PfMTIP or merozoite surface protein MSP1 produced overlapping staining patterns.

ImmunoEM was subsequently used to detect proteins in ultra thin merozoite sections using affinity-purified rabbit anti-PfGAP45 and anti-PfGAP50 separately. Both antibodies reacted well, with a number of gold particles being observed in individual merozoites (figure 3.5). The distribution of gold particles observed for each antibody was similar, the majority being located around the periphery of parasites, within ~50 nm of the surface.

3.2.4 PfGAPs form a complex with PfMyoA and PfMTIP

Initial immunoprecipitations were performed using affinity purified rabbit anti-PfGAP45. Regardless of lysis conditions, the antibody repeatedly precipitated a number of non-specific proteins, as assessed by control experiments performed using pre-immune serum. In an attempt to improve this, pre-immune serum was incubated with supernatants overnight to immunoprecipitate non-specific proteins. Unfortunately, no significant reduction in background was observed. However, in similar experiments, mouse PfGAP45 antiserum immunoprecipitated appreciably fewer non-specific proteins. Immunoprecipitation from SDS-lysed late schizonts identified a ~37-39 kDa doublet corresponding to PfGAP45 (figure 3.6 A, panel A, lane 2). Additional bands of ~90 kDa, ~78 kDa, ~75 kDa, 50 kDa, ~45 kDa and ~30 kDa were precipitated when parasites were lysed in NP-40 (figure 3.6 A, panel A, lane 4).

Western blotting was performed on immunoprecipitated samples from NP-40-lysed parasite extracts using rabbit antibodies specific for the other three known components of the tetrameric motor complex (figure 3.6, panel B). The ~90 kDa band was detected using PfMyoA antiserum whereas ~45 kDa and ~30 kDa bands were identified as PfGAP50 and PfMTIP respectively.

To analyse the composition of the tetrameric complex in greater detail, antibodies raised against all four components were used in parallel to immunoprecipitate proteins from NP-40-lysed late schizonts (figure 3.6 B). Interestingly, each antibody appeared to precipitate components of the complex in varying proportions. The relative intensities of bands observed in each

immunoprecipitation were measured using ImageJ and are represented as a percentage of total intensity (table 3.2). Although all four antibodies appear to precipitate PfMyoA, PfMTIP and PfGAP50, bands corresponding to PfGAP45 were not visible in any immunoprecipitations except those performed with PfGAP45 antiserum.

3.2.5 The tetrameric motor complex is assembled in two stages

To investigate the dynamics of the *P. falciparum* motor complex over time, immunoprecipitations using mouse PfGAP45 antiserum were performed on samples obtained from pulse-chase labelling experiments described in section 2.5.3 (figure 3.7). To retain interactions within the complex, samples were extracted using NP-40 buffer.

For each protein component, relative intensities of bands detected at each timepoint were analysed using image J and represented as a percentage of total intensity (table 3.3). Throughout the timecourse, ~90 kDa and ~30 kDa bands corresponding to PfMyoA and PfMTIP respectively both show an overall decrease in intensity. In addition to these proteins, the ~37 kDa corresponding to PfGAP45 was observed after radiolabelling for 15 min (t=0). However, the intensity of this band decreased in the sample extracted 60 min post-labelling (t=60) and was very faint 2 h post-labelling (t=120). Interestingly, ~39 kDa and ~45 kDa bands (corresponding to PfGAP45 and PfGAP50 respectively) that were very faint in the pulse increased in intensity throughout the chase.

3.2.6 PfGAP45 is directly associated with parasite membranes

If the trimeric complex of PfMyoA, PfMTIP and PfGAP45 is formed in the cytoplasm, it may have a different solubility profile to that of the membrane-associated tetrameric complex. To determine relative solubility profiles for these different complexes, mouse PfGAP45 antiserum was used to immunoprecipitate proteins from samples labelled in pulse-chase experiments. For each timepoint,

schizont pellets were lysed in a sequential series of buffers described in section 2.5.4, to extract proteins according to their location within cells (figure 3.8).

In all samples analysed, the antiserum precipitated only PfGAP45. At each timepoint in the labelling experiment, PfGAP45 could only be extracted in the presence of a detergent. For each timepoint, the intensity of bands observed in each sample was measured using ImageJ and represented as a percentage of total intensity (Table 3.4). At t=0 (pulse), a greater proportion of PfGAP45 was soluble in NP-40 than at any other timepoint and by t=120, the majority was extracted in DOC.

3.3 Discussion

Results presented in this chapter provide significant evidence to suggest a conserved myosin motor complex exists throughout Apicomplexa that may underlie a common mechanism of invasion.

As suggested by the microarray data, *P. falciparum* orthologues of GAP45 and GAP50 are expressed in the blood stage invasive merozoite at ~42 h post-invasion. However, it cannot be confirmed whether levels of translation correlate directly to that of transcription as protein would need to have been extracted at similar timepoints throughout the erythrocytic cycle. In the case of PfGAP45, the presence of a doublet in schizonts suggests the protein is either processed or modified within the parasite. Given that the single band observed in free merozoites corresponds to a higher molecular mass, post-translational modification would seem more likely. This is supported by results obtained from pulse-chase labelling experiments: apparent molecular masses observed for PfGAP45 increase throughout the timecourse

Another intriguing observation is that although PfGAP45 migrates at molecular masses of ~37-40 kDa, ProtParam calculates a mass of 23,631.8 Da for the protein. Such anomalous migration has been observed previously in *T. gondii* (Gaskins, Gilk et al. 2004) and more recently in *P. falciparum* (Baum, Richard et al. 2006; Jones, Kitson et al. 2006). The phenomenon has been attributed to either a high content of glutamic acid that can inhibit SDS binding or the presence of a putative coiled-coil region that may give rise to an extended conformation. Given that PfGAP45 may be modified in the parasite, one or more of these modifications may also affect the mobility of this protein in SDS-PAGE.

In non-reducing SDS-PAGE conditions, PfGAP45 appears to separate at higher molecular masses. This suggests the protein contains intra-molecular cystines that may affect protein conformation and thus mobility. In contrast, bands detected for PfGAP50 all corresponded to approximately the same apparent molecular mass. This suggests the protein is neither modified within the parasite, nor does it contain cystines.

Both GAPs are predominantly associated with parasite membranes. Solubility tests were performed on the assumption that cell lysis using hyptonic and high salt buffers would not disrupt intra-complex associations. If that were the case, it would seem likely that PfGAP45 only remains in association with parasite membranes by means of an interaction with another component of the membrane-bound complex. However, in analyses performed using material obtained from pulse-chase labelling experiments, it became apparent that high salt does in fact disrupt the tetrameric complex. In the absence of the other complex components, PfGAP45 is not extracted in high salt buffer. Therefore, the protein must be directly associated with membranes. Milder detergents repeatedly extracted the ~37 kDa form of PfGAP45 more readily than the ~39 kDa form. This implies the latter may have a stronger association with membranes.

Although PfGAP50 is proposed to be the anchor for the tetrameric complex (Gaskins, Gilk et al. 2004), a small proportion is extracted in high salt buffer. Although the mobility of this form was not significantly altered, a small deviation in molecular mass may not be discernible by SDS-PAGE. Thus, it may be that some PfGAP50 is in fact modified or processed in the parasite resulting in disruption of membrane attachment. Alternatively, it may be that this fraction of the total extracted PfGAP50 represents protein that has just been translated on ribosomes in the ER.

Both GAPs are found in a peripheral location comparable to that of tetrameric complex component PfMTIP and merozoite surface protein MSP1. However, evidence suggests these proteins are located in the IMC and plasma membrane respectively (Holder and Freeman 1981; Bergman, Kaiser et al 2003; Baum, Richard et al. 2005; Jones, Kitson et al. 2006, Green, Martin et al. 2006).

P. falciparum merozoites are among the smallest of apicomplexan zoites. As a consequence, parasite morphology is not easily resolved using microscopic techniques. Immunofluorescence and immunoEM analyses performed here could not conclusively ascertain which membrane system PfGAPs are associated with. The conditions used in immunoEM can often lead to poor resolution of parasite

morphology in comparison to standard transmission EM. This is apparent in images presented here, as it is difficult to identify pellicular membranes in some regions of parasites, let alone distinguish between them. Additionally, the gold particles used to detect proteins were 2 nm in diameter. As the distance between the merozoite surface and the IMC appears to be less than 200 nm (also observed in Baum, Richard et al. 2006), analyses within such a small range are unlikely to be accurate.

In developing merozoites within schizonts, PfGAP45 is found in complex with PfMTIP, PfMyoA, and PfGAP50. This evidence is in concordance with that recently obtained for *P. falciparum* (Baum, Richard et al. 2006; Jones, Kitson et al. 2006) and confirms that the tetrameric complex comprises the same constituent proteins as the equivalent complex from *T. gondii* tachyzoites (Gaskins, Gilk et al. 2004), implying a high degree of conservation within the phylum. The identities of additional co-precipitated proteins corresponding to molecular masses ~78 kDa, ~75 kDa and ~50 kDa are currently unknown. Very recent evidence suggests that the ~50 kDa band may in fact correspond to protein kinase B (PKB) (Vaid, Thomas et al. 2008); a discovery that is discussed further in chapter five. Perhaps the other two bands represent additional kinases or phosphatases that may be important in modifying components of the motor complex. There is also a possibility they are breakdown products of PfMyoA, as the antiserum used in Western blotting was not raised against the full length protein.

When the complex is extracted using antibodies raised against the four different protein components, the intensity of bands observed within and between lanes corresponding to each immunoprecipitation varies significantly. Similar variations have been observed previously in *P. falciparum* (Baum, Richard et al. 2006). In any given sample, band intensity may not directly correspond to protein abundance. This is because incorporation of [^{35}S] is related to the number of cysteine and methionione residues contained within proteins. In general, higher molecular mass proteins will contain a greater number of these residues and incorporate more radiolabel. In addition, individual polyclonal antisera and

antibody preparations used to extract the complex may comprise differing quantities of antibody specific for the antigen in question. Hence, the absolute quantity of protein precipitated may also vary for each antibody. Nonetheless, given that variation in radiolabel incorporation will be constant, relative band intensities observed in each lane should be the same if all expressed protein is complexed and the population of complexes is homogenous. It may be that the complex is unstable under the conditions used in these experiments and as a result, only small quantities could be isolated. However, it is also possible that at this timepoint in erythrocytic development, merozoites may actually contain a mixture of free protein, di-, tri- and tetrameric complexes.

Pulse-chase labelling experiments confirm that in concordance with *T. gondii* (Gaskins, Gilk et al. 2004), an initial ternary complex of PfMyoA, PfMTIP and PfGAP45 is likely to form in the cytosol prior to association with PfGAP50 at the IMC or plasma membrane. However, the fact that PfGAP45 and the ternary complex comprising PfGAP45, PfMyoA and PfMTIP appeared to be wholly associated with membranes conflicts with evidence from *T. gondii* suggesting the ternary complex is not membrane-bound (Gaskins, Gilk et al. 2004). It may be that the timepoint at which these analyses were made (~42-44 h post-invasion) is a little too late to extract cytoplasmic PfGAP45 and the ternary complex. It is unclear whether the trimeric complex is more stable than the tetrameric complex under lysis conditions used in these experiments. This may explain why the intensity of bands corresponding to PfMyoA and PfMTIP decreases as the tetrameric complex forms. Alternatively, the latter may in fact comprise less of these two proteins. Given the implication that subsets of complexes may exist at the timepoint being analysed here, it is possible that certain components of the motor complex have additional roles in the parasite that are yet to be discovered. Interestingly, this phenomenon was not observed in the *T. gondii* timecourse (Gaskins, Gilk et al. 2004). In fact, intensities of bands corresponding to TgMyoA and TgMLC1 appear to increase in the chase. Once again, this may underlie a functional difference between the two parasites.

Collectively, data obtained from parasite labelling experiments imply that formation of the tetrameric complex may be a highly dynamic and intricate process that is far from being fully deciphered.

Table 3.1

Solubility of PfGAPs in developing merozoites

	(% protein extracted)					
	Hypotonic	**High salt**	**NP-40**	**DOC**	**SDS**	**pellet**
PfGAP45 (~37 kDa)	0	0	55.55	44.45	0	0
PfGAP45 (~39 kDa)	0	0	67.60	32.40	0	0
PfGAP50	0	15.24	47.65	13.10	19.16	4.86

Table 3.2

Immunoprecipitation of the tetrameric complex

	Antibodies used in immunoprecipitation			
	α-PfGAP50	**α-PfGAP45**	**α-PfMTIP**	**α-PfMyoA**
PfMyoA	22.63	28.576	56.38	55.88
PfGAP50	64.95	9.251	10.63	25.66
PfGAP45	0	40.695	0	0
PfMTIP	12.42	21.478	32.99	18.46

Table 3.3

Variation in the motor components ~42-44 h post-invasion

	t=0	**t=15**	**t=30**	**t=60**	**t=120**
PfMyoA	24.3	20.4	22.0	19.1	14.2
PfGAP50	13.4	16.5	21.5	23.7	24.9
PfGAP45 (~39 kDa)	9.9	10.9	15.7	28.1	28.7
PfGAP45 (~37 kDa)	23.2	21.8	23.6	20.9	11.3
PfMTIP	23.0	19.8	22.2	18.7	16.2

Table 3.4

Variation in solubility of PfGAP45 ~42-44 h post-invasion

	(% protein extracted)				
	Hypotonic	**High salt**	**NP-40**	**DOC**	**SDS**
t=0	0	0	52.03	32.09	15.88
t=15	0	0	42.13	40.78	17.09
t=30	0	0	44.47	38.34	17.19
t=60	0	0	42.47	40.50	17.02
t=120	0	0	32.40	46.25	21.35

Figure 3.1

Transcriptional profiles of genes coding for PfGAPs

Intraerythrocytic transcriptional profiles for *PFL1090w* (A) and *PFI0880c* (B) (coding for PfGAP45 and PfGAP50 respectively) in *P. falciparum* 3D7 (red), HB3 (blue) and Dd2 (yellow) cell lines (Bozdech, Llinas et al. 2003; Bozdech, Zhu et al. 2003; Llinas, Bozdech et al. 2006). DNA microarrays using long oligonucleotides representing predicted open reading frames (ORFs) in the 3D7 genome were used to examine mRNA expression across 48 individual 1 h timepoints in the intraerythrocytic cycle. To measure the relative abundance of mRNAs throughout the cycle, total RNA from each timepoint (labelled with Cy5) was compared to an arbitrary reference pool of total RNA (labelled with Cy3) from all timepoints in a standard two-color competitive hybridization (Eisen and Brown, 1999). Transcriptional profiles are represented by the mean-centered series of ratio measurements for the corresponding oligonucleotide(s).

(A)

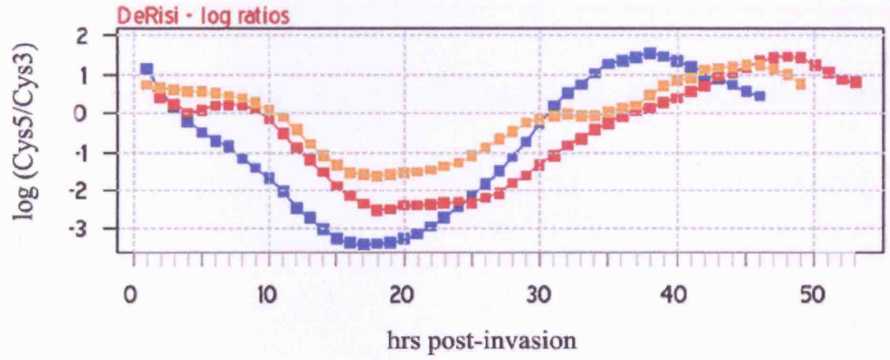
DeRisi - log ratios
log (Cys5/Cys3)
2
1
0
-1
-2
-3
0
10
20
30
40
50
hrs post-invasion

(B)

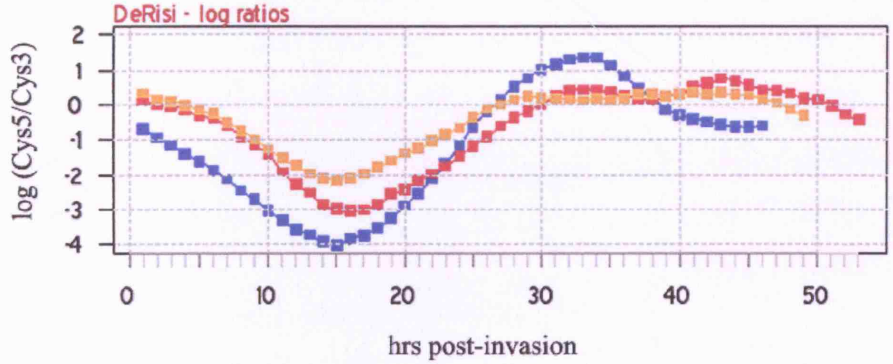
DeRisi - log ratios
log (Cys5/Cys3)
2
1
0
-1
-2
-3
-4
0
10
20
30
40
50
hrs post-invasion


HB3
3D7
DD2

Figure 3.2

PfGAPs are expressed in the late blood stages

Western blot analyses of protein extracted from late schizonts (~42 h post-invasion) and free merozoites, separated by SDS-PAGE in both reducing (R) and non-reducing (NR) conditions. (A) In reducing conditions, mouse PfGAP45 antiserum detected a ~37-39 kDa doublet in schizonts and a single ~40 kDa band in free merozoites. A similar pattern was observed in non-reducing conditions, except bands appeared to shift, i.e. separate at slightly higher apparent molecular masses. (B) Mouse PfGAP50 antiserum detected a ~45 kDa band in both schizonts and free merozoites, regardless of conditions used. Molecular mass markers are shown on the left hand side of panels.

(A)


R
NR
kDa
Sch
Mer
Sch
Mer
75
50
37
25

(B)

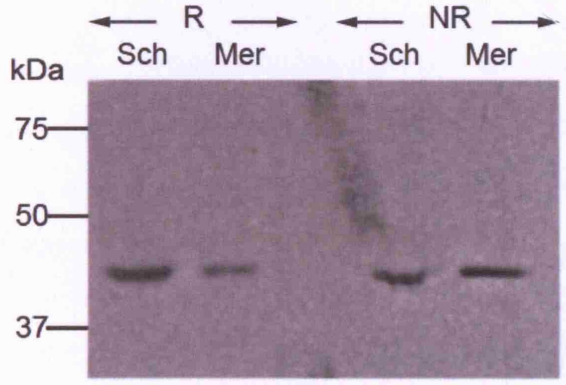
R
NR
kDa
Sch
Mer
Sch
Mer
75
50
37

Figure 3.3

PfGAPs are predominantly associated with membranes

Western blot analyses of late schizonts (~42 h post-invasion) extracted in a sequential series of buffers designed to separate proteins according to their location within cells. (A) Detection using mouse PfGAP45 antiserum demonstrated that the majority of PfGAP45 was extracted in NP-40; the remainder in DOC. Where fairly equal quantities of the ~39 kDa band were soluble in both detergents, a higher proportion of the ~37 kDa was soluble in NP-40. (B) Blots probed with mouse PfGAP50 antiserum showed that different proportions of PfGAP50 were extracted in various conditions. A small proportion was soluble in high salt, with the majority extracted in NP-40. Some protein was extracted in DOC as well as SDS, although a fraction was insoluble even in SDS (visible in the pellet lane). See table 3.1 for more precise estimates of relative band intensities. Asterisks represent possible non-specific detection of parasite haemoglobin. This may have occurred as the protein is likely to be highly concentrated in samples extracted using hypotonic lysis buffer. Molecular mass markers are shown on the left hand side of panels.

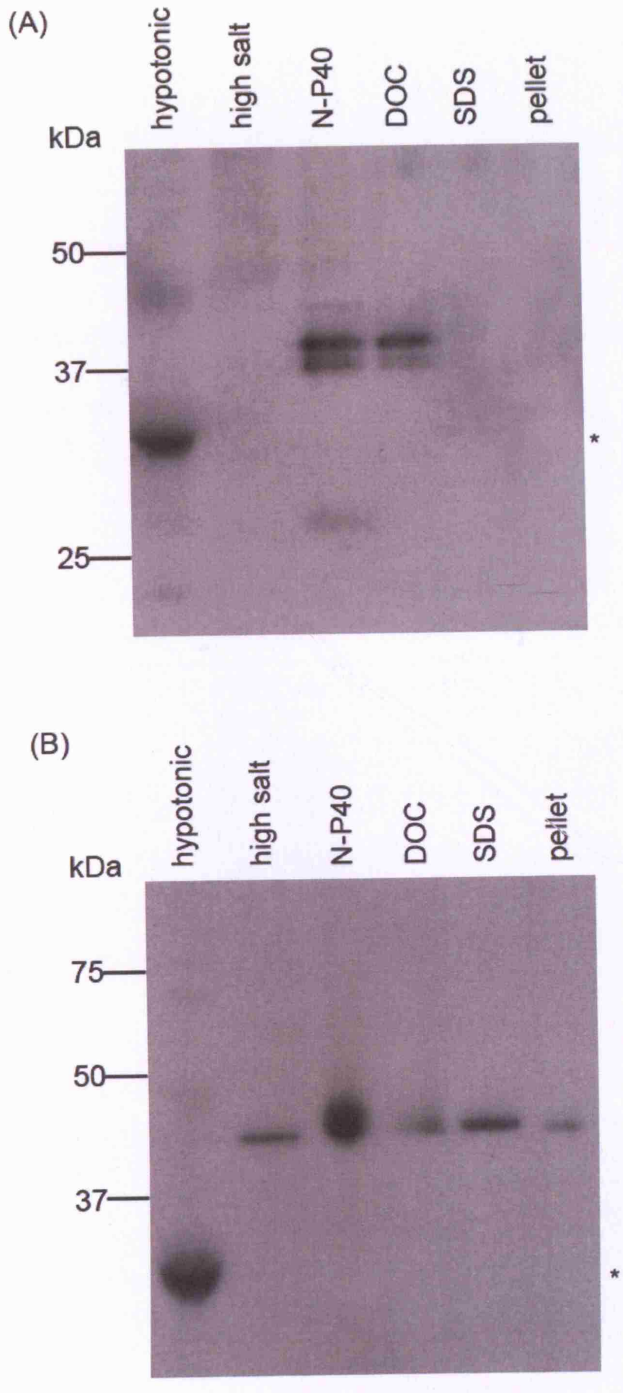
(A)
hypotonic
high salt
N-P40
DOC
SDS
pellet
kDa
50
37
25
*
(B)
hypotonic
high salt
N-P40
DOC
SDS
pellet
kDa
75
50
37
*

Figure 3.4

PfGAPs are located at the periphery of merozoites

Indirect co-immunofluorescence assays performed on late schizonts (~42 h post-invasion). Mouse PfGAP45 (A) or rabbit PfGAP50 (B) antisera both gave a pattern of fluorescence corresponding to location around the periphery of developing merozoites. Staining patterns were indistinguishable from those detected using antibodies raised against another component of the glideosome (PfMTIP), or surface protein MSP1/MSP1$_{19}$. However, they did not co-localise with patterns observed using antibodies raised against proteins located in apical organelles (EBA175, RhopH2 and PfAMA-1).

(A)

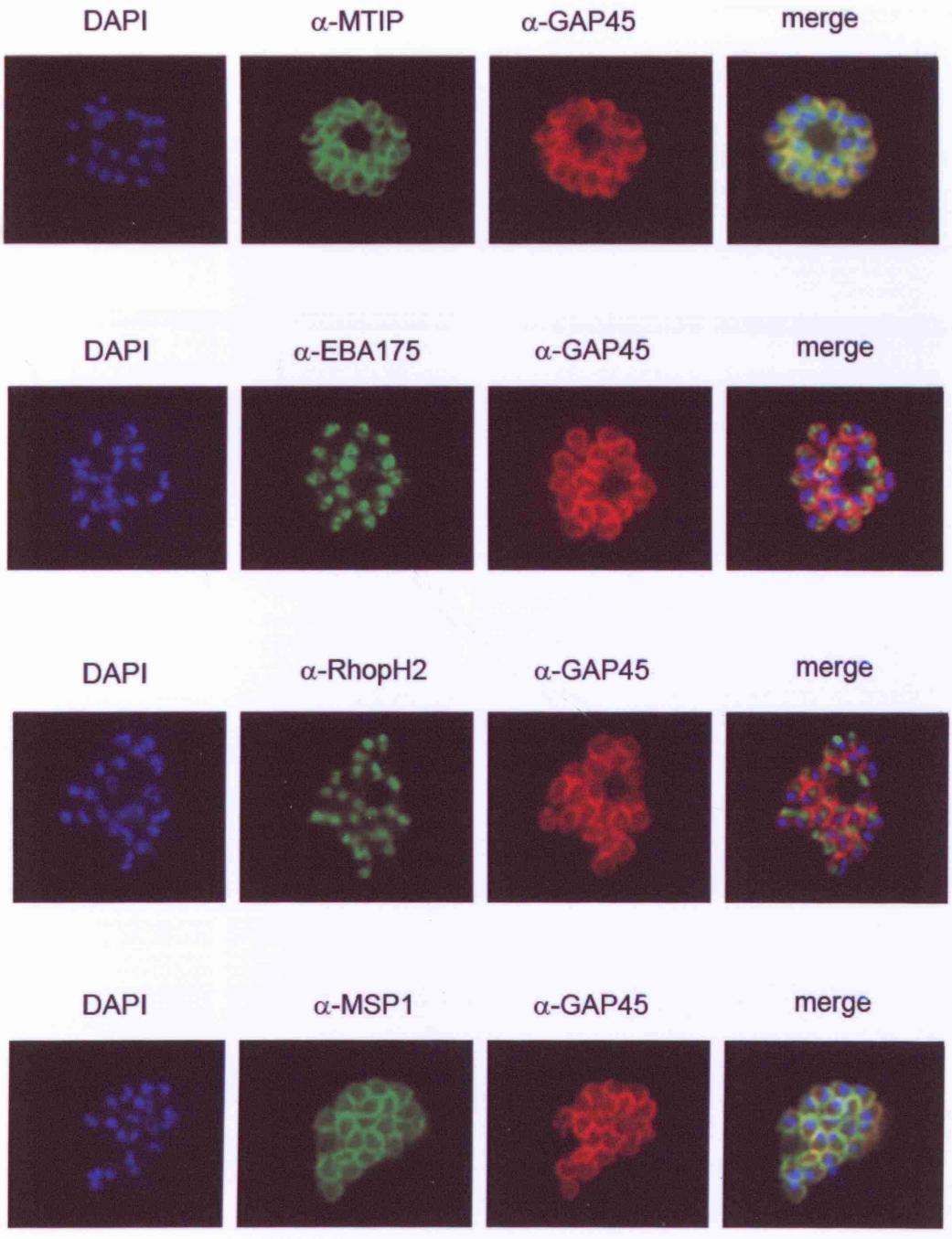
DAPI
α-MTIP
α-GAP45
merge
DAPI
α-EBA175
α-GAP45
merge
DAPI
α-RhopH2
α-GAP45
merge
DAPI
α-MSP1
α-GAP45
merge

(B)

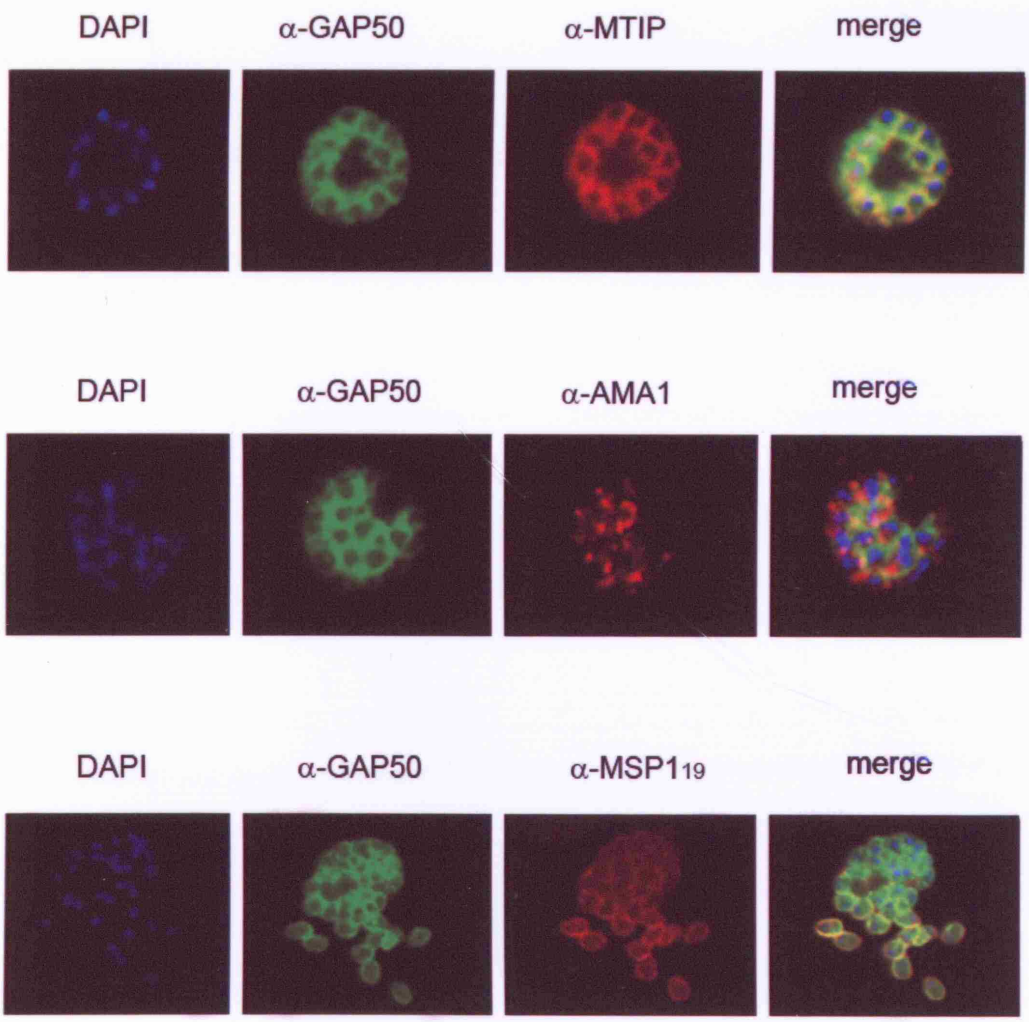
DAPI
α-GAP50
α-MTIP
merge
DAPI
α-GAP50
α-AMA1
merge
DAPI
α-GAP50
α-MSP1$_{19}$
merge

Figure 3.5

PfGAPs are associated with pellicular membranes

Immunoelectron microscopy of ultra-thin merozoite sections labelled with affinity-purified rabbit anti-PfGAP45 (A) and PfGAP50 (B). R, rhoptries; M, micronemes; pmn, pellicular membrane network. For both antibodies, the majority of gold particles decorated the periphery of merozoites, with minimal cytoplasmic or extracellular staining. Staining was confined to an electron-dense region of the periphery which extends ~50 nm from the cell surface and contains the pellicular membranes (plasma membrane and IMC). Merozoites labelled with pre-immune sera did not give rise to any staining. (C) Magnification of merozoite periphery stained with anti-PfGAPs.

(A)

α-GAP45

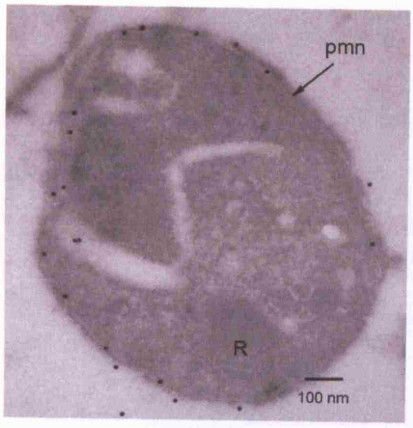

pre-immune

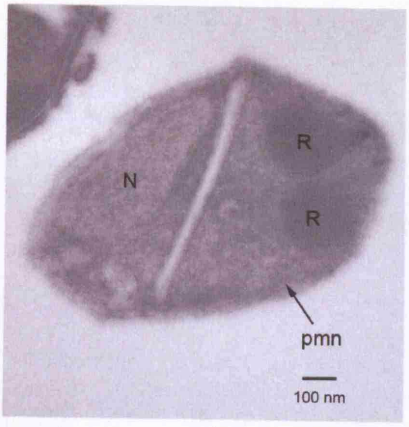

(B)

α-GAP50

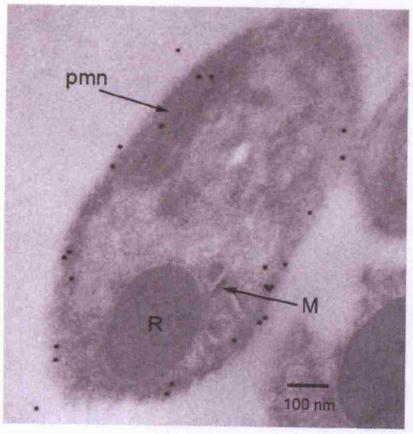

pre-immune

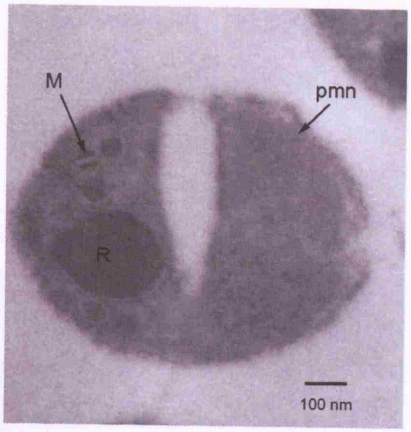

(C)

α-GAP45

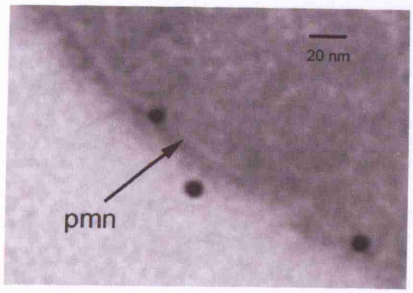

α-GAP50

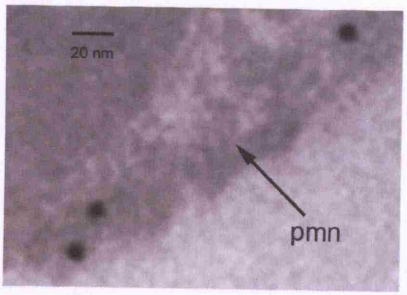

Figure 3.6

The tetrameric complex is conserved in *P. falciparum*

(A) Panel a: Autoradiograph of immunoprecipitation of [^{35}S]-labelled late schizonts (~42 h post-invasion) using mouse PfGAP45 antiserum. When parasites were extracted in SDS, PfGAP45 migrated as a ~37-39 kDa doublet (lane 2). In NP-40, the antiserum precipitated additional ~90, ~75, ~50, ~45 and ~30 kDa bands (lane 4). Lanes 1 and 3 are control immunprecipitations performed using pre-immune serum. Panel b: Western blot analyses of proteins precipitated from extracts prepared in NP-40. Mouse PfGAP45 antiserum precipitated PfMyoA (~90 kDa), PfGAP50 (~45 kDa) and PfMTIP (~30 kDa) (lane 1). Lane 2 contains control immunoprecipitations performed using pre-immune serum. Asterisks represent cross-reactivity of antisera with immunoglobulin heavy and light chains. (B) Autoradiograph of immunoprecipitation of [^{35}S]-labelled late schizonts (~42 h post-invasion) using antibodies raised against all four components of the tetrameric complex (as marked above each lane). Each antibody appeared to precipitate varying quantities of individual complex components (see table 3.2 for estimates of relative band intensities). Molecular mass markers are shown on the left hand side of panels.

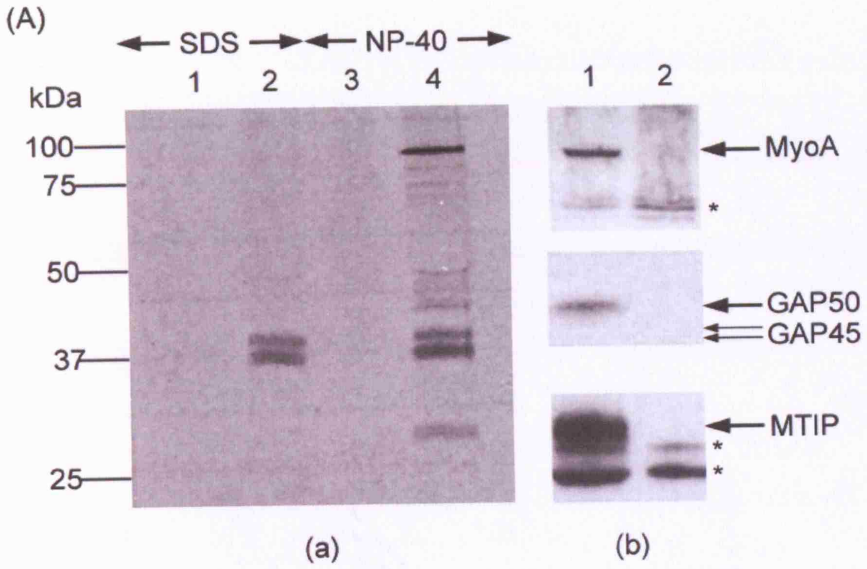
(A)
SDS
NP-40
1
2
3
4
kDa
100
75
50
37
25
(a)
1
2
MyoA
*
GAP50
GAP45
MTIP
*
*
(b)

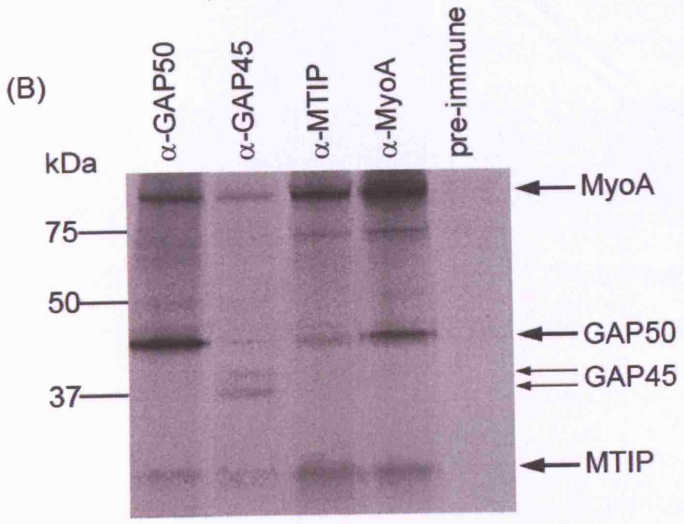
(B)
α-GAP50
α-GAP45
α-MTIP
α-MyoA
pre-immune
kDa
75
50
37
MyoA
GAP50
GAP45
MTIP

Figure 3.7

The *P. falciparum* tetrameric complex is formed in two stages

Autoradiograph of immunoprecipitations performed on samples extracted in NP-40 during pulse-chase labelling experiments, using mouse PfGAP45 antiserum. At t=0, corresponding to 15 min of labelling, bands of ~90 kDa (PfMyoA), ~37 kDa (PfGAP45) and ~30 kDa (PfMTIP) were observed (lane 1). Very faint ~39 and ~45 kDa bands corresponding to PfGAP45 and PfGAP50 are also discernible. During the chase (lanes 3, 5, 7 and 9), the ~39 and ~45kDa bands increased in intensity whereas bands corresponding to PfMyoA and PfMTIP decreased in intensity (see table 3.3 for more precise estimations of relative band intensities). Lanes 2, 4, 6 and 8 are control immunoprecipitations using pre-immune serum. Asterisks represent ~75 kDa and ~50 kDa bands whose identities are unknown. Molecular mass markers are shown on the left hand side of panels.

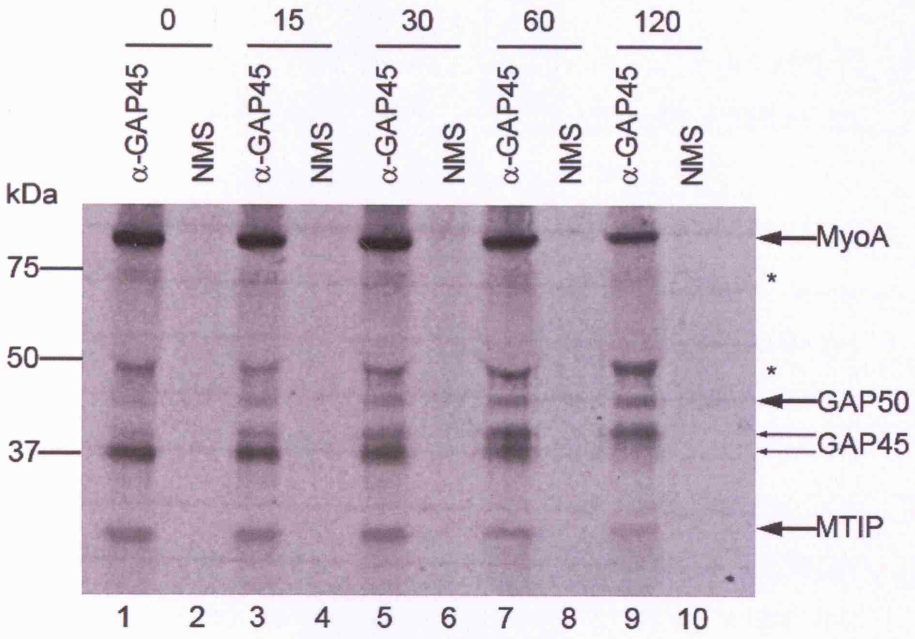
0
15
30
60
120
α-GAP45
NMS
kDa
75
50
37
MyoA
*
*
GAP50
GAP45
MTIP
1 2 3 4 5 6 7 8 9 10

Figure 3.8

PfGAP45 is directly associated with membranes

Immunoprecipitations performed on late schizonts (~42 h post-invasion) from pulse-chase labelling experiments, extracted in a series of buffers designed to separate proteins according to their location within cells. At each timepoint and under all buffer conditions, mouse PfGAP45 antiserum precipitated only bands of molecular masses corresponding to PfGAP45 (t=0, ~37 kDa; t=15, t=30 and t=60, ~37-39 kDa doublet; t=120, ~37 kDa). At t=0, the majority of PfGAP45 was extracted in NP-40 whereas by t=120, a greater proportion was extracted in DOC. See table 3.4 for more precise estimates of relative band intensities. Asterisks represent ~50 and ~47 kDa bands of unknown identity. Molecular mass markers are shown on the left hand side of panels.

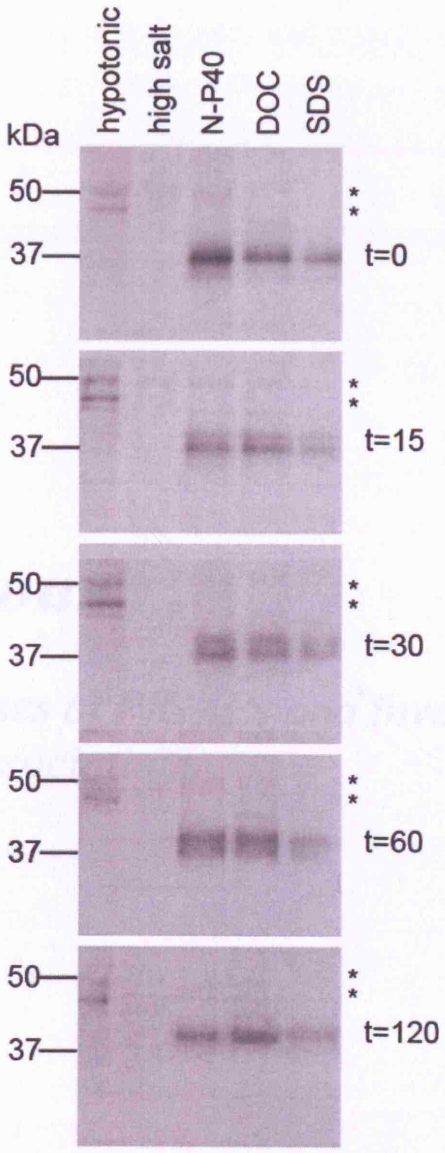
hypotonic
high salt
N-P40
DOC
SDS
kDa
50
37
t=0
t=15
t=30
t=60
t=120

Chapter Four

Structural analyses of PfGAPs and investigation of intra-complex associations

4.1 Introduction

The biological activity of a protein is often dependent on its ability to fold into a specific, stable conformation. At present, little is known about the three-dimensional structure of GAPs. Given that orthologues have been identified in a number of apicomplexan parasite species and sequences appear to be highly conserved (Gaskins, Gilk et al. 2004), GAPs could also exhibit similar structural features across the genera that may underlie function. The first half of this chapter is therefore focussed on analysing both the secondary and tertiary structure of recombinant PfGAPs as well as their conformational stability.

As yet, there is limited evidence for direct interactions between components of the tetrameric complex. The only well-defined interaction is that of MyoA and MTIP. Titration of a fluorescently labelled peptide comprising the C-terminal 17 residues of PfMyoA with full length recombinant PfMTIP demonstrated there is a high affinity interaction (K_d 235(±35) nM) between these two species (Green, Martin et al. 2006). More recent crystallographic studies have supported this evidence and provided valuable insights into the conformation of this complex (Bosch, Turley et al. 2006; Bosch, Turley et al. 2007). The most recently described complexes comprise residues 63-204 of PfMTIP bound to residues 803-816 of *P. yoelii* (Py)MyoA. In this structure, the hinge region connecting the two domains of PfMTIP is kinked. This intrinsic flexibility allows both N and C-terminal domains to interact with specific residues in PyMyoA, effectively clamping the protein around the peptide.

Although it has been demonstrated in *T. gondii* and *P. falciparum* that GAPs are components of the tetrameric motor complex (Gaskins, Gilk et al 2004; Baum, Richard et al. 2006; Jones et al, 2006), until very recently, their individual associations within that complex had not been defined. However, an interaction between PfGAP45 and PfMTIP was recently identified in glutathione *S*-transferase (GST) pull-down experiments using recombinant forms of both proteins expressed in *E. coli* (Vaid, Thomas et al. 2008). This information was not known at the start of this project and thus, analyses were undertaken on the

presumption that in the cytoplasm, PfGAP45 could potentially interact with either PfMTIP or PfMyoA.

Evidence from *T. gondii* (Gaskins, Gilk et al 2004) and described here for *P. falciparum* (section 3.2.5) suggests GAP50 does not associate with the other three components of the complex until they have reached their membrane destination. Furthermore, the precise topology of GAP50 within the IMC/plasma membrane is yet to be confirmed. Consequently, it was decided research would be better geared towards specific interactions of PfGAP45 at present. The remainder of this chapter describes various methods used to identify potential associations with either PfMTIP or PfMyoA. Recombinant PfMTIP used in these experiments was expressed and purified by Dr. Judith Green, NIMR, UK. The fusion protein was expressed in *E. coli* and comprised an N-terminal S-tag and hexa-His tag.

Unfortunately, attempts at expressing and purifying full length recombinant PfMyoA have not yet produced yields suitable for these studies. The crystal structure of scallop smooth muscle myosin subfragment-1 (S1) shown in figure 4.1 A (Houdusse, Szent-Gyorgyi et al. 2000) illustrates the spatial arrangement of a myosin heavy chain and its constituent light chains. The structure comprises a number of sub-domains: domain 1, domain 2 (upper and lower 50kDa), the converter region and domain 3 that contains binding sites for both essential (ELC) and regulatory light chains (RLC) (Rayment, Rypniewski et al. 1993)

The structure of chicken skeletal muscle myosin S1 was the first to be solved and residues constituting different sub-domains, binding sites and the catalytic site have all been defined (Rayment, Holden et al. 1993; Rayment, Rypniewski et al. 1993). An alignment of chicken skeletal muscle myosin S1 and PfMyoA amino acid sequences is shown in figure 4.1 B. In the chicken myosin, regions of domain 3 that bind light chains are located downstream of the converter domain (707-774), corresponding to residues 699-765 of PfMyoA. PfMTIP interacts with the extreme C-terminus of PfMyoA (802-818) (Green, Martin et al. 2006); a region that overlaps with the regulatory light chain binding domain of the

chicken myosin (808-842). As residues 766-802 of PfMyoA overlap with the essential light chain binding domain of the chicken myosin (783-806), it was concluded there may be space for interaction of PfMyoA with another protein, such as calmodulin or PfGAP45. Two overlapping peptides, GAKILTKIQREKLVEWEN and VEWENCVSVIEAAILKHKYKQKVNKN (residues 762-779 and 775-800 respectively) were therefore designed to encompass this region of PfMyoA. Both peptides were successfully synthesised by Dr. Graham Bloomberg, Bristol, UK (section 2.6.6).

The sulphydryl group of a cysteine residue is potentially the most chemically reactive functional group in a protein. Thus, it is possible to direct a fluorescent probe at this residue by choosing the appropriate chemically reactive fluorophore (Haugland 2005) provided the peptide or recombinant protein being labelled contains only one of these residues. Synthetic PfMyoA peptides were designed to comprise one cysteine for labelling (section 2.6.6) and was deduced experimentally that recombinant PfMTIP contained only one free sulphydryl group (section 2.10.2).

Free cysteines were successfully labelled with the environmentally sensitive probe, MIANS. The fluorescence intensity and to a lesser extent, the emission wavelengths of their protein conjugates tend to be very sensitive to substrate binding, folding and unfolding of the protein, changes in ionic strength and association of the labelled protein with another protein, membranes or nucleic acids (Haugland 2005). Owing to the long lifetimes of excited fluorescent molecules (nanoseconds), fluorescence can also be used to monitor the rotational motion of molecules. Fluorescence polarisation can be used to monitor protein-protein interactions as larger molecular mass complexes will have increased rotational correlation times and higher polarisation values (Fu 2004). To probe for potential interactions, emission spectra and polarisation values for labelled PfMyoA peptides and recombinant PfMTIP were obtained in the absence and presence of recombinant PfGAP45 (section 4.3.3.3).

In order to derive any structural or functional information for PfGAPs, sufficient quantities of both proteins were needed. However, to isolate significant quantities of GAPs from *P. falciparum*, a large amount of parasite material and highly specific antibodies would be required. Therefore, recombinant forms of both proteins were initially expressed in *E. coli* to obtain greater yields for subsequent analyses. Their expression and purification are discussed in the relevant sections.

Results described in this chapter suggest that recombinant PfGAP45 expressed in *E. coli* does not interact with either PfMTIP or PfMyoA. However, as described within the relevant sections, the protein appears to comprise considerably less overall secondary structure than is predicted. Therefore, it may be that the *E. coli* protein is misfolded. If correct folding is required for interaction of PfGAP45 with the other motor components, it was thought this may explain negative results obtained thus far.

Misfolding of recombinant proteins is common in *E. coli* (Baneyx and Mujacic 2004). Rapid induction that leads to the expression of large quantites of protein means folding mediators are depleted and rates of protein aggregation are often higher than that of proper folding. Additionally, *E. coli* is not able to support many post-translational modifications required for some proteins to fold successfully. In contrast, the methylotropic yeast *Pichia pastoris (P. pastoris)* possesses eukaryotic features such as a secretory pathway based on compartmentalized endomembranes, which is better equipped for post-translational modifications (Cereghino and Cregg 2000). Thus, PfGAP45 was subsequently expressed in *P. pastoris* and its overall secondary structure compared to that of the *E. coli* protein.

Protein expression in yeast can be problematic as this organism has a different synonymous codon preference to that of *E. coli* (Akashi 2001; Sinclair and Choy 2002). Furthermore, high A/T versus C/G content and frequent lysine and arginine repeats in the *Plasmodium* genome are thought to hinder the successful expression of many malarial antigens in heterologous systems (Yadava

and Ockenhouse 2003). As a consequence, *PFL1090w* (the gene coding for PfGAP45) was optimised for expression in *P. pastoris* (see section 2.3.9).

4.2 Theory and data analysis

4.2.1 Circular dichroism (CD) spectroscopy

Circular dichroism is the differential absorption of left-handed versus right-handed circularly polarised light that occurs due to structural asymmetry. Therefore, it can be utilised to examine the conformation of proteins and peptides. In the far-UV region (190-250 nm), the amide bond is the predominant chromophore with minimal contribution from aromatic residues. The bond itself is planar and will therefore have no intrinsic CD signal. The differential absorbance depends predominantly upon the asymmetry imposed by the presence of secondary structure conformations (α-helices, β-sheet, random coil). Moreover, individual secondary structure conformations will produce characteristic CD spectra that allow overall contributions of each type to be calculated for any given protein. In the aromatic near-UV region (250-340 nm), CD spectra result from absorbances of Phe, Tyr, Trp and cystinyl groups. The intensity of absorbance reflects the environment surrounding these aromatic amino acids. Residues that are rigidly held in space or that interact electronically with surrounding residues will give rise to more intense signals in this region. Therefore, spectra recorded in the near-UV region can provide information about the tertiary or quarternary structure of a protein.

The molar or mean residue CD extinction coefficient at any given wavelength can be calcuated using:

$$\Delta\varepsilon_M = \frac{\Delta A}{l \cdot C} \quad \text{or} \quad \Delta\varepsilon_{MRW} = \frac{\Delta A \cdot MRW}{l \cdot C} \quad \text{respectively.}$$

l is the path length of the cell (cm) and C is the protein concentration (M for $\Delta\varepsilon_M$ and mg ml^{-1} for $\Delta\varepsilon_{MRW}$).

ΔA is calculated from:

$$\Delta A = S.3x10^{-5}$$

Where S is the signal recorded at any given wavelength (millidegrees).
The mean residue weight (MRW) of a protein can be calculated from:

$$MRW = \frac{MW}{N\,Res}$$

where Nres is the number of residues in the polypeptide sequence.

CD can also be used to determine the conformational stability of a protein. The three-dimensional structure of a protein can be stabilised by electrostatic, van der Waals and hydrophobic interactions as well as by hydrogen bonding. If a protein is subjected to high (or low) temperature, extreme pH, high concentrations of chemical denaturants (such as guanidium hydrochloride (GuHCl) or urea) or pressure, these interactions are broken and native structure can be lost. An unfolded state forms that is considered to have a more random and fluctuating structure with its amino acid side chains more exposed to the surrounding solvent. In thermal unfolding, the transition is induced by increasing temperature at a constant rate and recording absorbance at a specific wavelength sensitive to changes in secondary structure conformations (e.g. 220 nm). For a simple two-state unfolding transition, the unfolding constant (K) defines a dynamic equilibrium between native and unfolded states:

$$Native(N) \overset{K}{\rightleftharpoons} Unfolded(U) \qquad \text{where } K = \frac{[U]}{[N]}$$

K is related to the free energy of unfolding (ΔG) by:

$$K = e^{\left(\frac{-\Delta G}{RT}\right)} \qquad (4.1)$$

ΔG is expressed in cal mol^{-1}, T is the absolute temperature (°K) and R is the universal gas constant (1.987 cal $°K^{-1}$ mol^{-1}).

The variation of free energy of unfolding with temperature is defined by the Gibbs-Helmholtz equation:

$$\Delta G_{(T)} = \Delta H_o - T\Delta S_o + \Delta C_p\left[T - T_o - T \cdot \ln\left(\frac{T}{T_o}\right)\right]$$

where T is the temperature chosen for analysis, $\Delta G_{(T)}$ is the ΔG at the chosen temperature, ΔH_o and ΔS_o (cal mol^{-1}) are the enthalpy and entropy changes at a reference temperature (T_o) and ΔC_p is the change in heat capacity at constant pressure (cal $°K^{-1}$).

When the temperature corresponding to the midpoint of the unfolding transition is used as the reference temperature, the above equation can be re-written as:

$$\Delta G_{(T)} = \Delta H_m\left(1 - \frac{T}{T_m}\right) + \Delta C_p\left[T - T_m - T \cdot \ln\left(\frac{T}{T_m}\right)\right] \qquad (4.2)$$

where T_m is the midpoint of the unfolding curve and ΔH_m is the enthalpy change at the midpoint temperature.

The change in optical signal observed as a function of temperature can be described by:

$$\text{Signal} = \text{Opt}_N \cdot F_N + \text{Opt}_U \cdot F_U \quad (4.3)$$

where Opt_N and Opt_U are the optical signals corresponding to the native and unfolded states respectively and F_N and F_U represent fractions of the native and unfolded states. In practice, the values of Opt_N and Opt_U are often linearly-dependent on the temperature and can be defined by:

$$\text{Opt}_N = I_N + S_N T$$
$$\text{Opt}_U = I_U + S_U T$$

thus, in a plot of Signal against T, I_N and I_U are the *y*-intercept values extrapolated for slopes representing Opt_N and Opt_U respectively and S_N and S_U are the slopes. F_U and F_N can be calculated from K as follows:

$$F_U = \frac{K}{(1+K)} \quad (4.4)$$

$$F_N = 1 - F_U \quad (4.5)$$

Experimental data were fitted to equations 4.1-4.5 (with $I_N, I_U, S_N, S_U, T_m, \Delta H_m$ and ΔC_p as the variables) using CURFIT, a standard non-linear least squares program designed by Dr. Stephen Martin (NIMR, UK). In practice, ΔC_p is poorly defined by the data and was kept constant (at zero) in the fit.

The binding of a ligand to the native and/or unfolded state of a protein must affect the stability of the protein. The change in stability that results from

ligand binding is known as the ligand interaction free energy ($\Delta\Delta G$). For two-state unfolding, the simplest case is that the ligand binds to a single site on only the native form of the protein. Here, the ligand interaction free energy is given by:

$$\Delta\Delta G = -RT \ln\left(\frac{1}{1+K_L[L]}\right)$$

where K_L is the association constant for ligand binding to the native state and $[L]$ is the free ligand concentration (M).

4.2.2 Fluorescence spectroscopy

Fluorescence is an optical phenomenon. Molecules that fluoresce absorb photons at a specific wavelength, causing electrons to be excited to a higher energy state. This state is unstable and excess energy is dissipated in several ways, one of which involves the emission of photons at a lower energy and a longer wavelength. Emission spectra are very sensitive to changes in the environment of the fluorophore. Therefore, the affinity of a protein for a target protein or peptide labelled with an extrinsic fluorophore (within the range 1 nM - 2 μM) can be accurately determined if ligand binding causes some change in optical signal of the labelled species.

A binding interaction with simple 1:1 stoichiometry can be defined by:

$$P + L \underset{k_{off}}{\overset{k_{on}}{\rightleftharpoons}} PL \qquad \text{where} \qquad K_d = \frac{[k_{off}]}{[k_{on}]} = \frac{[P][L]}{[PL]} \qquad (4.4)$$

P is the protein, L is the ligand and PL is the complex, with [ ] representing concentrations (M). K_d is the dissociation constant and is used to define the strength of interaction between P and L. k_{on} and k_{off} represent association and dissociation rate constants respectively (M^{-1} s^{-1} and s^{-1}).

The law of conservation of mass states that in a closed system, the mass of the products must equal that of the reactants. Hence:

$$P_t = [PL] + [P]$$
$$L_t = [PL] + [L]$$

where t represents total protein and ligand. By fitting these into equation 4.4 and rearranging, $[PL]$ can be calculated from:

$$[PL] = \frac{(P_t + L_t + K_d) - \left[(P_t + L_t + K_d)^2 - 4P_tL_t\right]^{0.5}}{2} \qquad (4.5)$$

$[P]$ and $[L]$ can then be calculated from the conservation of mass equations.

For any mixture of protein and ligand, the observed optical signal is given by:

$$\text{Signal} = S_L \cdot [L] + S_P \cdot [P] + S_{PL} \cdot [PL]$$

where S represents the signal observed for either protein, ligand or complex.
Using the conservation of mass equations, this can be re-written as:

$$\text{Signal} = S_P \cdot P_t + S_L \cdot L_t + (S_{PL} - S_P - S_L) \cdot [PL] \qquad (4.6)$$

In the above equation, $[PL]$ can be defined by equation 4.5. Experimental data were fitted to equation 4.6 (with K_d, S_L, S_P and S_{PL} as the variables), using CURFIT (Dr. Stephen Martin, NIMR, UK).

When a fluorescent molecule is excited with plane polarised light, light is emitted in a fixed polarised plane, provided that the molecule remains stationary throughout the excited state. If the molecule rotates and tumbles out of this plane during the excited state, light is emitted in a different plane from the excitation light, i.e. it becomes depolarised. The extent to which light is depolarised depends on the lifetime of the fluorescent probe and the rotational correlation time (dependent on shape and molecular mass). To monitor rotation, vertically polarized light is used to excite the fluorophore and the intensity of emitted light can be monitored in vertical and horizontal planes. Polarisation can then be calculated by:

$$P = \left(\frac{I_{\parallel} - I_{\perp}}{I_{\parallel} + I_{\perp}} \right)$$

where $I_{\parallel}$ and $I_{\perp}$ are the fluorescence intensities with polarisers parallel and perpendicular respectively.

4.3 Results

4.3.1 Preparation of recombinant PfGAPs expressed in *E. coli*

Membrane proteins or proteins that are extensively hydrophobic tend to be poorly expressed in *E. coli* and are often found in inclusion bodies (Baneyx and Mujacic 2004). The extreme N and C-termini of PfGAP50 are both largely hydrophobic and thus DNA encoding only residues 27-366 was amplified and used for subsequent cloning.

Genes or parts of genes encoding PfGAP45 and PfGAP50 were successfully amplified from parasite genomic DNA and cloned into *E. coli* expression vectors pQE60 and pET32Xa/LIC respectively (described in section 2.3). Once transformed into appropriate cells, a series of small scale expression trials were set up to examine protein expression and solubility. It was subsequently deduced that cultures induced overnight at 18°C gave rise to the maximum yield of soluble protein in both cases. To obtain sufficient quantites of both proteins for purification and further analyses, larger culture volumes were inoculated and expression based on the optimised conditions (section 2.4.2).

Both expression vectors give rise to proteins containing a hexa-His tag. Immobilised metal affinity chromatography (IMAC) was therefore used to capture recombinant proteins by means of this tag and separate them from other proteins synthesised by the host (full method described in section 2.6.1). Initial experiments were performed using Ni-NTA resin (figure 4.2 A). Samples from each progressive stage in the purification process were analysed using coomassie blue-stained SDS-PAGE gels (panel 1) and by Western blotting with anti-His antibodies, to confirm tagged protein identities (panel 2).

For PfGAP50, elution fractions (lanes labelled 50 and 250) contained a ~55 kDa band corresponding to the recombinant protein. Although preparations of PfGAP50 exhibited a high degree of purity, PfGAP45 was not so well purified using this resin. Although the predominant elution product was a ~36 kDa band, a number of additional bands were repeatedly observed regardless of wash

conditions used. Western blotting confirmed that the ~36 kDa band corresponded to recombinant PfGAP45 and other bands observed were contaminating *E. coli* proteins. In an attempt to improve the purity of PfGAP45 preparations, Ni-NTA resin was replaced with TALON™ IMAC resin. TALON™ resin has been shown to reduce contamination in preparations as it has stricter requirements for the spatial arrangement of histidine residues (Clontech 2001). As shown by coomassie blue staining (figure 4.2 B, panel 1), although PfGAP45 appeared to have a slightly lower affinity for the resin, contamination in the eluted samples was significantly reduced. Western blotting was repeated (panel 2) and confirmed that the single ~36 kDa band observed corresponded to the recombinant protein.

For recombinant PfGAP45, the only extraneous part of the protein sequence was at the extreme C-terminus, where a 4 amino acid linker was followed by the hexa-His tag. Although this region represented only ~5% of the overall sequence, it cannot be ruled out that these residues may make a small contribution to the overall secondary structure.

In contrast, it was deemed necessary to remove the large N-terminal tag from recombinant PfGAP50. The tag constituted ~27% of the overall amino acid sequence and comprised ~12 kDa *E. coli* Trx, whose conformation would likely contribute to the overall secondary structure calculated for the fusion protein. To allow efficient removal of this tag, the pET32Xa/LIC plasmid sequence encodes a factor Xa cleavage site (IleGluGlyArg↓) downstream of the hexa-His tag sequence. For maximum cleavage efficiency, the amount of enzyme used (per mg recombinant protein) as well as the length and temperature of incubation were optimised (see section 2.6.2).

As shown in figure 4.3 A, when 1 mg protein was subjected to overnight treatment, the majority of the full length product (~55 kDa) was successfully cleaved into ~40 kDa and ~15 kDa bands. As the predicted molecular mass for PfGAP50 (using ProtParam) is 38.188 kDa, it was deduced that the larger molecular mass cleavage product corresponded to PfGAP50 and the smaller, to the N-terminal tags. PfGAP50 was subsequently purified from any remaining full

length fusion protein and tags by IMAC. Figure 4.3 B shows that Ni-NTA column flow-through fractions contained only the ~40 kDa band corresponding to PfGAP50.

As the quantity of protein used in these experiments was greatly in excess of factor Xa (1: 20 enzyme: protein by mass), attempts were not made to remove the enzyme from samples. Although it was considered unlikely, it cannot be ruled out that the enzyme may make a small contribution to the CD spectra obtained for the recombinant protein.

4.3.2 Structural analyses

4.3.2.1 Secondary structure prediction for recombinant PfGAPs

A number of programs can be used to predict the secondary structure a protein is most likely to adopt, based on its amino acid sequence. One such program, PSIPRED (Jones 1999; Bryson, McGuffin et al 2005), was used to predict the most likely conformations of both PfGAP45 and PfGAP50 (figure 4.4 A and B respectively).

PSIPRED predicts that PfGAP45 is a mostly α-helical protein comprising 41% α-helix, 8% β-sheet and 51% random coil. The full length sequence of PfGAP50 is predicted to form a mixed α/β protein comprising 24% α-helix, 24.7% β-sheet and 51.1% random coil. However, in *T. gondii*, direct amino acid sequencing of purified parasite protein showed that the first residue of the mature protein corresponded to residue 51 of the predicted coding sequence (Gaskins, Gilk et al. 2004). This implies that the N-terminus of GAP50 acts as a cleavable signal peptide.

SignalP is a program that predicts the presence and location of signal peptide cleavage sites within amino acid sequences (Nielsen, Engelbrecht et al 1997; Bendtsen, Nielsen et al. 2004). This program was used to predict the likelihood and position at which the N-terminus of PfGAP50 might be cleaved if it were to act as a signal peptide. The program uses two different methods to

analyse sequences, one of which (Hidden Markov Model or HMM) includes prediction of signal anchors as well as signal peptides. Using the first method (Neural Network or NN), the N-terminal 25 amino acids were predicted to act as a signal peptide, with cleavage occurring at IKC↓QL. However, by analysis with HMM, the sequence was predicted to encode a signal anchor with ~92% confidence.

Whether this region indeed encodes a signal peptide or anchor cannot be confirmed until it is experimentally determined. If it is a signal peptide, the predicted secondary structure would then comprise 22% α-helix, 26% β-sheet and 52% random coil. However, as discussed in section 4.3.1, recombinant PfGAP50 was expressed as a truncated protein comprising only 339 of the predicted 396 amino acids. Thus, factoring the loss of the N and C-termini into PSIPRED gives a predicted overall secondary structure content of 17% α-helix, 29% β-sheet and 55% random coil.

Interestingly, it has been suggested that GAP45 contains a putative coiled-coil domain (Gaskins, Gilk et al. 2004; Jones, Kitson et al. 2006). Coiled-coils are structural motifs in which 2-7 α-helices are intertwined forming a super-coil that is usually left-handed. Coiled-coils usually contain heptad repeats that allow hydrophobic amino acids to interact along the face of each helix, effectively burying them away from the aqueous solution (figure 4.5).

COILS (Parry 1982; Lupas 1996) is a program designed to predict the probability of a sequence forming coiled-coils. By performing a scan using the default parameters, the program predicted that the N-terminal portion (~100 amino acids) of PfGAP45 has a high probability of forming coiled-coils. However, ~50% of this region is comprised of either positively or negatively charged residues. As coiled-coils are usually solvent-exposed, all but the **a** and **d** positions of the heptad repeat have a high likelihood of being occupied by hydrophilic residues (figure 4.5). When set to default, the program will give equal weighting to all amino acid positions and thus will be biased towards sequences rich in charged residues. Thus, a second scan was performed where weighting was given

to positions **a** and **d** being hydrophobic, to reduce the risk of false-positive identification. The resulting probability decreased significantly suggesting that PfGAP45 may not actually form coiled-coils. Again, this cannot be proved until experimentally determined.

4.3.2.2 Conformational analyses of recombinant PfGAPs using CD

To determine the actual content of secondary structure in both recombinant PfGAPs, far-UV CD spectra were recorded and the resulting percentages of each type of conformation estimated.

Recombinant PfGAP45 produced a spectrum characteristic of a protein with little overall secondary structure (figure 4.6 A, trace A). However, the position and intensity of the low wavelength band suggest it is not entirely unstructured. Analyses using standard calculation methods (Sreerama et al, 2000) gave 8% α-helix, 24% β-sheet, 20% turn and 48% random coil. Cooling PfGAP45 samples to 2°C did not change the far-UV CD spectrum. The spectrum was also unaffected by pH (range 2-8), the addition of Ca^{2+} (1 mM) and Mg^{2+} (5 mM), or changes in salt concentration ([NaCl] = 50-500 mM). These spectra are not shown in the figure as they were all identical. However, the addition of 80% (v/v) of the helicogenic solvent trifluoroethanol (TFE) produced a spectrum characteristic of a protein with high α-helical content, prominent bands being observed at 207 and 222 nm (figure 4.6 A, trace B). Analysis of this spectrum gave 64% α-helix, 3% β-sheet, 14% turn and 19% random coil.

In contrast, spectra recorded for recombinant PfGAP50 were characteristic of a protein with an ordered conformation and high content of overall secondary structure (figure 4.6 B). The relative percentages of each conformation were calculated as 22% α-helix, 24% β-sheet, 20% turn and 34% random coil.

Near-UV CD spectra were also recorded for both recombinant proteins, to examine their tertiary structure. For PfGAP45, a broad peak was observed at ~275 nm that most likely corresponds to absorption by tyrosine and there was a

characteristic tyrosine shoulder ~6 nm to the red (figure 4.7 A). The signal observed at longer wavelengths (~295-310 nm) may correspond to absorbance by cystines. For PfGAP50, bands observed at ~295 nm and ~288 nm likely correspond to the ^1L_b transitions of tryptophan and the maximum observed at ~275 nm, to the broad ^1L_a transition of tryptophan and absorption by tyrosine (figure 4.7 B).

If a protein is folded into a three-dimensional conformation, the strength of interactions maintaining this conformation dictates its stability. By far-UV and near-UV CD analyses, recombinant PfGAP50 appeared to have an ordered conformation. To determine its conformational stability, unfolding was monitored as a function of temperature using far-UV CD absorbance at 220 nm (figure 4.8 A). The signal remained fairly constant (~ -1.8 M^{-1} cm^{-1}) between 20°C and 40°C where it then became more negative, reaching a minimum of ~ -2.4 M^{-1} cm^{-1} at ~55°C. As the temperature increased above 55°C, the signal became less negative, coinciding with increased turbidity of the sample. As precipitation had occurred, the experiment was repeated and samples were re-cooled after heating to 55°C. Far-UV CD spectra obtained at 20°C, 30°C, 45°C, 55°C and after re-cooling to 20°C are shown in figure 4.8 B, traces A-E respectively. At each sample temperature, the overall secondary structure content was calculated and values obtained are shown in table 4.1. Results indicate that after 40°C, PfGAP50 undergoes an α-β transition that is retained upon cooling to 20°C.

4.3.3 Interactions of PfGAPs within the tetrameric complex

4.3.3.1 Co-immunoprecipitations

To test the possibility that PfGAP45 binds to PfMTIP, recombinant proteins were mixed and incubated in an aqueous buffer before being pulled-down by means of an appropriate affinity tag.

Evidence from *T. gondii* suggests all but the extreme C-terminus of GAP50 is contained within the lumen of the IMC (Gaskins, Gilk et al. 2004). If

this is the case, the remainder of the protein would be unlikely to interact with other components of the tetrameric complex. Taking this into account, recombinant PfGAP50 that had not been treated with factor Xa was used as an internal control.

Although all three recombinant proteins contained a hexa-His tag, only PfMTIP and PfGAP50 contained an S-tag and were used to extract PfGAP45. To ensure S-tagged proteins bound S-protein agarose as expected, controls were set up whereby proteins were incubated in the absence of their potential binding partners (figure 4.9 A). As expected, PfGAP45 (~36 kDa) did not bind S-protein agarose (lanes 1 and 2) whereas PfGAP50 (~55 kDa) appeared to bind with high affinity (lanes 5 and 6). PfMTIP (~30 kDa) also bound the resin but with an apparently lower affinity. As shown in lanes 3 and 4, a small proportion of the protein remained in the flow-through. In mixed samples (figure 4.9 B), the proportions of each protein observed in relevant fractions remained the same. Bands corresponding to PfGAP45 were not observed in either of the eluted fractions (lanes 2 and 4 for PfMTIP and PfGAP50 respectively).

4.3.3.2 CD analyses

The far-UV CD spectra of recombinant PfGAP45 and PfMTIP (concentrations determined as described in section 2.6.3) recorded at the same concentration (5.5 μM) are shown in figure 4.10 A, plots A and B respectively. The spectrum of PfMTIP is characteristic of a protein with a high α-helical content (Analysis using standard calculation methods (Sreerama et al, 2000) gave 38% α-helix, 13% β-sheet, 21% turn, and 28% random coil). The far-UV CD spectrum recorded for a 1:1 mixture of the two proteins is identical to the sum of the component spectra (plots C and D respectively).

Thermal unfolding of PfMTIP in the presence and absence of PfGAP45 was also studied (Figure 4.10 B). The unfolding of 3.5 μM PfMTIP in 20 mM phosphate buffer (pH 7.2) conforms to a simple two-state transition between native and denatured forms and is >95% reversible as assessed by restoration of

the native spectrum upon cooling. Analysis of the first derivative of the unfolding curve yielded a transition midpoint temperature, T_m, of 48.8 ± 0.2 °C (Trace A). When unfolding was repeated in the presence of 4.5 μM PfGAP45, the apparent T_m was essentially unchanged at 49.3 ± 0.2 °C (Trace B).

4.3.3.3 Fluorimetric analyses

The emission spectra observed for MIANS bound to recombinant PfMTIP and PfMyoA peptide 2 (2 μM) are shown in figure 4.11 A and B respectively, traces labelled A. Spectra recorded for PfMyoA peptide 1 are not shown as results obtained were similar to those observed for peptide 2.

Emission maxima (E_{max}) for labelled PfMyoA peptides 1 and 2 (443 nm) were consistent with the probes being solvent exposed. In contrast, the observed E_{max} for labelled PfMTIP was at a shorter wavelength (430 nm), suggesting that the probe was buried in a more hydrophobic environment. Addition of 6 M guanidine hydrochloride shifted E_{max} to 443 nm and reduced the intensity. As shown in the traces labelled B, addition of 10 μM PfGAP45 did not give rise to a significant change in the observed emission spectra.

Polarisation values were also recorded for both labelled PfMyoA peptides (0.08 and 0.09 for peptides 1 and 2 respectively) and recombinant PfMTIP (0.27). Likewise, addition of PfGAP45 did not give rise to a significant change in any of the recorded values.

4.3.4 Preparation of recombinant PfGAP45 in *P. pastoris*

The gene coding for PfGAP45 (*PFL1090w*) was optimised for expression in *P. pastoris* and successfully cloned into pPIC9K by GENEART GmbH, Regensburg, Germany. Subsequent to transformation of constructed plasmids, screening with geneticin® identified a number of clones containing multiple copies of the gene. As multiple gene copies can give rise to higher levels of protein expression (Cregg, Vedvick et al. 1993) and references therein), clones

that were able to grow on the highest concentrations of geneticin® (4 mg ml^{-1}) were selected.

Following induction with methanol, samples of the growth medium were analysed for expression of PfGAP45 at 24 h intervals. Maximal protein expression was obtained 96 h post-induction, after which significant proteolytic degredation occured. Recombinant PfGAP45 was expressed with a C-terminal hexa-His tag and was subsequently purified from the culture medium using Ni-NTA resin as described in section 2.6.1. SDS-PAGE analysis of fractions eluted from the resin showed that samples predominantly contained a ~48 kDa protein, although a faint ~37 kDa band was also observed (figure 4.12 A, lanes marked 50 and 250). Western blotting using anti-His antibodies and mouse PfGAP45 antiserum confirmed that the ~48 kDa band corresponded to recombinant PfGAP45 (figure 4.12 B, panels A and B respectively, lanes 2).

The predicted molecular mass for recombinant PfGAP45 expressed in *P. pastoris* was calculated by ProtParam as 26.136 kDa. Although PfGAP45 appears to migrate anomalously in SDS-PAGE, the observed molecular mass was much larger than would be expected. By comparison, recombinant PfGAP45 expressed in *E. coli* has a predicted molecular mass of 24710.8 Da (ProtParam) and migrates at ~36 kDa (figure 4.2). Furthermore, the proteins bands were smeared in appearance.

The addition of glycans to a protein can affect SDS-binding and consequently, its mobility in SDS-PAGE (Yoshimasu et al, 2002). It was considered unlikely that the mass difference observed corresponded to the addition of N-linked glycans. *N*-glycosylation is highly specific and thus, potential consensus sites were removed from the gene coding sequence prior to cloning. In lower eukaryotes such as *P. pastoris*, *O*-oligosaccharides are composed solely of mannose (Man) residues and *O*-mannosylation can occur on serine or threonine residues (Cereghino and Cregg 2000) and references therein).

To test whether recombinant PfGAP45 expressed in *P. pastoris* comprised carbohydrate, protein was separated by SDS-PAGE and gels stained using either

coomassie blue (figure 4.13 A, panel A) or periodic acid/schiff's reagent (PAS) (Sigma-Aldrich) (panel B). Erythrocyte membranes comprise a number of glycoproteins that can be stained with PAS. Membrane ghosts were generated by lysing and washing erythrocytes (50% haematocrit) in a hypotonic lysis buffer (5 mM $NaPO_4$, pH 8.0). Recombinant PfGAP45 expressed in *E. coli* was used as a negative control. While bands corresponding to a number of erythrocyte membrane proteins as well as both recombinant proteins were easily discernible in coomassie-stained gels, only a ~70 kDa erythrocyte glycoprotein and the ~48 kDa band corresponding to the *Pichia* protein were successfully detected using PAS (lanes 1 and 3 respectively).

In an attempt to remove either N or O-linked glycans, PfGAP45 was treated for 2 h with PNGase F (an *N*-glycosidase), α1-2, 3 mannosidase or α1-6 mannosidase using reaction conditions stated in the supplied protocols (New England Biolabs). Treated samples were then analysed by SDS-PAGE (figure 4.13 B, lanes 2, 3 and 4 respectively). By comparison with un-treated protein (lane 1), none of the enzymes produced any discernible change in mobility.

4.3.5 Far-UV CD of recombinant PfGAP45 expressed in *P. pastoris*

Evidence suggests that post-translational glycosylation does not affect the conformation of proteins (Yoshimasu, Ahn et al. 2002). Therefore, the far-UV CD spectrum of glycosylated recombinant PfGAP45 expressed in *P. pastoris* was recorded and directly compared to that previously observed for the *E. coli* protein (figure 4.14, traces A and B respectively). The shape and intensity of the observed spectra were very similar. Estimation of secondary structure content using standard calculation methods (Sreerama and Woody 2000) gave 5.4% α-helix, 18.3% β-sheet, 17.1% turn and 59.2% random coil.

4.4 Discussion

Expression of PfGAPs in *E. coli* was successful and yielded sufficient quantities of recombinant protein for subsequent analyses. In comparison with predictions made by PSIPRED, PfGAP45 appears to have a significantly lower content of α-helix and is more random overall. In contrast, although precise contributions of both α-helix and β-sheet show slight deviations, the overall content of secondary structure observed for PfGAP50 is similar to that of the prediction.

The near-UV CD spectrum recorded for PfGAP50 demonstrates that the protein is folded into an ordered conformation. Interestingly, the spectrum is unusually intense, especially in the region 260-280 nm that corresponds primarily to absorption by tyrosine residues. The amino acid sequence of PfGAP50 contains 20 tyrosine residues. However, near-UV CD intensity is not always proportional to the number of aromatic residues. Some proteins containing large numbers of aromatic residues can have less intense signals owing to cancelling effects of positive and negative signals. Nonetheless, the larger the number of tyrosines, the more likely it is that some are in close proximity to one another. Thus, if there is some kind of interaction between tyrosine residues in PfGAP50, this can also give rise to a more intense near-UV CD signal.

In many proteins, heat-induced misfolding leads to formation of β-sheet-rich fibrillar aggregates that resemble natural amyloid (Benjwal, Verma et al. 2006) and references therein). Thus, it is unknown whether the α-β transition that occurs in PfGAP50 prior to aggregation is of any functional significance. However, as the protein must be able to tolerate human body temperature (37°C), the β-rich form may actually represent its active conformation in the blood. Unfortunately, if protein aggregation and unfolding are concomitant, the transition is inherently irreversible and cannot be analyzed by equilibrium thermodynamics. Thus, the conformational stability of PfGAP50 cannot be established at present.

Although PfGAP45 appears to have a low content of secondary structure, the fact that cooling did not alter the spectrum suggests this cannot be attributed to the protein being unstable and partially unfolded at room temperature. Furthermore, the effect of TFE on resulting spectra clearly demonstrates it has the propensity to form an ordered structure. The intensity of CD spectra recorded in the near-UV in fact suggests that it may have some well-defined tertiary structure. The amino acid sequence of PfGAP45 contains 6 cysteines; 5 of which are located in the C-terminal 45 residues (figure 4.14). The presence of bands corresponding to absorbance by cystines therefore suggests it may be the C-terminal portion of PfGAP45 that is folded.

Collectively, results obtained from a number of experiments suggest that PfGAP45 does not interact with PfMTIP or the PfMyoA tail. There are, of course, a number of limitations to individual experimental techniques that should be considered in the interpretation of these results.

Far-UV CD can be used to identify a protein interaction if there is a concomitant change in the secondary structure of either component. Thus, if the interaction between recombinant PfGAP45 and PfMTIP did not induce a significant change in the conformation of either counterpart, it would not be detected using this method. Furthermore, although fluorescence is a more sensitive technique, the interaction may occur in a region of the labelled protein/peptide that does not significantly alter the environment of the probe. Nonetheless, if there were an interaction, the molecular mass of the complex would be greater and fluorescence polarisation expected to change.

Perhaps the most interesting observation is that in co-immunoprecipitation experiments, recombinant PfMTIP does not co-precipitate quantites of recombinant PfGAP45 that would be visible in coomassie blue-stained SDS-PAGE gels. Although this method is often less useful if an interaction is of low affinity, experiments recently performed using similar proteins expressed in *E. coli* produced results contradictory to those shown here (Vaid, Thomas et al. 2008). While the reaction buffer used was very similar (50 mM Tris-HCl pH 7.5,

50 mM NaCl, 1 mM DTT) recombinant PfMTIP was expressed with an N-terminal GST tag and PfGAP45, a 33 amino acid N-terminal T7 and hexa-His tag (Dr P. Sharma, personal communication). It is worth noting that despite controls being performed to confirm GST does not interact with recombinant PfGAP45, whether the T7-His tag itself interacts with PfMTIP was not tested. However, it must also be considered that if the extreme C-terminus of PfGAP45 is absolutely required for association with PfMTIP, a C-terminal tag may either interfere with the structure of this region or block the binding site. Furthermore, it is not known whether the N-terminally tagged form of PfGAP45 comprises a higher content of secondary and/or tertiary structure than the C-terminally tagged protein.

Interestingly, another group have tranfected and expressed PfGAP45 tagged at the C-terminus with green fluorescent protein (GFP) and shown that parasite development is not affected (Baum, Richard et al. 2006). However, it is possible that the potential binding domain may still be accessible in the GFP mutant or that endogenous PfGAP45 is sufficient to sustain function despite the presence of the episomal GFP copy.

It cannot be disregarded that PfGAP45 is also misfolded in *P. pastoris.* The recombinant protein was also expressed with a C-terminal hexa-His tag that may interfere with structure. Alternatively, PfGAP45 may require parasite-specific factors in order to fold. However, it is intriguing that by comparison with the same protein expressed in *E. coli*, the two have a strikingly similar content of overall secondary structure.

Secondary structure prediction programs do not always accurately predict the true conformation of a protein from an amino acid sequence. Such programs will make a prediction partially based on the probability of a given residue being present in motifs contained in proteins whose structure has been solved (Chou and Fasman 1974) as cited by (Chen, Gu et al. 2006). One residue that is often found in α-helices is glutamic acid. As the N-terminal region of PfGAP45 is rich in glutamic acid (figure 4.14), it is possible that the program has given bias to these residues and a number of the predicted helices may not actually form. It is

possible then, that a large proportion of PfGAP45 does not actually form an ordered structure; a property that may be intrinsic to its function within the parasite.

By comparing amino acid sequences of various GAP45 orthologues, the extreme N and C-terminus are considerably more conserved than the residues separating them (figure 4.14). The N-terminus is predicted to comprise a consensus sequence required for *N*-myristoylation (Gaskins, Gilk et al. 2004) whereas precise function of the C-terminus is unknown. It may be that the C-terminal region of PfGAP45 adopts a more ordered structure and/or is involved in binding one or more of the additional complex components.

Alongside *N*-myristoylation, it has been suggested that GAP45 may also be palmitoylated and/or phosphorylated within parasites (Jones, Kitson et al. 2006; Johnson, Rajfur et al. 2007). If one or more of these modifications exist, it is possible they may induce conformational changes in the protein that would not occur in either of the recombinant forms. It has been documented that some completely or partially unfolded proteins can undergo a structural transition and thus increase in fold upon binding a target (Fink 2005). Therefore, it may be that GAP45 remains fairly unstructured until it is bound to one or more of the other complex components.

Table 4.1

Secondary structure contents of PfGAP50 during thermal unfolding

Temperature (°C)	*Secondary structure (%)*			
	α-helix	**β-sheet**	**turn**	**random coil**
20	22.4	23.0	21.1	33.4
30	22.2	23.7	20.1	33.9
45	18.2	27.4	20.6	33.8
55	16.8	28.9	21.4	33.1
Re-cooled to 20	17.6	27.8	20.7	33.8

Figure 4.1

The structure of myosins

(A) Crystal structure of scallop smooth muscle myosin S1 docked to an actin filament (Houdousse, Szent-Gyorgyi et al. 2000). S1 sub-domains (Rayment 1993) are colour coded as follows: domain 1, green; domain 2 upper 50 kDa, red; domain 2 lower 50 kDa, purple; converter region, grey; domain 3, pink. Regulatory and essential light chains are depicted in red and yellow respectively. (B) Alignment of chicken skeletal muscle myosin II S1 (CSMM) and PfMyoA amino acid sequences. Coloured bars running along the top of the sequences represent S1 subdomains, as described in (A). Coloured bars underneath the sequences represent binding domains. Conserved Walker motifs that are required for ATP-binding are depicted in blue and residues that are involved in binding regulatory and essential light chains are highlighted in red and yellow respectively.

(A)

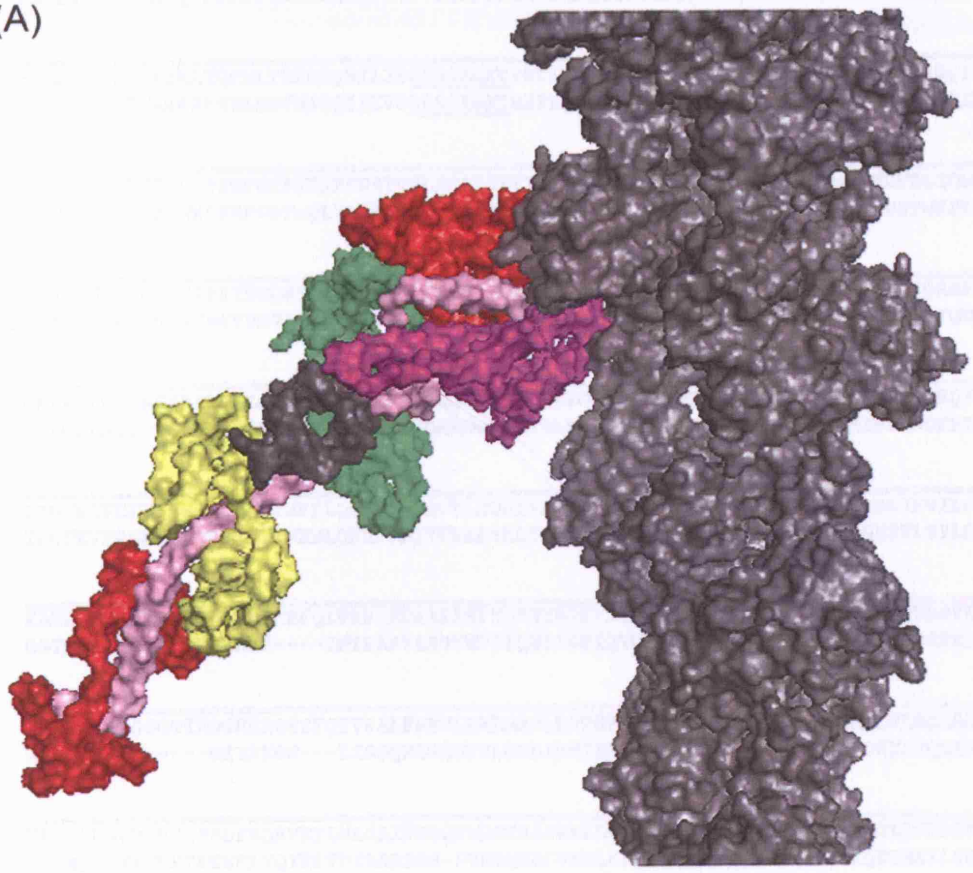

(B)

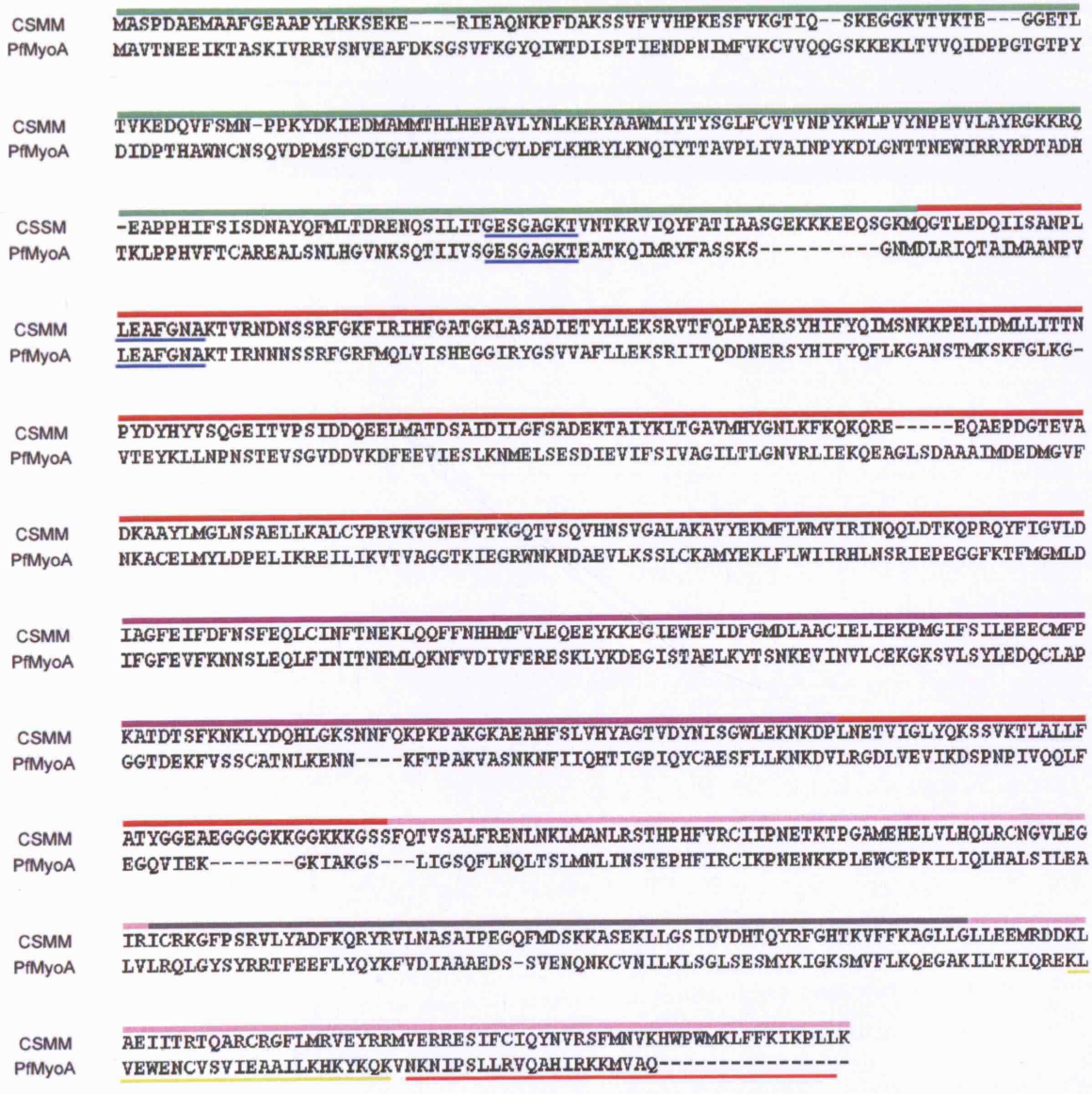
CSMM MASPDAEMAAFGEAAPYLRKSEKE----RIEAQNKPFDAKSSVFVVHPKESFVKGTIQ--SKEGGKVTVKTE---GGETL
PfMyoA MAVTNEEIKTASKIVRRVSNVEAFDKSGSVFKGYQIWTDISPTIENDPNIMFVKCVVQQGSKKEKLTVVQIDPPGTGTPY
CSMM TVKEDQVFSMN-PPKYDKIEDMAMMTHLHEPAVLYNLKERYAAWMIYTYSGLFCVTVNPYKWLPVYNPEVVLAYRGKKRQ
PfMyoA DIDPTHAWNCNSQVDPMSFGDIGLLNHTNIPCVLDFLKHRYLKNQIYTTAVPLIVAINPYKDLGNTTNEWIRRYRDTADH
CSSM -EAPPHIFSISDNAYQFMLTDRENQSILITGESGAGKTVNTKRVIQYFATIAASGEKKKEEQSGKMQGTLEDQIISANPL
PfMyoA TKLPPHVFTCAREALSNLHGVNKSQTIIVSGESGAGKTEATKQIMRYFASSKS----------GNMDLRIQTAIMAANPV
CSMM LEAFGNAKTVRNDNSSRFGKFIRIHFGATGKLASADIETYLLEKSRVTFQLPAERSYHIFYQIMSNKKPELIDMLLITTN
PfMyoA LEAFGNAKTIRNNNSSRFGRFMQLVISHEGGIRYGSVVAFLLEKSRIITQDDNERSYHIFYQFLKGANSTMKSKFGLKG-
CSMM PYDYHYVSQGEITVPSIDDQEELMATDSAIDILGFSADEKTAIYKLTGAVMHYGNLKFKQKQRE-----EQAEPDGTEVA
PfMyoA VTEYKLLNPNSTEVSGVDDVKDFEEVIESLKNMELSESDIEVIFSIVAGILTLGNVRLIEKQEAGLSDAAAIMDEDMGVF
CSMM DKAAYLMGLNSAELLKALCYPRVKVGNEFVTKGQTVSQVHNSVGALAKAVYEKMFLWMVIRINQQLDTKQPRQYFIGVLD
PfMyoA NKACELMYLDPELIKREILIKVTVAGGTKIEGRWNKNDAEVLKSSLCKAMYEKLFLWIIRHLNSRIEPEGGFKTFMGMLD
CSMM IAGFEIFDFNSFEQLCINFTNEKLQQFFNHHMFVLEQEEYKKEGIEWEFIDFGMDLAACIELIEKPMGIFSILEEECMFP
PfMyoA IFGFEVFKNNSLEQLFINITNEMLQKNFVDIVFERESKLYKDEGISTAELKYTSNKEVINVLCEKGKSVLSYLEDQCLAP
CSMM KATDTSFKNKLYDQHLGKSNNFQKPKPAKGKAEAHFSLVHYAGTVDYNISGWLEKNKDPLNETVIGLYQKSSVKTLALLF
PfMyoA GGTDEKFVSSCATNLKENN----KFTPAKVASNKNFIIQHTIGPIQYCAESFLLKNKDVLRGDLVEVIKDSPNPIVQQLF
CSMM ATYGGEAEGGGGKKGGKKKGSSFQTVSALFRENLNKLMANLRSTHPHFVRCIIPNETKTPGAMEHELVLHQLRCNGVLEG
PfMyoA EGQVIEK-------GKIAKGS---LIGSQFLNQLTSLMNLINSTEPHFIRCIKPNENKKPLEWCEPKILIQLHALSILEA
CSMM IRICRKGFPSRVLYADFKQRYRVLNASAIPEGQFMDSKKASEKLLGSIDVDHTQYRFGHTKVFFKAGLLGLLEEMRDDKL
PfMyoA LVLRQLGYSYRRTFEEFLYQYKFVDIAAAEDS-SVENQNKCVNILKLSGLSESMYKIGKSMVFLKQEGAKILTKIQREKL
CSMM AEIITRTQARCRGFLMRVEYRRMVERRESIFCIQYNVRSFMNVKHWPWMKLFFKIKPLLK
PfMyoA VEWENCVSVIEAAILKHKYKQKVNKNIPSLLRVQAHIRKKMVAQ----------

Figure 4.2

Purification of recombinant PfGAPs (*E. coli*)

Purification of recombinant PfGAP45 and PfGAP50 expressed in *E. coli* using Ni-NTA (A) or TALON (B) resin (PfGAP45 only). Supernatant (S), Flowthrough (F) and subsequent wash (10, 20) and elution (50, 250) fractions are identified at the top of each panel, numbers representing concentrations of imidazole used in each step (mM). SDS-PAGE gels stained using coomassie blue are shown in panels labelled 1 and corresponding Western blot analyses using α-His antibodies, in panels labelled 2. Recombinant PfGAP45 and PfGAP50 separated at apparent molecular masses of ~36 and ~55 kDa respectively. Asterisks represent small quantites of contaminating *E. coli* proteins and molecular mass markers are shown on the left hand side of the panels.

(A)

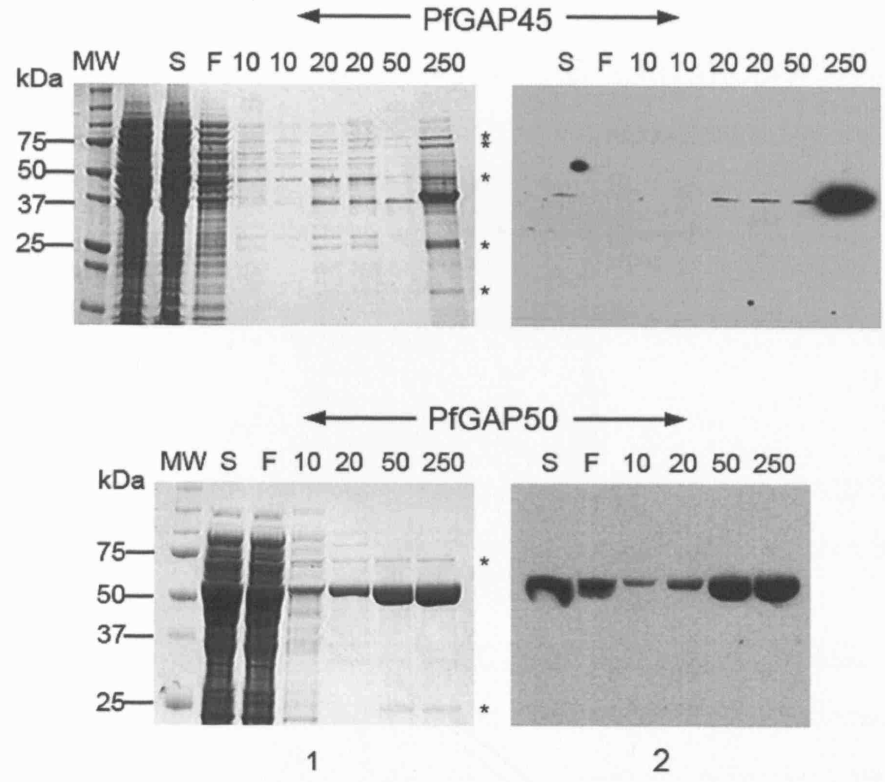
PfGAP45
MW S F 10 10 20 20 50 250
S F 10 10 20 20 50 250
kDa
75
50
37
25
PfGAP50
MW S F 10 20 50 250
S F 10 20 50 250
kDa
75
50
37
25
1
2

(B)

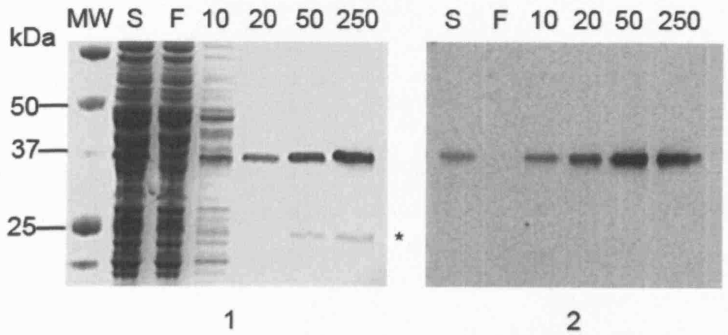
MW S F 10 20 50 250
S F 10 20 50 250
kDa
50
37
25
1
2

Figure 4.3

Removal of the N-terminal tag from recombinant PfGAP50

Coomassie-stained SDS-PAGE gels depicting factor Xa cleavage of the N-terminal tag from recombinant PfGAP50. (A) By comparison with un-treated samples (lane 1), enzymatic digestion of PfGAP50 gave rise to two additional cleavage products with apparent molecular masses ~41 and ~14 kDa (lane 2). (B) After purification using Ni-NTA resin, flowthrough fractions contained only the ~41 kDa protein corresponding to cleaved PfGAP50. Molecular mass markers are shown on the left hand side of panels.

(A)

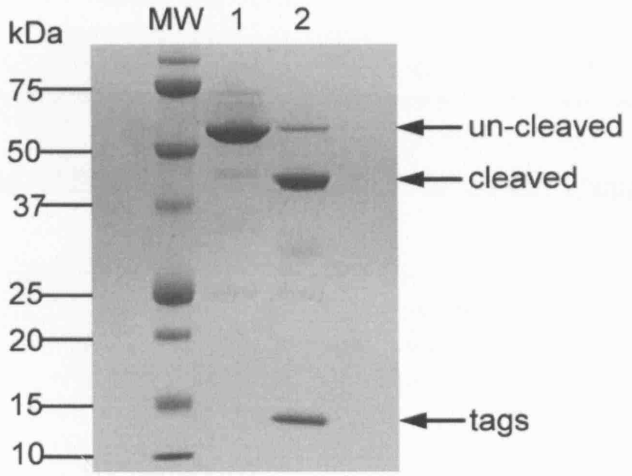
kDa
MW
1
2
75
50
37
25
20
15
10
un-cleaved
cleaved
tags

(B)

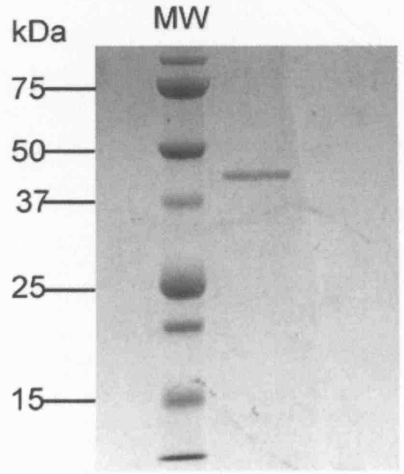
kDa
MW
75
50
37
25
15

Figure 4.4

Secondary structure predictions for PfGAPs

Predicted secondary structure of PfGAP45 (A) and PfGAP50 (B) using PSIPRED (Jones, 1999; Bryson et al, 2005). Diagrammatical representations are explained in the key below amino acid sequences.

(A)

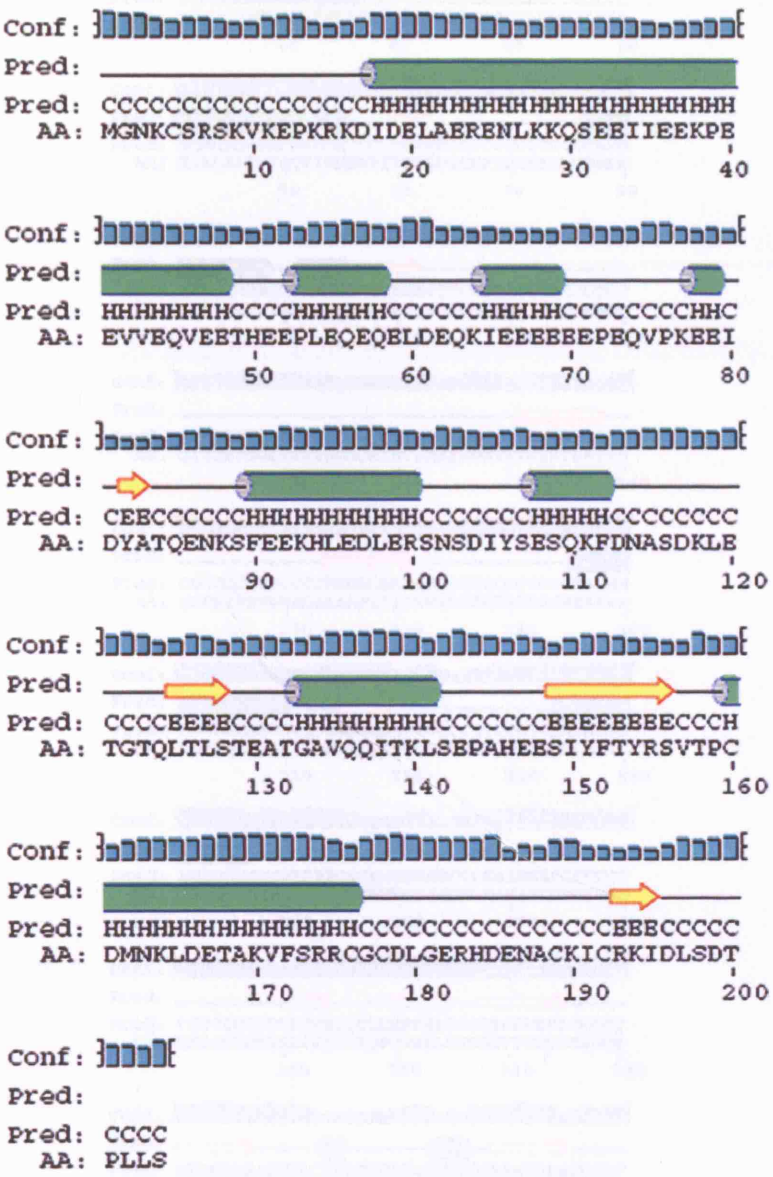
Conf:
Pred:
Pred: CCCCCCCCCCCCCCCCHHHHHHHHHHHHHHHHHHHHHH
AA: MGNKCSRSKVKEPKRKDIDELAERENLKKQSEEIIEEKPE
10 20 30 40
Conf:
Pred:
Pred: HHHHHHHHCCCCHHHHHHCCCCCCHHHHHCCCCCCCCHHC
AA: EVVEQVEETHEEPLEQEQELDEQKIEEEEEEPEQVPKEEI
50 60 70 80
Conf:
Pred:
Pred: CEECCCCCCHHHHHHHHHHHCCCCCCCHHHHHCCCCCCCC
AA: DYATQENKSFEEKHLEDLERSNSDIYSESQKFDNASDKLE
90 100 110 120
Conf:
Pred:
Pred: CCCCEEEECCCCHHHHHHHHHCCCCCCCEEEEEEEECCCH
AA: TGTQLTLSTEATGAVQQITKLSEPAHEESIYFTYRSVTPC
130 140 150 160
Conf:
Pred:
Pred: HHHHHHHHHHHHHHHHHCCCCCCCCCCCCCCCCCEEECCCCC
AA: DMNKLDETAKVFSRRCGCDLGERHDENACKICRKIDLSDT
170 180 190 200
Conf:
Pred:
Pred: CCCC
AA: PLLS

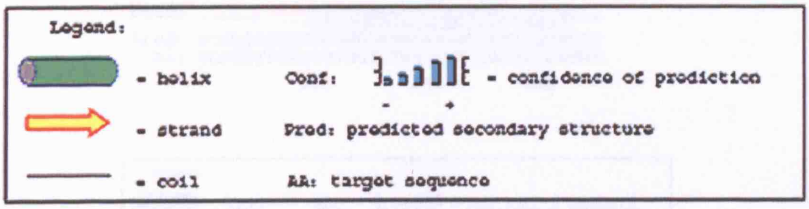
Legend:
= helix
= strand
= coil
Conf:
- +
= confidence of prediction
Pred: predicted secondary structure
AA: target sequence

(B)

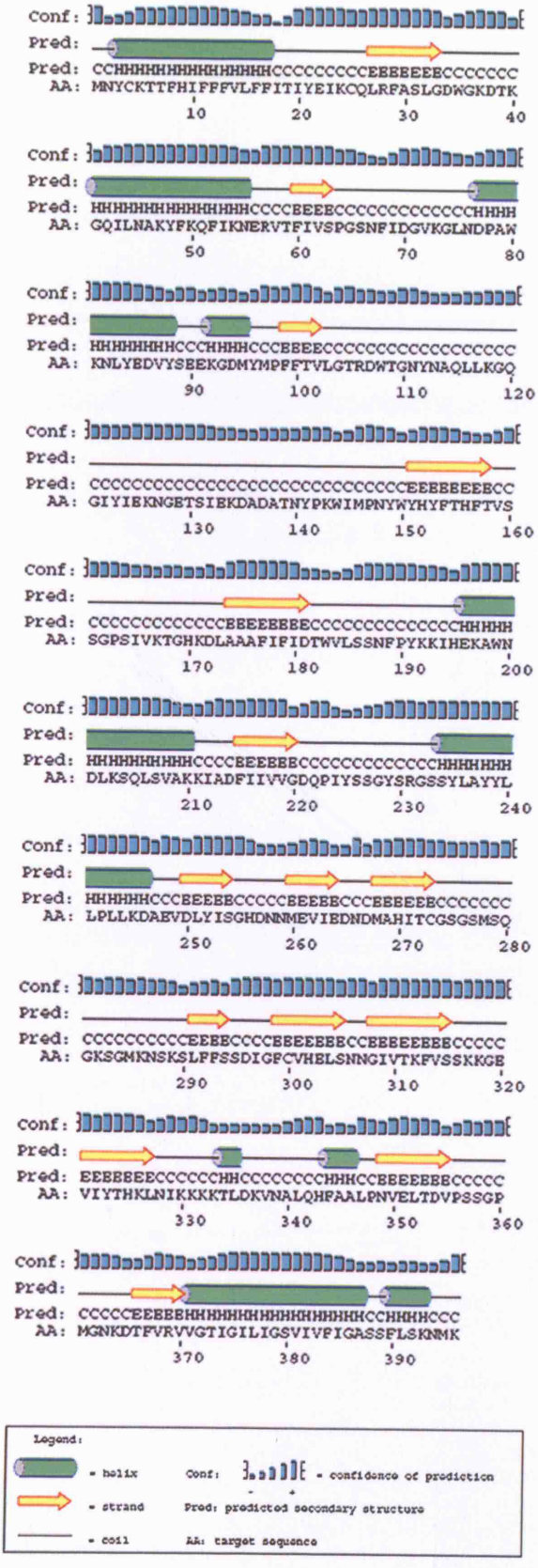
Conf:
Pred:
Pred: CCHHHHHHHHHHHHHHHCCCCCCCCCCEEEEEEECCCCCCC
AA: MNYCKTTPHIFFFVLFFITIYEIKCQLRFASLGDWGKDTK
10 20 30 40
Pred: HHHHHHHHHHHHHHHCCCCEEEECCCCCCCCCCCCCCHHHH
AA: GQILNAKYFKQFIKNERVTFIVSPGSNFIDGVKGLNDPAW
50 60 70 80
Pred: HHHHHHHHCCCHHHHCCCEEEECCCCCCCCCCCCCCCCCC
AA: KNLYEDVYSEEKGDMYMPFFTVLGTRDWTGNYNAQLLKGQ
90 100 110 120
Pred: CCCCCCCCCCCCCCCCCCCCCCCCCCCCCCCCEEEEEEEECC
AA: GIYIEKNGETSIEKDADATNYPKWIMPNYWYHYFTHFTVS
130 140 150 160
Pred: CCCCCCCCCCCCCEEEEEEEECCCCCCCCCCCCCCCHHHHH
AA: SGPSIVKTGHKDLAAAFIFIDTWVLSSNFPYKKIHEKAWN
170 180 190 200
Pred: HHHHHHHHHHCCCCEEEEEECCCCCCCCCCCCCCHHHHHH
AA: DLKSQLSVAKKIADFIIVVGDQPIYSSGYSRGSSYLAYYL
210 220 230 240
Pred: HHHHHHHCCCEEEEECCCCCEEEEECCCEEEEEECCCCCCC
AA: LPLLKDAEVDLYISGHDNNMEVIEDNDMAHITCGSGSMSQ
250 260 270 280
Pred: CCCCCCCCCCEEEECCCCEEEEEEECCEEEEEEECCCCCC
AA: GKSGMKNSKSLFFSSDIGFCVHELSNNGIVTKFVSSKKGE
290 300 310 320
Pred: EEEEEECCCCCCCHHCCCCCCCCHHHCCEEEEEECCCCC
AA: VIYTHKLNIKKKKTLDKVNALQHFAALPNVELTDVPSSGP
330 340 350 360
Pred: CCCCCEEEEEHHHHHHHHHHHHHHHHCCHHHHCCC
AA: MGNKDTFVRVVGTIGILIGSVIVFIGASSFLSKNMK
370 380 390
Legend:
= helix
= strand
= coil
Conf: - +
= confidence of prediction
Pred: predicted secondary structure
AA: target sequence

Figure 4.5

Helical wheel presentation of an α-helical coiled coil motif

In the heptad repeat, positions **a** and **d** (yellow) are typically occupied by hydrophobic (Leu, Ile, Val, Met) that form an interaction surface at the interface of the helices. In contrast, positions **e** and **g** (red) are frequently occupied by charged amino acids (most commonly Glu and Lys) that form inter-helical ionic interactions. Polar residues are often found in the remaining positions, **b**, **c**, and **f**, which are solvent exposed and located at the opposite side of the motif (Pagel, Vagt et al. 2005).

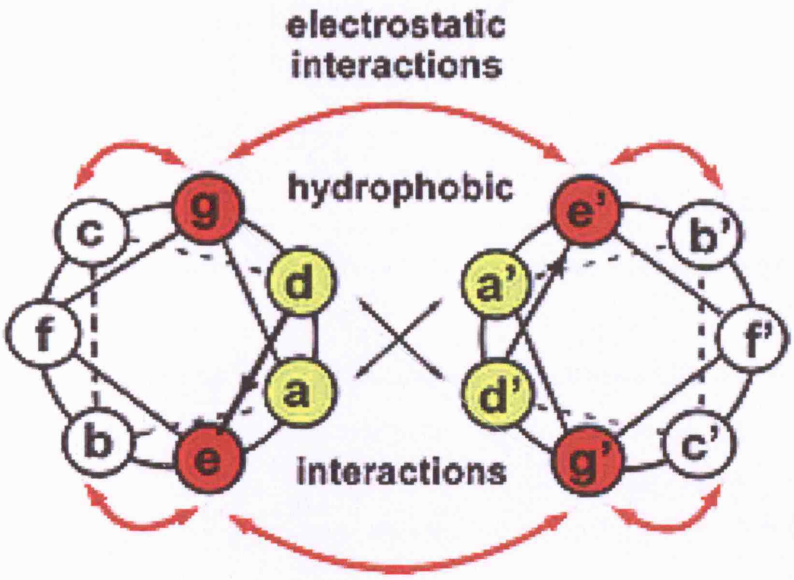
electrostatic
interactions
hydrophobic
interactions
g
c
d
f
a
b
e
e'
b'
a'
f'
d'
g'
c'

Figure 4.6

The secondary structure of recombinant PfGAPs (*E. coli*)

Far-UV CD spectra of recombinant PfGAP45 (A) and PfGAP50 (B) expressed in *E. coli*, recorded in PBS (traces labelled A) and in the case of PfGAP45, 80% (v/v) TFE (trace B).

(A)

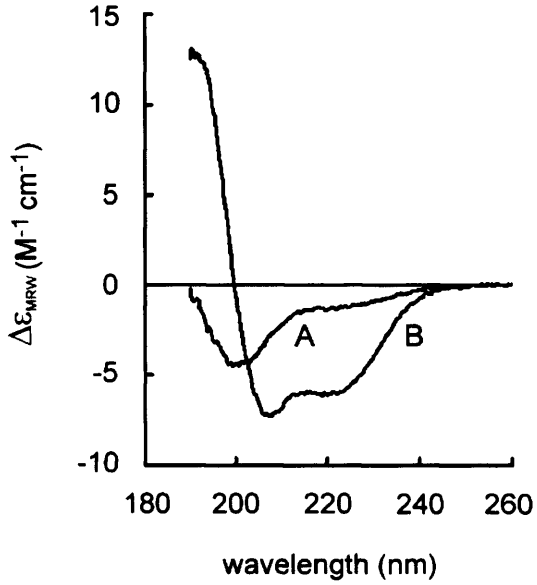
15
10
5
0
-5
-10
180
200
220
240
260
A
B
wavelength (nm)
$\Delta\varepsilon_{MRW}$ (M^{-1} cm^{-1})

(B)

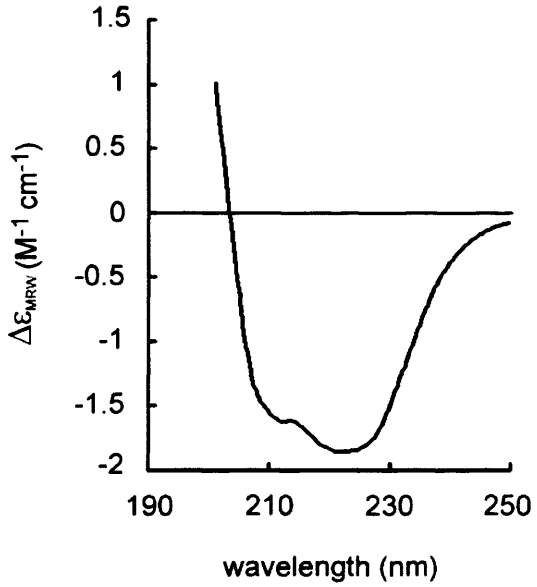
1.5
1
0.5
0
-0.5
-1
-1.5
-2
190
210
230
250
wavelength (nm)
$\Delta\varepsilon_{MRW}$ (M^{-1} cm^{-1})

Figure 4.7

The tertiary structure of recombinant PfGAPs (*E. coli*)

Near-UV CD spectra of recombinant PfGAP45 (A) and PfGAP50 (B) expressed in *E. coli*, recorded in PBS.

(A)

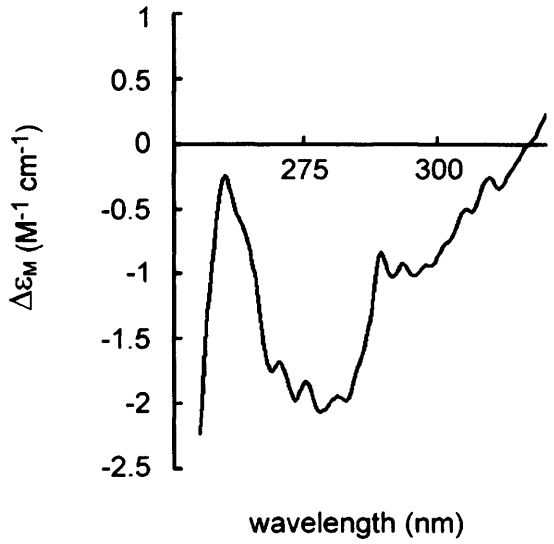
1
0.5
0
-0.5
-1
-1.5
-2
-2.5
275
300
Δε_M (M^-1 cm^-1)
wavelength (nm)

(B)

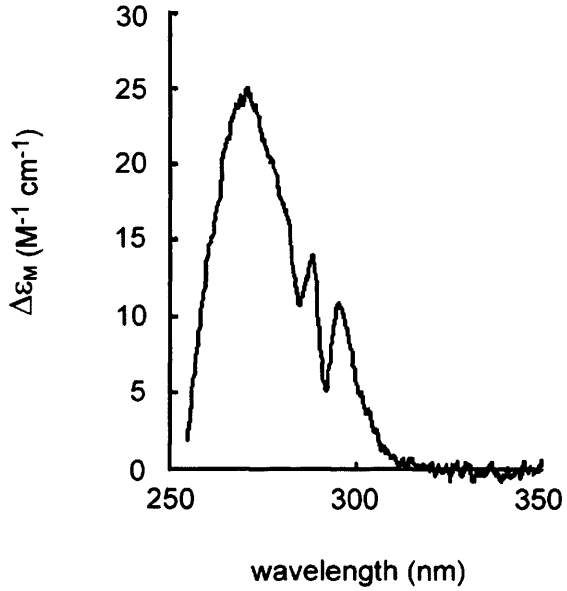
30
25
20
15
10
5
0
250
300
350
Δε_M (M^-1 cm^-1)
wavelength (nm)

Figure 4.8

Conformational stability of recombinant PfGAP50

Thermal unfolding of recombinant PfGAP50 monitored using far-UV CD absorbance. (A) Initial experiments performed by monitoring the CD signal at a single wavelength (220 nm) while increasing the temperature from 20-85°C. (B) Far-UV CD spectra recorded at 20°C, 30°C, 45°C, 55°C and 20°C after re-cooling (traces A-E respectively).

(A)

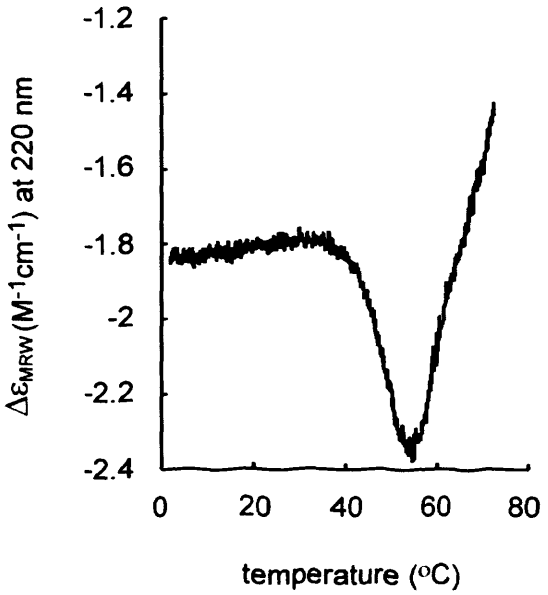
-1.2
-1.4
-1.6
-1.8
-2
-2.2
-2.4
0
20
40
60
80
Δε_MRW (M⁻¹cm⁻¹) at 220 nm
temperature (°C)

(B)

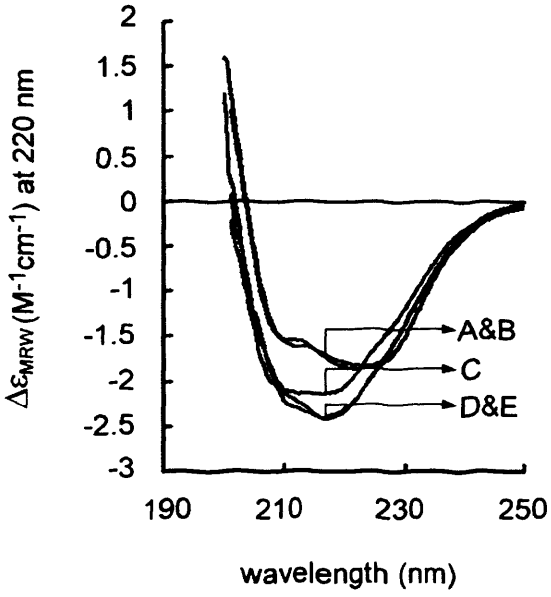
2
1.5
1
0.5
0
-0.5
-1
-1.5
-2
-2.5
-3
190
210
230
250
Δε_MRW (M⁻¹cm⁻¹) at 220 nm
wavelength (nm)
A&B
C
D&E

Figure 4.9

PfMTIP does not co-precipitate with PfGAP45 *in vitro*

Investigation of the potential interaction between recombinant PfGAP45 and recombinant PfMTIP by *in vitro* co-immunoprecipitation. Protein samples were incubated with S-agarose and corresponding flowthrough (F) and elution (E) fractions separated by SDS-PAGE. Recombinant PfGAP50 that had not been treated with factor Xa was used as a negative control for association with PfGAP45. (A) To test their affinity for S-agarose, PfGAP45 (lanes 1 and 2), PfMTIP (lanes 3 and 4) and PfGAP50 (lanes 5 and 6) alone were incubated with the resin. (B) Prior to incubation with S-agarose, PfGAP45 was mixed with equimolar quantites of PfMTIP (lanes 1 and 2) or PfGAP50 (lanes 3 and 4). Asterisks represent proteolytic breakdown of PfGAP50 and molecular mass markers are shown on the left hand side of the panels.

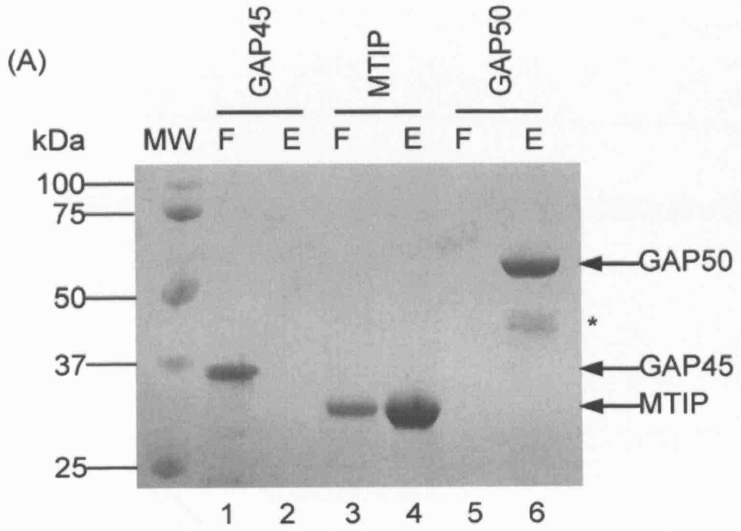
(A)
GAP45
MTIP
GAP50
kDa
MW
F
E
F
E
F
E
100
75
50
37
25
GAP50
*
GAP45
MTIP
1
2
3
4
5
6

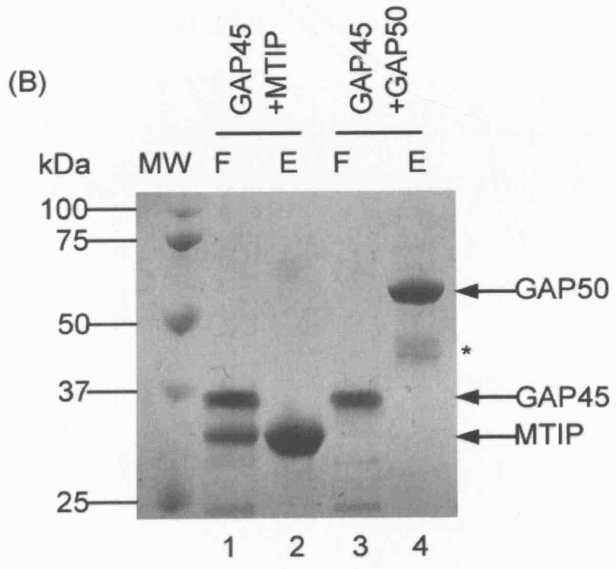
(B)
GAP45
+MTIP
GAP45
+GAP50
kDa
MW
F
E
F
E
100
75
50
37
25
GAP50
*
GAP45
MTIP
1
2
3
4

Figure 4.10

PfMTIP-PfGAP45 interaction is not detectable by CD analyses

Investigation of the potential interaction between recombinant PfGAP45 and recombinant PfMTIP using CD analyses. (A) Far-UV CD spectra of PfGAP45 (trace A), PfMTIP (trace B), PfGAP45+PfMTIP (trace C) and the appropriate weighted sum of trace A and B (trace D). (B) The first derivative of the far-UV CD signal (at 220 nm) recorded for PfMTIP with respect to temperature, in the absence (trace A) and presence (trace B) of PfGAP45.

(A)

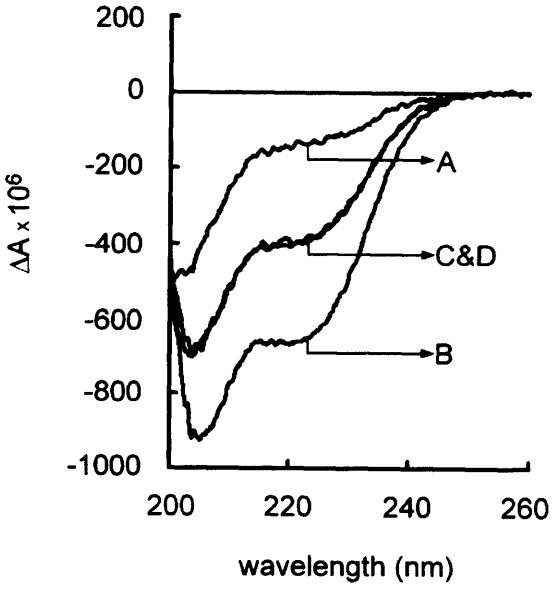
200
0
-200
-400
-600
-800
-1000
ΔA x 10⁶
A
C&D
B
200
220
240
260
wavelength (nm)

(B)

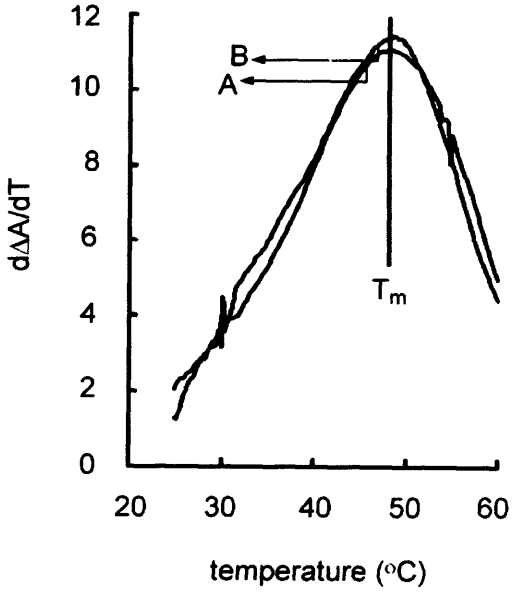
12
10
8
6
4
2
0
dΔA/dT
B
A
Tm
20
30
40
50
60
temperature (°C)

Figure 4.11

PfMTIP-PfGAP45 interaction is not detectable by fluorescence analyses

Investigation of the potential interaction between recombinant PfGAP45 and recombinant PfMTIP using fluorescence spectroscopy. Emission spectra of extrinsic fluorophore MIANS bound to recombinant PfMTIP (A) or synthetic PfMyoA tail peptide 2 (B) in the absence (traces labelled A) and presence (traces labelled B) of recombinant PfGAP45.

(A)

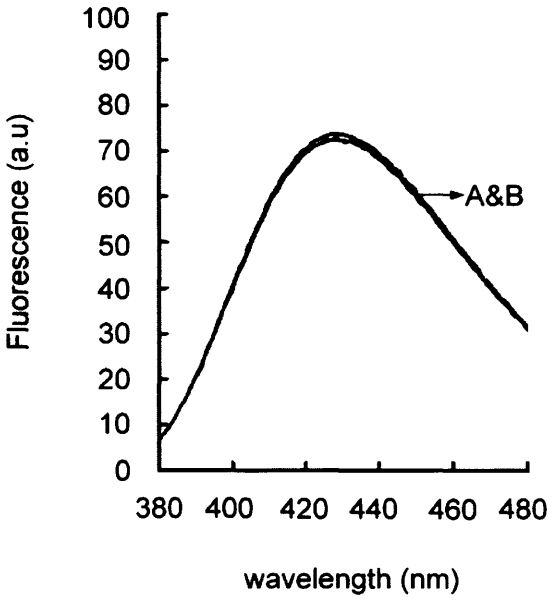
100
90
80
70
60
50
40
30
20
10
0
Fluorescence (a.u)
A&B
380
400
420
440
460
480
wavelength (nm)

(B)

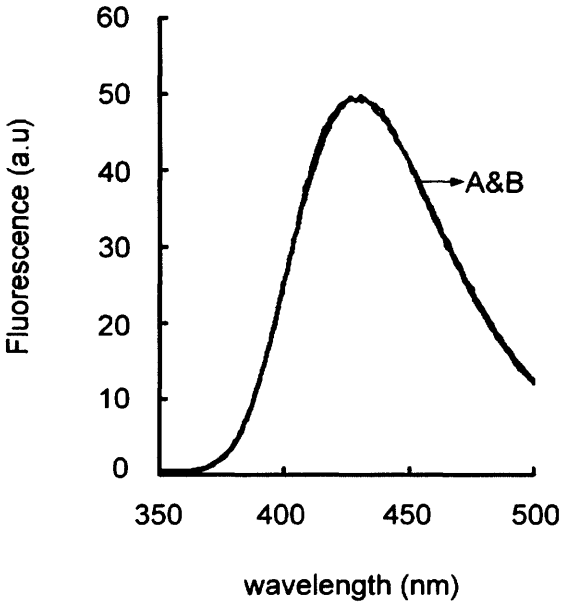
60
50
40
30
20
10
0
Fluorescence (a.u)
A&B
350
400
450
500
wavelength (nm)

Figure 4.12

Purification of recombinant PfGAP45 (*P. pastoris*)

(A) Coomassie blue-stained SDS-PAGE gel showing purification of recombinant PfGAP45 expressed in *P. pastoris* using Ni-NTA resin. Supernatant (S), Flowthrough (F) and subsequent wash (10, 20) and elution (50, 250) fractions are identified at the top of each panel, numbers representing concentrations of imidazole used in each step (mM). The predominant elution product was a ~48 kDa protein that was smeared in appearance. (B) Western blot analyses of eluted fractions (lane 2) using α-His antibodies (panel A) and mouse α-PfGAP45 (panel B) confirm the ~48 kDa protein corresponds to hexa-His tagged PfGAP45. Recombinant protein expressed in *E. coli* was used as a positive control in both cases (lane 1). Asterisks represent cross-reactivity with contaminating *E. coli* proteins that may have been present in the original preparation used to raise the antiserum. Molecular mass markers are shown on the left hand side of the panels.

(A)

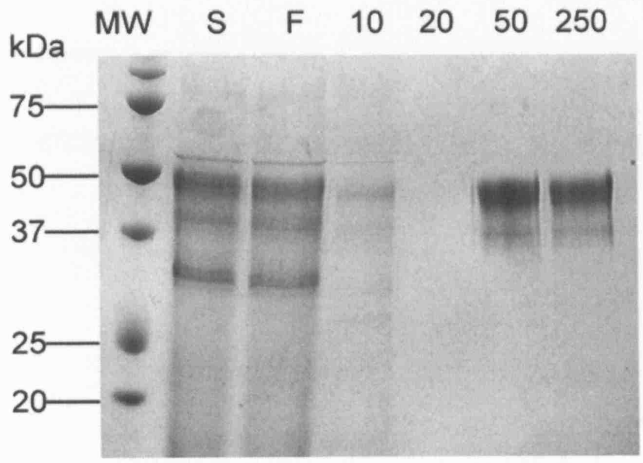
MW
S
F
10
20
50
250
kDa
75
50
37
25
20

(B)

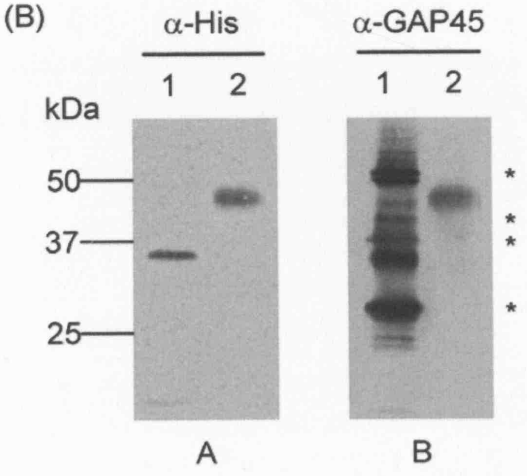
α-His
α-GAP45
1
2
1
2
kDa
50
37
25
*
*
*
*
A
B

Figure 4.13

PfGAP45 is glycosylated in *P. pastoris*

(A) (Panel A): Coomassie-stained SDS-PAGE gel showing relative mobilities of erythrocyte membrane proteins (lane 1) and recombinant PfGAP45 expressed in *E. coli* or *P. pastoris* (lanes 2 and 3 respectively). (Panel B): Duplicate SDS-PAGE gel stained using PAS. (B) Coomassie-stained SDS-PAGE gel showing resulting mobilities of recombinant PfGAP45 expressed in *P. pastoris* subsequent to treatment with specific glycosidases. By comparison with the expected molecular mass of ~48 kDa observed in untreated samples (lane 1), digestion with either PNGase F (lane 2), α-1,2,3 mannosidase (lane 3) or α-1,6 mannosidase (lane 4) did not affect this mobility. Molecular mass markers are shown at the left hand side of the panels.

(A)

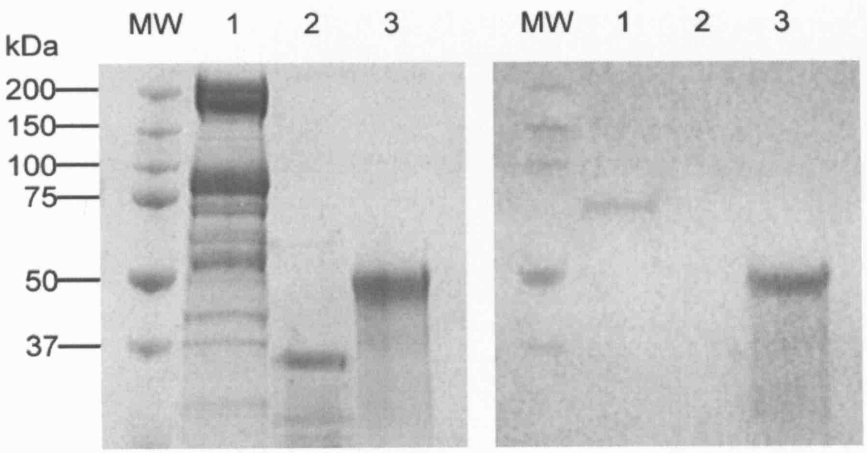
MW 1 2 3
kDa
200
150
100
75
50
37
MW 1 2 3
A
B

(B)

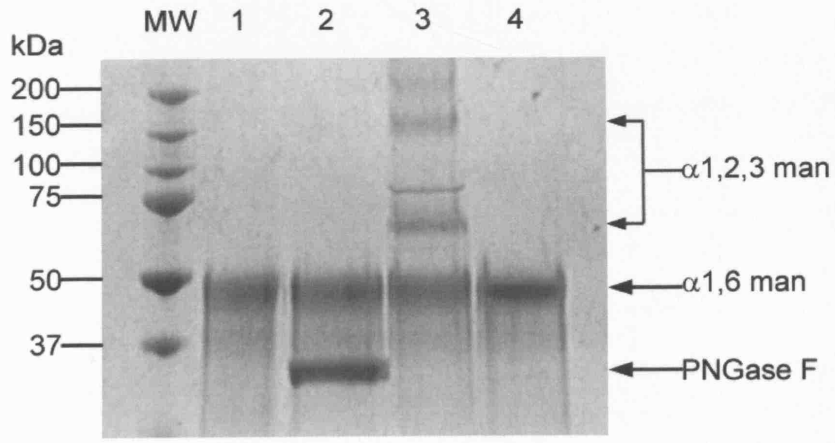
MW 1 2 3 4
kDa
200
150
100
75
50
37
α1,2,3 man
α1,6 man
PNGase F

Figure 4.14

Different recombinant forms of PfGAP45 adopt a similar conformation

Far-UV CD spectra of recombinant PfGAP45 expressed in *P. pastoris* (trace A) and *E. coli* (trace B), both recorded in PBS.

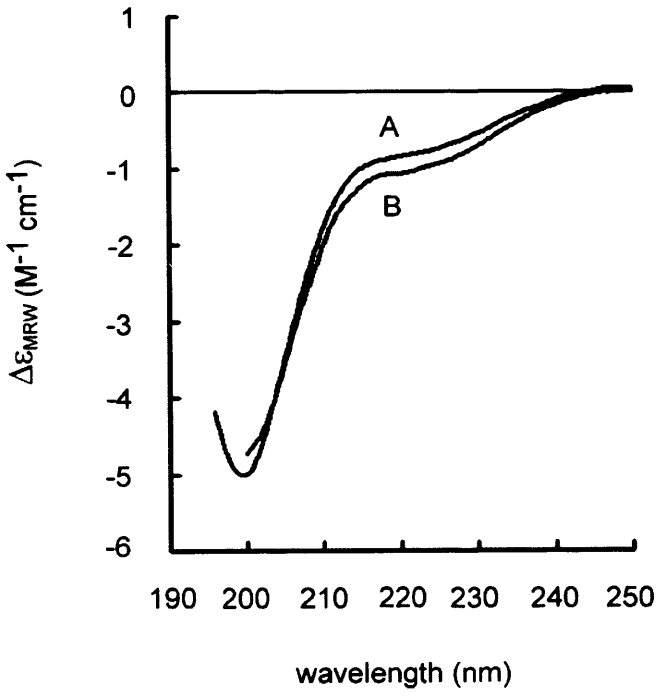
1
0
-1
-2
-3
-4
-5
-6
A
B
190 200 210 220 230 240 250
wavelength (nm)
$\Delta\varepsilon_{MRW}$ (M^{-1} cm^{-1})

Figure 4.15

Comparison of apicomplexan GAP45 amino acid sequences

Alignment of GAP45 sequences from different apicomplexan parasites. Amino acid residues identical in at least four of the six sequences are highlighted in black; similar residues in gray. The amino-terminal *N*-myristoylation and possible palmitoylation sites are indicated with an asterisk. Tg: *Toxoplasma (T). gondii*, Nc: *Neospora (N). caninum*, Pf: *Plasmodium (P). falciparum*, Py: *Plasmodium (P). yoelii*, Cp: *Cryptosporidium (C). parvum.*

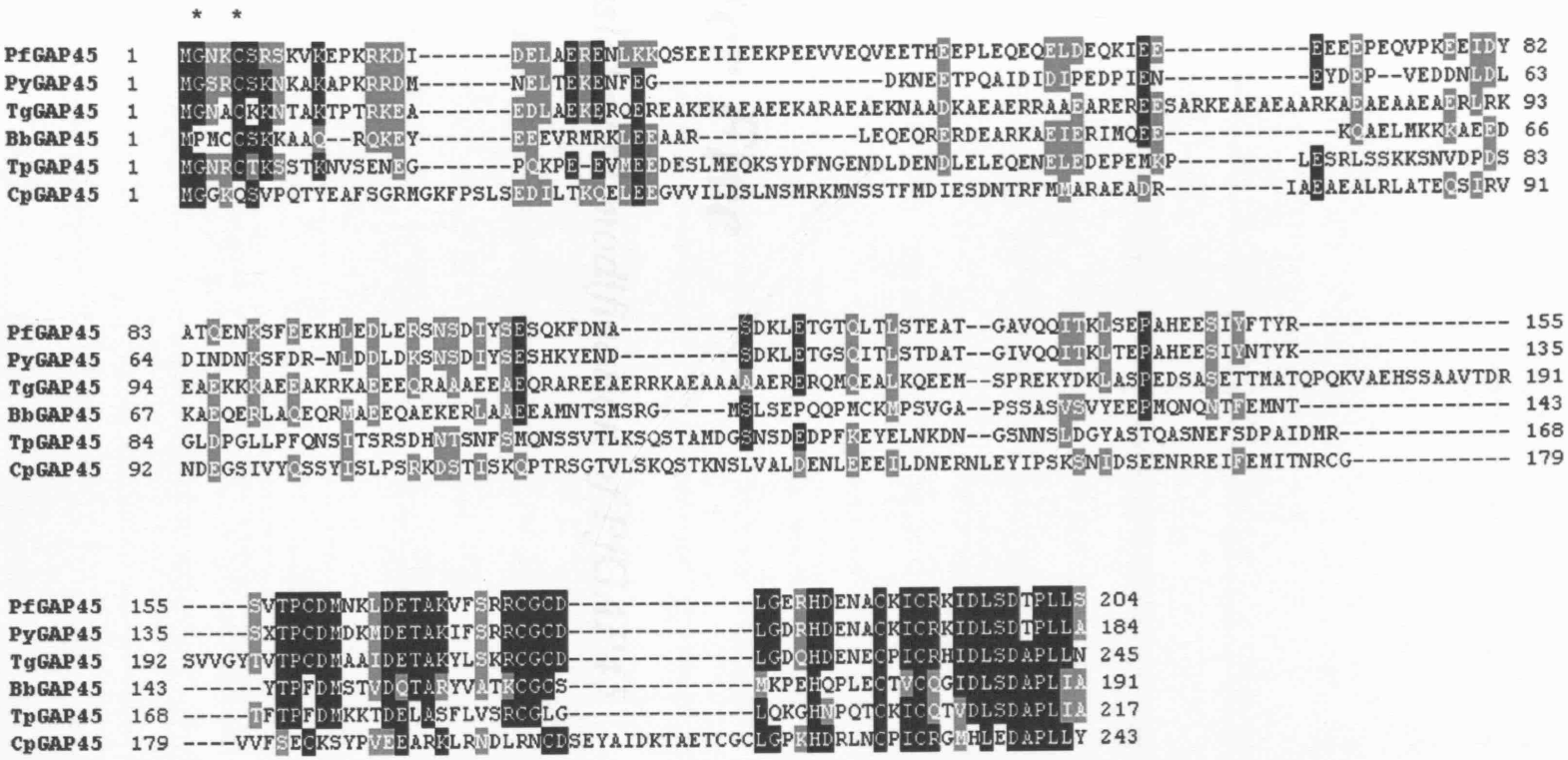
PfGAP45 1 MGNKCSRSKVKEPKRKDI-------DELAERENLKKQSEEIIEEKPEEVVEQVEETHEEPLEQEQELDEQKIEE----------EEEEPEQVPKEEIDY 82
PyGAP45 1 MGSRCSKNKAKAPKRRDM-------NELTEKENFEG----------DKNEETPQAIDIDIPEDPIEN----------EYDEP--VEDDNLDL 63
TgGAP45 1 MGNACKKNTAKTPTRKEA-------EDLAEKERQEREAKEKAEAEEKARAEAEKNAADKAEAERRAAEARERERSARKEAEAEAARKAEAEAAEAPRRRK 93
BbGAP45 1 MPMCCSKKAAQ--RQKEY-------EEEVRMRKLEEAAR----------LEQEQREDEARKAEIERIMQEE----------KQAELMKKKAEEE 66
TpGAP45 1 MGNRCTKSSTKNVSENEG-------PQKPE-EVMEEDESLMEQKSYDFNGENDLDENDLELEQENELEDEPEMKP---------LESRLSSKKSNVDPDS 83
CpGAP45 1 MGGKQSVPQTYEAFSGRMGKFPSLSEDILTKQELEEGVVILDSLNSMRKMNSSTFMDIESDNTRFMMARAEADR---------IAEAEALRLATEQSIRV 91
PfGAP45 83 ATQENKSFEEKHLEDLERSNSDIYSESQKFDNA---------SDKLETGTQLTLSTEAT--GAVQQITKLSEPAHEESIVFTYR---------- 155
PyGAP45 64 DINDNKSFDR-NLDDLDKSNSDIYSESHKYEND---------SDKLETGSQITLSTDAT--GIVQQITKLTEPAHEESIVNTYK---------- 135
TgGAP45 94 EAEKKKAEEAKRKAEEQCRAAAEEAEQRAREEAERRKAEAAAAAERERQMQEALKQEEM--SPREKYDKLASPEDSASETTMATQPQKVAEHSSAAVTDR 191
BbGAP45 67 KAEQERLAQEQRMAEEQAEKERLAAEEAMNTSMSRG-----MSLSEPQQPMCKLPSVGA--PSSASVSVYEEPMQNQNTPEMNT---------- 143
TpGAP45 84 GLDPGLLPFQNSITSRSDHNTSNFSMQNSSVTLKSQSTAMDGSNSDEDPFKEYELNKDN--GSNNSLDGYASTQASNEFSDPAIDMR---------- 168
CpGAP45 92 NDEGSIVYQSSYISLPSRKDSTISKQPTRSGTVLSKQSTKNSLVALDENLEEEILDNERNLEYIPSKSNIDSEENRREIFEMITNRCG---------- 179
PfGAP45 155 -----SVTPCDMNKLDETAKVFSRRCGCD----------LGERHDENACKICRKIDLSDTPLLS 204
PyGAP45 135 -----SXTPCDMDKMDETAKIFSRRCGCD----------LGDRHDENACKICRKIDLSDTPLLA 184
TgGAP45 192 SVVGYTVTPCDMAAIDETAKYLSKRCGCD----------LGDQHDENECPICRHIDLSDAPLLN 245
BbGAP45 143 ------YTPFDMSTVDQTARYVATKCGCS----------MKPEHQPLECTVCQGIDLSDAPLIA 191
TpGAP45 168 -----TFTPFDMKKTDELASFLVSRCGLG----------LQKGHNPQTCKICQTVDLSDAPLIA 217
CpGAP45 179 ----VVFSECKSYPVEEARKLRNDLRNCDSEYAIDKTAETCGCLGPKHDRLNCPICRGPHLEDAPLLY 243

Chapter Five

Post-translational modification of PfGAP45

5.1 Introduction

Proteins can be modified either co- or post-translationally and many of these adaptations can be intrinsic to their specific function. Examples of the biological effects of protein modifications include: phosphorylation for signal transduction, ubiquitination for proteolysis, attachment of fatty acids for membrane anchoring or association, glycosylation for protein half-life, targeting, cell-cell and cell-matrix interactions, and carboxylation in protein-ligand binding to name a few (Graves, Martin et al. 1994).

From pulse-chase experiments performed in section 3.2.5, it appears that PfGAP45 undergoes at least one type of post-translational modification. Throughout the time course (~42-44 h post-invasion), molecular masses observed for PfGAP45 appear to increase (figure 3.7). Several prediction programs for protein modification can be found at The Expert Protein Analysis System (ExPASy) Proteomics Server of the Swiss Institute for Bioinformatics (SIB). A number of these programs were utilised in order to identify potential modifications of PfGAP45 that may occur in the parasite. The results obtained led to experimental work being focussed on potential lipidation (*N*-myristoylation and palmitoylation) and phosphorylation of the protein.

N-myristoylation is a co-translational lipid anchor modification of many eukaryote and viral proteins whereby a 14-carbon saturated fatty acid is covalently attached to a glycine residue by an amide bond. The myristoyl-CoA: NMT recognizes a sequence motif of appropriate substrate proteins at the N-terminus and attaches the lipid moiety to an absolutely required N-terminal glycine residue. Protein *S*-palmitoylation is the reversible post-translational attachment of a 16-carbon lipid moiety to the sulphydryl group of a cysteine residue by means of a thioester linkage. Although the consensus site and mechanisms involved are not well-defined, the reaction is thought to be catalysed by palmitoyltransferases (PATs) and the preferred substrate is palmitoyl-CoA. Phosphorylation is another post-translational modification prevalent in a number of prokaryotic and

eukaryotic proteins. It involves the ATP-dependent enzymatic addition of a phosphate group to a serine, threonine or tyrosine residue by a specific kinase.

Calcium-dependent protein kinases (CDPKs) are a multigene family of kinases found in plants and alveolates (Harper and Harmon 2005) and their members possess a unique internal mode of regulation. The highly conserved N-terminal serine/threonine kinase domain is contiguous with a C-terminal calmodulin-like calcium-binding domain (CaM-LD) and an autoinhibitory junction (J) domain separates the two.

The kinase is normally inhibited by association of the J domain with the active site. Upon activation, Ca^{2+}-binding to the CaM-LD induces a conformational change allowing the N-lobe of the CaM-LD to associate with the J domain, removing it from the active site (Chandran, Stollar et al. 2006).

Current evidence suggests that *Plasmodium* encodes five CDPK isoforms as well as some other structurally-related kinases, each expressed predominantly at specific phases in the life-cycle (Ward, Equinet et al. 2004). *P. berghei* (Pb) CDPK3 and PbCDPK4 are both expressed in the sexual stages. Ookinetes without a functional CDPK3 gene (ΔCDPK3) have reduced ability to glide as well as invade the mosquito midgut whereas sporozoites are indistinguishable from wild-type parasites (Ishino, Orito et al. 2006; Siden-Kiamos, Ecker et al. 2006). PbCDPK4 is important in regulating cell-cycle progression in male gametocytes and may have an additional role in ookinete infectivity (Billker, Dechamps et al. 2004). Collectively, these data imply CDPKs have distinct but highly specific roles in different life-cycle stages.

More recently, it has also been shown that another CDPK, CDPK1, is a target for KT5926 in *T. gondii* tachyzoites (Kieschnick, Wakefield et al. 2001). As this inhibitor blocks the ability of parasites to attach to host cells and move over substrates, this implies a potential role for CDPK1 in invasion and/or gliding. PfCDPK1 was first identified by Zhao et al (Zhao, Kappes et al. 1993) and microarray analyses suggest that expression is restricted to the late blood stages (Bozdech, Llinas et al. 2003; Bozdech, Zhu et al. 2003; Le Roch, Zhou et al.

2003). PfCDPK1 appears to be associated with parasite membranes by virtue of a dually acylated N-terminus; Gly2 is *N*-myristoylated and Cys3 is palmitoylated (Möskes, Burghaus et al. 2004).

Evidence has shown that PfCDPK1 phosphorylates the exogenous substrates casein and histone as well as *P. falciparum* raf kinase inhibitor protein (PfRKIP) (Zhao, Franklin et al. 1994; Kugelstadt, Winter et al. 2007). RKIP exists in a number of species as an active regulator in a variety of signalling pathways. In *P. falciparum,* it appears to modulate the activity of PfCDPK1, possibly affecting phosphorylation of additional substrates.

Previous immunoEM analyses have suggested that PfCDPK1 is located in the PVM of developing parasites (Moskes, Burghaus et al. 2004). However, more recent work has demonstrated that the kinase is located at the periphery of both developing merozoites within late schizonts and free merozoites. Patterns of fluorescence overlap with those of PfMTIP, PfGAP45 and surface protein, MSP1 (Green et al, unpublished). Given the timing and location of expression, it was deemed possible that one or more of the motor proteins may be substrates for CDPK1.

Recombinant PfCDPK1 was subsequently expressed in *E. coli* and purified to homogeneity by Dr Judith Green, NIMR, UK. Kinase assays performed have shown that recombinant PfMTIP is a substrate for PfCDPK1 (Green et al, unpublished). A large proportion of this chapter therefore describes research geared towards investigating the possibility that PfGAP45 is also a substrate for this kinase. All experiments in this chapter were performed using recombinant PfGAP45 expressed in *E. coli.*

Mass spectrometry is an analytical tool that can be utilised to determine the molecular mass of a sample. Depending on the methods and instrumentation used, molecular masses of large biomolecules can be measured to within an accuracy of 0.01% of the total mass of the sample. This makes the technique sensitive enough to detect even small deviations in mass, such as amino acid substitutions or post-translational modifications.

Two different methods were utilised in order to analyse the phosphorylation of recombinant PfGAP45 by recombinant PfCDPK1. Electrospray ionisation mass spectrometry (ESI-MS) is a "soft" ionisation method, as the sample is ionised by the addition or removal of protons, with little extra energy remaining to induce fragmentation. Thus, ESI-MS was used to analyse intact phosphorylated recombinant PfGAP45.

Another "soft" ionisation method, matrix-assisted laser desorption/ionisation (MALDI), was used to identify phosphorylation sites within recombinant PfGAP45. Although MALDI-time-of-flight (TOF) is a powerful tool for the characterisation of phosphopeptides, their acidity means they are often poorly ionised (Annan and Carr 1996). This can lead to poor sensitivity of detection within complex peptide mixtures. To improve and simplify data quality and analyses, recombinant PfGAP45 phosphopeptides were enriched by purification from unmodified peptides using gallium (III) resin (Pierce). Phosphate groups selectively bind immobilised gallium and isolated phosphopeptides were subsequently eluted in buffers compatible with MALDI-TOF (see section 2.10.4).

By using a reflectron-TOF instrument, phosphopeptides can be identified based on the presence of characteristic fragment ions. Selection and fragmentation of parent ions $[M+H^+]$ that are metastable i.e. sufficiently stable to be transported out of the ion source but not to survive the flight to the detector, is known as post-source decay (PSD). The major fragment ion observed for both serine and threonine phosphopeptides is $[MH-H_3PO_4]^+$ or $MH-98$ Da.

5.2 Results

5.2.1 *In silico* prediction of co- and post-translational modifications

NMT- the myristoyl predictor is a program used to predict the likelihood that a given sequence will be myristoylated. The program consists of terms evaluating amino acid type preferences at sequence positions close to the N-terminus as well as terms penalising deviations from the physical property pattern of amino acid side-chains encoded in multi-residue correlation within the motif sequence (Maurer-Stroh, Eisenhaber et al. 2002). As described in section 4.4, the extreme N-terminus of GAP45 is well conserved across the genera (figure 4.13) and the sequences of most species contain an N-terminal glycine. One notable exception to this is in *Babesia bovis* (*B. bovis*), where this residue is proline. Nevertheless, the NMT prediction program suggested that the N-terminal 20 amino acids of PfGAP45 are a "reliable" target for *N*-myristoylation.

CSS-Palm 2.0 (Zhou, Xue et al. 2006) is a recently updated prediction program that uses a data set of experimentally-determined palmitoylation sites to determine the probability of a cysteine within a given protein sequence being palmitoylated. The amino acid sequence of PfGAP45 contains 6 Cys residues but only one, Cys5 is present in the N-terminus and was suggested to be a strong candidate for palmitoylation. This residue, like Gly2, is also highly conserved across Apicomplexa although in some *Cryptosporidium* species i.e. *C. parvum*, it is replaced by glutamine (figure 4.13).

NetPhos 2.0 (Blom, Gammeltoft et al. 1999) predicts the likelihood of a serine, threonine or tyrosine residue being phosphorylated in a given sequence. The program works by analysing the sequence space around target residues in comparison to verified protein phosphorylation sites from the PhosphoBase database developed by the same group (http://www.cbs.dtu.dk/databases /PhosphoBase). As no tyrosine kinases have yet been identified in *Plasmodium* (Kappes, Doerig et al. 1999), these residues were excluded in the query. Predicted phosphorylation sites within the PfGAP45 protein sequence are shown in table 5.1. Out of a possible 28 residues, 10 serines and 4 threonines were predicted as likely

candidates for phosphorylation with residues 89, 101, 103, 128, 158 and 173 scoring highly.

5.2.2 *In vitro N*-myristoylation of PfGAP45

To examine the possibility that recombinant PfGAP45 is *N*-myristoylated, *in vitro N*-myristoylation assays were performed using recombinant PfNMT and a ^{3}H-labelled myristate, myristoyl-CoA. Recombinant PfNMT (Gunaratne, Sajid et al. 2000) was expressed from a synthetic gene generated with codon usage optimised for *E. coli* and purified to homogeneity (Bowyer, Gunaratne et al. 2007). Recombinant PfARF1 was used as a positive control as its acylation had been demonstrated previously (Bowyer et al, unpublished). The gene was subcloned from a construct producing an N-terminal GST fusion protein (Stafford et al, 1996) to produce a C-terminally hexa-His-tagged protein also expressed in *E. coli* (Bowyer, unpublished data). Aliquots of both recombinant PfNMT and PfARF1 were kindly donated by Dr Paul Bowyer, Stanford University, CA, USA, as well as information regarding optimal assay conditions (section 2.9.1).

As shown in figure 5.1 A, panel 2, assays performed using PfARF1 and PfGAP45 gave rise to radiolabelled bands of apparent molecular masses ~20 kDa and ~36 kDa (lanes 3 and 4 respectively). These values correspond to molecular masses observed for the recombinant proteins separated by SDS-PAGE and stained using coomassie blue (Figure 5.1 A, panel 1).

To confirm specificity of PfNMT and that myristate was indeed attached to the N-terminal glycine of PfGAP45, a Gly2Ala variant was expressed in *E. coli* and purified using the same methods as described for wild-type PfGAP45. In the same assay, although wild-type PfGAP45 was reproducibly acylated (figure 5.1 B, panel 2, lane 3) the ~36 kDa band observed for the PfGAP45 variant in coomassie-blue stained SDS-PAGE gels (figure 5.1 B, panel 1, lane 4) was not radiolabelled in the corresponding autoradiograph.

5.2.3 Modification of PfGAP45 in the parasite

To elucidate whether PfGAP45 is *N*-myristoylated and palmitoylated *in vivo*, schizonts were tightly synchronised at ~42 h post-invasion and labelled for 2 h with [^{3}H] myristic acid or [^{3}H] palmitic acid. Immunoprecipitations using mouse PfGAP45 antiserum were performed on ^{3}H-labelled parasite extracts in order to detect acylated PfGAP45. As confirmation that PfGAP45 was being expressed at this time, immunoprecipitations were also performed on extracts of the same parasite culture grown for 2 h in the presence of [^{35}S] methionine and cysteine. Immunoprecipitation of both ^{35}S-labelled schizonts and schizonts labelled with [^{3}H] myristic acid identified a ~37-39 kDa doublet (Figure 5.2 A, panels A and B respectively). From schizonts labelled with [^{3}H] palmitic acid, the antibody precipitated a single band of ~39 kDa (Figure 5.2 A, panel C).

To investigate possible phosphorylation of PfGAP45 in the parasite, schizonts synchronised at ~42 h post-invasion and purified merozoites were lysed in 1% (v/v) NP-40 immunoprecipitation buffer (recipe in section 2.77) and treated with lambda phosphatase as described in the supplied protocol (New England Biolabs). Lambda phosphatase is a protein phosphatase that will remove phosphate groups from serine, threonine and tyrosine residues. Mouse PfGAP45 antiserum was used to detect protein in parasite extracts via Western blotting (figure 5.2 B). In un-treated schizonts and merozoites (lanes 1 and 2), the antiserum detected ~37-39 kDa and ~37-40 kDa doublets respectively whereas a single band of ~37 kDa was detected in treated extracts (lanes 3 and 4).

5.2.4 PfGAP45 is a substrate for PfCDPK1 *in vitro*

To test whether recombinant PfCDPK1 was capable of phosphorylating recombinant PfGAP45, kinase assays were performed where [γ-^{32}P] ATP was used to monitor transfer of phosphate to the substrate. Proteins in each assay were separated by SDS-PAGE and phosphorylated bands detected by autoradiography. As evidence suggests that recombinant PfMTIP is a substrate for PfCDPK1 (Green et al, unpublished), this protein was used as a positive control.

Assays performed using PfCDPK1 alone gave rise to a radiolabelled ~68 kDa band corresponding to the same molecular mass observed for the protein in coomassie blue-stained SDS-PAGE gels (figure 5.3B and A respectively, lanes labelled 1). Radiolabelling was not observed when the same assay was repeated in the presence of 1 mM EGTA (lanes labelled 2), while supplementation with either PfGAP45 or PfMTIP gave rise to additional radiolabelled bands of ~36 kDa and ~30 kDa respectively (lanes 4 and 6). Although effectively stained using coomassie blue, ~67 kDa, ~22 kDa and ~40 kDa bands corresponding to BSA (Sigma-Aldrich), recombinant $MSP7_{22}$ (expressed and kindly donated by Dr. Madhu Kaddekoppala, NIMR, UK) and recombinant PfGAP50 respectively (lanes 7-9) were not detected by autoradiography.

The kinetic parameters of enzyme-substrate pairs were calculated by coupling the hydrolysis of ATP to two additional enzyme reactions (see figure 2.1). Phosphoenolpyruvate (PEP) is first converted to pyruvate by pyruvate kinase (PK), re-generating ATP. The subsequent conversion of pyruvate into lactate by lactate dehydrogenase (LDH) results in the oxidation of NADH, which, can be monitored by recording absorbance change at 340 nm (ΔA_{340}) over time (section 2.9.3). Initial addition of recombinant PfCDPK1 to the reaction buffer resulted in a signal change that most likely corresponded to autophosphorylation. Subsequent titration with either ATP or recombinant PfGAP45 increased the rates of signal change, with values for K_M being determined as 96 ± 28 μM and 18 ± 5 μM respectively (figure 5.4 A and B).

5.2.5 Isolation of recombinant PfGAP45 phosphopeptides

Phosphorylated PfGAP45 was prepared by scaling up kinase assays described in section 2.9.2. The substrate concentration was increased to 100 μM and 1 mM ATP used in place of radiolabelled material. To ensure reactions had gone to completion, samples were incubated at 30°C overnight prior to analysis.

To identify the number of phosphates transferred to PfGAP45, protein samples were initally analysed by ESI-MS. The mass spectrum of phosphorylated recombinant PfGAP45 appeared to have four distinct multiply charged ion series (figure 5.5). The predicted molecular mass of intact recombinant PfGAP45 by ProtParam is 24710.8 Da and a molecular mass of 24711.67 ± 2.99 Da was calculated for ions comprising series A. Ions comprising additional series B-D gave molecular masses of 24795.29 ± 7.03, 24875.07 ± 5.54 and 24.958.46 ± 10.27 respectively. The errors described here represent the mean standard deviation in molecular masses calculated for all the peaks in a given series. Taking experimental error into account, the mass difference observed between each of these forms is ~80 Da, corresponding to the net addition of phosphate. This strongly suggests a total of three phosphates are incorporated as there is no obvious alternative explanation for this series.

In an attempt to isolate specific residues of recombinant PfGAP45 phosphorylated by recombinant PfCDPK1, protein samples were digested with endopeptidase Asp-N or trypsin and resulting peptides analysed by MALDI-TOF. Analyses of tryptic digests revealed one phosphopeptide, R↓SHHHHHH, spanning residues 208-214 of recombinant PfGAP45 (figure 5.6 A). In contrast, analyses of samples digested with Asp-N identified three phosphopeptides. The sequence of one of these, ↓DTPLLSGSRSHHHHHH, overlapped with that of the tryptic peptides and the two novel peptides, ↓DYATQENKSFEEKHLE↓D and ↓DLERSNSDIYSESQKF↓D spanned residues 81-96 and 97-112 respectively (figure 5.6 B).

In the case of all three peptides, only a single residue was phosphorylated and peaks corresponding to metastable fragmentation were observed. However, in all analyses performed, fragment ions observed corresponded to a loss of ~85 Da. This is because the instrument was calibrated presuming all ions produced would have the same kinetic energy as the parent ion. As this type of decay occurs after ionisation, the fragment ions would have less kinetic energy and thus be incorrectly focussed by the ion reflector. As a consequence, they are assigned an inaccurate molecular mass value.

To acquire correct molecular masses for the fragment ions, PSD scans were performed on peptides derived from Asp-N digests using appropriate reflector voltages obtained from calibration with [Glu]-fibrinopeptide. For each of the three phosphopeptides and their corresponding fragment ions, the true difference in mass was calculated as ~98 Da (figure 5.7).

5.2.6 Identification of phosphorylation sites within parasite-derived PfGAP45

5.2.6.1 Extraction of PfGAP45 from purified merozoites

Although evidence suggests PfGAP45 is expressed in merozoites (as described in chapter 3), precise quantities contained within individual parasites at any one time is unknown. Hence, in order to minimise contamination with additional erythrocyte proteins, PfGAP45 was extracted from purified merozoites rather than developing merozoites within schizonts. To obtain maximum protein yield and purity, 500 µl packed cells were used in each experiment and rabbit PfGAP45 antiserum affinity-purified and used to prepare affinity columns (section 2.7.2).

Merozoites were lysed using 0.5% (w/v) *N*-octylglucoside buffer (section 2.7.3). *N*-octylglucoside is a mild, non-ionic detergent less likely to cause antibody denaturation during the purification process or interfere with MALDI-TOF analyses (if any slight contamination exists in samples). The detergent was included in every buffer throughout the purification procedure so as to keep acylated PfGAP45 in solution. However, when parasites are lysed using

comparably mild detergents, the intact motor complex is extracted (section 3.2.4). As high salt has been shown to disrupt the tetrameric complex (section 3.2.6), purification buffers also contained high concentrations of salt (500 mM NaCl) to ensure intra-complex associations were disrupted. Once PfGAP45 had bound to the antibody column, protein was eluted using 0.1 M glycine pH 2.7 (neutralised with 1 M TrisHCl pH 9.0) in 1 ml fractions that were subsequently analysed by Western blotting.

In all 10 fractions, rabbit PfGAP45 antiserum predominantly detected a ~40 kDa band that was smudgy in appearance (figure 5.8 A). Additional higher molecular mass bands detected may correspond to cross-reactivity with small amounts of eluted antibody. However, similar patterns of background staining were observed in Western blotting experiments performed on both schizont and merozoite lysates using the same antiserum (data not shown). Therefore, there may be some cross-reactivity of the rabbit antibody with other parasite proteins and as a consequence, a small amount of these proteins were co-purified.

5.2.6.2. MALDI-TOF analyses

Eluted fractions containing PfGAP45 were pooled and concentrated to a final volume of 20 µl. Proteins were separated by SDS-PAGE and visualised using Colloidal Blue (Invitrogen) (figure 5.8 B). This stain is more sensitive than conventional Coomassie Blue (can detect up to 10 ng protein) and will give a clear background by de-staining in ultrapure water. The ~40 kDa band corresponding to PfGAP45 was excised from the gel, split into two pieces and protein digested with either trypsin or Asp-N.

A list of the peptides isolated by MALDI-TOF is given in table 5.2. Using the BLAST tool at NCBI, both sets of peptides were matched to the amino acid sequence of PfGAP45, although digestion with either enzyme gave only 23% sequence coverage. However, by analysing overlapping peptide fingerprints obtained from both enzyme digests, the total sequence coverage was calculated to be 42%.

As only a small amount of protein was available for analysis, it was not possible to enrich potential phosphopeptides. However, further manual analyses of the spectra obtained revealed two phosphopeptides: ↓ DYATQENKSFEEKHLE ↓ D was isolated from Asp-N digests and a previously unidentified tryptic peptide, K ↓ LSEPAHEESIYFTYR ↓ was identified, spanning residues 141-155 (figure 5.9 A and B respectively). In the case of both peptides, corresponding fragment ions were also present. However, as their signals were weak, it was not possible to perform PSD scans in order to confirm their true molecular masses. Nonetheless, the observed losses in molecular mass were equivalent to those observed in digests performed using recombinant PfGAP45 (MH−85 Da). Therefore, it was presumed the true losses in mass were also the same.

5.3 Discussion

In order for the motor to generate the large external force required for parasites to invade erythrocytes, one expects that myosin A must be firmly anchored to suitable structures within the merozoite. Until now, only putative transmembrane protein GAP50 has been suggested as a likely candidate for this role (Gaskins, Gilk et al. 2004). As it is clear that GAP50 is assembled in membranes prior to formation of the tetrameric complex, the mechanism by which cytoplasmic components of the complex reach their membrane-bound destination has, until now, remained elusive.

Results show that PfGAP45 is *N*-myristoylated both *in vitro* and in developing merozoites. Various studies have proved that *N*-myristoylation of cytoplasmic proteins is sufficient to target and promote membrane interaction (Resh 1999). However, the binding energy provided by this lipidation is fairly weak (10^{-4} M K_d) and insufficient to provide a stable anchorage (Resh 1999). Some *N*-myristoylated proteins are also palmitoylated via one or more cysteine residues either adjacent to, or within twenty amino acids of the N-terminus (Resh 1999; Navarro-Lérida, Alvarez-Barrientos et al. 2002). As PAT activity has only been found in membranes, this second acylation event is thought to occur at membranes and can provide a much higher affinity interaction (Shahinian and Silvius 1995).

Radiolabelling experiments indicate that PfGAP45 is palmitoylated in developing merozoites. It is proposed therefore, that *N*-myristoylation targets the protein and in turn, the ternary complex, to parasite membranes. The addition of a palmitate moiety then rigidly anchors the protein in its specific target membrane.

Although this mechanism for membrane attachment is likely to be highly conserved throughout the phylum, it may not be exclusive. Although *N*-myristoylation of *B. bovis* GAP45 is not possible, the presence of an additional cysteine (Cys4) at the N-terminus suggests the protein may be dually palmitoylated (figure 4.14). Indeed, CSS-Palm 2.0 predicts that in addition to Cys5, this residue is also a strong candidate for acylation. On the premise that two

fatty acids are better than one, it may be that the second palmitate merely enhances membrane association. However, biophysical characterization of acylated peptides indicates that hydrophobicity conferred by a single palmitate is sufficient to support stable membrane interaction (Pietzsch and McLaughlin 1993). For some proteins, dual or multiple palmitoylation appears to be sufficient for membrane targeting even in the absence of myristate. Although precise mechanisms are still unclear, the rate at which such proteins reach their destination is slower and the secretory pathway may be involved (van't Hof and Resh 1997; Gonzalo and Linder 1998).

In contrast, N-terminal palmitoylation cannot occur in *C. parvum* GAP45 as there are no available cysteines. Additional residues are present in the C-terminal domain that may be acylated although none are predicted to be suitable candidates (figure 4.14). Alternatively, interaction with one or more of the additional complex components at membranes may be sufficient for stable attachment. Collectively, these discrepancies suggest that although the motor complex and its individual constituents probably have a common role in parasite invasion, there may be subtle differences specific to individual species.

In addition to acylation, PfGAP45 is phosphorylated in the parasite. The addition of negative charge to the protein appears to significantly affect its mobility in SDS-PAGE (figure 5.2 B), suggesting a number of phosphate groups may be incorporated or that this modification introduces some conformational change that influences protein shape. Pulse-chase labelling experiments imply that the ternary complex predominantly comprises the ~37 kDa form of PfGAP45 (figure 3.7). Thus, using the increase in apparent molecular mass as a marker for phosphorylation, it would appear that modification occurs when the ternary complex reaches its target membrane and is associated with PfGAP50. As palmitoylated PfGAP45 has an apparent molecular mass of ~39 kDa, this suggests it is also phosphorylated. These observations might be expected given that PfCDPK1 appears to be located in the plasma membrane and if the addition of palmitate only occurs once the protein has reached its target membrane.

It is worth noting that in free merozoites, PfGAP45 has an apparent molecular mass of ~40 kDa. The presence of a ~37 kDa band in the sample shown in figure 5.2 is believed to result from small amounts of schizont contamination. This increase in apparent molecular mass implies that additional phosphorylation may occur between the timepoint at which schizonts were extracted (~42 h post-invasion) and merozoite release (~48 h), or subsequent to erythrocyte rupture. Additionally, upon treatment with lambda phosphatase, PfGAP45 extracted from released merozoites appears to have a smaller molecular mass than the same protein isolated from schizonts. Perhaps the protein is also processed somehow within the same timeframe described above.

Recombinant PfGAP45 is phosphorylated by PfCDPK1 *in vitro*. As previously observed for this kinase and a number of other CDPKs, its activity is critically dependent on Ca^{2+}. Autophosphorylation of the kinase is observed even in the absence of a protein substrate. However, in contrast with analyses performed using RKIP (Kugelstadt, Winter et al. 2007), phosphorylation of PfGAP45 does not enhance autophosphorylation. In the case of PfCDPK1, K_M values for potential endogenous substrates have not yet been published. However, by comparison to those obtained for Mg^{2+} ATP using casein (K_M 26 μM) or histone H1 (K_M 34 μM) as substrates (Zhao, Franklin et al. 1994), values calculated using NADH-coupled kinase assays appear to be within an appropriate range.

ESI-MS analysis of recombinant PfGAP45 phosphorylated by PfCDPK1 suggests that three phosphates are incorporated. Notably, for each charge state, peaks observed in each of the four series showed similar deviations in intensity. Therefore, incorporation of phosphate at each of the three residues does not appear to occur at the same rate i.e. non-stoichiometric. ESI-MS is often referred to as semi-quantitative as peak intensity depends on basicity, molecular mass and concentration of the species in question. Although addition of phosphate will alter basicity, it is presumed the effect would be minimal given the molecular mass of the protein.

MALDI-TOF analysis of peptides generated from phosphorylated recombinant PfGAP45 confirms the presence of three different phosphorylation sites. One of the sites, Ser208, is found in the linker/affinity tag incorporated at the C-terminus of the recombinant protein. It is possible that the tag sequence may have generated a consensus site for phosphorylation by PfCDPK1. The additional phosphopeptides identified in Asp-N digests unfortunately contain more than one serine or threonine residue. Consequentially, residues within PfGAP45 that may be phosphorylated are Thr84 or Ser89 (peptide 2) and Ser101, Ser103, Ser107 or Ser109 (peptide 3). According to the prediction program, only Ser89, Ser101 and Ser103 are considered likely candidates for phosphorylation. This suggests Ser89 is the most likely candidate residue in peptide 2 but either Ser101 or Ser103 in peptide 3 may be modified. However, in peptide 3, cleavage does not occur N-terminally of Asp104. Although this may result from partial cleavage, if phosphorylation occurs at the adjacent N-terminal residue, Ser103, this modification may interfere with proteolysis. Interestingly, both Ser101 and Ser103 are predicted to be phosphorylated with a very high degree of confidence. Despite this, only one residue in peptide 3 was found to be modified. Perhaps another kinase may catalyse phosphorylation at the additional residue or it may be that these residues are in close proximity and if both were modified, the negative charges would repel one another.

The successful isolation of phosphopeptide 2 from Asp-N digests of PfGAP45 extracted from merozoites implies that Thr84 or Ser89 may indeed be a target for PfCDPK1 *in vivo*. The absence of phosphopeptide 3 is not necessarily indicative of its lack of modification within the parasite. With such small quantities of parasite protein being available for analysis, phosphopeptide enrichment was not possible. Therefore, if levels of phosphorylation within the sample are low at this particular site, the mass spectrometer would be unlikely to detect the phosphopeptide.

Interestingly, by SDS-PAGE analysis, unmodified recombinant PfGAP45 and the same protein phosphoylated by PfCDPK1 have identical apparent

molecular masses (data not shown). This suggests there may be additional kinases involved in the phosphorylation of PfGAP45. Very recently, it has been shown that PfGAP45 is also phosphorylated by protein kinase B (PfPKB) (Vaid, Thomas et al. 2008). However, the precise sites that are modified are yet to be confirmed. Therefore, it may be one such site is contained within the tryptic peptide identified exclusively in protein extracted from parasites.

As incorporation of three phosphate groups does not alter the mobility of recombinant PfGAP45 in SDS-PAGE, there may in fact be more phosphorylation sites than have been successfully detected here. A proportion of the PfGAP45 sequence does not give rise to peptides favourable for analysis using MALDI-TOF. By analysis of resulting fingerprints, peptides isolated from parasite protein digests were biased towards the C-terminal region (table 5.2). The extreme N-terminus of PfGAP45 is dually acylated (figure 5.1 and 5.2 A) and thus unlikely to be solubilised in buffers compatible with mass spectrometry. In addition, a large stretch of the N-terminal domain is rich in acidic residues. As ionisation by MALDI is competitive and tends to favour peptides comprising basic amino acids, the signal corresponding to peptides derived from the N-terminus may be suppressed. Therefore, if there are phosphorylation sites in this region of PfGAP45 (as is predicted by NetPhos 2.0), they may be very difficult to detect using this method.

The fact that PfCDPK1 appears to phosphorylate two of the motor components (PfMTIP and PfGAP45) implies that this kinase may function in regulating the acto-myosin motor during invasion and/or gliding motility. Phosphorylation of RLCs by Ca^{2+}/calmodulin-dependent myosin light chain kinases appears to play a pivotal role in the regulation of myosin motors in various muscle and non-muscle tissues. In skeletal muscle, RLC phosphorylation potentiates the force and speed of contractions initiated by Ca^{2+} binding to troponin. It is thought the modification may promote movement of myosin heads away from the thick filament backbone. In smooth muscle and other non-muscle tissues, RLC phosphorylation plays a more central role. It promotes a significant

increase in actin-activated myosin ATPase activity and is sufficient for the initation of smooth muscle contraction (Gallagher, Herring et al. 1997; Kamm and Stull 2001) and references therein).

Although it is not known to which components PfGAP45 is directly associated, the protein is clearly an integral constituent of the myosin motor complex essential for host cell invasion (figure 3.2.4, Baum, Richard et al. 2006; Jones, Kitson et al, 2006). Consequently, phosphorylation may be critical to its function within the parasite. As there appear to be multiple phosphorylation events involving more than one kinase, individual modifications may have consequences applicable to specific stages in both complex formation and subsequent motor activity.

Phosphorylation that takes place prior to or in concurrence with palmitoylation may promote or increase affinity of interactions between specific components in the cytoplasm or at the membrane. Interestingly, phosphopeptides identified thus far are located in the low complexity region of GAP45 that exhibits poor conservation across the phylum (table 5.2 and figure 4.14). It may be that the addition of negative charge to this region induces a structural transition required for high affinity interaction with one or more of the other motor components. Additional phosphorylation that occurs subsequent to firm membrane attachment might be required for activation or regulation of the motor during invasion.

Table 5.1

Predicted phospborylation sites in PfGAP45

Sequence	Residue	Probability
KCSRSKVKE	Ser8	0.525
LKKQSEEII	Ser31	0.805
QVEETHEEP	Thr49	0.744
QENKSFEEK	Ser89	0.997
DLERSNSDI	Ser101	0.962
ERSNSDIYS	Ser103	0.956
FDNASDKLE	Ser116	0.699
QLTLSTEAT	Ser128	0.993
AHEESIYFT	Ser149	0.521
SIYFTYRSV	Thr153	0.500
YRSVTPCDM	Thr158	0.962
KLDETAKVF	Thr168	0.599
AKVFSRRCG	Ser173	0.989
KIDLSDTPL	Ser198	0.799

Table 5.2

Peptides identified in parasite-derived PfGAP45

Enzyme	Sequence	Residues
Trypsin:	DIDELAER	17-24
	DIDELAERENLK	17-28
	LSEPAHEESIYFTYR	141-155
	RCGCDLGER	175-183
	KIDLSDTPLLS	194-204
Asp-N:	DEQKIEEEEEEPEQVPKEEI	61-80
	DETAKVFSRRCGC	166-178
	DENACKICRKI	185-195
	DENACKICRKIDLS	185-198

Figure 5.1

PfGAP45 is a substrate for PfNMT *in vitro*

In vitro *N*-myristoylation assays. (A) (Panel 1): Coomassie-blue stained SDS-PAGE gel demonstrating the mobility of recombinant proteins used in each assay. PfGAP45 migrated at ~36 kDa (lanes 2 and 4), PfARF1 at ~20 kDa (lane 3) and PfNMT at ~51 kDa (lanes 1, 3 and 4). (Panel 2): Exposure of assay samples to X-ray film. Both recombinant PfARF1 and PfGAP45 were radiolabelled only in the presence of PfNMT (lanes 3 and 4 respectively). Asterisks represent breakdown products of recombinant PfGAP45 and molecular mass markers are shown in-between the two panels. (B) Assay using a Gly2Ala variant of recombinant PfGAP45. Where the wild-type recombinant protein was reproducibly radiolabelled (panel 2, lane 3), the variant protein that also migrated at ~36 kDa (panel 1, lane 4) was not detected in the corresponding autoradiograph (panel 2, lane 4).

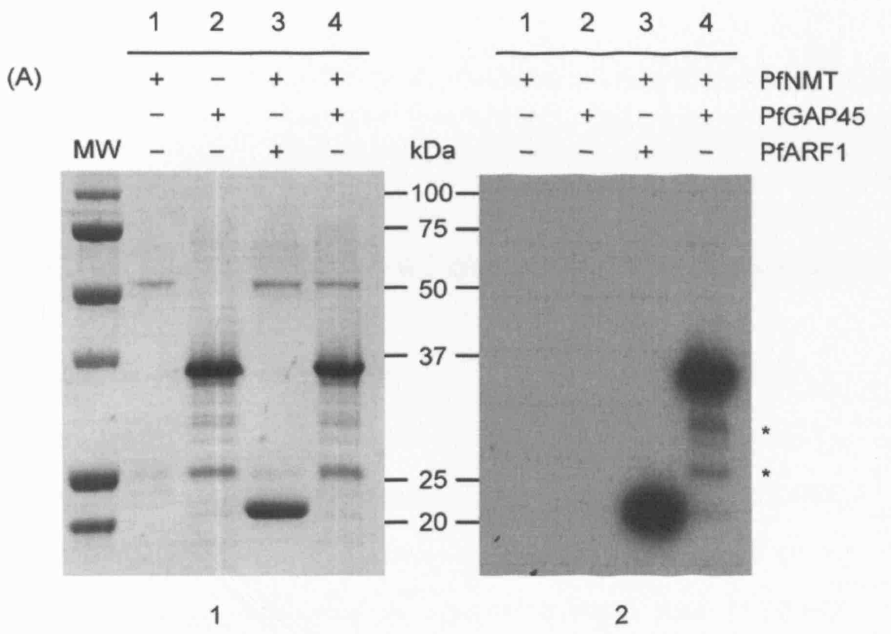
(A)
1 2 3 4
1 2 3 4
+ − + + + − + + PfNMT
− + − + − + − + PfGAP45
MW − − + − kDa − − + − PfARF1
100
75
50
37
25
20
*
*
1
2

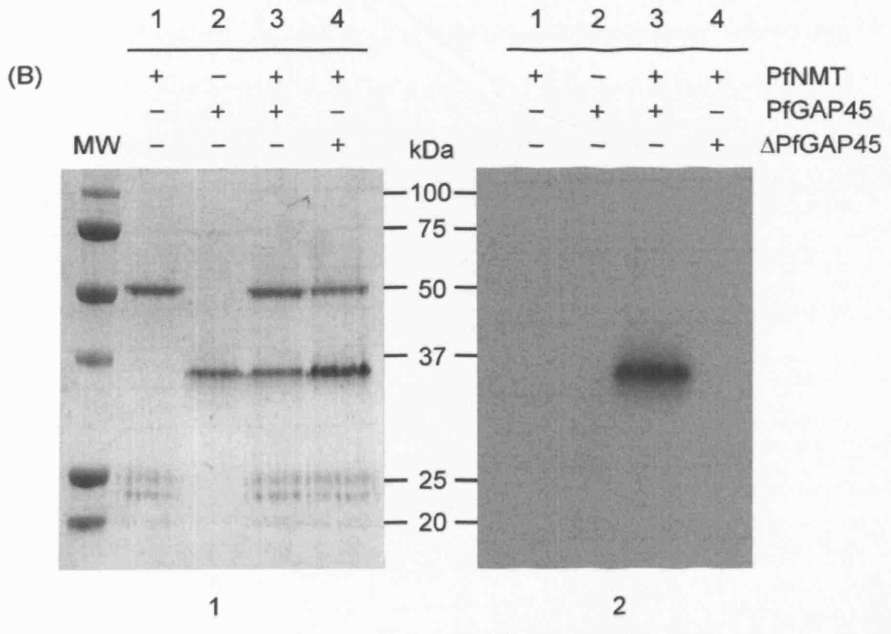
(B)
1 2 3 4
1 2 3 4
+ − + + + − + + PfNMT
− + + − − + + − PfGAP45
MW − − − + kDa − − − + ΔPfGAP45
100
75
50
37
25
20
1
2

Figure 5.2

PfGAP45 is dually acylated and phoshorylated in merozoites

(A) Autoradiographs showing immunoprecipitation of PfGAP45 from ^{35}S-labelled schizonts (panel 1) or schizonts grown in the presence of [^{3}H] myristic acid or palmitic acid (panels 2 and 3 respectively). All parasites were extracted in 1% (w/v) SDS. Mouse PfGAP45 antiserum precipitated either a ~37-39 kDa doublet (panels 1 and 2) or a single ~39 kDa band (panel 3). The asterisk represents potential contamination from unincorporated fatty acid used in the labelling procedure. Immunoprecipitations performed for each of the labelling experiments using normal mouse serum did not give rise to any radiolabelled bands (data not shown). (B) Western blot analysis of protein extracted from late-stage schizonts (SZ) or purified merozoites (MZ). Lanes 3 and 4 contain protein extracts treated with lambda phosphatase. In untreated samples (lanes 1 and 2), mouse PfGAP45 antiserum detected a ~37-39 or ~37-40 kDa doublet for schizonts and merozoites respectively. Subsequent to phosphatase treatment, the protein migrated as a single band of ~37 or ~36 kDa (for schizonts and merozoites respectively).

(A)

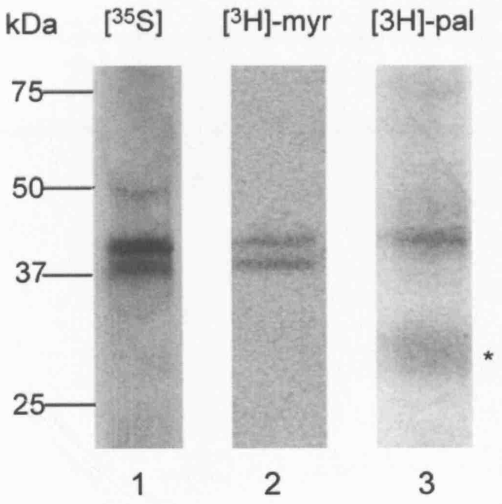
kDa
[35S]
[3H]-myr
[3H]-pal
75
50
37
25
*
1
2
3

(B)

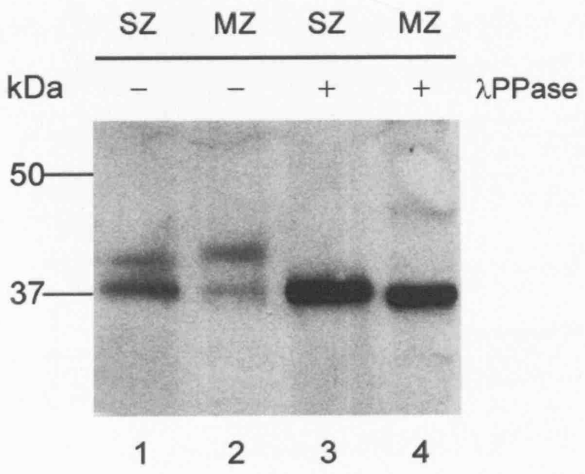
SZ
MZ
SZ
MZ
kDa
–
–
+
+
λPPase
50
37
1
2
3
4

Figure 5.3

PfGAP45 is a substrate for PfCDPK1 *in vitro*

In vitro [γ-^{32}P] ATP kinase assays. (A) Coomassie blue-stained SDS-PAGE gel showing relative mobilities of recombinant proteins used in each assay. Protein bands were observed at molecular masses ~68, 67, 40, 36, 30 and 22 kDa that correspond to recombinant PfCDPK1 (lanes 1,2,4,6,7,8 and 9), BSA (lane 8), PfGAP50 (cleaved with factor Xa) (lane 9), PfGAP45 (lanes 3 and 4), PfMTIP (lanes 5 and 6) and $MSP7_{22}$ (lane 7) respectively. (B) Exposure of protein samples from (A) to X-ray film. PfCDPK1 was always radiolabelled except in the presence of 1 mM EGTA (lane 2) and bands corresponding to PfGAP45 and PfMTIP were also radiolabelled when the kinase was present (lanes 4 and 6 respectively). Asterisks represent cleavage of the N-terminal tag from recombinant PfCDPK1 by low levels of factor Xa present in the PfGAP50 sample. Molecular mass markers are shown on the left hand side of the panels.

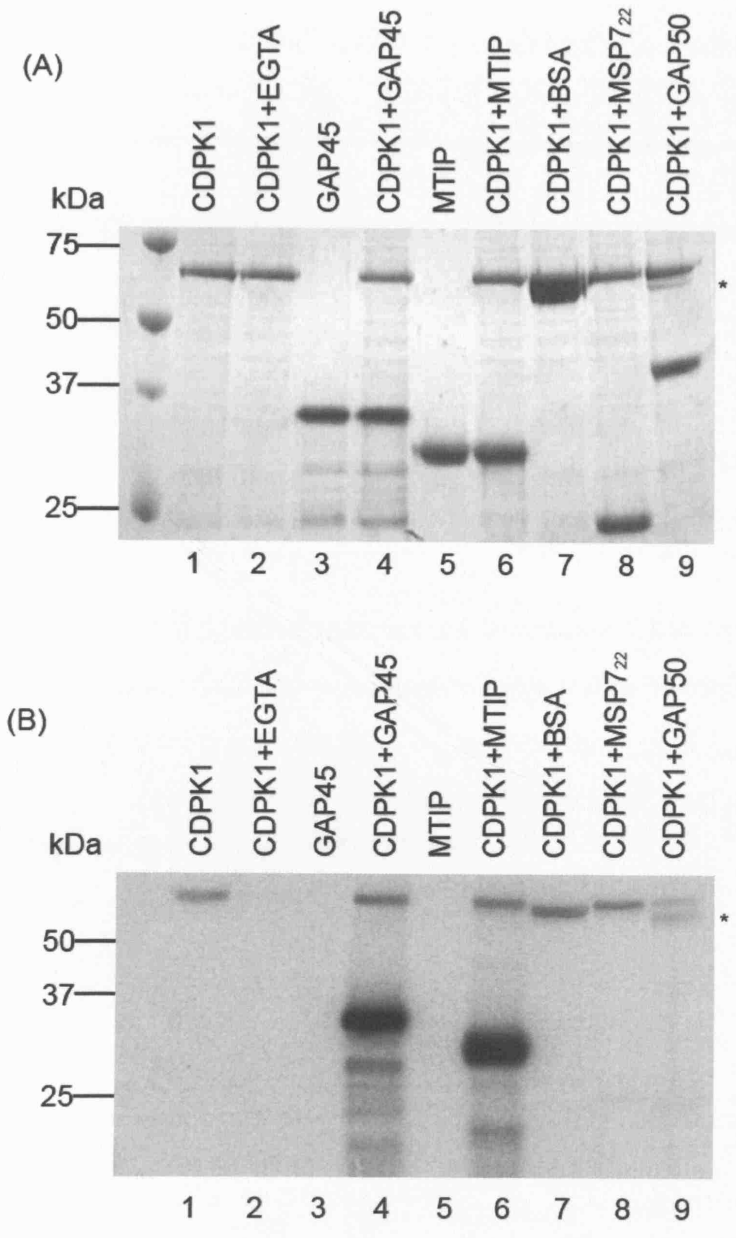
(A)
kDa
CDPK1
CDPK1+EGTA
GAP45
CDPK1+GAP45
MTIP
CDPK1+MTIP
CDPK1+BSA
CDPK1+MSP7$_{22}$
CDPK1+GAP50
75
50
37
25
*
1 2 3 4 5 6 7 8 9
(B)
kDa
CDPK1
CDPK1+EGTA
GAP45
CDPK1+GAP45
MTIP
CDPK1+MTIP
CDPK1+BSA
CDPK1+MSP7$_{22}$
CDPK1+GAP50
50
37
25
*
1 2 3 4 5 6 7 8 9

Figure 5.4

The kinetics of PfCDPK1-catalysed phosphorylation

In vitro NADH-coupled kinase assays using recombinant PfCDPK1. Shown here are plots of initial rates against concentration of ATP (A) or GAP45 (B). Values for K_M were calculated as 96 ± 28 μM and 18 ± 5 μM respectively using the non-linear least squares method (see section 2.9.3).

(A)

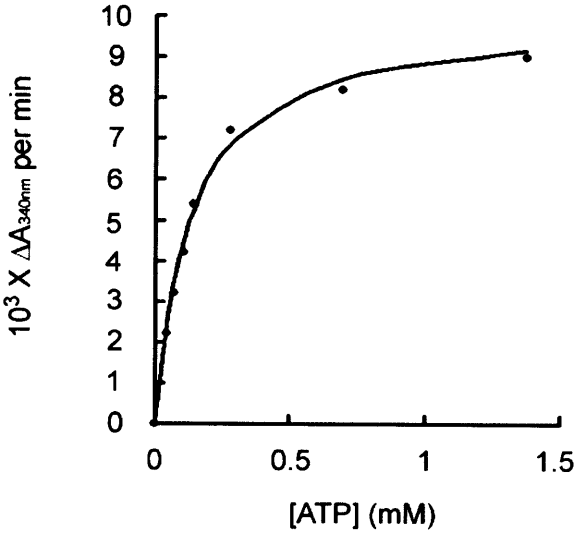
10
9
8
7
6
5
4
3
2
1
0
10^3 X ΔA_{340nm} per min
0
0.5
1
1.5
[ATP] (mM)

(B)

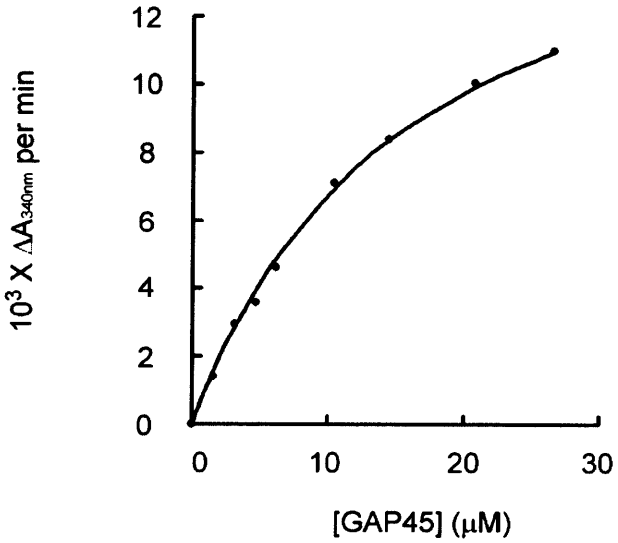
12
10
8
6
4
2
0
10^3 X ΔA_{340nm} per min
0
10
20
30
[GAP45] (μM)

Figure 5.5

Recombinant PfGAP45 is modified at three different sites

The mass spectrum observed for recombinant PfGAP45 phosphorylated *in vitro* by recombinant PfCDPK1, analysed by ESI-MS. Four distinct series were observed (A-D) and individual peaks used to calculate corresponding molecular masses (24711.67 ± 2.99, 24795.29 ± 7.03, 24875.07 ± 5.54 and 24.958.46 ± 10.27 respectively). Molecular masses of peaks comprising series A corresponded to the predicted mass of recombinant PfGAP45 (24710.8 Da) and increases in mass observed for the other three series (~80 Da) equates to the net addition of phosphate i.e. 1, 2 and 3 groups for series B, C and D respectively.

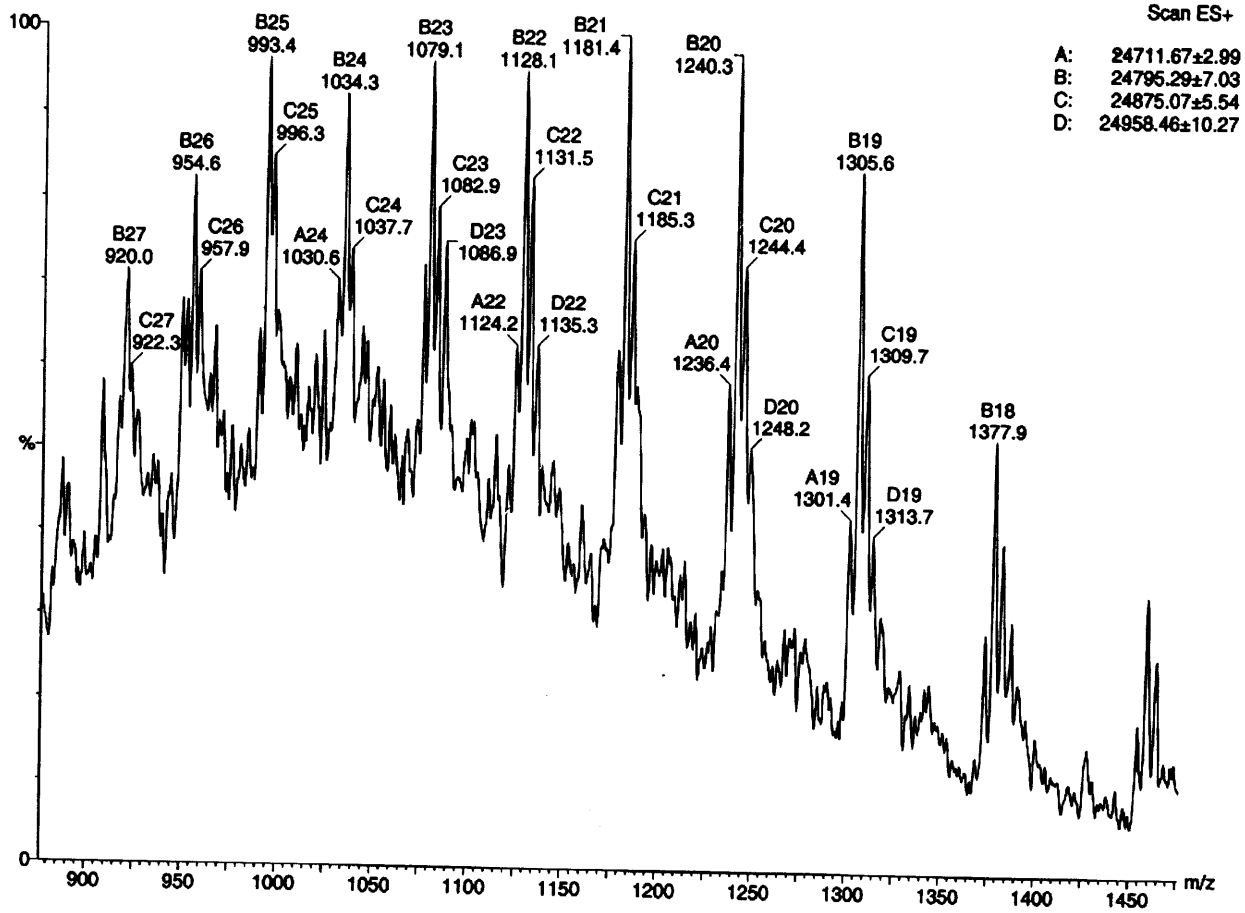
Scan ES+
A: 24711.67±2.99
B: 24795.29±7.03
C: 24875.07±5.54
D: 24958.46±10.27
100
%
0
B25 993.4
B24 1034.3
B23 1079.1
B22 1128.1
B21 1181.4
B20 1240.3
B26 954.6
C25 996.3
C22 1131.5
C23 1082.9
C21 1185.3
B19 1305.6
B27 920.0
C26 957.9
A24 1030.6
C24 1037.7
D23 1086.9
C20 1244.4
A22 1124.2
D22 1135.3
C27 922.3
A20 1236.4
C19 1309.7
D20 1248.2
B18 1377.9
A19 1301.4
D19 1313.7
900
950
1000
1050
1100
1150
1200
1250
1300
1350
1400
1450
m/z

Figure 5.6

Phosphates are incorporated between residues 81-112 of PfGAP45

Identification of recombinant PfGAP45 phosphopeptides using MALDI-TOF mass spectrometry. For analyses, PfGAP45 phosphorylated by recombinant PfCDPK1 (*in vitro*) was digested with either trypsin (A) or Asp-N (B) and phosphopeptides enriched using gallium (III) resin. One phosphopeptide (R↓S*HHHHHH*), spanning residues 208-214 of PfGAP45 was isolated from tryptic digests, whereas digestion with Asp-N revealed three phosphopeptides. The sequence of one of these (↓DTPLLSGSRS*HHHHHH*) overlapped with that of the tryptic peptide and the two novel peptides (↓DYATQENKSFEEKHLE↓D and ↓DLERSNSDIYSESQKF↓D) spanned residues 81-96 and 97-112 of the protein.

(A)

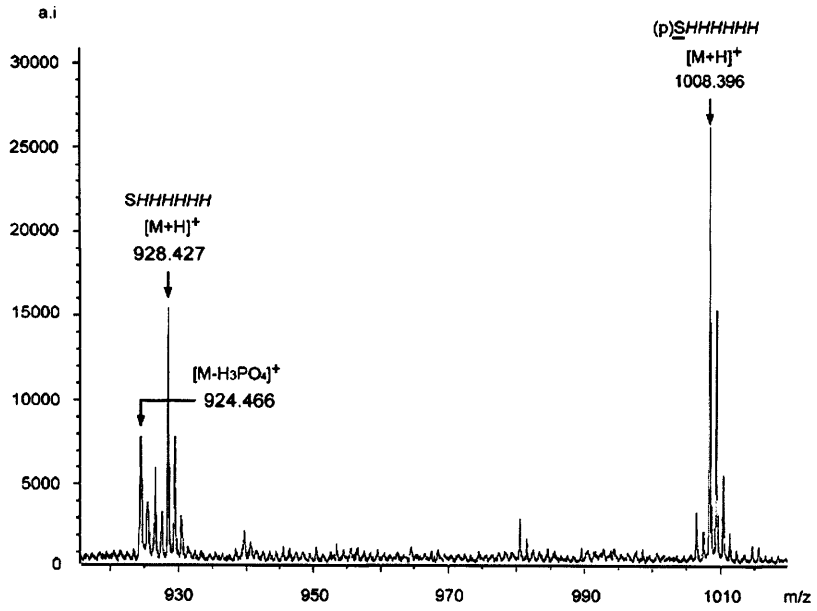
a.i
30000
25000
20000
15000
10000
5000
0
930
950
970
990
1010
m/z
(p)SHHHHHH
[M+H]+
1008.396
SHHHHHH
[M+H]+
928.427
[M-H3PO4]+
924.466

(B)

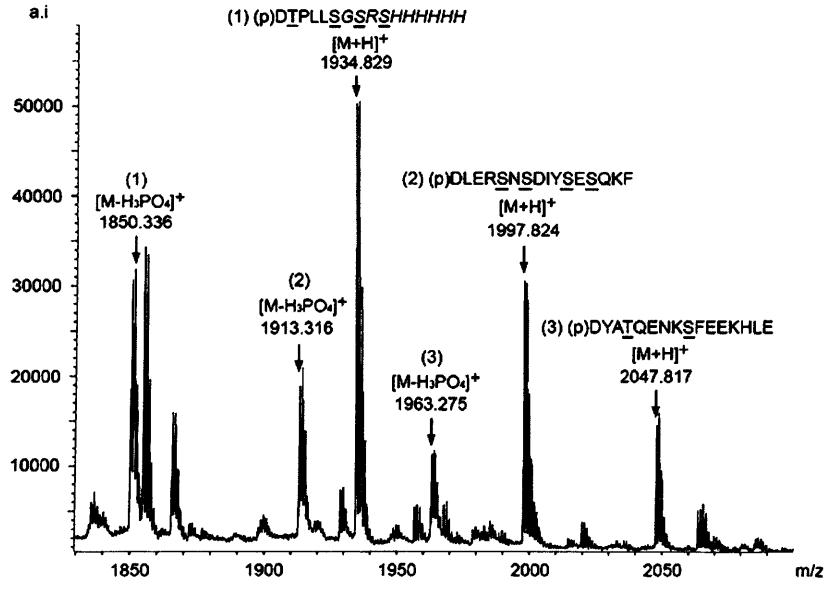
a.i
50000
40000
30000
20000
10000
1850
1900
1950
2000
2050
m/z
(1) (p)DTPLLSGSRSHHHHHH
[M+H]+
1934.829
(1)
[M-H3PO4]+
1850.336
(2)
[M-H3PO4]+
1913.316
(3)
[M-H3PO4]+
1963.275
(2) (p)DLERSNSDIYSESQKF
[M+H]+
1997.824
(3) (p)DYATQENKSFEEKHLE
[M+H]+
2047.817

Figure 5.7

Determination of metastable fragment ion true molecular masses

Post-source decay (PSD) scans performed using Asp-N digests of recombinant PfGAP45 phosphorylated by PfCDPK1 (*in vitro*) and enriched using gallium (III) resin. In the case of all three phosphopeptides (A-C respectively), although molecular masses of the parent ions ($[M+H]^+$) were unchanged, the true molecular masses lost due to fragmentation correspond to ~98 Da ($[MH-H_3PO_4]^+$).

(A)

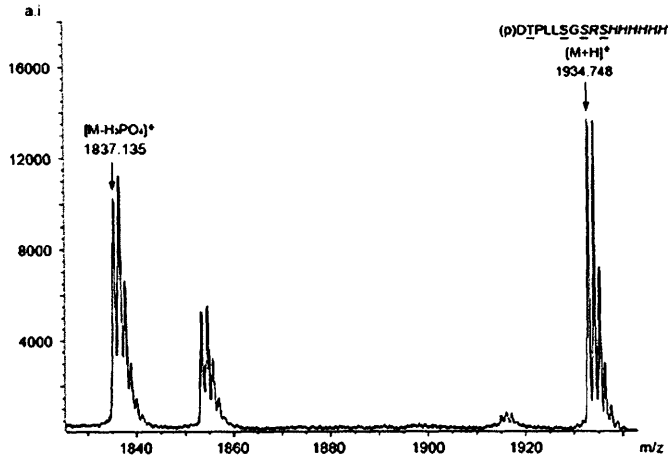
a.i
16000
12000
8000
4000
[M-H3PO4]+
1837.135
(p)DTPLLSGSRSHHHHHH
[M+H]+
1934.748
1840
1860
1880
1900
1920
m/z

(B)

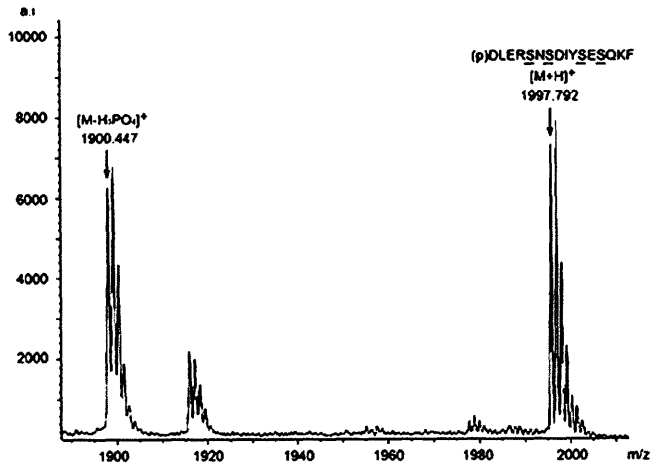
a.i
10000
8000
6000
4000
2000
[M-H3PO4]+
1900.447
(p)DLERSNSDIYSESQKF
[M+H]+
1997.792
1900
1920
1940
1960
1980
2000
m/z

(C)

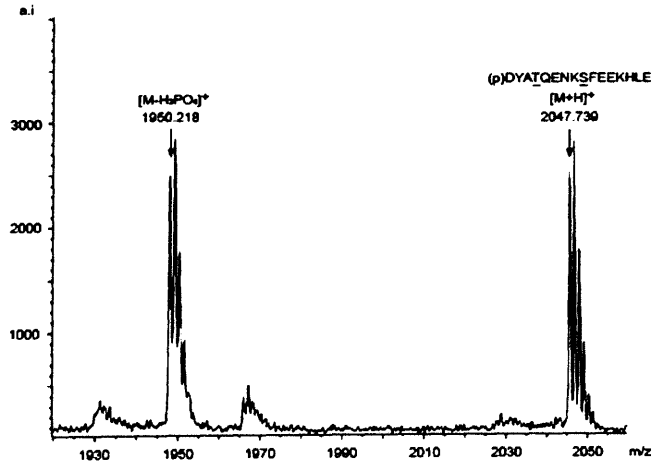
a.i
3000
2000
1000
[M-H3PO4]+
1950.218
(p)DYATQENKSFEEKHLE
[M+H]+
2047.739
1930
1950
1970
1990
2010
2030
2050
m/z

Figure 5.8

Purification of PfGAP45 from merozoites

Purification of PfGAP45 from merozoites (A) Western blot analysis of 1 ml fractions eluted stepwise from a rabbit anti-PfGAP45 affinity column. Mouse PfGAP45 antiserum predominantly detected a ~40 kDa band that had previously been observed for PfGAP45 in merozoites. Although most abundant in lanes 3 and 4, protein was detected in all 10 fractions. Asterisks represent either cross-reactivity of the antiserum with antibodies eluted from the column or co-purification of additional parasite proteins. (B) Pooled, concentrated fractions from (A) separated by SDS-PAGE and stained using colloidal blue. The ~40 kDa band corresponding to PfGAP45 was excised from the gel and analysed by MALDI-TOF. Asterisks represent contamination of the sample with additional parasite proteins. Molecular mass markers are shown on the left hand side of the panels.

(A)

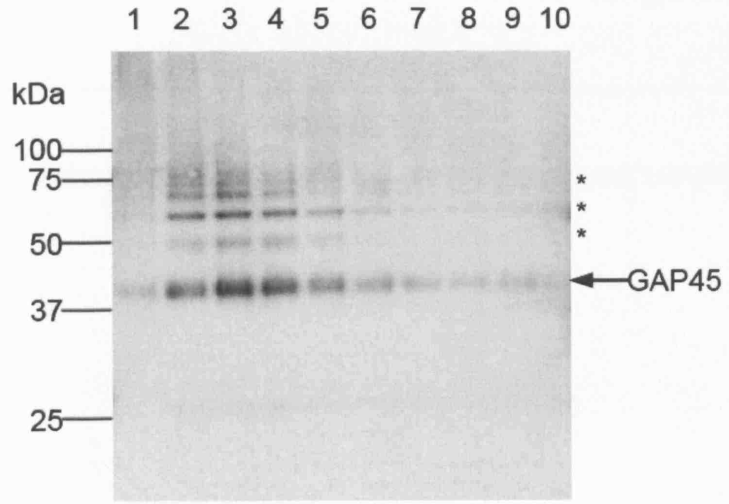
1 2 3 4 5 6 7 8 9 10
kDa
100
75
50
37
25
*
*
*
GAP45

(B)

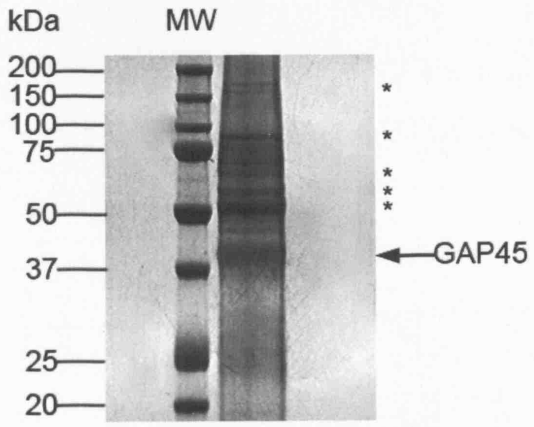
kDa
MW
200
150
100
75
50
37
25
20
*
*
*
*
*
GAP45

Figure 5.9

Identification of two parasite-derived phosphopeptides

Identification of parasite-derived PfGAP45 phosphopeptides using MALDI-TOF mass spectrometry. Bands corresponding to PfGAP45 were excised from SDS-PAGE gels and protein digested with either Asp-N (A) or trypsin (B). Manual analyses of the spectra obtained revealed two phosphopeptides. One previously identified peptide was isolated from Asp-N digests (↓ DYATQENKSFEEKHLE ↓ D) and a novel tryptic peptide was identified (K ↓ LSEPAHEESIYFTYR ↓), spanning residues 141-155 of PfGAP45.

(A)

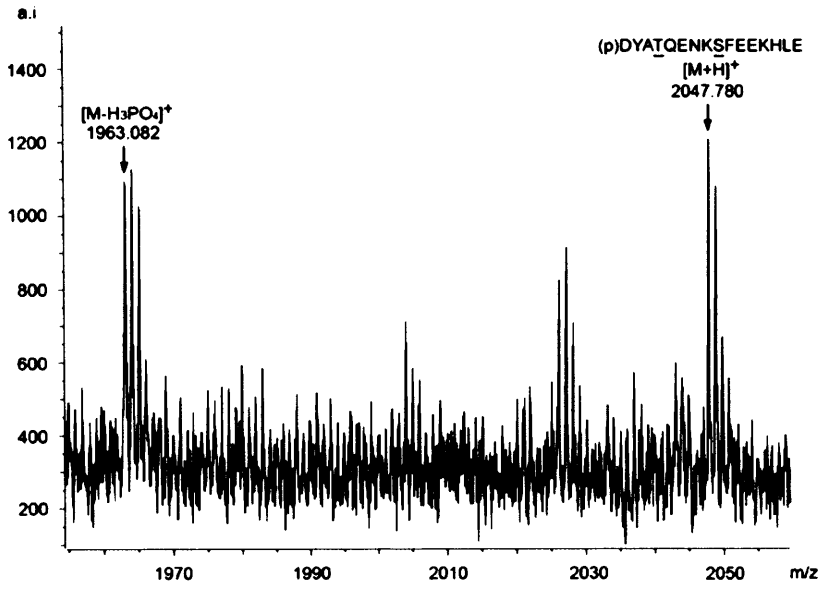
a.i
1400
1200
1000
800
600
400
200
[M-H3PO4]+
1963.082
(p)DYATQENKSFEEKHLE
[M+H]+
2047.780
1970
1990
2010
2030
2050
m/z

(B)

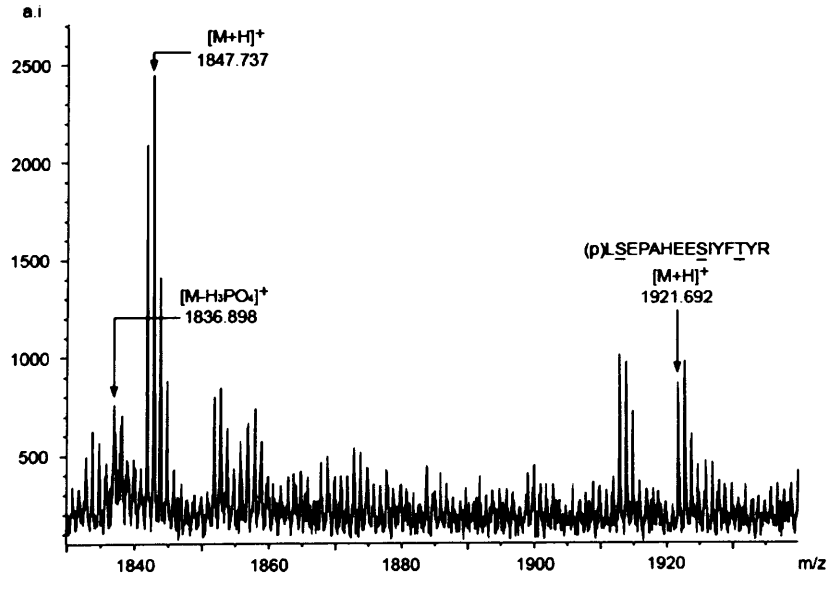
a.i
2500
2000
1500
1000
500
[M+H]+
1847.737
[M-H3PO4]+
1836.898
(p)LSEPAHEESIYFTYR
[M+H]+
1921.692
1840
1860
1880
1900
1920
m/z

Chapter Six

Conclusions and perspectives

Undeniably, any successful strategy for prevention or treatment of malaria requires an indepth understanding of the mechanisms adopted by the parasite to ensure its survival and propagation. The blockade of any process essential for parasite viability is the definitive milestone for any research group.

Host cell penetration and/or gliding motility are intricate processes that unify all known species of Apicomplexa. With the discovery that an acto-myosin based motor is critically required for both events, ablation of any function vital for activity is a much sought-after goal. However, using simplistic terms, in order to make or break something, you need to know how the pieces fit together.

The recent discovery that MyoA is found in a tetrameric protein complex poses important questions in regard to how the motor is both assembled at the right location and regulated during mechanical activity. As the GAPs also appear to be essential parasite proteins, deciphering their individual roles within the complex and in invasion/motility is a prerequisite for compiling a broader understanding of these processes.

6.1 Conservation of the tetrameric motor complex

Comparative analyses of GAP sequences from a wide range of apicomplexan parasites suggest both proteins are highly conserved. This would imply they have similar roles within these organisms. However, no two parasites are identical and within the genera, significant variation exists in the lifecycle and host range of individual species. As a consequence, direct extrapolation should not be made between different species purely based on sequence conservation; subtle differences observed within organisms may underlie unique functional aspects. Conservation of function can only truly be determined experimentally. Therefore, the primary goal of this research project was to establish that the same tetrameric complex exists in *P. falciparum* as has been recently identified in *T. gondii*.

Western blotting experiments performed on protein extracted from both late stage (~42 h post-invasion) schizonts and released merozoites successfully confirmed that both PfGAPs are expressed at a timepoint indicative of their

potential role in erythrocytic invasion. Solubility tests performed using the same parasite material deduced that, like in *T. gondii*, both PfGAPs are primarily associated with membranes.

Immunofluorescence and immunoEM analyses elucidated that PfGAPs, like TgGAPS, are located at the periphery of merozoites. However, their precise location within the pellicle could not be ascertained. As discussed in section 3.3, achieving high resolution of *P. falciparum* merozoite ultrastructure in these types of analyses can be difficult. It may be that some adaptation to the immunoEM procedure is necessary. For example, direct conjugation of primary antibodies to gold particles may decrease steric hinderance imposed by the use of a secondary antibody. Alternatively, dual labelling with either PfMTIP or PfMyoA could be attempted to illustrate spatial arrangement of the complex at the parasite surface. If successful, resulting evidence may constitute a model favouring one membrane location over the other.

Metabolic radiolabelling of parasite proteins expressed in late schizogony enabled the immunoprecipitated tetrameric complex to be successfully detected by autoradiography. However, further analysis is required to elucidate whether this complex comprises a 1:1 mixture of each protein component. If immunoprecipitations were repeated using monoclonal antibodies raised against one or more of the motor proteins, accurate quantitation might be possible. The recent discovery that PfPKB appears to co-precipitate with the tetrameric complex and the presence of additional un-idenitified species in immunoprecipitations performed here suggests there may be other proteins/co-factors associated with the complex that are important in regulation of the motor and/or function. If sufficient quantities of the complex could be extracted from parasites, it may be possible to identify some of these unknown components, using mass spectroscopy for example.

Pulse-chase labelling experiments also demonstrated that a conserved two-stage mechanism underlies formation of the tetrameric complex. However, residues important for acylations likely to traffic and anchor GAP45 at

membranes are not conserved in all apicomplexan species. These anomalies highlight the possibility that functional differences may exist between individual organisms. Given that results suggest there are subsets of di-, tri- and tetrameric complexes present in merozoites and that relative intensities of bands corresponding to each component vary over time (i.e. in pulse-chase experiments), one might speculate that there are additional roles for individual proteins or subsets of complexes in the parasite. Perhaps the identification of other components that interact with members of the complex will provide some insight into alternative functions for these proteins. A potentially important limitation with analyses performed in this chapter is that parasites synchronised at one specific timepoint (~42 h post-invasion) during the erythrocytic cycle were analysed. As microarray experiments suggest the PfGAPs are also expressed in earlier blood stages, it is possible they have alternative functions at these timepoints. Perhaps further analyses at the protein level could be carried out at a variety of timepoints in the erythrocytic cycle.

Collectively, results presented here suggest that a conserved tetrameric motor complex does exist in invasive apicomplexan zoites. Further investigation is undoubtedly required to define precisely how conserved the functions of individual proteins are both within the complex and ultimately, in mechanical activity of the motor.

6.2 Structure of PfGAPs

The successful production of recombinant PfGAPs in reasonable quantities facilitated an effective assessment of their secondary and tertiary structure. Recombinant PfGAP45 expressed in prokaryote and eukaryotic heterologous systems appeared to have a low overall content of secondary structure. This is despite the prediction that this protein has a high content of α-helix. However, examination of tertiary structure suggested the *E. coli* protein was at least partially folded.

Evidently, the precise nature of this unfolded state needs to be examined in greater detail. If expression of truncated forms of PfGAP45 is possible, their analysis using similar spectroscopic methods might determine whether specific regions form a more ordered conformation. If co- and/or post-translational modification are required for protein folding, the ability to reproduce at least two of these processes *in vitro* might be a valuable tool for evaluating their effects on structure. Whether association with other motor components imposes conformational changes on PfGAP45 can only be effectively examined once a direct interaction has been identified. Alternatively, if correct folding of PfGAP45 is dependent on host-specific factors, analysis of the parasite protein would be a necessity. Unfortunately, extracting sufficient quantities for analyses would be an arduous task.

In contrast, analyses of recombinant PfGAP50 imply the protein is folded into an ordered conformation. The calculated content of secondary structure was compable to that of the prediction, suggesting the protein adopts a similar conformation in the parasite. Aggregation of heat-unfolded polypeptides is a commonly observed phenomenon that limits effective determination of conformational stability. Denatured states obtained under various unfolding conditions can exhibit different physical properties, despite being instinguishable thermodynamically (Creighton 1993). As an alternative to temperature, the unfolding of PfGAP50 could therefore be monitored by treatment with chemical denaturants such as GuHCl or urea.

Naturally, for both PfGAPs, detailed examination of protein architecture could only be obtained using alternative methods such as X-ray crystallography.

6.3 Direct intra-complex associations

Although results presented in this report confirm that both PfGAPs do form part of a tetrameric protein complex, direct interactions of either protein with other members of the complex were not successfully identified.

In *T. gondii*, it has been suggested that the short C-terminal tail (residues 427-431) of TgGAP50 participates in intra-complex association (Gaskins, Gilk et al. 2004). While expression of a full-length TgGAP50-YFP (yellow fluorescent protein) fusion protein was not deleterious to parasite growth, stable transfectants could not be obtained with a mutant protein missing this domain. Immunoprecipitation of the complex from parasites transiently expressing TgGAP50Δ(427-431)YFP showed that unlike TgGAP50-YFP, the mutant protein did not interact with the other subunits (Gaskins, Gilk et al. 2004).

Given that GAP50 is proposed to be the principle membrane anchor for the motor, maintenance of firm association with other complex components comprising such a small stretch of amino acids might be deemed unfeasible. Interestingly, 3 out of the 6 residues are positively charged. Hence, it is possible this region is required for stable membrane anchorage through interaction with phospholipid head groups. Its deletion may therefore disrupt membrane association and account for observations made in *T. gondii*.

Elucidating the topological arrangement of GAP50 in membranes would seem a crucial goal in determining precisely how the motor complex is assembled. Although it has been proposed that the majority of the protein resides in the lumen of the IMC (Gaskins, Gilk et al. 2004), this has not been evaluated experimentally. Indeed, membrane trafficking in *P. falciparum* is still somewhat poorly defined. Nonetheless, one important factor to consider is the role of its N-terminal signal sequence. To elucidate the function of this region in PfGAP50, parasites could be transfected with a fusion protein comprising the N-terminal signal sequence linked to a detectable cytoplasmic protein such as GFP. Its fate could then be tracked by comparing extracts containing soluble or membrane-bound proteins.

Undoubtedly, potential interaction of the PfGAP50 tail with other proteins in the complex needs to be investigated. Experimentation using fluorescently-labelled synthetic peptides may help deduce whether this region is involved in binding and more specifically, to which components. Whether the remainder of

PfGAP50 participates in intra-complex associations could also be analysed using the truncated recombinant protein.

Despite extensive experimentation using a wide range of techniques, a direct interaction of PfGAP45 with either the PfMyoA tail or PfMTIP could not be established. Since there is evidence for an association between recombinant forms of PfGAP45 and PfMTIP *in vitro* (Vaid, Thomas et al. 2008), possible tagging and/or misfolding issues accompanying recombinant PfGAP45 used in these analyses need to be addressed. To rule out the possibility that C-terminal tagging of PfGAP45 interferes with conformation and/or binding, it may be necessary to express the protein with an N-terminal tag and repeat analyses. Additionally, although evidence suggests recombinant PfMTIP used in these analyses has an ordered conformation, it is important to confirm the binding site is intact. Therefore, repeating experiments with untagged or C-terminally tagged recombinant PfMTIP might also be desirable.

6.4 The role of PfGAPs

Although comprehensive evidence now exists to support GAPs being an integral part of the tetrameric motor complex that is essential for erythrocyte invasion, their precise functions are still unclear. While it is evident their characterisation will be an ongoing process, results obtained here perhaps represent one novel piece of a sizeable puzzle. There are also implications that the roles of PfGAPs and/or PfMyoA and PfMTIP may extend beyond that of their function in the invasive motor.

Results described in this report show that phosphorylation of at least two of the motor components occurs in merozoites. If modification by kinases has a regulatory role in the function of the motor, it is feasible to assume there may also be phosphatases that remove phosphates when appropriate. Besides its likely role in anchoring the tetrameric complex at membranes, it has recently been noted that GAP50 and its orthologues demonstrate 22-26% sequence identity with a number of plant and animal purple acid phosphatases (PAPs) (Gaskins, Gilk et al. 2004).

PAPs are required for phosphate acquisition by plants but besides a few enzymes that perform specific metabolic functions, a precise role has not been assigned to many of them (Olczak, Morawiecka et al. 2003). Despite this, all PAPs contain a binuclear metal core that is important for the coordination of phosphate. Consequently, a set of seven amino acids are highly conserved across the group.

As shown in a multiple aligment of various apicomplexan GAP50 sequences with rat PAP, many of the residues critical for enzymatic activity are not conserved (Gaskins, Gilk et al. 2004). By inspection of the conserved domain in PfGAP50, the region comprising residues 26-331 is assigned to the metallo-dependent phosphatase superfamily with a high degree of confidence (Superfamily 1.69 HMM library and genome assignments server). However, its classification into the sub-family of acid phosphatases is very weak. Perhaps apicomplexan GAP50 proteins represent a novel sub-family of enzymes that are as yet undefined.

As the truncated form of PfGAP50 successfully expressed here appears to adopt an ordered conformation, it would not be unfeasible to test for phosphatase activity. A number of assays can be used to monitor dephosphorylation and characterise enzyme kinetics, e.g. p-Nitrophenyl phosphate (pNPP) is proven to be an effective chromogenic substrate for all types of protein phosphatases. If GAP50 is in fact a phosphatase, this would represent a novel function within the parasite. It may be that this protein is important in downregulating the phosphorylation of either PfGAP45 or PfMTIP; a consequence that may affect activity of the acto-myosin motor during erythrocytic invasion. Alternatively, although residues required for catalysis are not conserved, PfGAP50 might bind phosphates on PfGAP45 or PfMTIP and prevent their removal until necessary.

Radiolabelling experiments revealed that PfGAP45 is dually acylated in the parasite. However, despite the strong possibility these lipidations are required for trafficking and subsequent attachment of the ternary complex to membranes, these hypotheses need to be tested *in vivo*. Parasites could be transfected with a series of constructs in order to express PfGAP45 mutants where Gly2, Cys5 or

both are replaced with alternative amino acids. Evaluation of resulting phenotypes should define a more precise role for these modifications. Although Cys5 is the most probable candidate for palmitoylation, it cannot be ruled out that one or more of the other 5 cysteines may in fact be modified. If mutation of Cys5 does not affect membrane association of PfGAP45, it may be necessary to analyse multiple variants where alternative cysteines are replaced individually or in combination.

In addition to acylation, PfGAP45 was found to be phosphorylated at multiple sites both *in vitro* and *in vivo*. However, further investigation is needed to identify which residues are modified. Tandom mass spectrometry (MS-MS) could be used to detect phosphorylation sites. Phosphopeptide mixtures are first ionised by nanospray-ESI (a low flow rate version of ESI-MS) in order to generate a mass spectrum. Protonated ions for individual phosphopeptides are then collided with an inert gas that induces fragmentation. Some of this fragmentation occurs across the peptide backbone and gives varying degrees of sequence information. Unfortunately, attempts at obtaining sequence information for PfGAP45 phosphopeptides have so far been unsuccessful. Peptide samples analysed so far did not give rise to phosphopeptide-related ions under nanospray conditions. If repeat experiments do not yield the required information, more time consuming analyses involving various mutant proteins or peptides might be necessary.

Results also indicate that PfCDPK1 is capable of phosphorylating PfGAP45 *in vitro*. Despite the existence of an overlapping peptide, further evidence is required to confirm PfGAP45 is indeed a substrate for this kinase *in vivo*. An important first step would be to show that the second phosphopeptide modified by the kinase *in vitro* is also modified in the parasite. As inherent technical difficulties and sequence constraints have somewhat plagued analyses thus far, the ability to extract larger quantites of PfGAP45 from parasites would likely be invaluable. This might be possible if a monoclonal antibody was raised against the protein and utilised in affinity columns. It should be noted however, that protein abundance is not likely to improve detection of PfGAP45 peptides

rich in acidic amino acids. Therefore, if there are additional sites contained in these regions, they may be extremely difficult to isolate.

In contrast to those raised against PfPKB (Vaid, Thomas et al. 2008), PfCDPK1 antibodies do not appear to co-precipitate proteins of the tetrameric complex (Green et al, unpublished data). This may not be suprising though, as many kinases only exhibit transient association with their substrate proteins. It is not known whether disruption of *Pfcdpk1* will result in a lethal phenotype. However, if phosphorylation of its substrates is essential for parasite survival, this may well be the case. However, if a conditional knockout could be generated such as that described for *TgmyoA* (Meissner, Schluter et al. 2002), downstream effects specific to the kinase could then be investigated.

In spite of analyses undertaken so far, a precise role for PfGAP45 has still not been ascertained. However, the identification of such extensive modification poses a number of questions that could be addressed in future research efforts. As stated in section 6.2, the ability to modify PfGAP45 *in vitro* might be crucial in evaluating possible effects. If one or more of the recognised modifications affect protein structure or interaction with another component, this could be monitored using CD and/or fluorescence spectroscopy. As the tetrameric complex can be effectively immunoprecitated from parasites, this may also be a valuable tool. If phosphorylation of PfGAP45 increases the affinity of its interaction with other components of the complex, treating extracts with phosphatases may significantly alter relative quantites of proteins precipitated.

Determining whether phosphorylation regulates the acto-myosin motor is a more complex task. The ability of the PfMyoA complex to bind and translocate Pfactin can be monitored by capturing the complex onto a surface with PfMTIP-specific antibodies (Green et al, 2006). It may be that if parasites are treated with phosphatases prior or subsequent to extraction of the complex, resulting velocities of Pfactin translocation may change. Of course, if it is possible to generate a *Pfcdpk1* conditional knockout, similar sets of experiments performed using these

parasites would confirm if any observed effects are also kinase and hence, protein specific.

Although far from complete, results presented in this report represent a significant contribution to the ongoing characterisation of GAPs. It is hoped that these insights will provide a loose framework for future research endeavors. In light of novel findings, an updated model for arrangement of the tetrameric complex at its target membrane is depicted in figure 6.1.

Figure 6.1

The updated glideosome complex

Updated model of the glideosome complex based on results obtained in this research project, adapted from figure 1.5. Depicted in black are 14-carbon myristate and 16-carbon palmititate moieties associated with PfGAP45 that may be important in targeting cytoplasmic PfMyoA and PfMTIP to membranes and anchoring proteins at these membranes. The letter P, depicted in orange represents the addition of one or more phosphate groups to specific serine or threonine residues of PfGAP45 and PfMTIP. The precise effects of phosphate addition on the proteins themselves and/or in regulation of the motor is still unknown but they may be multiple and complex. Although there is now evidence to suggest PfGAP45 interacts with PfMTIP (Vaid, Thomas et al. 2008), direct interactions between PfGAP45 or PfGAP50 and the other motor components were not identified in this project. As a result, the precise topology of the tetrameric complex as well as its arrangement within membranes is still poorly defined.

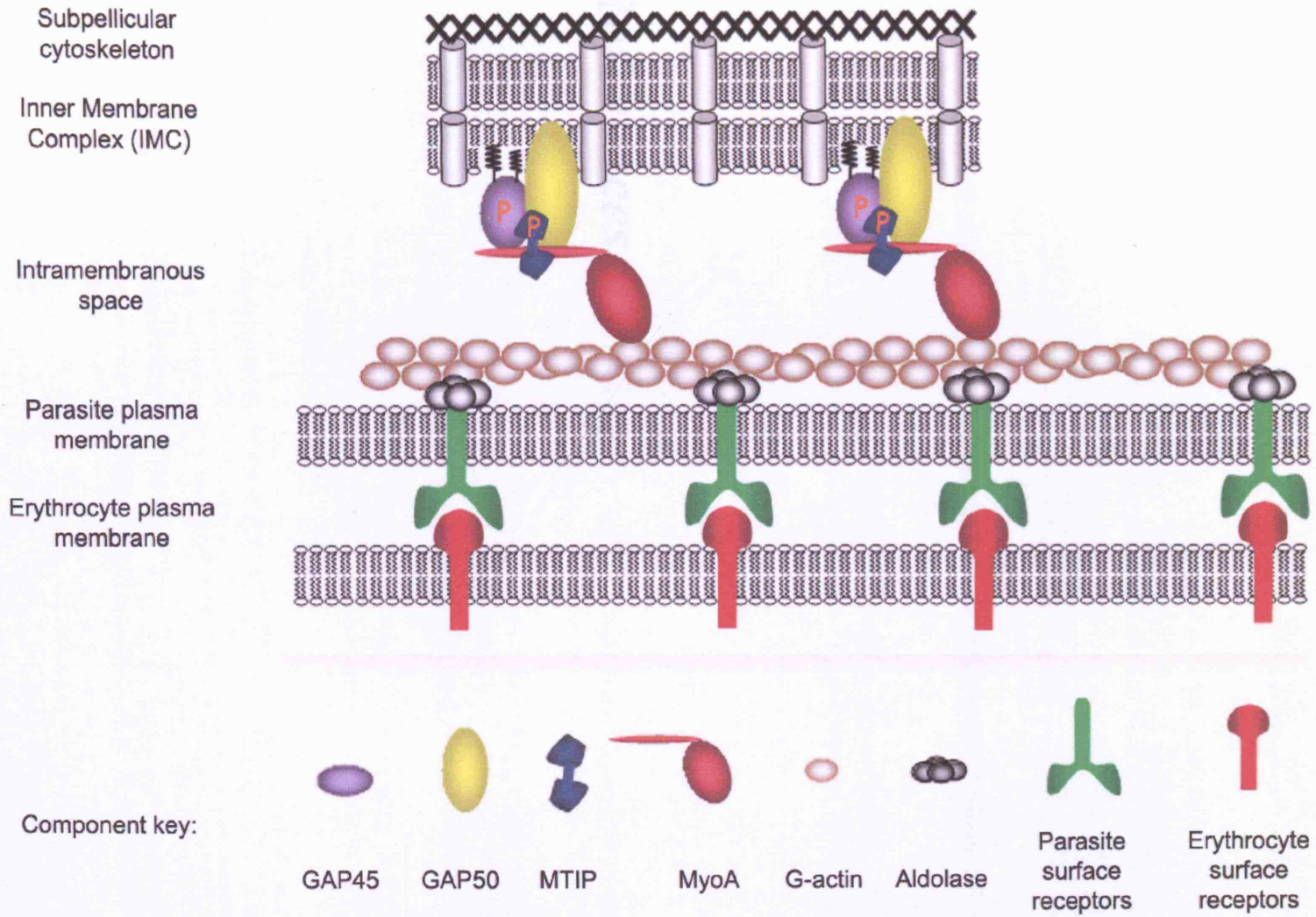
Subpellicular cytoskeleton
Inner Membrane Complex (IMC)
Intramembranous space
Parasite plasma membrane
Erythrocyte plasma membrane
P
P
P
P
Component key:
GAP45
GAP50
MTIP
MyoA
G-actin
Aldolase
Parasite surface receptors
Erythrocyte surface receptors

References

Abdalla, S. H. (1990). "Hematopoiesis in human malaria." Blood Cells **16**: 401.

Ahmed, H. (2004). Principles and reactions of protein extraction, purification and characterisation. Boca Raton, CRC Press.

Aikawa, M., L. H. Miller, et al. (1978). "Erythrocyte entry by malarial parasites. A moving junction between erythrocyte and parasite." J Cell Biol **77**(1): 72-82.

Aikawa, M., L. H. Miller, et al. (1981). "Freeze-fracture study on the erythrocyte membrane during malarial parasite invasion." J Cell Biol **91**(1): 55-62.

Aikawa, M. and T. M. Seed (1980). Morphology of *Plasmodia*. Malaria. J. P. Kreier. New York, Academic Press. **1:** 285-344.

Aikawa, M., M. Torii, et al. (1990). "Pf155/RESA antigen is localized in dense granules of Plasmodium falciparum merozoites." Exp Parasitol **71**(3): 326-329.

Aikins, M. K., J. Fox-Rushby, et al. (1998). "The Gambian National Impregnated Bednet Programme: Costs, consequences and net cost-effectiveness." Social Science & Medicine **46**(2): 181-191.

Akashi, H. (2001). "Gene expression and molecular evolution." Curr Opin Genet Dev **11**(6): 660-666.

Alexander, D. L., S. Arastu-Kapur, et al. (2006). "*Plasmodium falciparum* AMA1 binds a rhoptry neck protein homologous to TgRON4, a component of the moving junction in *Toxoplasma gondii*." Eukaryot Cell **5**(7): 1169-1173.

Alexander, D. L., J. Mital, et al. (2005). "Identification of the moving junction complex of *Toxoplasma gondii*: a collaboration between distinct secretory organelles." PLoS Pathog **1**(2): e17.

Amici, R. R. (2001). "The history of Italian parasitology." Veterinary Parasitology **98**(1-3): 3-30.

Annan, R. S. and S. A. Carr (1996). "Phosphopeptide analysis by matrix-assisted laser desorption time-of-flight mass spectrometry." Anal. Chem **68**(19): 3413-3421.

Arastu-Kapur, S., E. L. Ponder, et al. (2008). "Identification of proteases that regulate erythrocyte rupture by the malaria parasite *Plasmodium falciparum*." Nat Chem Biol **4**(3): 203-213.

Arrowood, M. J., C. R. Sterling, et al. (1991). "Immunofluorescent microscopical visualization of trails left by gliding *Cryptosporidium parvum* sporozoites." J Parasitol **77**(2): 315-317.

Baird, J. K. (1995). "Host age as a determinant of naturally acquired immunity to *Plasmodium falciparum*." Parasitol. Today **11**: 105-111.

Baird, J. K., T. R. Jones, et al. (1991). "Age-dependent acquired protection against *Plasmodium falciparum* in people having two years exposure to hyperendemic malaria." Am. J. Trop. Med. Hyg **45**: 65-76.

Baker, R. P., R. Wijetilaka, et al. (2006). "Two *Plasmodium* rhomboid proteases preferentially cleave different adhesins implicated in all invasive stages of malaria." PLoS Pathog **2**(10): e113.

Baneyx, F. and M. Mujacic (2004). "Recombinant protein folding and misfolding in *Escherichia coli*." Nat Biotechnol(22): 11.

Bannister, L. and G. Mitchell (2003). "The ins, outs and roundabouts of malaria." Trends Parasitol **19**(5): 209-213.

Bannister, L. H., G. A. Butcher, et al. (1975). "Structure and invasive behavior of *Plasmodium knowlesii* merozoites *in vitro*." Parasitology **71**: 483-491.

Bannister, L. H. and A. R. Dluzewski (1990). "The ultrastructure of red cell invasion in malaria infections: a review." Blood Cells **16**(2-3): 257-292.

Bannister, L. H., J. M. Hopkins, et al. (2000). "Ultrastructure of rhoptry development in *Plasmodium falciparum* erythrocytic schizonts." Parasitology **121**(Pt 3): 273-287.

Bannister, L. H. and G. H. Mitchell (1989). "The fine structure of secretion by *Plasmodium knowlesi* merozoites during red cell invasion." J Protozool **36**(4): 362-367.

Bannister, L. H. and G. H. Mitchell (1995). "The role of the cytoskeleton in *Plasmodium falciparum* merozoite biology: an electron microscopic view." Annals of Tropical Medicine and Parasitology **89**(2): 105-111.

Bannister, L. H., G. H. Mitchell, et al. (1986). "Lamellar membranes associated with rhoptries in erythrocytic merozoites of *Plasmodium knowlesi*: a clue to the mechanism of invasion." Parasitology **92**: 291-303.

Barale, J. C., T. Blisnick, et al. (1999). "*Plasmodium falciparum* subtilisin-like protease 2, a merozoite candidate for the merozoite surface protein 1-42 maturase." Proc Natl Acad Sci U S A **96**(11): 6445-6450.

Barragan, A. and L. D. Sibley (2002). "Transepithelial migration of Toxoplasma gondii is linked to parasite motility and virulence." J Exp Med **195**(12): 1625-1633.

Baruch, D. I. (1999). "Adhesive receptors on malaria-parasitized red cells." Baillieres Best Pract Res Clin Haematol **12**: 747–761.

Baruch, D. I., J. A. Gormely, et al. (1996). "*Plasmodium falciparum* erythrocyte membrane protein 1 is a parasitized erythrocyte receptor for adherence to CD36, thrombospondin, and intercellular adhesion molecule 1." Proc Natl Acad Sci U S A **93**(8): 3497-3502.

Baruch, D. I., B. L. Pasloske, et al. (1995). "Cloning the *P. falciparum* gene encoding PfEMP1, a malarial variant antigen and adherence receptor on the surface of parasitized human erythrocytes." Cell **82**: 77-87.

Bastianelli, G., A. Bignami, et al. (1898). "Coltivazione delle semilune malariche dell'Uomo nell'Anopheles claviger Fabr. (sinonimo Anopheles maculipennis Meig.)." Atti Acc. Lincei, Rend Sc. Mat. Fis. Nat **S.5**(7): 313-314.

Baum, J., A. G. Maier, et al. (2005). "Invasion by *P. falciparum* merozoites suggests a hierarchy of molecular interactions." PLoS Pathog **1**(4): e37.

Baum, J., A. T. Papenfuss, et al. (2006). "Regulation of apicomplexan actin-based motility." Nat Rev Microbiol **4**(8): 621-628.

Baum, J., D. Richard, et al. (2006). "A conserved molecular motor drives cell invasion and gliding motility across malaria life cycle stages and other apicomplexan parasites." J. Biol. Chem. **281**(8): 5197-5208.

Baum, J., C. J. Tonkin, et al. (2008). "A malaria parasite formin regulates actin polymerization and localizes to the parasite-erythrocyte moving junction during invasion." Cell Host Microbe **3**(3): 188-198.

Bement, W. M. and M. S. Mooseker (1995). "TEDS rule: a molecular rationale for differential regulation of myosins by phosphorylation of the heavy chain head." Cell. Motil. Cytosceleton **31**(2): 87-92.

Bendtsen, J. D., H. Nielsen, et al. (2004). "Improved prediction of signal peptides: SignalP 3.0." J Mol Biol **340**(4): 783-795.

Benjwal, S., S. Verma, et al. (2006). "Monitoring protein aggregation during thermal unfolding in circular dichroism experiments." Protein. Sci **15**(3): 635-639.

Bergman, L. W., K. Kaiser, et al. (2003). "Myosin A tail domain interacting protein (MTIP) localizes to the inner membrane complex of *Plasmodium* sporozoites." J Cell Sci **116**(1): 39-49.

Billker, O., S. Dechamps, et al. (2004). "Calcium and a calcium-dependent protein kinase regulate gamete formation and mosquito transmission in a malaria parasite." 117 **4**(503-514).

Black, C. G., L. Wang, et al. (2003). "Apical location of a novel EGF-like domain-containing protein of *Plasmodium falciparum*." Mol Biochem Parasitol **127**(1): 59-68.

Blackman, M. J., H. Fujioka, et al. (1998). "A subtilisin-like protein in secretory organelles of *Plasmodium falciparum* merozoites." J Biol Chem **273**(36): 23398-23409.

Blackman, M. J., H. G. Heidrich, et al. (1990). "A single fragment of a malaria merozoite surface protein remains on the parasite during red cell invasion and is the target of invasion-inhibiting antibodies." J Exp Med **172**(1): 379-382.

Bloland, P. B., E. M. Lackritz, et al. (1993). "Beyond chloroquine: implications of drug resistance for evaluating malaria therapy efficacy and treatment policy in Africa." J Infect Dis **167**: 932-937.

Blom, N., S. Gammeltoft, et al. (1999). "Sequence and structure-based prediction of eukaryotic protein phosphorylation sites." J Mol Biol **294**(5): 1351-1362.

Bosch, J., C. A. Buscaglia, et al. (2007). "Aldolase provides an unusual binding site for thrombospondin-related anonymous protein in the invasion machinery of the malaria parasite." Proc Natl Acad Sci U S A **104**(17): 7015-7020.

Bosch, J., S. Turley, et al. (2006). "Structure of the MTIP-MyoA complex, a key component of the malaria parasite invasion motor." Proc Natl Acad Sci U S A **103**(13): 4852-4857.

Bosch, J., S. Turley, et al. (2007). "The closed MTIP-myosin A-tail complex from the malaria parasite invasion machinery." J Mol Biol **372**(1): 77-88.

Bowyer, P. W., R. S. Gunaratne, et al. (2007). "Molecules incorporating a benzothiazole core scaffold inhibit the N-myristoyltransferase of *Plasmodium falciparum*." Biochem J **408**(2): 173-180.

Bozdech, Z., M. Llinas, et al. (2003). "The transcriptome of the intraerythrocytic developmental cycle of *Plasmodium falciparum*." PLoS Biology **1**(1): E5.

Bozdech, Z., J. Zhu, et al. (2003). "Expression profiling of the schizont and trophozoite stages of *Plasmodium falciparum* with a long-oligonucleotide microarray." Genome Biology **4**(2): R9.

Bradley, P. J., C. Ward, et al. (2005). "Proteomic analysis of rhoptry organelles reveals many novel constituents for host-parasite interactions in *Toxoplasma gondii*." J Biol Chem **280**(40): 34245-34258.

Bray, D. (2001). Cell movements: from molecules to motility New York, Garland Publishing.

Bryson, K., L. J. McGuffin, et al. (2005). "Protein structure prediction servers at University College London." Nucleic Acids Res **33**(Web Server issue): W36-38.

Buscaglia, C. A., I. Coppens, et al. (2003). "Sites of interaction between aldolase and thrombospondin-related anonymous protein in *Plasmodium*." Mol Biol Cell **14**(12): 4947-4957.

Campbell, G. H., L. H. Miller, et al. (1984). "Monoclonal antibody characterization of *Plasmodium falciparum* antigens." Am J Trop Med Hyg **33**(6): 1051-1054.

Camus, D. and T. J. Hadley (1985). "A *Plasmodium falciparum* antigen that binds to host erythrocytes and merozoites." Science **230**(4725): 553-556.

Capanno, E. (2006). "Battista Grassi: a zoologist for malaria." Contributions to Science **3**(2): 187-195.

Carruthers, V. and J. C. Boothroyd (2007). "Pulling together: an integrated model of *Toxoplasma* cell invasion." Curr Opin Microbiol **10**(1): 83-89.

Carruthers, V. B. and M. J. Blackman (2005). "A new release on life: emerging concepts in proteolysis and parasite invasion." Mol Microbiol **55**(6): 1617-1630.

Carruthers, V. B., O. K. Giddings, et al. (1999). "Secretion of micronemal proteins is associated with *Toxoplasma* invasion of host cells." Cell Microbiol **1**(3): 225-235.

Carruthers, V. B. and L. D. Sibley (1997). "Sequential protein secretion from three distinct organelles of *Toxoplasma gondii* accompanies invasion of human fibroblasts." Eur J Cell Biol **73**(2): 114-123.

Carruthers, V. B. and L. D. Sibley (1999). "Mobilization of intracellular calcium stimulates microneme discharge in *Toxoplasma gondii*." Mol Microbiol **31**(2): 421-428.

Carter, R. and K. N. Mendis (2002). "Evolutionary and historical aspects of the burden of malaria." Clin. Microbiol. Rev. **15**(4): 564-594.

Cereghino, J. L. and J. M. Cregg (2000). "Heterologous protein expression in the methylotrophic yeast *Pichia pastoris*." FEMS Microbiol. Rev **24**: 45-66.

Chandran, V., E. J. Stollar, et al. (2006). "Structure of the regulatory apparatus of a calcium-dependent protein kinase (CDPK): a novel mode of calmodulin-target recognition." J Mol Biol **357**(2): 400-410.

Chandre, F., F. Darriet, et al. (1999). "Status of pyrethroid resistance in *Anopheles gambiae*." Bull W.H.O **77**.

Chang, P. and D. M. Dwyer (1976). "Multiplication of a human parasite (*Leishmania donovani*) in phagolysosomes of hamster macrophages *in vitro*." Science **193**: 678-680.

Chaparro-Olaya, J., A. R. Dluzewski, et al. (2003). "The multiple myosins of malaria: The smallest malaria myosin, *Plasmodium falciparum* myosin-B (Pfmyo-B) is expressed in mature schizonts and merozoites " European Journal of Protistology **39**(4): 423-427.

Chaparro-Olaya, J., G. Margos, et al. (2005). "*Plasmodium falciparum* myosins: transcription and translation during asexual parasite development." Cell Motil Cytoskeleton **60**(4): 200-213.

Charron, A. J. and L. D. Sibley (2004). "Molecular partitioning during host cell penetration by *Toxoplasma gondii*." Traffic **5**(11): 855-867.

Chaturvedi, S., H. Qi, et al. (1999). "Constitutive calcium-independent release of *Toxoplasma gondii* dense granules occurs through the NSF/SNAP/SNARE/Rab machinery." J Biol Chem **274**(4): 2424-2431.

Chen, H., F. Gu, et al. (2006). "Improved Chou-Fasman method for protein secondary structure prediction." BMC Bioinformatics **7**(S4): S14.

Chen, Q., M. Schlichtherle, et al. (2000). "Molecular aspects of severe malaria." Clin. Microbiol. Rev. **13**(3): 439-450.

Chou, P. Y. and G. D. Fasman (1974). "Prediction of protein conformation." Biochemistry **13**(2): 222-245.

Clontech (2001). "Protein purification products overview." Clontechniques **XVI**(1): 27-32.

Coluzzi, M. (1994). "Malaria and the Afrotropical ecosystems: impact of man-made environmental changes." Parassitologia **36**: 223-227.

Coluzzi, M. (1999). "The clay feet of the malaria giant and its African roots: hypotheses and inferences about origin, spread and control of *Plasmodium falciparum*." Parassitologia **41**(1-3): 277-283.

Conseil, V., M. Soête, et al. (1999). "Serine protease inhibitors block invasion of host cells by *Toxoplasma gondii*." Antimicrob Agents Chemother **43**(6): 1358-1361.

Cook, P. F., M. E. J. Neville, et al. (1982). "Adenosine cyclic 3',5'-monophosphate dependent protein kinase: kinetic mechanism for the bovine skeletal muscle catalytic subunit." Biochemistry **21**(23): 5794-5799.

Cowman, A. F., R. B. Saint, et al. (1985). "Conserved sequences flank variable tandem repeats in two S-antigen genes of *Plasmodium falciparum*." Cell **40**(4): 775-783.

Cregg, J. M., T. S. Vedvick, et al. (1993). "Recent advances in the expression of foreign genes in *Pichia pastoris*." Biotechnology **11**(8): 905-910.

Creighton, T. E. (1993). Proteins: structures and molecular properties. New York, W.H. Freeman and Company.

Culvenor, J. G., K. P. Day, et al. (1991). "*Plasmodium falciparum* ring-infected erythrocyte surface antigen is released from merozoite dense granules after erythrocyte invasion." Infect Immun **59**(3): 1183-1187.

Curtis, C. F., J. E. Miller, et al. (1998). "Can anything be done to maintain the effectiveness of pyrethroid-impregnated bednets against malaria vectors? ." Phil Trans R Soc Lond **353**: 1769–1775

David, P. H., S. M. Handunnetti, et al. (1988). "Rosetting: a new cytoadherence property of malaria-infected erythrocytes." Am J Trop Med Hyg **38**: 289-297.

DeLano, W. L. (2002). The PyMOL Molecular Graphics System. Palo Alto, CA, USA, DeLano Scientific.

Dobrowolski, J., V. Carruthers, et al. (1997). "Participation of myosin in gliding motility and host cell invasion by *Toxoplasma gondii*." Mol. Microbiol. **26**: 163-173.

Dobrowolski, J. and L. Sibley (1996). "*Toxoplasma* invasion of mammalian cells is powered by the actin cytoskeleton of the parasite." Cell **84**: 933-939.

Dobrowolski, J. M., I. R. Niesman, et al. (1997). "Actin in the parasite *Toxoplasma gondii* is encoded by a single copy gene, ACT1 and exists primarily in a globular form." Cell Motil Cytoskeleton **37**(3): 253-262.

Doury, J. C., S. Bonnefoy, et al. (1994). "Analysis of the high molecular weight rhoptry complex of *Plasmodium falciparum* using monoclonal antibodies." Parasitology **108**(Pt 3): 269-280.

Drew, D. R., R. A. O'Donnell, et al. (2004). "A common cross-species function for the double epidermal growth factor-like modules of the highly divergent *Plasmodium* surface proteins MSP-1 and MSP-8." J Biol Chem **279**(19): 20147-20153.

Dubey, J. P., D. S. Lindsay, et al. (1998). "Structures of *Toxoplasma gondii* tachyzoites, bradyzoites, and sporozoites and biology and development of tissue cysts." Clin. Microbiol. Rev. **11**(2): 267-299.

Dubremetz, J. F., A. Achbarou, et al. (1993). "Kinetics and pattern of organelle exocytosis during *Toxoplasma gondii*/host-cell interaction." Parasitol Res **79**(5): 402-408.

Dubremetz, J. F. and E. Ferreira (1978). "Capping of cationised ferritin by coccidian zoites." J Protozool **25**: 9B.

Duraisingh, M. T., T. Triglia, et al. (2003). "Phenotypic variation of *Plasmodium falciparum* merozoite proteins directs receptor targeting for invasion of human erythrocytes." EMBO J **22**(5): 1047-1057.

Entzeroth, R. (1985). "Invasion and early development of *Sarcocystis muris* (Apicomplexa, Sarcocystidae) in tissue cultures." J Protozool **32**(3): 446-453.

Facer, C. A. and M. Tanner (1997). "Clinical trials of malaria vaccines: progress and prospects." Adv Parasitol **39**: 1-68.

Field, S. J., J. C. Pinder, et al. (1993). "Actin in the merozoite of the malaria parasite, *Plasmodium falciparum*." Cell Motil Cytoskeleton **25**(1): 43-48.

Fink, A. L. (2005). "Natively unfolded proteins." Current Opinion in Structural Biology **15**(1): 35-41.

Florens, L., X. Liu, et al. (2004). "Proteomics approach reveals novel proteins on the surface of malaria-infected erythrocytes." Mol Biochem Parasitol **135**(1): 1-11.

Florens, L., M. P. Washburn, et al. (2002). "A proteomic view of the *Plasmodium falciparum* life cycle." Nature **419**(6906): 520-526.

Forney, J. R., D. K. Vaughan, et al. (1998). "Actin-dependent motility in *Cryptosporidium parvum* sporozoites." J Parasitol **84**(5): 908-913.

Foth, B. J., M. C. Goedecke, et al. (2006). "New insights into myosin evolution and classification." Proc Natl Acad Sci U S A **103**(10): 3681-3686.

Foussard, F., Y. Gallois, et al. (1990). "Isolation of the pellicle of *Toxoplasma gondii* (Protozoq, Coccidia): characterization by electron microscopy and protein composition." Parasitol. Res **76**(7): 563-565.

Francis, C. L., T. A. Ryan, et al. (1993). "Ruffles induced by *Salmonella* and other stimuli direct macropinocytosis of bacteria." Nature **364**: 639-642.

Fraser, T. S., S. H. Kappe, et al. (2001). "Erythrocyte-binding activity of *Plasmodium yoelii* apical membrane antigen-1 expressed on the surface of transfected COS-7 cells." Mol Biochem Parasitol **117**(1): 49-59.

Frevert, U., I. Usynin, et al. (2006). "Nomadic or sessile: can Kupffer cells function as portals for malaria sporozoites to the liver?" Cell Microbiol **8**(10): 1537-1546.

Fu, H. (2004). Protein-protein interactions: methods and applications. Totowa, Humana Press.

Galan, J. E. and J. B. Bliska (1996). "Cross-talk between bacterial pathogens and their host cells." Annu Rev Cell Dev Biol **12**: 221-255.

Galinski, M. R. and J. W. Barnwell (1996). "*Plasmodium vivax*: merozoites, invasion of reticulocytes and considerations for malaria vaccine development." Parasitol Today **12**(1): 20-29.

Gallagher, P. J., B. P. Herring, et al. (1997). "Myosin light chain kinases." J Muscle Res Cell Motil **18**(1): 1-16.

Gantt, S., C. Persson, et al. (2000). "Antibodies against thrombospondin-related anonymous protein do not inhibit Plasmodium sporozoite infectivity *in vivo*." Infect. Immun **68**(6): 3667-3673.

Garnham, P. C. C. (1966). Malaria parasites and other Haemosporidia. Oxford, Blackwell Scientific Publications

Gaskins, E., S. Gilk, et al. (2004). "Identification of the membrane receptor of a class XIV myosin in *Toxoplasma gondii*." J. Cell Biol. **165**(3): 383-393.

Gilberger, T. W., J. K. Thompson, et al. (2003). "A novel erythrocyte binding antigen-175 paralogue from *Plasmodium falciparum* defines a new trypsin-resistant receptor on human erythrocytes." J. Biol. Chem **278**(16): 14480-14486.

Gilson, P. R., T. Nebl, et al. (2006). "Identification and stoichiometry of glycosylphosphatidylinositol-anchored membrane proteins of the human malaria parasite *Plasmodium falciparum*." Mol Cell Proteomics **5**(7): 1286-1299.

Glushakova, S., D. Yin, et al. (2005). "Membrane transformation during malaria parasite release from human red blood cells." Curr. Biol **15**(18): 1645-1650.

Goel, V. K., X. Li, et al. (2003). "Band 3 is a host receptor binding merozoite surface protein 1 during the *Plasmodium falciparum* invasion of erythrocytes." Proc Natl Acad Sci U S A **100**(9): 5164-5169.

Golgi, C. (1889). "Sul ciclo evolutivo dei parassiti malarici nella febbre terzana; diagnosi differenziale tra i parassiti endoglobulari malarici della terzana e quelli della quartana." Arch. Sci. Med **13**: 173-196.

Gonzalo, S. and M. E. Linder (1998). "SNAP-25 palmitoylation and plasma membrane targeting require a functional secretory pathway." Mol Biol Cell **9**(3): 585-597.

Gordon, J. L. and L. D. Sibley (2005). "Comparative genome analysis reveals a conserved family of actin-like proteins in apicomplexan parasites." BMC genomics **12**(6): 179.

Grassi, B. (1900). "Studi di uno zoologo sulla malaria." Atti. Reale Accad. Lincei Mem **3**: 299-511.

Graves, D. J., B. L. Martin, et al. (1994). Co- and Post-Translational Modification of Proteins: Chemical Principles and Biological Effects. New York, Oxford University Press.

Green, J. L., L. Hinds, et al. (2006). "*Plasmodium* thrombospondin related apical merozoite protein (PTRAMP) is shed from the surface of merozoites by PfSUB2 upon invasion of erythrocytes." Mol Biochem Parasitol **150**(1): 114-117.

Green, J. L., S. R. Martin, et al. (2006). "The MTIP-myosin A complex in blood stage malaria parasites." Journal of Molecular Biology **355**(5): 933-941.

Guerin, P. J., P. Olliaro, et al. (2002). "Malaria: current status of control, diagnosis, treatment, and a proposed agenda for research and development." The Lancet Infectious Diseases **2**(9): 564-573.

Guillet, P., D. Alnwick, et al. (2001). "Long lasting treated mosquito nets: a break through in malaria prevention." Bull. W. H. O **79**: 998.

Gunaratne, R., M. Sajid, et al. (2000). "Characterization of *N*-myristoyltransferase from *Plasmodium falciparum*." Biochem j **1**(348): 459-463.

Gupta, S., R. W. Snow, et al. (1999). "Immunity to non-cerebral severe malaria is acquired after one or two infections." Nat. Med **5**: 340-343.

Hackett, F., M. Sajid, et al. (1999). "PfSUB-2: a second subtilisin-like protein in *Plasmodium falciparum* merozoites." Mol Biochem Parasitol **103**(2): 183-195.

Hakansson, S., H. Morisaki, et al. (1999). "Time-lapse video microscopy of gliding motility in *Toxoplasma gondii* reveals a novel, biphasic mechanism of cell locomotion." Mol Biol Cell **10**(11): 3539-3547.

Hall, T. (1999). "BioEdit: a user-friendly biological sequence alignment editor and analysis program for Windows 95/98/NT." Nucl. Acids Symp. Ser **41**: 95-98.

Harper, J. F. and A. Harmon (2005). "Plants, symbiosis and parasites: a calcium signalling connection." Nat Rev Mol Cell Biol **6**(7): 555-566.

Harper, J. M., E. F. Hoff, et al. (2004). "Multimerization of the *Toxoplasma gondii* MIC2 integrin-like A-domain is required for binding to heparin and human cells." Mol Biochem Parasitol **134**(2): 201-212.

Harris, P. K., S. Yeoh, et al. (2005). "Molecular identification of a malaria merozoite surface sheddase." PLoS Pathog **1**(3): 241-251.

Haugland, R. P. (2005). The Handbook—A Guide to Fluorescent Probes and Labeling Technologies. Eugene, Molecular Probes, Invitrogen.

Hay, S. I., C. A. Guerra, et al. (2004). "The global distribution and population at risk of malaria: past, present, and future " The Lancet Infectious Diseases **4**(5): 327-336.

Healer, J., S. Crawford, et al. (2002). "Independent translocation of two micronemal proteins in developing *Plasmodium falciparum* merozoites." Infect. Immun **70**(10): 5751-5758.

Heintzelman, M. and J. Schwartzman (1999). "Characterisation of myosin-A and myosin-C: two class XIV unconventional myosins from *Toxoplasma gondii.*" Cell Motil. Cytoskeleton **44**: 58-67.

Heintzelman, M. B. (2006). "Cellular and molecular mechanics of gliding locomotion in eukaryotes." Int Rev Cytol **251**: 79-129.

Heintzelman, M. B. and J. D. Schwartzman (1997). "A novel class of unconventional myosins from *Toxoplasma gondii.*" Journal of Molecular Biology **271**(1): 139-146.

Herm-Gotz, A., S. Weiss, et al. (2002). "*Toxoplasma gondii* myosin A and its light chain: a fast, single-headed, plus-end-directed motor." EMBO J. **21**(9): 2149-2158.

Hettmann, C., A. Herm-Gotz, et al. (2000). "A dibasic motif in the tail of a class XIV apicomplexan myosin is an essential determinant of plasma membrane localization." Mol. Biol. Cell **11**(4): 1385-1400.

Hiller, N. L., T. Akompong, et al. (2003). "Identification of a stomatin orthologue in vacuoles induced in human erythrocytes by malaria parasites. A role for microbial raft proteins in apicomplexan vacuole biogenesis." J Biol Chem **278**(48): 48413-48421.

Hirunpetcharat, C., J. H. Tian, et al. (1997). "Complete protective immunity induced in mice by immunization with the 19-kilodalton carboxyl-terminal fragment of the merozoite surface protein-1 (MSP1[19]) of *Plasmodium yoelii* expressed in *Saccharomyces cerevisiae*: correlation of protection with antigen-specific antibody titer, but not with effector CD4+ T cells." J Immunol **159**(7): 3400-3411.

Holder, A. A. and R. R. Freeman (1981). "Immunization against blood-stage rodent malaria using purified parasite antigens." Nature **294**(5839): 361-364.

Holder, A. A., R. R. Freeman, et al. (1985). "Isolation of a *Plasmodium falciparum* rhoptry protein." Mol Biochem Parasitol **14**(3): 293-303.

Houdusse, A., A. G. Szent-Gyorgyi, et al. (2000). "Three conformational states of scallop myosin S1." Proc Natl Acad Sci U S A **97**(21): 11238-11243.

Howell, S. A., I. Well, et al. (2003). "A single malaria merozoite serine protease mediates shedding of multiple surface proteins by juxtamembrane cleavage." J Biol Chem **278**(26): 23890-23898.

Hu, K., D. S. Roos, et al. (2002). "A novel polymer of tubulin forms the conoid of *Toxoplasma gondii*." J Cell Biol **156**(6): 1039-1050.

Hume, J. C. C., E. J. Lyons, et al. (2003). "Human migration, mosquitoes and the evolution of *Plasmodium falciparum*." Trends in Parasitology **19**(3): 144-149.

Huynh, M. H., C. Opitz, et al. (2004). "Trans-genera reconstitution and complementation of an adhesion complex in *Toxoplasma gondii*." Cell Microbiol **6**(8): 771-782.

Huynh, M. H., K. E. Rabenau, et al. (2003). "Rapid invasion of host cells by *Toxoplasma* requires secretion of the MIC2-M2AP adhesive protein complex." EMBO J **22**(9): 2082-2090.

Ishino, T., Y. Chinzei, et al. (2005). "Two proteins with 6-cys motifs are required for malarial parasites to commit to infection of the hepatocyte." Mol Microbiol **58**(5): 1264-1275.

Ishino, T., Y. Orito, et al. (2006). "A calcium-dependent protein kinase regulates *Plasmodium* ookinete access to the midgut epithelial cell." Mol Microbiol **59**(4): 1175-1184.

Jarcho, S. (1993). Quinine's predecessor: Francesco Torti and the early history of cinchona. Baltimore, Johns Hopkins University Press.

Jewett, T. J. and L. D. Sibley (2003). "Aldolase forms a bridge between cell surface adhesins and the actin cytoskeleton in apicomplexan parasites." Mol Cell **11**(4): 885-894.

Johnson, J. G., N. Epstein, et al. (1980). "Factors affecting the ability of isolated *Plasmodium knowlesi* merozoites to attach to and invade erythrocytes." Parasitology **80**(3): 539-550.

Johnson, T. M., Z. Rajfur, et al. (2007). "Immobilization of the type XIV myosin complex in *Toxoplasma gondii*." Mol Biol Cell **18**(8): 3039-3046.

Jones, D. T. (1999). "Protein secondary structure prediction based on position-specific scoring matrices." J Mol Biol **292**(2): 195-202.

Jones, M. L., E. L. Kitson, et al. (2006). "*Plasmodium falciparum* erythrocyte invasion: a conserved myosin associated complex." Mol Biochem Parasitol **147**(1): 74-84.

Kamm, K. E. and J. T. Stull (2001). "Dedicated myosin light chain kinases with diverse cellular functions." J Biol Chem **276**(7): 4527-4530.

Kaneko, O., J. Mu, et al. (2002). "Gene structure and expression of a *Plasmodium falciparum* 220-kDa protein homologous to the *Plasmodium vivax* reticulocyte binding proteins." Mol Biochem Parasitol **121**(2): 275-278.

Kappe, S., T. Bruderer, et al. (1999). "Conservation of a gliding motility and cell invasion machinery in apicomplexan parasites." J. Cell Biol. **147**(5): 937-944.

Kappes, B., C. D. Doerig, et al. (1999). "An overview of *Plasmodium* protein kinases." Parasitol Today **15**(11): 449-454.

Kariuki, M. M., X. Li, et al. (2005). "Two *Plasmodium falciparum* merozoite proteins binding to erythrocyte band 3 form a direct complex." Biochem Biophys Res Commun **338**(4): 1690-1695.

Karunaweera, N. D., G. E. Grau, et al. (1992). "Dynamics of fever and serum levels of tumor necrosis factor are closely associated during clinical paroxysms in *Plasmodium vivax* malaria." Proc Natl Acad Sci U S A **89**(8): 3200-3203.

Kato, K., D. C. Mayer, et al. (2005). "Domain III of *Plasmodium falciparum* apical membrane antigen 1 binds to the erythrocyte membrane protein." Proc Natl Acad Sci U S A **102**(15): 5552-5557.

Kieschnick, H., T. Wakefield, et al. (2001). "*Toxoplasma gondii* attachment to host cells is regulated by a calmodulin-like domain protein kinase." J Biol Chem **276**(15): 12369-12377.

King, C. A. (1981). "Cell surface interaction of the protozoan Gregarina with concanavalin A beads - implications for models of gregarine gliding." Cell Biol Int Rep **5**(3): 297-305.

King, C. A. (1988). "Cell motility of sporozoan protozoa." Parasitol Today **4**(11): 315-319.

Kitchen, S. F. (1949). Symptomology: general considerations. Malariology. M. F. Boyd. Philadelphia, Saunders. **2:** 966-1045.

Klotz, F. W., T. J. Hadley, et al. (1989). "A 60-kDa *Plasmodium falciparum* protein at the moving junction formed between merozoite and erythrocyte during invasion." Mol Biochem Parasitol **36**(2): 177-185.

Krishnegowda, G., A. M. Hajjar, et al. (2005). "Induction of proinflammatory responses in macrophages by the glycosylphosphatidylinositols of *Plasmodium falciparum*: cell signaling receptors, glycosylphosphatidylinositol (GPI) structural requirement, and regulation of GPI activity." J. Biol. Chem **280**: 8606-8616.

Krotoski, W. A., W. E. Collins, et al. (1982). "Demonstration of hypnozoites in sporozoite-transmitted *Plasmodium vivax* infection." Am J Trop Med Hyg **31**(6): 1291-1293.

Kugelstadt, D., D. Winter, et al. (2007). "Raf kinase inhibitor protein affects activity of *Plasmodium falciparum* calcium-dependent protein kinase 1." Mol Biochem Parasitol **151**(1): 111-117.

Kwiatkowski, D. (1995). "Malarial toxins and the regulation of parasite density." Parasitol. Today **11**: 206-212.

Kwiatkowski, D., J. G. Cannon, et al. (1989). "Tumour necrosis factor production in *falciparum* malaria and its association with schizont rupture." Clin Exp Immunol **77**(3): 361-366.

Langreth, S. G., J. B. Jensen, et al. (1978). "Fine structure of human malaria *in vitro*." J Protozool **25**(4): 443-452.

Langreth, S. G. and E. Peterson (1985). "Pathogenicity, stability, and immunogenicity of a knobless clone of *Plasmodium falciparum* in Colombian owl monkeys." Infect Immun **47**: 760-766.

Laveran, A. (1880). "Note surun nouveau parasite trouve dans le sang de plusiers malades attients de fievre palustre." Bull. Acad. Med: 1235-1236 (premiere note) 1346-1347 (deuxieme note).

Le Roch, K. G., Y. Zhou, et al. (2003). "Discovery of gene function by expression profiling of the malaria parasite life cycle." Science **301**(5639): 1503-1508.

Lebrun, M., A. Michelin, et al. (2005). "The rhoptry neck protein RON4 re-localizes at the moving junction during *Toxoplasma gondii* invasion." Cell Microbiol **7**(12): 1823-1833.

Lengler, C. (2004). "Insecticide-treated bednets and curtains for preventing malaria." Cochrane Database of Systematic Reviews.

Leriche, M. A. and J. F. Dubremetz (1990). "Exocytosis of *Toxoplasma gondii* dense granules into the parasitophorous vacuole after host cell invasion." Parasitol Res **76**(7): 559-562.

Lew, A. E., A. R. Dluzewski, et al. (2002). "Myosins of *Babesia bovis*: molecular characterisation, erythrocyte invasion, and phylogeny." Cell Motil Cytoskeleton **52**(4): 202-220.

Lewit-Bentley, A. and S. Rety (2000). "EF-hand calcium-binding proteins." Current Opinion in Structural Biology **10**(6): 637-643.

Li, X., H. Chen, et al. (2004). "A co-ligand complex anchors *Plasmodium falciparum* merozoites to the erythrocyte invasion receptor band 3." J Biol Chem **279**(7): 5765-5771.

Liendo, A., T. T. Stedman, et al. (2001). "*Toxoplasma gondii* ADP-ribosylation factor 1 mediates enhanced release of constitutively secreted dense granule proteins." J Biol Chem **276**(21): 18272-18281.

Ling, I. T., L. Florens, et al. (2004). "The *Plasmodium falciparum* clag9 gene encodes a rhoptry protein that is transferred to the host erythrocyte upon invasion." Mol Microbiol **52**(1): 107-118.

Linse, S. and S. Forsén (1995). "Determinants that govern high-affinity calcium binding." Adv Second Messenger Phosphoprotein Res **30**: 89-151.

Litsios, S. (2002). Malaria control and the future of international public health. The contextual determinants of malaria. E. A. Casman and H. Dowlatabadi. Washington DC, Resources for the Future: 292-328.

Llinas, M., Z. Bozdech, et al. (2006). "Comparative whole genome analysis of three Plasmodium falciparum strains." Nucleic. Acids. Res **34**(4): 1166-1173.

Looareesuwan, S., M. Ho, et al. (1987). "Dynamic alteration in splenic function during acute *falciparum* malaria." New England Journal of Medicine **317**: 675-679.

Lovett, J. L. and L. D. Sibley (2003). "Intracellular calcium stores in *Toxoplasma gondii* govern invasion of host cells." J Cell Sci **15**(116): 3009-3016.

Lupas, A. (1996). "Prediction and analysis of coiled-coil structures." Methods Enzymol **266**: 513-525.

Luse, S. A. and L. H. Miller (1971). "*Plasmodium falciparum* malaria. Ultrastructure of parasitized erythrocytes in cardiac vessels." Am J Trop Med Hyg **20**: 655-660.

Mann, T. and C. Beckers (2001). "Characterization of the subpellicular network, a filamentous membrane skeletal component in the parasite *Toxoplasma gondii*." Mol Biochem Parasitol **115**(2): 257-268.

Marchiafava, E. and A. Celli (1885). "Weitere Untersuchungen über die Malariainfection." Fortschritte der Medicin **3**: 787-806.

Margos, G., I. Siden-Kiamos, et al. (2000). "Myosin-A expressions in sporogonic stages of *Plasmodium*." Molecular and Biochemical Parasitology **111**(2): 465-469.

Marshall, V. M., A. Silva, et al. (1997). "A second merozoite surface protein (MSP-4) of *Plasmodium falciparum* that contains an epidermal growth factor-like domain." Infect Immun **65**(11): 4460-4467.

Marshall, V. M., W. Tieqiao, et al. (1998). "Close linkage of three merozoite surface protein genes on chromosome 2 of *Plasmodium falciparum*." Mol Biochem Parasitol **94**(1): 13-25.

Matuschewski, K., M. M. Mota, et al. (2001). "Identification of the class XIV myosins Pb-MyoA and Py-MyoA and expression in *Plasmodium* sporozoites." Molecular and Biochemical Parasitology **112**(1): 157-161.

Matuschewski, K., A. C. Nunes, et al. (2002). "*Plasmodium* sporozoite invasion into insect and mammalian cells is directed by the same dual binding system." EMBO J **21**(7): 1597-1606.

Maurer-Stroh, S., B. Eisenhaber, et al. (2002). "N-terminal *N*-myristoylation of proteins: prediction of substrate proteins from amino acid sequence." Journal of Molecular Biology **317**(4): 541-557.

Mayer, D. C., O. Kaneko, et al. (2001). "Characterization of a *Plasmodium falciparum* erythrocyte-binding protein paralogous to EBA-175." Proc Natl Acad Sci U S A **98**(9): 5222-5227.

McColl, D. J. and R. F. Anders (1997). "Conservation of structural motifs and antigenic diversity in the *Plasmodium falciparum* merozoite surface protein-3 (MSP-3)." Mol Biochem Parasitol **90**(1): 21-31.

McCormick, C. J., D. S. Tuckwell, et al. (1999). "Identification of heparin as a ligand for the A-domain of *Plasmodium falciparum* thrombospondin-related adhesion protein." Mol Biochem Parasitol **100**(1): 111-124.

McCoubrie, J. E., S. K. Miller, et al. (2007). "Evidence for a common role for the serine-type *Plasmodium falciparum* serine repeat antigen proteases: implications for vaccine and drug design." Infect Immun **75**(12): 5565-5574.

Meissner, M., D. Schluter, et al. (2002). "Role of *Toxoplasma gondii* myosin A in powering parasite gliding and host cell invasion." Science **298**(5594): 837-840.

Menard, R., A. A. Sultan, et al. (1997). "Circumsporozoite protein is required for development of malaria sporozoites in mosquitoes." Nature **385**(6614): 336-340.

Mendis, K., B. J. Sina, et al. (2001). "The neglected burden of *Plasmodium Vivax* malaria." Am J Trop Med Hyg **64**(S1-2): 97-106.

Mendis, K. N., P. H. David, et al. (1991). "Antigenic polymorphism in malaria: is it an important mechanism of immune evasion?" Immunol. Today **12**(3): A34-37.

Miller, L. H., D. I. Baruch, et al. (2002). "The pathogenic basis of malaria." Nature **415**(6872): 673-679.

Miller, S. K., R. T. Good, et al. (2002). "A subset of *Plasmodium falciparum* SERA genes are expressed and appear to play an important role in the erythrocytic cycle." J Biol Chem **277**(49): 47524-47532.

Miltenyi, S., W. Muller, et al. (1990). "High gradient magnetic cell separation with MACS." Cytometry **11**(2): 231-238.

Mital, J., M. Meissner, et al. (2005). "Conditional expression of *Toxoplasma gondii* apical membrane antigen-1 (TgAMA1) demonstrates that TgAMA1 plays a critical role in host cell invasion." Mol Biol Cell **16**(9): 4341-4349.

Mitchell, G. H. and L. H. Bannister (1988). "Malaria parasite invasion: interactions with the red cell membrane." Crit Rev Oncol Hematol **8**(4): 225-310.

Mitchell, G. H., A. W. Thomas, et al. (2004). "Apical membrane antigen 1, a major malaria vaccine candidate, mediates the close attachment of invasive merozoites to host red blood cells." Infect Immun **72**(1): 154-158.

Mizuno, Y., A. Makioka, et al. (2002). "Effect of jasplakinolide on the growth, invasion, and actin cytoskeleton of *Plasmodium falciparum*." Parasitol Res **88**(9): 844-888.

Mooseker MS and R. Cheney (1995). "Unconventional myosins." Annu. Rev. Cell Dev. Biol **11**: 633-675.

Mordue, D. G., N. Desai, et al. (1999). "Invasion by *Toxoplasma gondii* establishes a moving junction that selectively excludes host cell plasma membrane proteins on the basis of their membrane anchoring." J Exp Med **190**(12): 1783-1792.

Morrissette, N. S., J. M. Murray, et al. (1997). "Subpellicular microtubules associate with an intramembranous particle lattice in the protozoan parasite *Toxoplasma gondii*." J Cell Sci **110**(Pt 1): 35-42.

Morrissette, N. S. and L. D. Sibley (2002). "Cytoskeleton of apicomplexan parasites." Microbiol Mol Biol Rev **66**(1): 21-38.

Möskes, C., P. A. Burghaus, et al. (2004). "Export of *Plasmodium falciparum* calcium-dependent protein kinase 1 to the parasitophorous vacuole is dependent on three N-terminal membrane anchor motifs." Mol Microbiol **54**(3): 676-691.

Mota, M. M. and A. Rodriguez (2004). "Migration through host cells: the first steps of *Plasmodium* sporozoites in the mammalian host." Cell Microbiol **6**(12): 1113-1118.

Müller, H. M., I. Reckmann, et al. (1993). "Thrombospondin related anonymous protein (TRAP) of *Plasmodium falciparum* binds specifically to sulfated glycoconjugates and to HepG2 hepatoma cells suggesting a role for this molecule in sporozoite invasion of hepatocytes." EMBO J **12**(7): 2881-2889.

Navarro-Lérida, I., A. Alvarez-Barrientos, et al. (2002). "Distance-dependent cellular palmitoylation of de-novo-designed sequences and their translocation to plasma membrane subdomains." J Cell Sci **115**(Pt 15): 3119-3130.

Nichols, B. A. and M. L. Chiappino (1987). "Cytoskeleton of *Toxoplasma gondii*." J Protozool **34**(2): 217-226.

Nichols, B. A., M. L. Chiappino, et al. (1983). "Secretion from the rhoptries of *Toxoplasma gondii* during host-cell invasion." J Ultrastruct Res **83**(1): 85-98.

Nielsen, H., J. Engelbrecht, et al. (1997). "Identification of prokaryotic and eukaryotic signal peptides and prediction of their cleavage sites." Protein Eng **10**(1): 1-6.

O'Donnell, R. A., T. F. de Koning-Ward, et al. (2001). "Antibodies against merozoite surface protein (MSP)-1(19) are a major component of the invasion-inhibitory response in individuals immune to malaria." J Exp Med **193**(12): 1403-1412.

O'Donnell, R. A., F. Hackett, et al. (2006). "Intramembrane proteolysis mediates shedding of a key adhesin during erythrocyte invasion by the malaria parasite." J Cell Biol **174**(7): 1023-1033.

O'Reilly, G. and F. Clarke (1993). "Identification of an actin binding region in aldolase." FEBS Lett **321**(1): 69-72.

Oaks, S. C., V. S. Mitchell, et al. (1991). Malaria: obstacles and opportunities. Washington.

Ogun, S. A. and A. A. Holder (1996). "A high molecular mass *Plasmodium yoelii* rhoptry protein binds to erythrocytes." Mol Biochem Parasitol **76**(1-2): 321-324.

Olczak, M., B. Morawiecka, et al. (2003). "Plant purple acid phosphatases - genes, structures and biological function." Acta Biochim Pol **50**(4): 1245-1256.

Pachebat, J. A., M. Kadekoppala, et al. (2007). "Extensive proteolytic processing of the malaria parasite merozoite surface protein 7 during biosynthesis and parasite release from erythrocytes." Mol Biochem Parasitol **151**(1): 59-69.

Pagel, K., T. Vagt, et al. (2005). "Directing the secondary structure of polypeptides at will: from helices to amyloids and back again?" Org Biomol Chem **3**(21): 3843-3850.

Pain, A., D. J. P. Ferguson, et al. (2001). "Platelet-mediated clumping of *Plasmodium falciparum*-infected erythrocytes is a common adhesive phenotype and is associated with severe malaria." Proceedings of the National Academy of Sciences **98**(4): 1805-1810.

Parry, D. A. (1982). "Coiled-coils in alpha-helix-containing proteins: analysis of the residue types within the heptad repeat and the use of these data in the prediction of coiled-coils in other proteins." Biosci Rep **2**(12): 1017-1024.

Pearce, J. A., K. Mills, et al. (2005). "Characterisation of two novel proteins from the asexual stage of Plasmodium falciparum, H101 and H103." Mol Biochem Parasitol **139**(2): 141-151.

Perkins, D. N., D. J. Pappin, et al. (1999). "Probability-based protein identification by searching sequence databases using mass spectrometry data." Electrophoresis **20**(18): 3551-3567.

Phillips, R. E. and G. Pasvol (1992). "Anaemia of *Plasmodium falciparum* malaria." Baillieres Clinical Haematology **5**: 315-330.

Pietzsch, M. and S. McLaughlin (1993). "Binding of acylated peptides and fatty acids to phospholipid vesicles: pertinence to myristoylated proteins." Biochemistry **32**(39): 10436-10443.

Pinder, J., R. Fowler, et al. (1998). "Actomyosin motor in the merozoite of the malaria parasite, *Plasmodium falciparum*: implications for red cell invasion." J Cell Sci **111**(13): 1831-1839.

Pizarro, J. C., B. Vulliez-Le Normand, et al. (2005). "Crystal structure of the malaria vaccine candidate apical membrane antigen 1." Science **308**(5720): 408-411.

Pollard, T. D. (2007). "Regulation of actin filament assembly by Arp2/3 complex and formins." Annu. Rev. Biophys. Biomol. Struct **36**: 451-477.

Pollard, T. D. and G. G. Borisy (2003). "Cellular motility driven by assembly and disassembly of actin filaments." Cell **112**(4): 453-465.

Powell, R. D., J. V. McNamara, et al. (1972). "Clinical aspects of acquisition of immunity to *falciparum* malaria." Proc. Helminthol. Soc. Wash **39**: 51-68.

Price, R. N., F. Nosten, et al. (1997). "Artesunate/mefloquine treatment of multi-drug resistant *falciparum* malaria." Trans R Soc Trop Med Hyg **91**: 574-577.

Rayment, I., H. M. Holden, et al. (1993). "Structure of the actin-myosin complex and its implications for muscle contraction." Science **261**(5117): 58-65.

Rayment, I., W. R. Rypniewski, et al. (1993). "Three-dimensional structure of myosin subfragment-1: a molecular motor." Science **261**(5117): 50-58.

Rayner, J. C. (2006). "Erythrocyte exit: out, damned merozoite! Out I say!" Trends Parasitol **22**(5): 189-192.

Rayner, J. C., M. R. Galinski, et al. (2000). "Two *Plasmodium falciparum* genes express merozoite proteins that are related to *Plasmodium vivax* and *Plasmodium yoelii* adhesive proteins involved in host cell selection and invasion." Proc Natl Acad Sci U S A **97**(17): 9648-9653.

Rayner, J. C., E. Vargas-Serrato, et al. (2001). "A *Plasmodium falciparum* homologue of *Plasmodium vivax* reticulocyte binding protein (PvRBP1) defines a trypsin-resistant erythrocyte invasion pathway." J Exp Med **194**(11): 1571-1581.

Resh, M. D. (1999). "Fatty acylation of proteins: new insights into membrane targeting of myristoylated and palmitoylated proteins." Biochimica et Biophysica Acta (BBA) - Molecular Cell Research **1451**(1): 1-16.

Rich, S. M. and F. J. Ayala (2003). "Progress in malaria research: the case for phylogenetics." Adv Parasitol **54**: 255-280.

Richie, T. L. and A. Saul (2002). "Progress and challenges for malaria vaccines." Nature **415**: 694-701.

Robson, K. J., U. Frevert, et al. (1995). "Thrombospondin-related adhesive protein (TRAP) of *Plasmodium falciparum*: expression during sporozoite ontogeny and binding to human hepatocytes." EMBO J **14**(16): 3883-3894.

Rogers, W. and S. Hoffman (1999). Malaria vaccines. Malaria. M. Wahlgren and P. Perlmann. Amsterdam, Harwood Academic Publishers.

Ronn, A., H. A. Msangeni, et al. (1996). "High level of resistance of *Plasmodium falciparum* to sulfadoxine-pyrimethamine in children in Tanzania." Trans R Soc Trop Med Hyg **90**: 179-181.

Ross, R. (1897). "On some peculiar pigmented cells found in two mosquitoes fed on malarial blood." Br. Med. J **ii**: 1786-1788.

Ross, R. (1898). "The role of the mosquito in the evolution of the malaria parasite." Lancet **ii**: 488-489.

Russell, D. G. and R. E. Sinden (1981). "The role of the cytoskeleton in the motility of coccidian sporozoites." J Cell Sci **50**: 345-359.

Sahoo, N., W. Beatty, et al. (2006). "Unusual kinetic and structural properties control rapid assembly and turnover of actin in the parasite *Toxoplasma gondii*." Mol Biol Cell **17**(2): 895-906.

Sam-Yellowe, T. Y., H. Shio, et al. (1988). "Secretion of *Plasmodium falciparum* rhoptry protein into the plasma membrane of host erythrocytes." J Cell Biol **106**(5): 1507-1513.

Samuel, B. U., N. Mohandas, et al. (2001). "The role of cholesterol and glycosylphosphatidylinositol-anchored proteins of erythrocyte rafts in regulating raft protein content and malarial infection." J Biol Chem **276**(31): 29319-29329.

Sanders, P. R., P. R. Gilson, et al. (2005). "Distinct protein classes including novel merozoite surface antigens in Raft-like membranes of *Plasmodium falciparum*." J Biol Chem **280**(48): 169-176.

Schmitz, S., M. Grainger, et al. (2005). "Malaria parasite actin filaments are very short." J Mol Biol **349**(1): 113-125.

Schofield, L. and F. Hackett (1993). "Signal transduction in host cells by a glycosylphosphatidylinositol toxin of malaria parasites." J. Exp. Med **177**: 145-153.

Scholtyseck, E. and H. Mehlhorn (1970). "Ultrastructural study of characteristic organelles (paired organelles, micronemes, micropores) of sporozoa and related organisms." Z Parasitenkd **34**(2): 97-127.

Selinsky, B. S. (2003). Membrane protein protocols. Expression, purification, and characterisation. Totowa, Humana Press.

Shahinian, S. and J. Silvius (1995). "Doubly-lipid-modified protein sequence motifs exhibit long-lived anchorage to lipid bilayer membranes." Biochemistry **34**(11): 3813-3822.

Shaw, M. K. and L. G. Tilney (1995). "The entry of *Theileria parva* merozoites into bovine erythrocytes occurs by a process similar to sporozoite invasion of lymphocytes." Parasitology **111**: 455-461.

Shaw, M. K. and L. G. Tilney (1999). "Induction of an acrosomal process in *Toxoplasma gondii*: visualization of actin filaments in a protozoan parasite." Proc Natl Acad Sci U S A **96**(16): 9095-9099.

Shaw, M. K., L. G. Tilney, et al. (1991). "The entry of *Theileria parva* sporozoites into bovine lymphocytes: evidence for MHC class I involvement." J Cell Biol **113**(1): 87-101.

Shin, S. C., J. P. Vanderberg, et al. (1982). "Direct infection of hepatocytes by sporozoites of *Plasmodium berghei*." J Protozool **29**(3): 448-454.

Sibley, L. D. (1995). "Invasion of vertebrate cells by *Toxoplasma gondii*." Trends Cell Biol **5**(3): 129-132.

Siden-Kiamos, I., A. Ecker, et al. (2006). "*Plasmodium berghei* calcium-dependent protein kinase 3 is required for ookinete gliding motility and mosquito midgut invasion." Mol Microbiol **60**(6): 1355-1363.

Sidjanski, S. and J. P. Vanderberg (1997). "Delayed migration of *Plasmodium* sporozoites from the mosquito bite site to the blood." Am J Trop Med Hyg **57**: 426-429.

Sinclair, G. and F. Y. Choy (2002). "Synonymous codon usage bias and the expression of human glucocerebrosidase in the methylotrophic yeast, *Pichia pastoris*." Protein Expr Purif **26**(1): 96-105.

Singh, S., M. Plassmeyer, et al. (2007). "Mononeme: A new secretory organelle in *Plasmodium falciparum* merozoites identified by localization of rhomboid-1 protease." Proc Natl Acad Sci U S A **104**(50): 20043-20048.

Smythe, J. A., R. L. Coppel, et al. (1988). "Identification of two integral membrane proteins of *Plasmodium falciparum*." Proc Natl Acad Sci U S A **85**(14): 5195-5199.

Sreerama, N. and R. W. Woody (2000). "Estimation of protein secondary structure from circular dichroism spectra: comparison of CONTIN,

SELCON, and CDSSTR methods with an expanded reference set." Analytical Biochemistry **287**(2): 252-260.

Stafford, W., R. Stockley, et al. (1996). "Isolation, expression and characterization of the gene for an ADP-ribosylation factor from the human malaria parasite, *Plasmodium falciparum*." Eur J Biochem **242**(1): 101-113.

Stahl, H. D., A. E. Bianco, et al. (1986). "Sorting large numbers of clones expressing *Plasmodium falciparum* antigens in *Escherichia coli* by differential antibody screening." Mol Biol Med **3**(4): 351-368.

Stephens, J. W. W. (1922). "A new malaria parasite of man." Ann Trop Med **16**: 383-388.

Stewart, M. J. and J. P. Vanderberg (1991). "Malaria sporozoites release circumsporozoite protein from their apical end and translocate it along their surface." J Protozool **38**(4): 411-421.

Stowers, A. W., V. Cioce, et al. (2001). "Efficacy of two alternate vaccines based on *Plasmodium falciparum* merozoite surface protein 1 in an *Aotus* challenge trial." Infect Immun **69**(3): 1536-1546.

Stubbs, J., K. M. Simpson, et al. (2005). "Molecular mechanism for switching of *P. falciparum* invasion pathways into human erythrocytes." Science **309**(5739): 1384-1387.

Sturm, A., R. Amino, et al. (2006). "Manipulation of host hepatocytes by the malaria parasite for delivery into liver sinusoids." Science **313**: 1287-1290.

Sultan, A. A., V. Thathy, et al. (1997). "TRAP is necessary for gliding motility and infectivity of *Plasmodium* sporozoites." Cell **90**(3): 511-522.

Tachado, S. D., P. Gerold, et al. (1996). "Glycosylphosphatidylinositol toxin of *Plasmodium* induces nitric oxide synthase expression in macrophages and vascular endothelial cells by a protein tyrosine kinase-dependent and protein kinase C-dependent signaling pathway." J Immunol **156**: 1897-1907.

Taliaferro, W. H. (1949). Immunity to the malarial infections. Malariology. M. F. Boyd. Philadelphia, The W. B. Saunders Co: 941.

Tardieux, I., X. Liu, et al. (1998). "A *Plasmodium falciparum* novel gene encoding a coronin-like protein which associates with actin filaments." FEBS Lett **441**(2): 251–256.

Taylor, H., M. Grainger, et al. (2002). "Variation in the expression of a *Plasmodium falciparum* protein family implicated in erythrocytic invasion." Infect. Immun **70**(10): 5779-5789.

Tetley, L., S. M. Brown, et al. (1998). "Ultrastructural analysis of the sporozoite of *Cryptosporidium parvum*." Microbiology **144**(Pt 12): 3249-3255.

Thompson, J., R. E. Cooke, et al. (2004). "PTRAMP; a conserved *Plasmodium* thrombospondin-related apical merozoite protein." Mol Biochem Parasitol **134**(2): 225-232.

Thompson, J., D. Higgins, et al. (1994). "CLUSTAL W: improving the sensitivity of progressive multiple sequence alignment through sequence weighting, position-specific gap penalties and weight matrix choice." Nucleic Acids Res **22**(22): 4673-4680.

Topolska, A. E., A. Lidgett, et al. (2004). "Characterization of a Membrane-associated Rhoptry Protein of *Plasmodium falciparum*." J Biol Chem **279**(6): 4648-4656.

Trager, W. and J. B. Jensen (1976). "Human malaria parasites in continuous culture." Science **193**(4254): 673-675.

Trager, W., C. Rozario, et al. (1992). "Transfer of a dense granule protein of *Plasmodium falciparum* to the membrane of ring stages and isolation of dense granules." Infect Immun **60**(11): 4656-4661.

Trape, J. F. and C. Rogier (1996). "Combating malaria morbidity and mortality by reducing transmission." Parasitol Today **12**(6): 236-240.

Triglia, T., M. T. Duraisingh, et al. (2005). "Reticulocyte-binding protein homologue 1 is required for sialic acid-dependent invasion into human erythrocytes by *Plasmodium falciparum*." Mol Microbiol **55**(1): 162-174.

Triglia, T., J. Healer, et al. (2000). "Apical membrane antigen 1 plays a central role in erythrocyte invasion by *Plasmodium* species." Mol Microbiol **38**(4): 706-718.

Trucco, C., D. Fernandez-Reyes, et al. (2001). "The merozoite surface protein 6 gene codes for a 36 kDa protein associated with the *Plasmodium falciparum* merozoite surface protein-1 complex." Mol Biochem Parasitol **112**(1): 91-101.

Utzinger, J., Y. Tozan, et al. (2001). "Efficacy and costeffectiveness of environmental management for malaria control." Trop Med Int Health **6**: 677-687.

Vaid, A., D. C. Thomas, et al. (2008). "Role of Ca2+/calmodulin-PfPKB signaling pathway in erythrocyte invasion by *Plasmodium falciparum*." J Biol Chem **283**(9): 5589-5597.

van't Hof, W. and M. D. Resh (1997). "Rapid plasma membrane anchoring of newly synthesized p59fyn: selective requirement for NH2-terminal myristoylation and palmitoylation at cysteine-3." J Cell Biol **136**(5): 1023-1035.

van Dijk, M. R., C. J. Janse, et al. (2001). "A central role for P48/45 in malaria parasite male gamete fertility." Cell **104**(1): 153-164.

van Vugt, M., A. Brockman, et al. (1998). "Randomized comparison of artemether-benflumetol and artesunate-mefloquine in treatment of multidrugresistant *falciparum* Malaria." Antimicrob. Agents Chemother. **42**(1): 135-139.

Vanderberg, J. P. (1974). "Studies on the motility of *Plasmodium* sporozoites." J Protozool **21**(4): 527-537.

Vanderberg, J. P. (1975). "Development of infectivity by the *Plasmodium* berghei sporozoite." J Parasitol **61**: 43-50.

Vlachou, D., T. Zimmermann, et al. (2004). "Real-time, *in vivo* analysis of malaria ookinete locomotion and mosquito midgut invasion." Cell Microbiol **6**(7): 671-685.

Wang, J., A. J. Morris, et al. (1996). "The molecular nature of the F-actin binding activity of aldolase revealed with site-directed mutants." J Biol Chem **271**(12): 6861-6865.

Ward, G. E., L. H. Miller, et al. (1993). "The origin of parasitophorous vacuole membrane lipids in malaria-infected erythrocytes." J Cell Sci **106**(Pt 1): 237-248.

Ward, P., L. Equinet, et al. (2004). "Protein kinases of the human malaria parasite *Plasmodium falciparum*: the kinome of a divergent eukaryote." BMC Genomics **5**(1): 79.

Webb, S. E., R. E. Fowler, et al. (1996). "Contractile protein system in the asexual stages of the malaria parasite *Plasmodium falciparum*." Parasitology **112**(Pt 5): 451-457.

Wemmer, K. A. and W. F. Marshall (2004). "Flagellar motility: all pull together." Curr. Biol **14**(23): R992-993.

Werner, E. B., W. R. Taylor, et al. (1998). "A *Plasmodium chabaudi* protein contains a repetitive region with a predicted spectrin-like structure." Mol Biochem Parasitol **94**(2): 185-196.

Wertheimer, S. P. and J. W. Barnwell (1989). "*Plasmodium vivax* interaction with the human Duffy blood group glycoprotein: identification of a parasite receptor-like protein." Exp Parasitol **69**(4): 340-350.

Wesseling, J. G., M. A. Smits, et al. (1988). "Extremely diverged actin proteins in *Plasmodium falciparum*." Mol Biochem Parasitol **30**(2): 143-153.

Wesseling, J. G., P. J. Snijders, et al. (1989). "Stage-specific expression and genomic organization of the actin genes of the malaria parasite *Plasmodium falciparum*." Mol Biochem Parasitol **35**(2): 167-176.

Wetzel, D. M., S. Hakansson, et al. (2003). "Actin filament polymerization regulates gliding motility by apicomplexan parasites." Mol Biol Cell **14**(2): 396-406.

White, N. J. (1997). "Assessment of the pharmacodynamic properties of antimalarial drugs *in-vivo*." Antimicrob Agents Chemother **41**: 1413-1422.

World Health Organisation, W. H. O. (1993). "Study group on the implementation of the global plan of action for malaria control 1993–2000. Implementation of the global malaria control strategy." World Health Organ Techn Rep Ser **839**: 1-57.

World Health Organisation, W. H. O. (2000). "Severe *falciparum* malaria." Trans. R. Soc. Trop. Med. Hyg **94**(S1): 1-9.

World Health Organisation, W. H. O. (2005). World malaria report.

Yadava, A. and C. F. Ockenhouse (2003). "Effect of codon optimization on expression levels of a functionally folded malaria vaccine candidate in prokaryotic and eukaryotic expression systems." Infect Immun **71**(9): 4961-4969.

Yamauchi, L. M., A. Coppi, et al. (2007). "*Plasmodium* sporozoites trickle out of the injection site." Cell Microbiol **9**(5): 1215-1222.

Yang, X., C. G. Adda, et al. (2007). "A partially structured region of a largely unstructured protein, *Plasmodium falciparum* merozoite surface protein 2 (MSP2), forms amyloid-like fibrils." J Pept Sci **13**(12): 839-848.

Yeoh, S., R. A. O'Donnell, et al. (2007). "Subcellular discharge of a serine protease mediates release of invasive malaria parasites from host erythrocytes." Cell **131**(6): 1072-1083.

Yoshimasu, M. A., J. K. Ahn, et al. (2002). "Soluble expression and purification of porcine pepsinogen from *Pichia pastoris*." Protein Expr Purif **25**(2): 229-236.

Yuda, M., T. Sawai, et al. (1999). "Structure and expression of an adhesive protein-like molecule of mosquito invasive-stage malarial parasite." J Exp Med **189**(12): 1947-1952.

Zhao, Y., R. M. Franklin, et al. (1994). "*Plasmodium falciparum* calcium-dependent protein kinase phosphorylates proteins of the host erythrocytic membrane." Mol Biochem Parasitol **66**(2): 329-343.

Zhao, Y., B. Kappes, et al. (1993). "Gene structure and expression of an unusual protein kinase from *Plasmodium falciparum* homologous at its carboxyl terminus with the EF hand calcium-binding proteins." J. Biol. Chem **268**(6): 4347-4354.

Zhou, F., Y. Xue, et al. (2006). "CSS-Palm: palmitoylation site prediction with a clustering and scoring strategy (CSS)." Bioinformatics **22**(7): 894-896.